UNIVERSITEIT VAN PRETORIA
UNIVERSITY OF PRETORIA
YUNIBESITHI YA PRETORIA

Accuracy and skill of the Conformal-Cubic Atmospheric Model in short-range weather forecasting over southern Africa

by
Christina Johanna Potgieter

Submitted in partial fulfilment of the requirements
for the degree of

MASTER OF SCIENCE

in the
Faculty of Natural and Agricultural Sciences
University of Pretoria

October 2006

UNIVERSITEIT VAN PRETORIA
UNIVERSITY OF PRETORIA
YUNIBESITHI YA PRETORIA

Accuracy and skill of the Conformal-Cubic Atmospheric Model in short-range weather forecasting over southern Africa

Christina Johanna Potgieter

Promoter: Prof. C.J. deW. Rautenbach
Department: Department of Geography, Geoinformatics and Meteorology
Faculty: Faculty of Natural and Agricultural Sciences
University: University of Pretoria
Degree: Master of Science

Summary

This dissertation reports on the use of the Conformal-Cubic Atmospheric Model (C-CAM) for short-range weather forecasting over southern Africa. Forecasts that were issued during a six month period in 2005 are verified in this study. The model ran at C100 resolution with 18 σ- levels in the vertical. A Schmidt stretching factor of 0.3 was used. The model ran in stand-alone mode, that is, no far-field nudging was provided by a driving model. The model was initialised once daily at 0000Z, from the Global Forecasting System (GFS) analysis field. The time-step used was 5 minutes. The integration period was four days, with the output fields written every six hours.

The forecasts are verified objectively against reanalysis data from the National Centers for Environmental Prediction (NCEP). Forecast accuracy and skill at the synoptic scale are evaluated by comparing the model forecast fields of 500 hPa geopotential heights and the vertically integrated moisture flux agains NCEP reanalysis. It is found that on average the C-CAM forecasts outscores persistence forecasts for all four days of the forecast, for all the months studied. Forecast errors in the 500 hPa height tend to develop in the westerly wind-regime south of the subcontinent. These errors tend to propagate northeastwards, contaminating the forecast fields over the subcontinent after two to three days. In the summer months, large errors in the simulated vertically integrated moisture flux propgate southwards from the tropics to South Africa.

Case studies of specific weather events are studied in order to determine the model's ability to predict specific weather events over South Africa. The distribution of the rainfall was predicted well but the areas where heavy rainfall occurred was forecast incorrectly. In the second case study, the prognostic model fields depicted the occurence of a severe thunderstorm event nearly two days in advance. Generally, it may be said that the C-CAM forecasts have skill for all four days of the forecasting period. Forecast accuracy start to decrease quite rapidly from the third day, though. This may place a time-limit on the use of the C-CAM set-up use here in event forecasting over southern Africa.

Akkuraatheid en vaardigheid van die Konformies-Kubiese Atmosferiese Model met korttermyn weervoorspelling oor suider Afrika

Christina Johanna Potgieter

Promotor: Prof. C.J. deW. Rautenbach
Departement: Departement Geografie, Geoinformatika en Meteorologie
Fakulteit: Fakulteit Natuur - en Landbouwetenskappe
Universiteit: Universiteit van Pretoria
Graad: Meester in Wetenskap

Samevatting

Die studie handel oor die gebruik van die Komformies-Kubiese Atmoferiese Model (C-CAM) in korttermyn weervoorspelling oor suider Afrika. Voorspellings uitgereik vir 'n ses maande periode gedurende 2005 word geverifieer. Die modellopies is gedoen met C100 horisontale resolusie en met 18 σ vlakke in die vertikaal. ‘n Schmidt strekfaktor van 0.3 is gebruik. Die model is daagliks om 0000Z onafhanklik geintegreer, vanaf die globale voorspellingsisteem analise veld. 'n Tydstap van 5 minute is gebruik. Die integrasie periode was telkens 4 dae, met uitvoervelde elke 6 uur.

In die studie word die voorspellings objektief geverifieer teen heranalsie data van die Nasionale Sentrums vir Omgewingsvoorspelling (NCEP). Voorspellings akkaraatheid en vaardigheid op die sinoptiese skaal word geevalueer deur die modelvoorspellings van 500 hPa hoogtes en die vertikaal geintegreerde vogvloed statisties te vergelyk met NCEP heranalise data. Daar word getoon dat die C-CAM voorspellings beter is as voortsettingsvoorspellings vir die hele 4-dag voorspellingsperiode. Voorspellingsfoute in die 500 hPa hoogte is geneig om in die westewindgordel suid van die subkontinent te ontwikkel en propageer dan noordooswaarts. Gedurende die somermaande plant groot foute in die vetikaal geintegreerde vogvloed suidwaarts voort, vanaf die trope na Suid Afrika.

Gevallestudies word ook in die studie gedoen, met die doel om die model se vermoe om spesifieke weersgebeurtenisse te voorspel te bepaal. In die geval van 'n afsnylaag wat bestudeer is, is die area waarin reenval voorgekom het goed voorspel, maar swaar neerslae is nie akkuraat voorspel nie. In die tweede gevallestudie is die gunstigheid vir swaardonderstorms omtrent twee dae vooruit korrek voorspel. In die algemeen is bevind dat die voorspellings vaardigheid het vir al vier dae van die voorspellingsperiode, alhoewel die akkuraatheid van voorspellings afneem na ongeveer drie dae. Dit kan 'n beperking plaas op die tydslimiet waarvoor C-CAM gebruik kan word om spesifieke weersgebeurtenisse te voorspel.

Acknowledgements

Many thanks and appreciation to:

- Prof. C.J. deW. Rautenbach (Head of the Department of Geography, Geoinformatics and Meteorology at the University of Pretoria).
- The scientists of CSIRO in Australia with the implementation of C-CAM.
- Francois Engelbrecht from the University of Pretoria for supplying already existed software developed by himself as well as for very useful imput on the structure of this study.
- The librarians of the South African Weather Service, Karin and Anastasia for helping with the quest to find articles.
- Coleen and Tracy from the South African Weather Service for all the data you provided.
- Noelien and Philip, my colleques from the Agricultural Research Counsil for assistance with GIS.
- Evert, Elizma, Stephan en Liezl wat my liefde vir weerstelsels deel en vir nuttige gesprekke daaroor.
- My familie - Ma, Stoffel, Annie, tannie Lettie en Leanie vir julle belangstelling asook vir my pa, alhoewel hy nie meer hier op aarde is nie, vir sy belangstelling tot hy nie meer kon nie.
- Francois, dankie vir jou ondersteuning en die baie koppies koffie.
- Aan God die eer vir die nodige geduld en deursettingsvermoe.

Contents

List of Symbols

c_p	specific heat at constant pressure
f_i	forecast value at the i^{th} grid point
$\bar{f}$	spatial average of the forecast values
m_d	mass of dry air
m_v	mass of water vapour
N	number of grid points
o_i	observed value at the i^{th} grid point
$\bar{o}$	spatial average of the observed values
p	pressure
p_0	standard pressure level
q	specific humidity
R	gas constant for dry air
u	zonal wind component
v	meridional wind component
$\mathbf{V}$	$\equiv (u,\, v)$, horizontal velocity
T	temperature
w	mixing ratio
z	geometric height
θ	potential temperature
θ_e	equivalent potential temperature

List of Figures

List of Tables

List of abbreviations

AGCM	Atmospheric General Circulation Model
AMSL	Above Mean-Sea Level
C-CAM	Conformal-Cubic Atmospheric Model
CLW	Coastal Low Workshop
CSIRO	Commonwealth Scientific and Industrial Research Organisation
DARLAM	Division of Atmospheric Research Limited Area Model
ECMWF	European Center for Medium Range for Weather Forecasting
GDAS	Global Data Assimilation System
GFS	Global Forecasting System
GrADS	Grid Analysis and Display System
IGY	International Geophysical Year
IT	Information Technology
ITC	Inter-Tropical Convergence
ITCZ	Inter-Tropical Convergence Zone
MFC	Moisture Flux Convergence
MM5	Fith-generation Pennsylvania State University-National Center for Atmospheric Research Meso-scale Model
MSG	Meteosat Second Generation
MSLP	Mean Sea-Level Pressure
NCAR	National Center for Atmospheric Research
NCEP	National Centers for Environmental Prediction
NWP	Numerical Weather Prediction
OAGCM	Ocean Atmosphere General Circulation Model
PC	Personal Computer
RMSE	Root Mean Square Error
SAWB	South African Weather Bureau
SAWS	South African Weather Service

SAST	South African Standard Time
SHR	Bulk Shear
SSI	Spectral Statistical Interpolation
SWIO	Southwest Indian Ocean
UKMO	United Kingdom Meteorological Office
UP	University of Pretoria
WRC	Water Research Commission

Chapter 1

Introduction

1.1 Background

The subcontinent of southern Africa is largely located in the subtropics, which implies that the upper air circulation over the region is predominantly anticyclonic and subsident. However, a great variety of weather systems occur over the region. The anticyclonic circulation is frequently interrupted by upper troughs from the westerly wind regime that propagate eastwards over the subcontinent. In the south frontal systems from the midlatitudes are the dominant systems in the austral winter. The northern parts are characterized by tropical weather systems in the austral summer, when the Inter-Tropical Convergence Zone (ITCZ) moves south of the equator. Tropical lows, easterly waves and meso-scale convective complexes are frequently observed over the northern subcontinent in summer. During seasons where the tropical circulation is particularly well defined, tropical lows occur frequently to the north of South Africa and even tropical cyclones sometimes make landfall over the coasts of Mozambique and South Africa. The subtropical highs normally devides the tropical systems from those of the midlatitudes. However, systems from these two flow regimes sometimes interact to produce widespread rainfall over the subcontinent. Superimposed on the great variety of synoptic-scale weather systems, smaller scale systems also occur to define the regional climate. These include coastal lows and berg winds along the South African and Namibian coast lines, and thunderstorms that develop over the highground regions of southern Africa.

Apart from the great variety of different types of weather systems that occur over the subcontinent, a specific type of system may also exhibit great variation in its track and intensity whilst moving over the region. Weather forecasting over southern Africa is therfore quite challenging. Operational forecasting over the region is still very much a “man-machine mix”. Forecasters would typically combine their knowledge and experience of local weather with Numerical Weather Prediction (NWP) guidance, as well as with satellite and radar images to compose daily weather forecasts. An issue of great importance to weather forecasting over the subcontinent, is the scarcity that exists in observational data. Over the whole subcontinent there are only a few weather stations where upper air soundings are being made on a daily basis. These include stations over South Africa (Irene, Polekwane, Betlehem, Bloemfontein, Springbok, De Aar, Cape Town, Port Elizabeth and Durban). To the north of South Africa even less observations are being made. Even surface observational data is sparse over the countries that are neighbouring South Africa. The situation is even worse over the Atlantic, Indian and the vast Southern Ocean that surrounds the subcontinent. The only regular upper air soundings over the oceans are provided by weather stations at remotely located islands such as Marion -and Gough Island. The surface observations from ships and weather buoys are also far and in between. The scarcity of observational data over southern Africa and the surrounding oceans impacts negatively on the need of providing NWP models with well-described initial conditions. Although the advances made in using meteorological satellite data as initial conditions for NWP models has led to a general increase in the accurcy of NWP in the southern hemisphere, the sparseness of weather station data remains a factor that is hampering weather prediction over the subcontinent.

Forecast fields from a number of NWP models are being used as forecasting guidance at the South African Weather Service (SAWS). These include predictions by the European Center for Medium Range Forecasting (ECMWF), the United Kingdom Meteorological Office (UKMO) and Global Forecasting System (GFS) global models. Since 1992, the Eta-model from the National Centers for Environmental Prediction (NCEP) has been running in-house at the SAWS (Riphagen, 1999; Riphagen et al., 2002). This model became the base model for the forecasts issued by the SAWS. The fith generation Pennsylvynia State-University-National Center for Atmospheric Research (NCAR) Meso-Scale Model (MM5) also runs operationally at the SAWS at present; it is mainly used for the generation of aviation forecasting products. In 2004 changes at NCEP persuaded the SAWS to obtain a new regional model for in-house forecasting, this time from the UKMO. The UKMO model (Davies et al., 2005) is presently being implemented at SAWS. At the University of Pretoria (UP) the Conformal-Cubic Atmospheric Model (C-CAM) has been running in-house since December 2004. The University of Pretoria (UP) is the only institution in South Africa other than the SAWS where a NWP model is used operationally.

An issue of great importance in NWP prediction is verifying a specific model's forecasts against observations over a given region. Unfortunately, the relative skill and accurcay of the NWP models used at the SAWS have apparently never been compared to each other in a formal study, although some results are available on the SAWS intranet. In this study, the potential of the C-CAM model to provide NWP guidance to weather forecasting over southern Africa is investigated. The accuracy and skill of the model are determined, with particular emphasis on how the model simulates the movement and evolution of weather systems over the country at the synoptic-scale.

1.2 Numerical weather prediction

Bjerknes (1904) was the first to realize that weather prediction is in principle an initial value problem, and that atmospheric behaviour is governed by the laws of physics. He also realized that the mathematical statement of these laws, which is a complex set of nonlinear partial differential equations, can not be solved analytically. In addition the atmospheric data available at the time was completely inadequate to describe the initial conditions (Haltiner and Williams, 1980). In particular, virtually no upper air observations were being made at that time.

Richardson (1922) was the first to attempt solving the equations numerically. However, Richardson obtained surface pressure changes an order of magnitude greater than observed. At the time, this failure was thought to be due primarily to the poor initial data available, particularly in the absence of upper air soundings. Perhaps even more important though, is that Richardson's numerical solution procedure would have led to the spurious growth of gravity and sound waves in the numerical solution (Holton, 1992). There was no immediate effort to repeat Richardson's experiment - and an important reason for this, is that the calculations that were performed using desk calculaters took months to complete. Thus, Richardson's pioneering effort at NWP was regarded as a failure.

It was only about three decades after Richardson's experiment that the first successes in NWP were achieved. By this time, three important developments have taken place. Firstly, theoretical research on the atmospheric equations has shown how the dynamical equations could be filtered of sound and gravity waves, by systematicaly introducing hydrostatic and geostrophic balance (Charney, 1948). Using the quasi-geostrophic equation set avoided the numerical difficulties that contributed to the failure of Richardson's solution of a more complicated equation set. Secondly, the invention of the radiosonde resulted in widespread observations of the upper atmosphere (e.g. Haltiner and Williams, 1980). The final breakthrough was the development of the first electronic computers the 1940s, making numerical weather prediction a practical posibility for the first time. In 1950 the first successful dynamical-numerical forecast was obtained for 500 hPa flow, by using an equivalent-barotropic vorticity model (Charney et al., 1956). Although this model was much simpler than Richardson's version, research on the numerical methods suitable for solving the atmospheric equations progressed rapidly. By the 1960's, hydrostatic primitive equation models with elaborate physical parameterization schemes were being used operationally. These models have since become highly evolved and sophisticated, and are today the primary tool for NWP (e.g. Janjic et al., 2001).

More recently, faster computers have made operational prediction possible using nonhydrostatic models based on the fully-elastic (unapproximated) atmospheric equations (see Engelbrect, 2006 for a recent review on nonhydrostatic models).

The growth of the surface and upper air observational network over the last five decades has resulted in the availability of more accurate initial conditions for use in NWP. However, over the oceans, Antarctica and many third world countries, especially in Africa, the observational network remains inadequate and is mostly deteriorating due to inadequate maintenance. The use of meteorological satellites to provide initialization data over data sparse regions have led to general improvements in model accuracy, in particular over the Southern Hemisphere. Data assimilation, the objective determination of the meteorological observations to be used as initial conditions at the model grid points over a given domain, subject to dynamical constraints, is another important branch of NWP (e.g. Haltiner and Williams, 1980). Additionally, NWP involves the display, distribution and verification of the forecasts obtained. The latter involves determining the accuracy and skill of a NWP model, against the background of the limits that exist in the predictability of the atmosphere.

1.3 Numerical weather prediction at the University of Pretoria

At UP research on numerical atmospheric prediction has traditionally focussed on the seasonal and longer time scales. In 1995 the CSIRO Mark 2 AGCM with an R21 spectral resolution was installed at the South African Weather Bureau (SAWB) by Rautenbach of UP, with the assistance of CSIRO researchers. A number of experiments were performed in order to determine the model's ability to simulate present-day climate over southern Africa, and to investigate ocean-atmosphere interaction (Jury et al., 1996; Jury et al., 2000). The model was subsequently used to produce experimental seasonal forecasts over the southern African region (Rautenbach, 2003). In 1999 research on the simulation of climate and climate change over southern Africa using regional climate models commenced at UP (Engelbrecht, 2000; Engelbrecht and Rautenbach, 2000). For this purpose the CSIRO's limited-area model DARLAM (Division of Atmospheric Research Limited Area Model) was implemented at UP by Engelbrecht and Rautenbach, with the asistance of CSIRO researchers McGregor and Katzfey. DARLAM's ability to simulate mid-summer and mid-winter climate over tropical and southern Africa was explored by Engelbrecht (2000), Engelbrecht et al. (2002) and Olwoch et al. (2003). The model was subsequently used to perform simulations of mid-summer and mid-winter climate change over the same region (Olwoch et al., 2007). More extensive simulations of climate and climate change over southern Africa have been performed at UP using the successor of DARLAM model, namely the variable resolution global model C-CAM (Engelbrecht, 2005).

C-CAM was implemented on computers at UP in 2003, as part of a project on model development funded by the Water Research Commission (WRC) in Pretoria. Various sensitivity studies were performed in order to improve the model's ability to simulate rainfall over southern Africa (Rautenbach et al., 2005). With the assistance of CSIRO researchers McGregor and Thatcher, the research group at UP managed to run C-CAM operationally for routine NWP over southern Africa in late 2004 (Rautenbach et al., 2005). UP is the first institution in South Africa, other than the SAWS, to accomplish this. During 2005 (the study period of this dissertation) the model was initialized once daily and a four-day forecast of high-resolution was produced. This dissertation reports on the the use of C-CAM as a tool for weather prediction over southern Africa.

1.4 The Conformal-Cubic Atmospheric model

Short-range weather forecasts produced by C-CAM are verified in this study. This Atmospheric General Circulation Model (AGCM) has been developed at CSIRO Marine and Atmospheric research, Australia. C-CAM is formulated on a quasi-uniform grid, derived by projecting the panels of a cube to the surface of the Earth (Rancic et al., 1996; McGregor 2005a). The model has the capability to run in variable resolution stretched-grid mode to provide high resoltion over the area of interest. In the latter case the model may run in conjunction with another simulation, by using sea-surface temperatures and far-field nudging of winds provided by the host model (McGregor and Dix, 2001, 2006). This approach of dynamic downscaling is highly flexible compared to the traditional limited-area modelling approach. It also avoids one of the main problems associated with limited-area models, namely reflections at the lateral boundaries (McGregor and Dix, 2001, 2006). C-CAM is a two-time-level semi-implicit semi-Lagrangian hydrostatic model. The C-CAM dynamics, numerics and physical parameterization schemes are discussed by McGregor (2005a) and McGregor and Dix (2001, 2006) (also see Chapter 3).

C-CAM has mostly been used to perform multi-year simulations of regional climate. These include simulations of present-day climate over various domains, with SSTs and far-field winds provided by NCEP reanalysis. Climate change simulations have also been carried out, with forcing provided by the CSIRO Mk3 Ocean-Atmosphere General Circulation Model (OACGM) (e.g. Engelbrecht, 2005). It has also been used for short-range weather-forecasting and to model the global transport of trace gasses.

1.5 Objectives of the research

As mentioned in section 1.3, a research project on atmospheric model development commenced at UP in 2003. As part of this project, C-CAM was implemented on a computer in Pretoria for the purpose of operational weather forecasting. The research in this thesis contributed to the mentioned research project (Rautenbach et al., 2005). The main goal of the research was to investigate the accuracy and skill of the C-CAM forecasts in predicting weather over southern Africa. The author (Potgieter) also assisted with the initial implementation of C-CAM on a computer in South Africa, and with maintaing the forecasting system once it was in place. The main objectives with the research outlined in the dissertation were:

Implementation of a local forecasting system based on C-CAM predictions, suitable for operational weather forecasting

In October 2004, C-CAM was implemented on a computer of UP located at the company NeTSYS International in Pretoria. The latter company provided the information technology (IT) infrastructure for the C-CAM forecasting system during 2004 and 2005. The main contribution of NeTSYS International was to download the analysis fields needed for model initialization on a daily basis. CSIRO scientist Thatcher implemented C-CAM on the computer at NeTSYS International, via remote access from Melbourne, Australia. The author contributed by suggesting which variables, pressure levels and time-levels should be availabe in the model output. During the project she continuously assisted with the manual transfer of the forecast data sets to data storage facilities at UP. She finally composed a number of scripts that facilitates the convenient use of the C-CAM forecasts in an operational forecasting environment.

To objectively determine the accuracy and skill of the C-CAM model in forecasting synoptic-scale weather systems over southern Africa

This was achieved by means of statistical evaluation of the C-CAM forecasts. Accuracy was determined verifying the C-CAM forecasts of 500 hPa geopotential heights and vertically integrated moisture flux agains NCEP reanalysis data. Secondly, point verification was done by means of comparing upper air sounding data at selected locations in South Africa to C-CAM forecasts at these points. Skill to predict synoptic scale patterns was evaluated by comparing the C-CAM forecasts against persitence forecasts based on NCEP reanalysis data. The statistical verification was done for six months of 2005 during which the C-CAM forecasting system ran smoothly. During the months not analysed too many forecasts were lost, largely because of power shortages at NeTSYS International, and because of a lack of data storage facilities.

To determine the usefulness of the C-CAM predictions in the forecasting of specific weather events over southern Africa

Uncertainty in the initial conditions and the nature of the atmospheric equations place a time limit on the predictability of the atmosphere. The second objective was achieved by firstly investigating how statistically determined model errors grow as a function of time. Secondly, C-CAM's ability to predict specific weather events were evaluated by two case studies. In the first case study, the C-CAM predictions of the track and intensity of a cut-off low system is compared to observed data. In the second case study, the C-CAM prognostic fields are used and analysed from a forecasters point of view to determine whether the tunderstorm under discussion could be predicted.

1.6 Organisation of the report

The growth of forecasting error in time over the southern African region, may be at least partially explained by the typical evolution and movement of the weather systems that characterize the region. Chapter 2 gives a literature overview of the great variety of weather systems that occur over southern Africa. The weather systems discussed range from the synoptic - to the meso-scale, and include troughs and lows over the land, ridges and anticyclones over the land, cold fronts, ridging high pressure systems, westerly waves and cut-off lows, coastal lows, tropical temperate troughs, tropical lows and easterly waves, tropical cyclones and topographically induced systems. The mean surface and upper air flow over southern Africa and the surrounding oceans, within which the different weather systems are embededed, is also discussed in Chapter 2.

The C-CAM forecasting system as used in the study is described in chapter three. This includes a brief discussion of the dynamics, numerics and physical parameterization schemes of C-CAM. Aspects of the model set-up over southern Africa, such as initialization, horizontal and vertical resolution, stretching factor and integration time are also discussed.

Chapter 4 describes the statistical verification of the C-CAM forecasts. The accuracy and skill of the predictions of 500 hPa height and the vertically integrated moisture flux over southern Africa, and how these change as a function of time during the integration period, are evaluated. Accuracy is also investigated by comparing the model forecasts against upper air soundings at selected weather stations. In Chapter 5, two case studies are discussed to subjectively determine the model's ability to predict specific weather events over the region. The case studies include a cut-off low that caused heavy rainfall along the Cape south coast, as well as a severe thunderstorm event. Conclusions on the research are presented in Chapter 6.

Chapter 2

Weather patterns over southern Africa

2.1 Introduction

The climate of southern Africa results from a great variety of weather systems that occur over the region. Situated in the descending component of the Hadley-cell circulation, great portions of southern Africa are under the influence of the subtropical high pressure belt in the austral winter. The anticyclones and subsidence associated with the subtropical high pressure belt cause dry winters over the interior regions of the subcontinent. South of the high pressure belt, midlatitude cyclones bring rainfall over the southern and western coastal areas of South Africa in the winter. In the austral summer, the subtropical high pressure belt shifts southwards. Over the land, the dominance of the high pressure belt ceases as it is replaced by a trough that links with the tropical regions. Most of the summer rainfall over the region oroginates from cloudbands that are aligned from the northwest to the southeast, in association with eastward propagating upper troughs. Extensive summer rainfall occurs when a westerly wave links up with an easterly wave or tropical low to the north. In such a case moisture transport takes place all the way from the tropics to the subcontinent and further southeastwards. This weather system is known as a tropical temperate trough. Tropical cyclones are a rare occurence over the subcontinent, but seasons where they occur are characterized by high rainfall totals and flooding.

Weather systems or circulation types over southern Africa has been identified and described by several authors of which the work of Taljaard (1995a), Harrison (1986) and Tyson (1986) are the most widely used. The classification methods used by these authors differ. Taljaard (1995a) described the circulation types that occur over southern Africa in summer and winter. He identified all the typical pressure distribution patterns on the surface as well as in the upper air and described these systems by means of specific examples. He used the location, intensity, temperature and certain structural features of cyclones, anticyclones, troughs and ridges to aid with his classification. His classification can be regarded as one of the most complete classifications of the different circulation patterns that occur over southern Africa. He also constructed the synoptic climatology for January and July over South Africa (Taljaard, 1995b). Harrison (1986) focused on identifying summer rain-producin circulation types. He had a statistical approach that he combined with satellite imagery. The most well known outcome of his work is probably the identification of the tropical-temperate trough as one of the important rain-producing systems over southern Africa. Tyson (1986) devided his classification into a few categories. He described the weather systems that form in the easterlies and westerlies that influence South Africa's weather. He described typical weather systems that are associated with fine or mildly disturbed conditions and he described some systems individually that can lead to significant rainfall over the country, e.g. tropical cyclones, thunderstorms and composite systems. The discussion in the remainder of this chapter largely follows the classification of southern African weather systems provided by these authors. Characteristics of the maritime weather patterns are also included in this literature overview, as the verification of C-CAM in chapter 4 involves extensive maritine areas surrounding southern Africa.

2.2 Study area

In this literature overview, circulation patterns that occur over tropical -and southern Africa, as well as the surrounding oceans are discussed (figure 2.1). During the austral summer, weather systems over South Africa (such as upper-air westerly waves, see section 2.5.6) interact from time-to-time with the circulation over tropical Africa. Some of the moisture that is transported southwards over South Africa during these connections, originates from north of the equator (see section 2.5.8). During the austral winter, cold fronts that originates from far southwest of South Africa, moves over the country (see section 2.5.4). The mean circulation over the southern ocean is therefore included in this literature overview.

2.3 Mean circulation patterns over southern Africa and the immediate ocean

2.3.1 Mean surface circulation over southern Africa

The mean circulation over southern Africa for the period 1981 to 1990 has been described by Taljaard (1995b). The circulation patterns and associated weather differ completely in mid-summer and mid-winter. Figure 2.1 shows the 850 hPa contours for January (1981-1990) over southern Africa, as obtained from Taljaard (1995b). Following the discussion of Taljaard (1995b), it may be seen

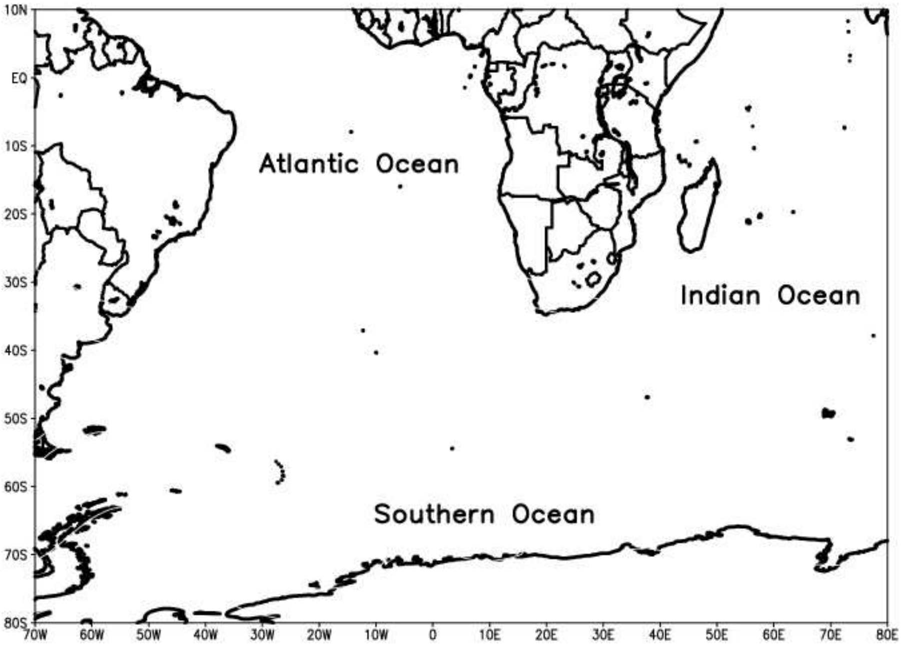

Figure 2.1: Area of interest in this study.

that in summer, a trough is seen to extend from northern Namibia across central Botswana to a low over southern Free State and northeastern Cape province. This low is located over the relatively low ground of the upper Orange River catchment. It is in the nature of a lee low west of the Lesotho mountian massif and north of the highground of the northeastern Cape (Taljaard, 1995b). The trough is flanked by a ridge extending eastwards along $30°S$ from the subtropical Atlantic Ocean and another at $25°S$ extending westwards from the Indian Ocean to Mpumalanga. A second minima in the trough occurs near Windhoek and is probaly caused by strong heating over the high ground of the Khomas Hochland during summer days (Taljaard, 1995b). The low over northeastern Cape Province is located over the relatively low ground of the upper Orange River catchment. It is also in the nature of a lee low west of the Lesotho mountain massif and north of the highground of northeastern Cape Province.

The semi-permanent ridge over Mpumalanga advects moist tropical air from the Mozambique Channel westwards and then southwards towards the Botswana trough. The opposite happens over the west coast where the Atlantic ridge mostly imports very dry subsided air to the regions west of the Botswana trough. It may be noted that the mean 850 hPa wind at Upington at 14:00 South African Standard Time (SAST) is northwesterly whereas it ought to be southerly according to the 850 hPa height distribution. In the late afternoon till early

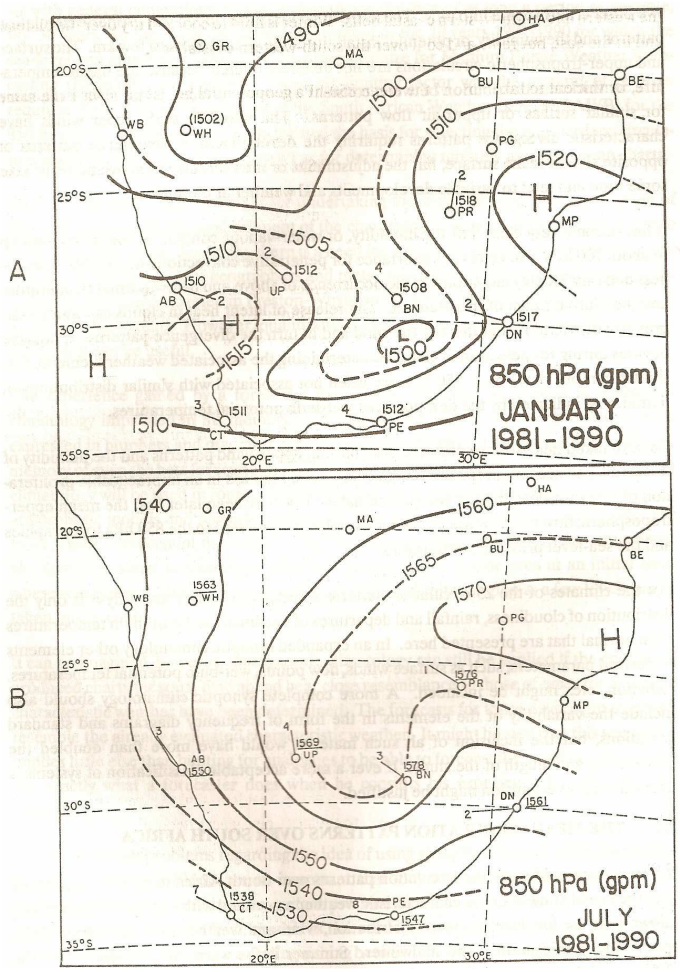

Figure 2.2: (A) Mean 850 hPa geopotential heights for January (1981-1990) and (B) July (1981-1990), (From Taljaard, 1995b).

morning it is actually southerly, but convective mixing sets in after sunrise, thereby transporting the momentum of the prevailing upper northwesterlies down to the surface during the day (Taljaard, 1995b).

In winter the heat lows and the Botswana trough are replaced by mean anticyclonic pressure and wind patterns over the plateau (Taljaard, 1995b). The 850 hPa contours during July for the period 1981 to 1990 are shown in figure 2.1, as obtained from Taljaard (1995b). The ridge over Mpumalnaga shifts about three degrees to the north, its axis now being located along $23°S$. However, anticyclone centres are so frequently located also over the central plateau that a weak secondary centre appears near the middle of the triangle between Pretoria, Upington and Bloemfoentein. The 14:00 SAST 850 hPa and surface winds over the region geostrophically corresponds to an anticyclonic center positioned about five degrees to the north. Once again, this is the result of convective downward flux of momentum from the 700 and 600 hPa levels in the afternoon, that dominates the surface wind. A peculiar feature is the cyclonic curvature of the contours over the highground of the eastern Freestate and Lesotho. The ridge-trough pattern over the Freestate, Lesotho and KwaZulu-Natal is likely to be dynamically produced by the predominant northwesterly flow across the Drakensberg mountain massif at the 850-600 hPa levles (Taljaard, 1995b). The pressure gradient steepens as the south coast is approached.

The mean circulation patterns over southern Africa is also described by Preston-Whyte and Tyson (1988). In general it is very similar to Taljaard's (1995a, 1995b) description. However, a difference is found in his description of the mean 850 hPa circulation during summer. The heat low over the Khomas Hochland as described by Taljaard (1995b), is not mentioned by Preston-Whyte and Tyson (1988). Instead, Preston-Whyte and Tyson (1988) describes that the trough over South Africa and Botswana is linked to a tropical low north of Botswana. Taljaard (1995b) does not mention a tropical low north of Botswana. However, this could be because his description focuses primarily on the region south of $20^{O}S$. Preston-Whyte and Tyson (1988) further describes that the centre of the tropical low wanders in an east-west direction along the southern branch of the ITCZ in the region of the Zaire Air Boundary and occasionally southward towards Namibia, Botswana, or Zimbabwe. The seasonal changes in the circulation over southern Africa are clearly evident in mean meridional sections through the atmosphere along $20°S$. It is apparent that tropical easterlies affect most of southern Africa throughout the year. At about $12°S$ low-level westerlies from the Atlantic Ocean extend to about 500 hPa in summer; in winter they weaken, become shallower and shift northward.

It may be noted that the change to a single high pressure cell takes place by March (Preston-Whyte and Tyson, 1988). This results in a northerly flow of moist air from the tropics over the western parts of southern Africa at a time when the air masses over Zimbabwe, Zambia and northern Botswana and

Namibia are still moist. This influx of moist air is largely responsible for the autumn rainfall maximum over the western regions at this time (Preston-Whyte and Tyson, 1988).

2.3.2 Mean mid- and upper air circulation over southern Africa

Taljaard (1953,1959) gave an in depth discussion on the mean summer and winter circulation in the lower troposphere over southern Africa. He compiled charts that represent the circulation on 2 km, 4 km and 6 km above mean sea-level (AMSL) (see figures 2.3, 2.4, 2.5). These charts are based upon observations published in the form of frequency tables and wind roses for southern African countries. These countries include South Africa, Namibia, southern Zimbabwe, Mozambique, Madagascar, Angola, Democratic Republic of the Congo and the former British East Africa.

Except for at the surface anticyclonic circulation dominates over southern Africa throughout the year (Taljaard, 1953, 1959; Preston-Whyte and Tyson, 1988). However, the position and intensity of the circulation changes during different seasons. A striking difference is also seen in the position of the high pressure system on the different levels. In general, the high pressure system is displaced north -and westwards on all levels during both summer and winter (Taljaard, 1953,1959, 1995a). A more detailed discussion follows below.

At 2 km AMSL above sea-level, the high pressure belt is indicated approximately along $27°S$ in summer. This high pressure belt consists of two cells over the Indian Ocean. The centre of the first cell is situated over Maputo and the centre of the second cell is situated southeast of Madagascar. Over the Atlantic ocean the centre of a cell in the high pressure belt is located at approximately $28°S$ and $15°E$. The high pressure cells at 2 km AMSL are like the sea-level high pressure cells not stationary. They vary in outline, intensity and in latitude of occurrence. They also move from west to east, but not as often as on sea-level. They are not always found in a definite position relative to the surface high pressure systems. The ITCZ at this level is at about $12 - 15°S$. It is not stationary at $15°S$ and is not always well marked. It is best developed during January.

During the winter, the centre of the cell that is situated over Maputo during the summer, is found over the eastern part of Limpopo Province. It is about $3°$ north of its position in summer. There is again a second cell present in the Indian Ocean high pressure belt. The location of this cell is very similar to where it is found during summer. Fairly strong easterly to southeasterly winds occur over the Indian Ocean north of the high pressure belt. The circulation over the continent is more intense in winter compared to summer, especially

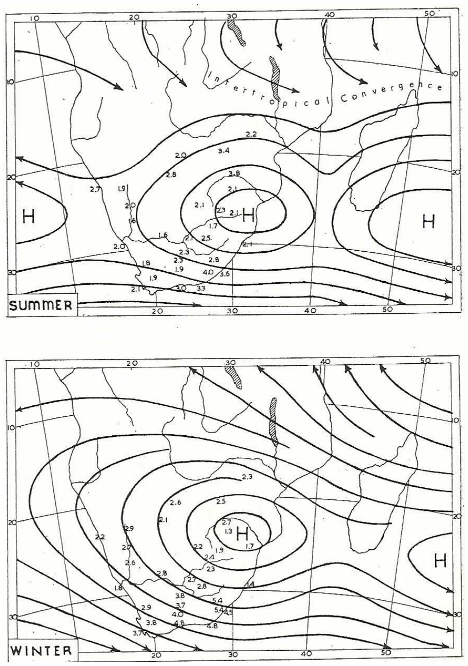

Figure 2.3: The mean streamlines on 2 km (AMSL) during summer (top) and winter (bottom) as obtained from Taljaard (1953).

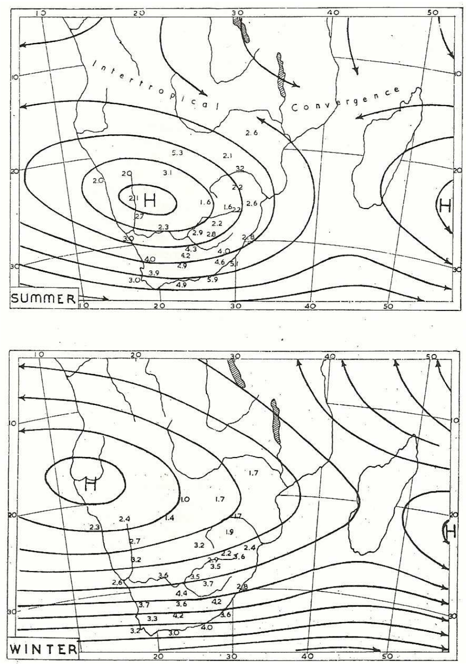

Figure 2.4: The mean streamlines on 4 km (AMSL) during summer (top) and winter (bottom) as obtained from Taljaard (1953).

over the southeastern part of South Africa. The Atlantic Ocean high pressure system is situated significantly more northwards ($20°S$) than during summer.

The position of the continental high pressure system at 4 km AMSL differs significantly during both summer and winter from 2 km to 4 km AMSL. During summer the high pressure system is situated at approximately $25°S$ and $20°E$ at 4 km AMSL - the core of the cell is displaced about 23 degrees due west form its position at 2 km AMSL. This significant displacement of the high pressure system between 2 km and 4 km AMSL causes a radical change in wind direction, and therefore in temperature and moisture content over almost all of South Africa. Whereas the circulation at 2 km AMSL brings in cool, humid maritime air from the north and east, the circulation at 4 km AMSL transports warm and drier continental air over the subcontinent.

At 4 km AMSL, a second cell is again to be seen in the Indian high pressure belt. The position of this cell is very similar to its 2 km AMSL position - it is not displaced westward with height. The position of the ITCZ at 4 km AMSL is quite similar as the 2 km AMSL position.

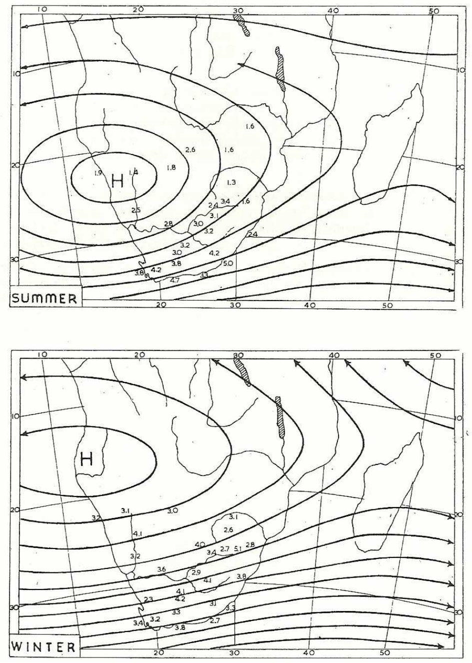

Figure 2.5: The mean streamflow on 6 km (AMSL) during summer (top) and winter (bottom) as obtained from Taljaard (1953).

The position of the continental high pressure system at 4 km AMSL during winter is about 20 degrees westward and 6 degrees northwards relative to its position at 2 km AMSL. The displacement is more in winter than in summer. The wind is on average westerly to southwesterly over South Africa at 4 km AMSL in winter.

There is no striking difference between the average circulation at 4 km and 6 km AMSL in both summer and winter. The wind over South Africa has a more southern component during both summer and winter at 6 km AMSL as compared to 4 km AMSL. Westerly and southwesterly winds are also more frequent at 6 km AMSL. The axis of highest pressure is located along approximately $20°S$ in summer and $15°S$ in winter at 6 km AMSL. The consequence of this is that westerly winds become more frequent over the immediate northern neighboring countries of South Africa, especially in winter.

Preston-Whyte and Tyson (1988) summarized the circulation of the mid -and upper troposphere. According to them, the mean anticyclone intensifies and moves northward in winter. Upper-level circumpolar westerlies expand and displace the upper tropical easterlies equatorward. This is in agreement with the work done by Taljaard (1953,1959). The westerlies extend equatorward then with the greatest increase from April to July, followed by a slow decline until October. The lowest speeds are observed in February to March. In the middle - and upper troposphere (500 and 200 hPa) during January, easterly flow is to be observed north of about $23°S$. This is also generally in agreement with Taljaard's (1953,1959) description of the circulation at 6 km AMSL (6 km can be compared with 500 hPa). Taljaard (1953, 1959) did not describe the circulation at 200 hPa, but according to Taljaard (1995a) the mean anticyclone on 200 hPa is situated close to, or slightly north of $20°S$. In winter subsidence occurs over much of southern Africa. In summer, flow tends to be poleward below about 500 hPa and equatorward above that level; at the 200 hPa level the flow is again poleward (Preston-Whyte and Tyson, 1988).

2.4 Mean maritime circulation patterns

2.4.1 Sea-level cyclone centres and tracks over the Southern Ocean

South of the subtropical high pressure belt, the westerly wind regime governs circulation over the Southern Ocean. Weather systems of the Southern Ocean have been actively studied for approximately hundered years up to date. However, this has always been challenging due to the sparseness of data over the vast Southern Ocean. The vastness of the ocean constitutes a data sparse region. Since the beginning of atmospheric observations over the Southern Ocean there has been considerabe inhomogenities in the temporal and spatial frequency of the observations. This is due to factors such as the occurrence of the World Wars, the popularity of whale hunting and conserted observation projects such as the International Geophysical Year (IGY). Of these, the IGY is probably the most significant in terms of studies that concern the weather systems of the Southern Ocean. During the IGY there was a dramatic increase in observation stations. The IGY commenced in July 1957 and the project ended in December 1958. Studies of the circulation patterns and the behavior of weather systems over the Southern Ocean that are based on the data collected during the IGY, has been considered to be more representative of the true nature of these systems than studies that are based on data prior to the IGY. A series of publications by Taljaard (1964, 1965,1967, 1972), Taljaard and van Loon (1962,1963,1964) and van Loon (1965) followed during and after the IGY. The work done by them can be considered as groundbreaking, since it was based on an optimum of observations as well as historically analysed charts. However, the fact that it is for a short period of time (18 months) must be kept in mind, since 18 months is not long enough to establish a normal behavior of pressure systems (Taljaard, 1967).

The advent of the modern era brought new opportunities for further investigation into the behavior of weather systems. The National Centers for Environmental Prediction-National Center for Atmospheric Research (NCEP-NCAR)

Reanalysis data make it possible to study the behavior of weather systems globally. Simmonds and Keay (2000) and Keable et al. (2002) studied the behavior of weather systems over the Southern Hemisphere based on NCEP-NCAR Reanalysis data covering the 40 year period 1958-1997. These analyses were obtained by assimilating past data into a frozen state-of-the-art analysis/forecast model system. This dataset can be regarded as one of the most complete, physically consistent datasets. Therefore the climatology of Southern Hemisphere cyclones obtained from this dataset is probably the most reliable yet (Simmonds and Keay, 2000).

Some contradiction exists between the work of Taljaard (1967), Simmonds and Keay (2000) and Lamb and Britton (1955) on where the most cyclogenesis occurs. Taljaard (1967) found that cyclogenesis occurs most frequently at approximately $45°S$ in all seasons and that the frequency of cyclongenesis is higher between $25°S$ and $40°S$ in winter than in summer. The formation of cyclones decrease poleward of $45°S$ but occasional periods occur when cyclogenesis is frequent even at $50-65°S$ (Taljaard, 1967). According to Simmonds and Keay (2000) and Lamb and Britton (1955), most cyclogenesis occurs at very high latitudes, and that the axis of the maximum lies on, or to the south of $60°S$. However, cyclolytic activity exceeds cyclogenesis in this region while cyclogenesis exceeds cyclolysis north of about $50°S$. Taljaard (1967) identified an area where there is a higher than normal frequency of cyclogenesis compared to other areas at a similar latitude. This area is subtropical South America and the adjacent Atlantic Ocean, particularly in winter. Simmonds and Keay (2000) found that the maximum number of cyclogenesis in the area identified by them, are found over the northern part of the Antarctic Peninsula as well as in the southern part of the Weddel Sea.

Cyclones are distributed frequently around Antarctica (Taljaard, 1967). Most systems occur south of $60°S$ (Simmonds and Keay, 2000). The most cyclone centres occur at $62-64°S$. That is $2-6°$equatorward of the hemispheric mean positions of the circumpolar low pressure trough. In summer the peak frequency is found at $62.5°S$ (Taljaard, 1967). The individual areas where high frequencies of cyclones are found are generally the same in all seasons:

- $60-70°S,\ 20-35°E$
- $60-65°S,\ 65-85°E$ (not evident in spring/autumn)
- $65-70°S,\ 70-85°W$
- $65-75°S,\ 30-50°W$

The areal distribution of cyclones over our area of interest shows a spiral arm of high frequency (it is best defined in austral winter), that stretches from subtropical South America to the Antarctic sector of the Indian Ocean. The frequencies are lower and the positions different during the transitional and summer months compared to the winter months (Taljaard, 1967, 1972). Seasonality in the number of cyclones was also found by Simmonds and Keay (2000). The maximum number of cyclones occur in winter with the minimum in summer. The second greatest frequency of cyclones occurs in the belt $10 - 30°S$. The same seasonality in the number of systems is found in this belt (Simmonds and Keay, 2000).

Cyclones are more intense in winter than in summer. The most intense systems are found immediately off the Antarctic coast, particularly in the Indian Ocean sector. The deepest systems occur at about $60°S$, well to the north of the circumpolar trough and in the region of greatest cyclone density. The mean depths of the systems are greater in winter and the axis of the greatest depth shifts south in winter. The largest systems (measured by their mean radius), occur near $60°S$ (Simmonds and Keay, 2000).

Cyclones move on average in an east-southeasterly direction (Taljaard, 1967). Their mean track lenght is 2315 km in winter and 1946 km in summer while individual systems travel in excess of 5000 km (Simmonds and Keay, 2000). The track intersects the latitude circles with an angle of $20 - 30°$. Towards the circumpolar trough, there is a tendency for the angle of intersection to increase where the mature and occluded systems slow down. Some centers that cross the mean position of the circumpolar trough recurve and move westwards, or enter Antarctica. Other systems continue their movement along the circumpolar trough in an easterly direction (Taljaard, 1967).

There are a few regions where cyclones frequently move east or even east-northeast. The extreme southwestern part of the Atlantic Ocean is such a region. After the cyclones cross Patagonia, the Drake Passage or the Antarctic Peninsula, they change course to east or east-northeast at first and then they turn sharply towards Antarctica again in the eastern Atlantic Ocean where they come to rest off the coast of Queen Maud Land between $0\ and\ 40°E$. About half of the cyclones that cross Patagonia, the Drake Passage or the Antarctic Peninsula have a northern component in their movement. The reason for this is probably because of the steering upper winds that have southerly components in that area (Taljaard, 1967, 1972).

2.4.2 Atlantic- and Indian high pressure systems

The belt of high pressure in the southern hemisphere is situated between $23°S$ and $43°S$. The core of the belt (subtropical ridge) is mostly situated nearer to the equator. On average, it is located a few degrees equatorward of the core of the zone with highest anticyclone frequency. It is especially so in the vicinity of the continental west coasts but it also happens in the mid-Atlantic at about $30°W$ during all seasons. The greatest concentration of cells exists in the

Atlantic Ocean between 0° and $15°W$ and in the Indian Ocean between 90°and $105°E$ (Taljaard, 1967,1972).

The speed of the high pressure cells in the high pressure belt vary in different areas. This has the consequence that the frequency of high pressure cells differs along the length of the high pressure belt. Generally, the systems are slow-moving in the eastern parts of the oceans or more specific $20 - 40°$off the continental west coasts. The frequencies are therefore higher over these areas as compared to where the systems advance more rapidly. Over the latter areas, the frequencies are low. Between $45°S$ and the Antarctic coast the frequency of anticyclones is near zero over the Indian Ocean and the eastern part of the Atlantic Ocean. The anticyclones that do occur here is usually of moderate intensity and short lived. Moderate numbers of anticyclones occur over the southwestern part of the Atlantic Ocean. The distribution is quite variable from month to month and season to season. An area where a belt of fairly frequent anticyclones are found extends from West Antarctica across the Weddell Sea to the southwestern part of the Atlantic Ocean. It fades out at about $25°W$. Anticyclones that follow this track (or a track more northerly) manage to break through the westerlies about once a month to reach the subtropics. Another factor that influence the frequency distribution of anticyclones is the preferred regions where old cells dissipate and where new cells form. The most obvious area (also referred to as 'graveyard') of anticyclones are found off the continental west coasts. The high pressure cells become quasi-stationary here and weaken while it retreats northward into the trade-wind belts. Simultaneously, younger and stronger cells take over from the southwest. These areas are referred to as 'cradles'. In our study area, such an area is found off the South African south and east coasts. Anticyclones of polar origin are very rare over the southern ocean (Taljaard, 1967,1972).

The strongest anticyclones (1030-1040 hPa) are most numerous about 4° poleward of the cores of highest frequency and quite far south of the subtropical ridge. The strongest systems in winter occur about 10° south of the average ridge axis. Two kinds of strong anticyclones occurs poleward of $40°S$. Firstly, cold systems which form in intensifying ridges consisting of surges of cold air in the rear of the last members of cyclone families and secondly, warm blocking systems which intensify as they extend to higher latitudes from the subtropical ridge (Taljaard, 1967,1972).

The most marked breaks in the belt of high anticyclonic frequency are found over the continental west coasts and the regions west and south of these coasts. High pressure cells in the high pressure belt over the Atlantic Ocean that nears South Africa mostly extend elongated ridges eastward over the southern parts of South Africa or over the sea south of land. The ridges are usually formed 5° off the coast in summer and over the southern part of the country in winter. New closed cells appear in the forward part of the ridge. This new cell is a few hundred kilometers east or southeast from the original cell of high pressure. This process is referred to as 'budding' in our forecasting jargon. The original cell of high pressure retreats then westwards and northwards (Taljaard, 1967).

On average, anticyclones move eastward with a weak equatorward component. New systems have the tendency to develop south of the main high pressure system belt and to dissipate north of this belt. One of three such areas in the Southern Hemisphere where new systems develop is off the southwest coast of South Africa. The latter is the only area that falls in the area of the study (Taljaard, 1967). The mean speed of anticyclones is greatest about 10° south of the subtropical ridge. The cells further equatorwards are slow moving (Taljaard, 1967).

A striking feature that occurs in all seasons, are the crowding of anticyclone tracks in a narrow zone in the Indian Ocean, approximately from $30°E$ to $90°E$. It rarely happens that anticyclones move from the Antarctic across the middle latitudes to the subtropics. A moderate number of systems move from West Antarctica into the Weddell Sea. It then moves in a northeasterly direction across the southwestern Atlantic but they seldom reach subtropical latitudes before dissipating (Taljaard, 1967).

2.4.3 Mean 500 hPa cyclone characteristics

Upper-level systems are also significant determinants of weather and climate. When these systems become displaced out of the main westerly flow of the mid-latitudes, they can become cut-off lows or cut-off/blocking highs (Keable et al., 2002). These systems are very important individual systems, although they do not occur on a regular basis over South Africa. Cut-off lows are systems with a high potential of good rainfall over a wide area (Taljaard, 1985). Blocking highs can obstruct the progression of weather systems and have therefore a significant effect on regional weather (Keable et al., 2002). It is such a system that contributed to the extensive rainfall during the February 1988 floods (Lindesay and Jury, 1991).

The behavior and characteristics of 500 hPa cyclones have been studied on a regular basis mostly since the IGY. The observational network increased significantly during the IGY and was then for the first time adequate for the analysis of 500 hPa maps over the continents and immediate surroundings, but it was still deficient over the extensive ocean areas. However, Taljaard and van Loon (1960) developed a method to extrapolate the 500 hPa circulation from the surface maps. Approximately 40 years after this pioneering work of Taljaard and van Loon (1960) a study, based on the same dataset that was utilized in the construction of a synoptic climatology of surface cyclones (Simmonds and Keay, 2000), was done by Keable et al. (2002) to determine the behavior of 500 hPa cyclones. According to Keable et al. (2002), this data set is superior to what previous researchers have had access to.

Over the ocean, most 500 hPa cyclones occur close to the latitude of the surface circumpolar trough during all seasons. The maxima of Antarctic continental system density occur between the Weddell Sea and the South Pole and over Queen Maud Land. In summer this last maximum appears just off the coast. In the subtropics, the most systems occur in the southern Mozambique Channel in al seasons (Keable et al., 2002).

Favoured areas of 500 hPa cyclogenesis are very similar to the areas where maximum system density is found, namely between the Weddell Sea and the South Pole and over Queen Maud Land. As with the maximum system density, the favoured area of cyclogenesis appears just off the coast of Queen Maud Land in summer. Other areas where cyclogenesis takes place regularly are just to the east of the southern tip of South America and in the southern Mozambique Channel (particularly in summer). The Antarctic continental systems show quasi-stationary behaviour since cyclolytic activity coincides closely with those of system density and cyclogenesis. The systems in the Mozambique Channel are also quasi-stationary. This may be associated with the interaction of the high Madagascan topography and the tropical easterlies. Cyclogenesis exceeds cyclolysis in the midlatitude oceanic regions north of about $60°S$ as well as over the Antarctic Peninsula and Weddell Sea regions. The opposite is true for an approximately $10°$latitude belt surrounding the Antarctic coast. Over most of Antarctica, cyclogenesis exceeds cyclolysis, indicating that many of the cyclones that form here are exported out (Keable et al., 2002).

The most intense systems occupy a zonally orientated band that is approximately $10 - 15°$wide and centred on about $50° - 60°S$ in summer and futher southward at about $60° - 70°$ in winter. The mean radius of systems in summer and winter also exhibits a zonally orientated band. A difference to that of the intensity of the systems, is that the axis of maximum radius appears to move slightly northward in winter rather than southward. Also, the maxima of the cyclone radii decrease in winter, whereas the maxima in intensity increase in winter. Generally, maximum system depth occurs where both the mean intensity and radius of the systems are large. It is noteworthy to mention that there is a system depth maximum in the east central Indian Ocean at about $50°S$ all year round (Keable et a., 2002).

The maximum average speed of over 14 ms^{-1} is attained by systems at about $50°S$ in the western and central Indian Ocean all year round (Keable et al., 2002). This belt is also the one of greatest mobility at the surface (Jones and Simmonds, 1993). In the latitudes $20 - 40°S$, the average speeds of movement vary considerably during the different seasons. There is generally not a great deal of seasonal variation evident in the mid-to-high latitudes. Greater seasonality is apparent equatorward of $40°S$. A movement of systems is on average in a slightly north of due east direction, particularly in the eastern Atlantic and Indian Oceans (Keable et al., 2002).

2.5 Weather systems over southern Africa

2.5.1 Introduction

Sunny skies and very little or no rain prevails more than 70% of the time over the interior of South Africa, even in summer (Taljaard, 1995a). From the previous section we can recall that South Africa is most of the time under the influence of anticyclonic flow. This results generally in sunny skies and moderate to high temperatures at the surface. When there is a deviation in this mean flow pattern, a wide variety of weather can be experienced. This can range from heatwave conditions to extreme rainfall events. Deviations in the flow from the mean, results in different weather systems to occur over the subcontinent. Most weather systems are characteristic to a specific season but can occur all year round (except for tropical weather systems that are nearly without exception seasonally dependent). In this section, the characteristic weather systems of South Africa are discussed.

2.5.2 Troughs and lows over the land

Surface lows and troughs are discussed in this section. Most lows over the land are shallow systems. Their central height are approximately 10-30 hPa lower than over the surrounding areas. The most common of these lows are heat lows and topographic lee lows (see section 2.5.11). Heat lows occur frequently in summer over the highground of central Namibia as well as over the central interior of South Africa. Other lows found over the land that are generally shallow, are the lows along cold fronts, or also referred to as frontal waves. They are infrequent and occur only once or twice each July. These lows are usually confined to the eastern half of the plateau and tend to develop when one branch of an eastward moving high pressure system takes shape along the east coast while the other branch trails behind over the plateau. A kind of low that occurs over the land but that is not shallow, is the low that is associated with cut-off lows. These lows are an extension of the low in the upper air. Less than half of the mid-winter cut-off lows which affect South Africa are reflected by closed lows on land (Taljaard, 1995a).

Troughs occur on a daily basis over South Africa during the summer. The trough axis is mostly found in variable positions over the central interior but occurs on the west coast from time to time as well as over the far northeastern part of the country. The trough moves to the west coast when a strong high is situated over the eastern part of the country. It is under these conditions that berg wind conditions develop along the west coast. When the trough is situated over the far northeastern part of the country (this is not the topographically induced trough as discussed in section 2.5.11), it is usually in the form of a frontal trough or as a manifestation of a strong upper air system.

Cloud development is favored eastward of the trough axis. The air in circulation is more moist over the latter areas as compared to west of the trough axis, especially during periods when this trough is connected to the Botswana trough (see section 2.3.1) which aids in transporting moist tropical air southwards. In extreme cases, this trough is connected to a tropical low. The latter system normally forms over Namibia or Botswana (see section 2.5.9).

2.5.3 Ridges and anticyclones over the land

The semi-permanent ridge over the northeastern part of the country steers moist air from Mozambique westward in over the eastern parts of South Africa, east of the surface trough. However, on a daily basis the weather associated with high pressure systems over South Africa can vary significantly. Surface high pressure systems that ridge along the south -and east coasts advects cool, moist air in over the country to variable degrees that depend on their strength. This type of system is discussed in section 2.5.5. When preceded by cold fronts, surface high pressure systems are associated with cold, dry air. Strong cold fronts are accompanied by strong anticyclones in their wake. When an anticyclone is associated with below (above) normal temperatures in the lowest 2-3 km, it is referred to as a cold (warm) high. Cold highs are the anticyclones that follow in the wake of cold fronts. Warm highs develop when anticyclones form over land when cold air has not been introduced over the land for a couple of days or when an anticyclone that followed a cold front becomes stationary over the land for at least three days. Subsidence and surface heating takes then place under cloudless skies during the day (Taljaard, 1995a). Heatwaves develop under these conditions.

Anticyclonic circulation in the mid -and upper levels of the troposphere over the country are usually associated with stable conditions and sunny skies. However, in summer it is not always the case. Cloud development can then take place around the periphery of the high pressure system. This usually happens around the southeastern and eastern periphery. This periphery usually co-incides with the highground areas of the eastern part of the country which aid in the development of convective clouds, so that isolated thunderstorms may occur over these highground areas. Rainfall from this circulation pattern is very limited. However, there are cases where mid-level anticyclones play an important role in the occurrence of extensive rainfall events over southern Africa. Here the position of the anticyclone is of fundamental importance (Taljaard, 1995a; 1996). At 700 hPa, the anticyclone should be centred over the east coast, or further to the east. Even the 500 hPa anticyclone should preferably be located east of

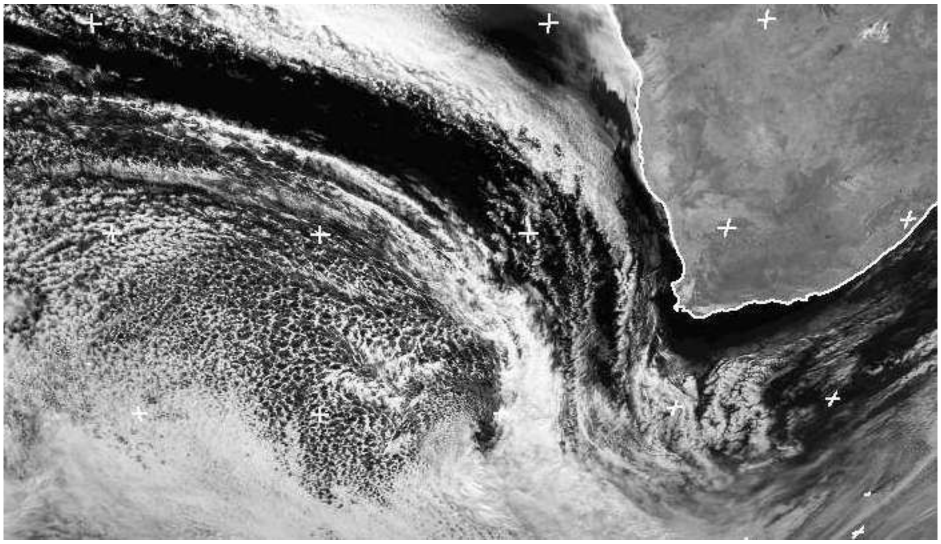

Figure 2.6: A cold front approaching South Africa seen on a MSG (channel 2) satellite image on 13 August 2006 at 1200Z (Copyright Eumetsat @ 2006)

the central plateau. In such a case a northerly air current is generated on the western periphery of the high, which aids with the transport of tropical air into South Africa. Often the transport of moisture is of sufficient depth to produce significant rainfall events (Taljaard, 1995a).

2.5.4 Cold fronts

Cold fronts (see figure 2.6) are important determinants of the weather and climate of southern Africa, particularly southern South Africa where they are the primary contributor to rainfall. They occur together with westerly waves, depressions, or cut-off lows (see section 2.5.6) and are mostly a winter feature when the amplitude of westerly disturbances is greatest (Preston-Whyte and Tyson, 1988). Cold fronts vary in intensity, shape, speed of propogation and the tracks followed (Taljaard, 1995a). The weather associated with fronts vary therefore as well - from slight cooling and light rain along the southern coastal belt to extreme cold conditions and rain that moves in over the interior, as well as snow over the mountainous regions. The Cape south coast is known as being very windy because of the passage of frontal systems.

Cold fronts enter South Africa from the west or southwest once to twice per week and sweep over the southern part of the country in winter (Taljaard, 1995a), whilst they are fewer and less well defined in summer (Taljaard, 1972). They are aligned northwest to southeast and they advance eastward with a northern component over the plateau. The cyclone associated with the front occur mostly south of $40°S$, but when it is intense, it can produce severe weather over the coastal belts. Occasionally systems develop closer the the land or even east of the land at $30-35°S$. Lows seldom develop as waves on cold fronts over the land, but when they do they are almost always weak. A diffluent flow pattern at 300 hPa over the central and northern parts of the land is a frequent phenomenon associated with cold fronts over southwestern Cape (Taljaard, 1995a).

When a cold front approaches South Africa and it is within 5 to 10 degrees of longitude off the west coast, the pressure gradient increases close to the front and over the western part of the country where northwesterly winds dominate. A ridge is usually present over the far northeastern part of the country. A broad current of relatively warm air flows southwards between the ridge and the cold front. A pseudo-front (also referred to as the leader front) forms sometimes over the western interior. This leader front forms when cool sub-inversion maritime air along the west coast deepens ahead of an approaching cold front and spills over on to the plateau where the much warmer continental air is normally present. The main front is usually 300-400 km away when the leader front becomes evident over the southwestern part of the land. Drizzle and rain occurs usually ahead of the main front and is enhanced over the mountainous areas. In cases of strong systems, heavy rainfall occurs over the mountainous areas. The leader front becomes less sharply defined as it moves eastward over the plateau. It becomes more difficult to disinguish between the main and the leader front as they advance eastward and northward so that only a broad transitional zone can be identified after the leading edge of the cold air has advanced about 1000 km from the west coast. A band of mid-level cloud forms characteristically over the land ahead of and above the leader front. This cloud band move from northwest to southeast and can produce light showers over the southern and eastern parts of the country (Taljaard, 1995a, 1972).

After the cold front moves in over the southwestern part of the country, the rainfall distribution pattern stays very similar to when the front was situated just off the coast. However, there is a decrease in the mean rainfall. The rainfall is mostly confined to the escarpment areas. To the east of the escarpment, a sharp decrease is found in the rainfall amounts, except in the case of a strong system. The winds back now to westerly and the rain becomes showery. The precipitation is now of a convective nature due to the deepening of an unstable cold air layer. A wind shift, from northerly to westerly, is also associated with the movement of the coastal low that precedes the cold front. Berg wind conditions develop usually ahead of the cold front and coastal low in the descending northerly flow (Taljaard, 1995a).

As the cold front moves eastward, the rain spread along the south coast and the adjacent interior. Some showers can occur over the central and eastern interior far ahead of the cold front due to convective development or the formation of thick mid-level cloud. This development is the result of warmer, more moist air that flows southwards ahead of the cold front and is then forced to rise against the colder, more dense air. The upper-air trough that usually accompanies frontal systems over the land aid in the upliftment of the air (Taljaard, 1995a).

With the eastward movement of cold fronts over the land, high pressure systems ridge in behind it and advects cold, dry air in over the country. Subsidence sets in behind the cold fronts, so that dry adiabatic warming of the subsiding air and absorption of solar radiation at the surface under clear skies during the day raises the temperature at the surface back to normal within a day or two and often to well above normal within three to four days. The onset of northerly flow also adds to the rising temperature (Taljaard, 1995a).

The degree to which a cold front advance over the country is dependent on the pressure gradient between the frontal trough and the high pressure system following it. Only a few cold fronts manage to advance across South Africa and they do so only when a deep low pressure system develop close to the east of the land and is followed by moderate to strong high pressure systems over the western and central parts of the country (Taljaard, 1995a). For cold air to reach Zimbabwe, a cut-off low system or a high amplitude upper-air trough must be present over the east coast or in the Mozambique Channel in order to establish the necessary pressure gradient that will drive the cold air northward (Taljaard, 1995b).

2.5.5 Ridging high pressure systems

Ridging high pressure systems occur along the South African coast in summer and winter but is more characterstic of summer (Taljaard, 1996) since cold fronts dominate the winter circulation. Taljaard (1995a) described the ridging process of an anticyclone around the South African coast during summer and winter. In summer, the first stage is characterized by the Atlantic subtropical anticyclone that extends a ridge eastwards to the west coast and high pressure that dominates over the western and central part of South Africa. Relatively cool and dry air is advected by the high pressure system in over the southwestern and western part of the country. Humid tropical air usually persists over the northeastern part of the country until it is replaced by cooler maritime air from the east and southeast when the advancing anticyclone or ridge reaches the east coast. The dry air spread occasionally to the northeastern part of the country.

The second stage of the ridging anticyclone in summer is characterised by the high pressure system that moves eastwards to be situated south of the country. The wind remains southwesterly along the southeast and east coasts but after the highest pressure passes by it rapidly backs to southeast, east and finally northeast. The wind along the Western Cape coast is easterly to southeasterly during this stage. A coastal low usually develops on the west coast, south of

Walvis Bay, and migrates southwards with time. The pressure normally falls rapidly along the south and southeast coasts until the coastal pressure minimum passes by. This is followed by southwesterly to southerly winds, rising pressure, significant cooling and cloudiness. The cooler air and cloudiness spreads inland but are bounded by the main escarpment that is situated 200-300 km from the coast. Occasionally the cloud moves across the escarpment. What happens next during the ridging process is an important event for South African rainfall. Before the cooler, stable air reaches the northeastern part of the country as the high pressure system continues to move east -and northwards along the coast, there is a westward movement of warm, humid tropical air from KwaZulu-Natal and Mozambique over the northeastern part of the country. This happens as soon as the lowest pressure has passed by, but before the cold air reaches these areas. This process is referred to as ’undercutting’ - the warm air is undercut by the invading cooler air. The amount of rainfall during these events is dependent on the humidity and temperature of the air over KwaZulu-Natal and Mozambique that moves westwards.

The third stage of an eastward-moving high pressure system in summer is reached when it is situated just east of the country at sea level, a ridge is present at 850 hPa over the northeastern part of the country and an upper ridge exists above the east coast. With the pressure being lower over the central and western part of the country, a broad current of tropical air starts to flow southwards. The expected rainfall depends much on the humidity of this air mass. The humidity of the air mass can be quite low at first due to the usual preceding influx of dry air from the west and south. Rainfall is also limted when the cool, stable air moves to far inland or when the flow pattern becomes anti-cyclonic over the eastern part of the country. When a cold front approaches the land while the high pressure system is receding, an inverted V-trough forms on 850 hPa. The axis of this trough is usually somewhere over the central interior stretching to the south or southeast coast. Here it is located a short distance to the rear of the coastal pressure minimum.

The main difference between summer and winter ridging anticyclones, is that the anticyclones is separated by cold frontal troughs in winter. The track of these high pressure systems is also more northwards in winter, so that they advance eastward across or immediately south of the land. In a typical frequent sequence of events of a ridging anticyclone in winter, the high pressure cell in the Atlantic Ocean extends a ridge eastward behind the cold front, while the main cell of high pressure stays west of the land. On 850 hPa, a ridge becomes visible over the western part of the Northern Cape, shortly after the cold front enters the country. The pressure rises sharply along the southern coast in the wake of the cold front. The ridge that extends eastwards is mostly centred overland or just off the coast. The characteristic feature of this type of ridging is the coastwise ridge over KwaZulu-Natal that stretches to Mpumalanga, as well as a remnant high over the eastern part of the Northern Cape, instead of

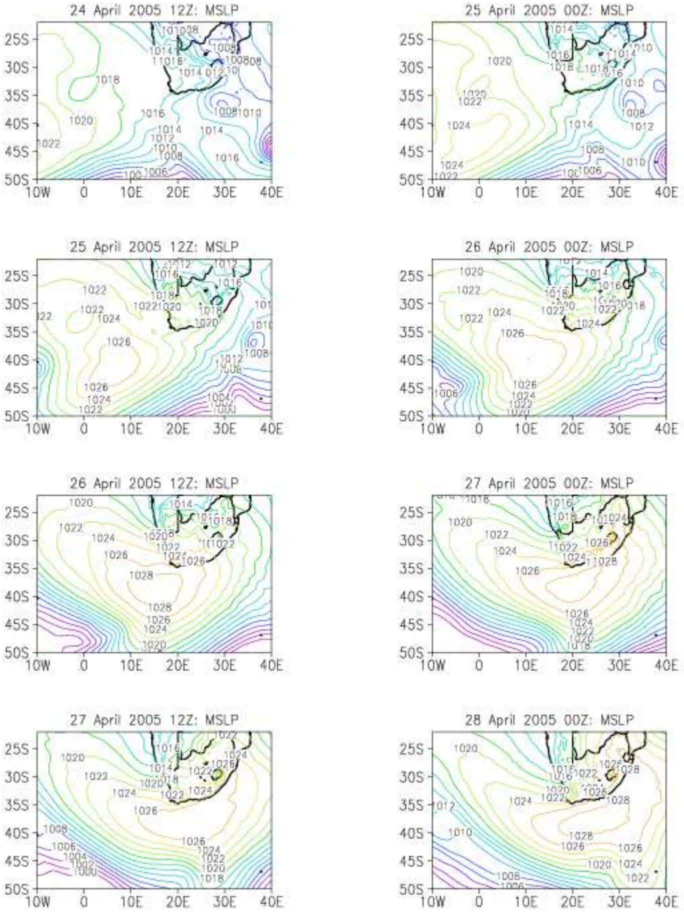
24 April 2005 12Z: MSLP

25 April 2005 00Z: MSLP

25 April 2005 12Z: MSLP

26 April 2005 00Z: MSLP

26 April 2005 12Z: MSLP

27 April 2005 00Z: MSLP

27 April 2005 12Z: MSLP

28 April 2005 00Z: MSLP

Figure 2.7: C-CAM prognosis of a high pressure system migrating eastwards south of the land.

the main high that occupies the plateau. This pattern occurs when the pressure rise along the south and east coasts is particularly strong. During the last stage of this sequence of events the pressure distribution is back to normal with only one centre of high pressure which is situated over the northeastern part of the country, linked to the Indian Ocean high east of the land (Taljaard, 1995a).

Types of ridging processes that occur less frequently are found when the anticyclone migrates eastwards south of the land. This type of ridging event is illustrated by the C-CAM prognosis displayed in figure 2.7 (note that the set-up of the C-CAM model over southern Africa is discussed in chapter 3). The track that the high pressure system follows is south of it's most common course. When the anticyclone is moving eastwards while it is close to the coast, an anticyclone forms over the southern interior and tracks eastward (south of it's usual course as well) in association with the maritime anticyclone. By the end of this ridging process, these anticyclones is found east of the land in the Indian Ocean while ridges are extended westward over the eastern part of the country (Taljaard, 1995a).

A related type of ridging process that occurs even more infrequently is when the anticyclone that moves eastward south of the land, is situated significantly southward of it's usual position (also see figure 2.7). Typically, the centre of such a high pressure system is approximately at $40°S$. This type of ridging is characteristically accompanied by a cut-off low (Taljaard, 1995a).

2.5.6 Westerly waves and cut-off lows

The circulation over southern Africa is in general anticyclonic (Preston-Whyte and Tyson, 1988). However, this anticyclonic circulation is regularly interrupted by upper-air westerly waves of varying amplitude, wavelenghts and wind speeds. They are characteristically asymmetric. Westerly waves have a greater influence on the upper level flow in winter as the westerly belt is situated more northwards during this season. The result of this is that the general anticyclonic circulation is replaced by almost due westerlies at high levels in winter (Taljaard, 1995a).

Westerly waves contribute to the destabilization of the atmosphere and therefore aid in the development of thunderstorms during summer and frontal cloudbands in winter. In winter cold fronts precede the upper trough axis by 5 to 10 degrees of longitude. This indicates that the systems are baroclinic (Taljaard, 1995a). High amplitude troughs in summer is sometimes associated with the development of squall lines.

A cut-off low system (figure 2.8) is an intense form of an upper air westerly wave trough. It is defined as a cold low which has become displaced out of the basic westerly current and lies equatorward of this current. It starts as a trough in the upper westerlies, deepens into a closed circulation and extends downwards to the surface (Preston-Whyte and Tyson, 1988). Based on data for a 10 year period (1973-1982), the frequency of cut-off low systems that have a lifespan of more than 2 days over and in the immediate vicinity of South Africa is 11 per year. They occur mostly in autumn (March to May and spring (August to October) (Taljaard, 1985). When short and long-lived cut-off low systems are considered, their average lifespan is approximately 3 days. When cut-off low systems that last for at least 2.5 days are considered, their average lifespan increases to 4 days (Taljaard, 1985).

Cut-off lows generally cause widespread, moderate rain over South Africa. For these systems that do not induce heavy falls of rain, the rainfall caused is indistinguishable from the rainfall associated with westerly wave troughs (Taljaard,

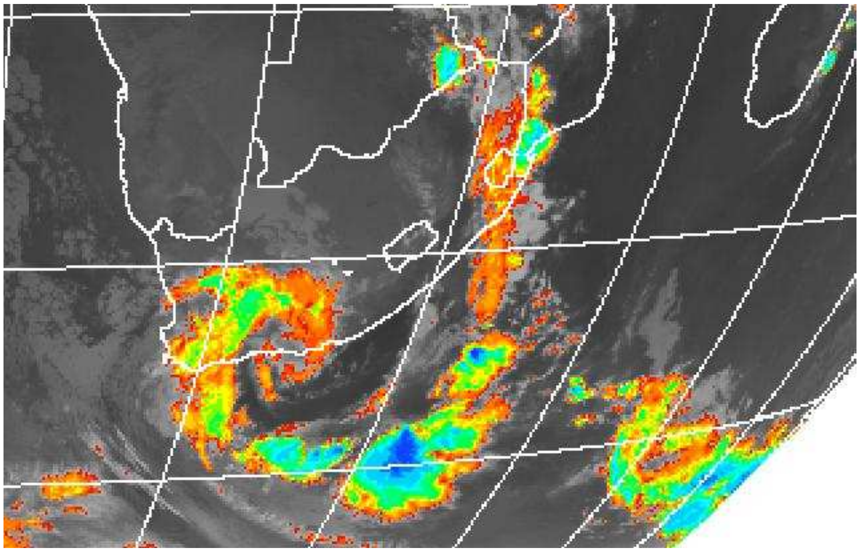

Figure 2.8: A Meteosat 7 infrared image of a cut-off low system captured on 24 March 2003 at 0600Z (Copyright Eumetsat @ 2006)

1985). About 20% of cut-off lows produce heavy rainfall over South Africa, in particular over the southern and eastern coastal belts (Taljaard, 1985). Heavy rainfall typically occurs when the system is still baroclinic and when a surface low is present some hundreds of kilometers east of the upper low (Taljaard, 1995a). It may also be noterd that cut-off lows are most of the time responsible for rain during winter over the summer rainfall area (Taljaard, 1995a).

The Laingsburg flood (Estie, 1981) is one of the most well-known rainfall events over southern Africa caused by a cut-off low system. Another cut-off low system that caused memorable floods occurred on 1 September 1968 at Port Elizabeth (Hayward and van den Berg, 1968). More recently, a cut-off low system that has lead to an extreme rainfall event occurred on 22 December 2004 over the southern coastal belt. From Mossel Bay eastwards along the coast to approximately Port Alfred, heavy rain occurred in isolated places. Some roads that link coastal towns had to be closed. A cut-off low system that has lead to a major flood and snow event occurred between 1-3 August 2006. The Cape south coast experienced one of the most extensive floods in years, while snowfalls occurred as far north over the country as Gauteng.

The typical synoptic sequence associated with the development, maturity and decay of cut-off low systems has been described by Taljaard (1985). He investigated just more than a hundred cut-off low cases, and identified five stages during the life cycle of a typical cut-off low system.

In the first stage a moderate upper air trough is situated just west of southern Africa with the high-level winds (300 hPa) all slightly north of westerly over South Africa. Over the ocean two surface systems are of importance. Firstly, a stronger than normal high pressure system is typically situated southwest of the country, more or less located near Gough Island and with its latitudinal position being 5-10 degrees south of its mean position. Secondly, a cold front is typically nearing Cape Town. Over the land a trough or closed low is indicated over the western part of the plateau by the 850 hPa contours. Relatively warm, moist air flows from the north over the central and eastern parts. Along the coast pressures falls significantly ahead of the cold front and rise to its rear. Light to moderate falls can occur along the south coast as onshore flow commences in the wake of the cold front.

The second stage is characterized by the intensification of the upper air trough. Over the western part of the country the upper-level winds back to southwesterly while the winds become northwesterly elsewhere. At the surface the Atlantic high pressure system advances east-south-eastwards through about 10 degrees of longitude and cold air is advected in over the southwestern part of the country. The trough or closed low on 850 hPa shifts north -and eastwards while warm air advection continues to its east. Moderate to heavy rain can occur along the south and the east coastal belts in the stronger onshore flow. Falls might exceed 40 mm just east of the 850 hPa trough (roughly 1000 km ahead of the 300 hPa trough axis).

A closed low in the higher levels is for the first time present at the third stage. Fresh to strong west-northwesterly to northwesterly winds occur over the northern areas of the country while southeasterly to northeasterly winds occur south of the centre of the cut-off low. At sea-level the high pressure system may extend a ridge further eastwards, or it can propagate eastwards along $40°S$. The cold air advances over most of the country. Exceptions are the extreme northeastern areas and the area east of the 850 hPa trough, where warm air advection takes place over the Free State areas extending northwestwards towards Namibia. It is in this area where cool air eventually undercuts the warmer, moister air comining from the north, that the best rainfall occurs. Along the coast further rainfall is unlikely because the onshore flow or undercutting has ceased. Rising pressures can still occur over most areas, but mainly southeast of the land. A next cold front appears near Gough Island. The advancement of this front toward South Africa leads to the eastward retreat of the cut-off low over South Africa during the next two to three days.

The forth stage appears not very different from the previous stage at first glance but the upper air ridge has advanced far to the east. This is also relfected at sea-level where a closed high pressure cell is situated just east of the land. The centre of the cut-off low system tends to be slow moving during this stage, especially if the surface high is strong or intensifying. The cold front southwest of the land is still making its way to South Africa.

The last stage of the lifecycle of a cut-off low system characterizes the collapse of it, which is often sudden. During this stage, falling pressure occurs south and close east to the land. The next cold front is still approaching from the southwest and the upper warm anitcyclone south of the land has weakened to a ridge. As the cut-off low is moving out over the southeast coast there is often a weak onshore flow to the rear of the surface coastal low that is associated with the cut-off low. Light rain may still fall along this coastal strip in the weak onshore flow.

2.5.7 Coastal lows

A coastal low is a small area of relatively lower pressure which appears in the lower levels of the atmosphere, below 700 hPa, along the coast (CLW, 1984). The pressure gradient is directed from the land towards the coast and the associated wind therefore as well. They occur all year round and propagate around the southern African coast from the west coast, south of about $28°S$, southwards and then eastwards towards the KwaZulu-Natal coast where it usually fills up. Coastal lows north of about $28°S$, can remain stationary for many days and can even propagate northwards. The reason for this can be the orientation of the coastline. North of about $28°S$, the Namibian coast is aligned almost due north-south, whereas it is aligned more or less northwest to southeast south of about $28°S$. South of the Orange River the southward movement of coastal lows are induced by the falling pressures further south due to nearing westerly troughs. There is a tendency for coastal lows to weaken in the vicinity of St Helena Bay and to reform along the south coast in the vicinity of Mossel Bay. The systems often intensify along the south coast as they advance eastward but occasionaly they weaken and stop moving eastward. They can also redevelop further to the west (Taljaard, 1995c).

The formation of coastal lows is a two-fold process. Firstly, the primary cause is considered to be the adiabatic warming of the air as it descends from the interior plateau to the lower lying areas at sea level. The increase in the temperature of the air at sea level leads to a density change of the air. This results then in the creation of lower pressure that takes the form of a coastal low. The other mechanism that contributes to coastal low formation is based on the conservation of potential vorticity. Cyclonic vorticity is generated on the lee side of the escarpment areas where the air parcel decelerates and its depth increases. The cyclonic vorticity fosters the development of an area of lower pressure (Taljaard, 1995c).

Different types of coastal lows are found along or close to the coast. The first type of coastal low is where the pressure is higher off the coast than along the

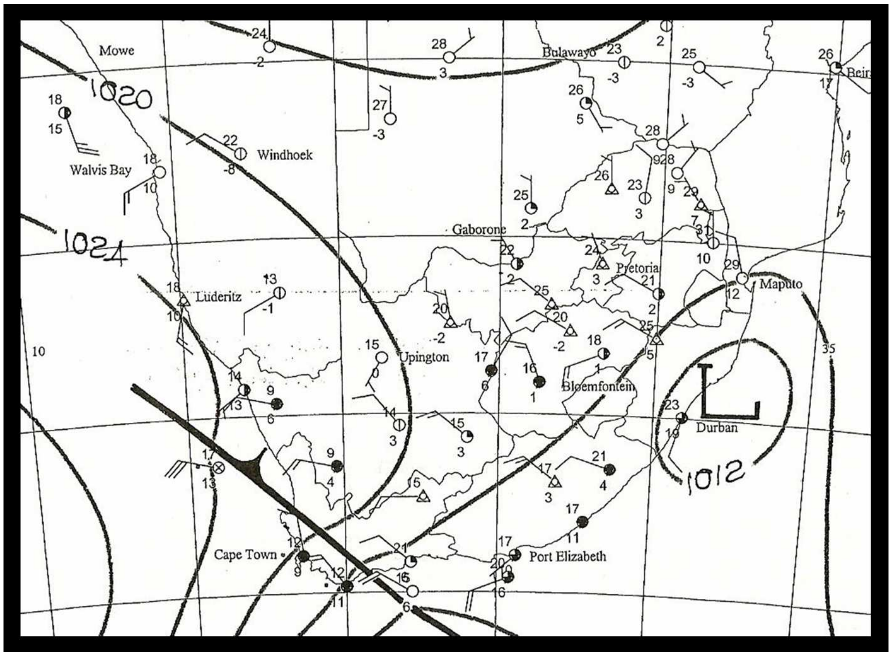

Figure 2.9: A coastal low preceding a cold front by a few hundred kilometers along the east coast on 21 July 2006 (from the Daily Weather Bulletin, South African Weather Systems).

coast. This coastal low along the west coast mostly falls in this category. It also occurs just south of the land when a high pressure belt induces dominant easterly winds. When a pressure minimum develops in such a case, the isobars are cyclonically curved over the adjacent ocean. The second type of coastal low (see figure 2.9) is the most common type of coastal low along the south and southeast coast in summer and almost the only type of coastal low along these coasts in winter. It is associated with approaching cold fronts and with some troughs between anticyclones when they advance eastwards at the latitude of the south coast. These coastal lows precede cold fronts by several hundred kilometers and they occur where a northwesterly wind blows from the plateau (Taljaard, 1995c). Most coastal lows on the Cape South Coast extend beyond 100 km offshore (Hunter, 1987). A third kind of coastal low occurs in association with cut-off low systems (Taljaard, 1995c).

Seasonality is found in the behavior of coastal lows. They are usually weak along the Namibian coast in winter and they are located further to the north compared to summer. The consequence of this is that only a few systems that develops north of Walvis Bay move southwards during winter (Taljaard, 1995c).

Apart from the wind shift (north/northeasterly to southwesterly) that accompanies the passage of a coastal low, the weather can otherwise vary significantly. This is to a certain extent dependent on the location of the coastal low as well as the season. For example, berg winds typically occur from March to September. They occur along the coastal belts of Namibia, the Cape Provinces, KwaZulu-Natal and even southern Mozambique (Taljaard, 1995c). Hot and windy weather precedes the coastal low in berg wind conditions. As the coastal low passes, cool air is advected in along the coast and adjacent interior. Shallow low-level clouds can form depending on the moisture content of the air that is moving in along the coast after the passage of the coastal low. During summer time, a coastal low can aid in thunderstorm formation along the southeast -and east coast and their immediate interior. Along the west coast, coastal lows are often associated with fog. When a deep coastal low (approximately 1000 hPa) is followed by a strong high pressure system along the east coast, a good chance exists for what is known as the 'southwesterly buster'. This is a very strong wind from the southwest that has a very rapid onset.

2.5.8 Tropical-temperate troughs

The dominant summer rainfall-producing system on the synoptic scale over southern Africa is the tropical-temperate trough (Harrison, 1984; Washington and Todd, 1999; Todd et al., 2004). It is the most important late-summer rainfall-producing system in particular and is characterized by a trough linking an area of convection over tropical or subtropical southern Africa with a mid-latitude depression to the south of the subcontinent (Harangozo and Harrison, 1983; Harrison, 1984). Approximately 39% of the mean annual rainfall could be attributed to this link (Crimp et al., 1997). A distinctive meridional cloudband marks the position of the tropical-temperate trough along the leading edge of the upper westerly wave that occurs with the system, and indicates the effective organization of convection in a northwest to southeast aligned zone across central southern Africa (Harrison, 1984). Cloudbands that form a continuous link between the tropical and temperate circulations are also observed in the central-western Pacific and over South America (Harangozo and Harrison, 1983). The formation of tropical-temperate links over these areas are semi-permanent, whereas the tropical-temperate links over southern Africa exists only during the austral summer months (Todd et al., 2004). The frequency of band formation appears to be roughly constant and independent of the rainfall but marked variations in the location of the bands are observed between wet and dry months (Harrison, 1984).

The importance of these systems was realized as early as 1970, when Johnson described a type of system which forms a long cloudband that is oriented NNW-SSE. It stretches from Angola or the Congo to South Africa where it is evidently associated with a frontal trough. This cloudband moves eastward throughout its length, but more rapidly so in the south. It forms along a trough which develops on the west side of an extensive high. This system described by Johnson (1970) is undoubtly the tropical temperature trough. The only difference is that Johnson (1970) stated that it occurs probably more during winter, although it affects southern Africa at all seasons occasionally. This contradicts more modern literature (Harrison, 1984; Lindesay and Jury, 1991) that highlighted it's importance as a late-summer rainfall-producing system. Today, by means of satellite imagery it is known that the tropical temperate trough is a summer feature.

Harangozo and Harrison (1983) investigated the synoptic circulation associated with southern African cloudbands during wet, dry and near-average Januaries. For this study they considered two months that were generally dry over the interior of southern Africa (1969 and 1973), a month with near-average rainfall (1971) and two relatively wet months (1974 and 1976). They located daily cloud band positions by making use of polar orbiting satellite imagery. The surface and upper air synoptic circulations associated with these bands were obtained from charts supplied by the SAWB. In this study, they identified the synoptic circulation pattern that is associated with the formation of summer cloudbands and determined how it varies during wet and dry periods. They found that tropical lows, subtropical troughs and temperate wave disturbances are the synoptic circulation patterns which are frequently associated with cloudbands over southern Africa (figure 2.10). Tropical lows, cold fronts near the subconintent and westerly waves over the land were associated with all the observed cloudbands during the five months they studied. During the wet months the tropical lows were most frequently situated over the central-western subcontinent, while they

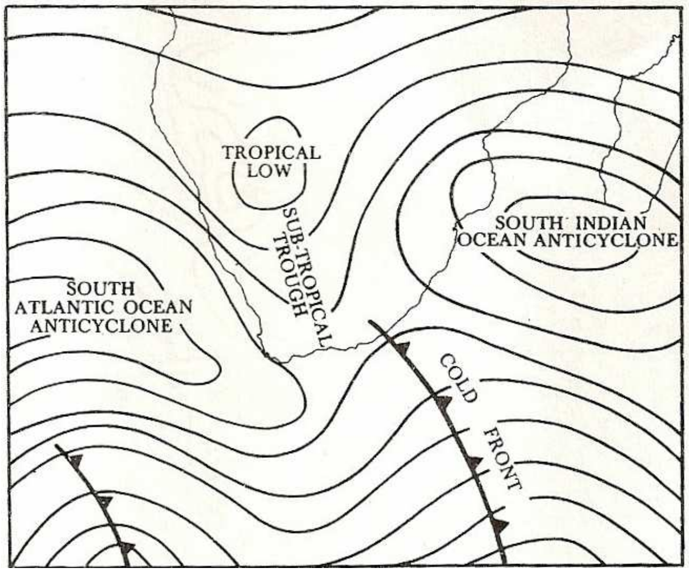

Figure 2.10: The synoptic circulations associated with cloudband formation over southern Africa (from Harangozo and Harrison, 1983).

were situated over the eastern subcontinent during the three drier months. The position of the low is also displaced northwards during the drier months, from $20°S$ to $15°S$ between the wet and dry months respectively. The frequency of cold fronts and westerly waves changed little during the months under investigation. It may be noted that Jury and Pathack (1993) found that the tropical low locates over southeast Angola or soutwest Zambia and forms preferentially during the period December to March at the furthest southwestern limit of the ITCZ.

The subtropical troughs often co-incide spatially with cloudbands. These troughs are indicated as low pressure troughs on the surface charts. No changes in the overall frequency or locations of the subtropical troughs were observed between the wet and dry months. In studies by Taljaard (1953) and Rubin (1956) it appears that deepening of the trough co-incides with periods of heavier rains. The trough is in general associated with a well-defined boundary that seperates moist air from dry air to the west. Thunderstorms develop within a 300 km zone extending eastwards from the moisture-boundary. This region is therefore a zone of surface convergence (Taljaard, 1959). The position of the trough is a good indicater of the western boundary of the cloudband (Harrison, 1984).

Although cloudbands were in all cases associated with tropical lows, cold fronts and westerly waves during this study period, the opposite were not true. Cloudbands failed to appear over the subcontinent on numerous occasions when both tropical lows and cold fronts were present. Surface synoptic circulations are therefore unreliable guides to the presence of cloudbands (Harangozo and Harrison, 1983). Streten (1973) indicated that the cloudbands appear to form uniquely on the leading edges of cyclone wave troughs. This happens when a tropical low that is situated over central Africa extends throughout much of the troposphere (Harangozo and Harrison, 1983). The days when cloudbands failed to develop were most frequent in the three drier months. A clear area were then present between the tropical and temperate cloud masses. On this basis, Harangozo and Harrison (1983) then proposed that a necessary condition for cloudband formation is the coupling of tropical lows with westerly waves. Given that the frequency of tropical lows and westerly waves varied little and that westerly waves were situated over South Africa during the study months, the position of tropical lows between wet and dry months may also be important in explaining cloudband development. It is noteworthy to mention that Taljaard (1996) questioned that the cloudbands regularly stretch directly southwards from tropical lows along the inter-ocean convergence zone/inter-tropical convergence zone.

Satellite imagery reveals two basic forms taken by the bands (Harrison, 1984). The band can terminate at the southern coast at a coastal disturbance or the band can connect to the temperate cyclone completely (Harrison, 1984) as seen on the satellite image of 17 January 2006 1800Z (figure 2.11). It happens frequently that the form where the band terminates at a coastal disturbance precedes the form where the connection to the temperate cyclone is complete (Harrison, 1984a). The spatial rainfall distributions produced by the bands are very similar (Harrison, 1984).

The water vapour transport associated with tropical-temperate troughs has been investigated by Todd et al. (2004) for the months of November to February. Daily satellite rainfall estimates, together with NCEP reanalysis data are used in their study. They found that tropical-temperate trough rain bands are zones of pronounced water vapour convergence. These convergence zones extend from equatorial southern Africa to the midlatitudes. The tropical-temperate trough transports water vapour that converges over equatorial southern Africa poleward, through a coupling of cyclonic circulation to the west and by an anticyclonic circulation to the east of the tropical-temperate trough axis. The maximum poleward transport occurs along the leading easternmost edge of the temperate disturbance. The latter was also found by Harrison (1986). The circulation pattern associated with such an event is characterised by an anomalously strong Indian Ocean high, displaced eastward from its mean position, and a cyclonic circulation over the continent. The cyclonic circulation is situated where the midlatitude transient links with the continental low.

There is a seasonal difference in the nature of tropical-temperate trough events and the associated water vapour transport fields. The water vapour circulation

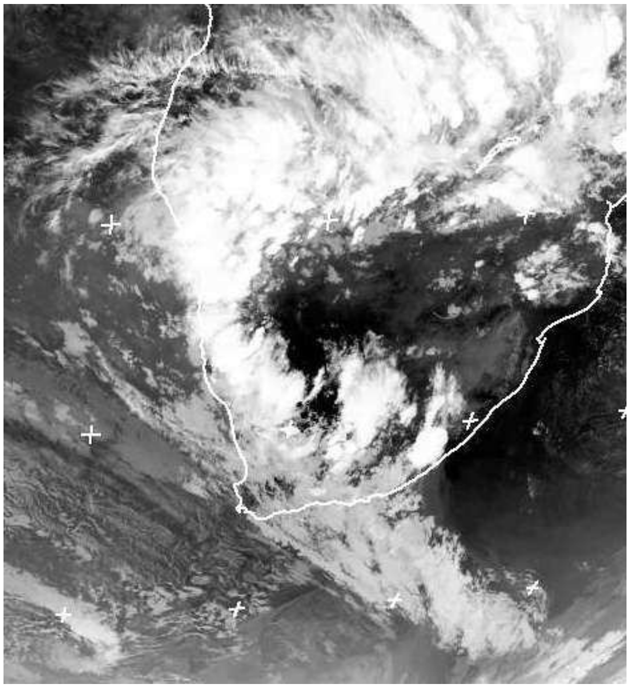

Figure 2.11: A cloudband associated with a tropical-temperate trough is seen over the western part of South Africa on this Meteosat Second Generation infrared satellite image (channel 9), captured on 17 January 2006 1800Z (Copyright Eumetsat @ 2006)

differ from the early to the late summer. The role of tropical circulation in late summer is greater than in early summer when the midlatitude circulation dominates. Tropical-temperate trough events during the late summer months tend to have a preferential location over the southwest Indian Ocean (SWIO) associated with the eastward progression of the Indian Ocean high over the summer season as well as increased thermal forcing of an upper-level westerly wave over southern Africa (Todd et al., 2004). The leading edge of this upper-level westerly wave lies over Madagascar in high summer (Harrison, 1986).

During early summer (November and December) and January (late summer) the poleward water vapour flux over southern Africa is driven by three main paths of anomalous water vapour flux, whilst February is characterized by moisture fluxes that originate mostly from only two regions. The first moisture source in early summer and January, that contributes to the poleward water vapour flux, is a northerly flux from the northern Indian Ocean which is linked to a zonal easterly flux. In early summer, this easterly flux is between $120°E$ and $45°E$ centred on $5°N$. Secondly, a westerly flux from the western part of southern Africa centred on $10°S$ brings moisture to the tropical-temperate trough in early summer and January. Thirdly, the moisture flux in the cyclonic flow around the tropical-temperate trough aids in the poleward water vapour flux over southern Africa. There are two main differences between the January and early summer moisture flux patterns. Firstly, in January the easterly water vapour flux is situated more southward than in early summer (centred on $15°S$ compared to $5°N$ in November). Secondly, the water vapour flux over the western part of southern Africa is stronger in January than in early summer. The consequence of this is that moisture convergence occurs further to the east in January. During the late summer two characteristic water vapour flux patterns are found. The first pattern is associated with January and correspond to a certain extent with the early summer pattern. The second pattern is associated with February. During February, the rain band lies further to the west than in January. The water vapour flux anomalies are similar to other months, except that the anomalous moisture flux into the tropical-temperate trough region emerges largely from only two regions, namely the Indian Ocean and the southern part of tropical Africa. Anomalous moisture divergence occurs over the Congo Basin centred on $25°E$, $5°S$ (Todd et al., 2004).

A case study illustrating many of the above mentioned concepts are described by Lindesay and Jury (1991). During February 1988 a major flood-producing tropical-temperate trough occurred over South Africa. During this event the cirulation pattern was characterized by the poleward displacement of the mid-latitude westerlies, a well developed high pressure anomaly over the SWIO and Mozambique Channel, a southward shift in the ITC, and anomalously strong near-surface easterlies in the trade wind belt which resulted in strong inflow of maritime air over the east coast of southern Africa. Moisture inflow during this period was mostly from the Congo Basin and over the east coast between

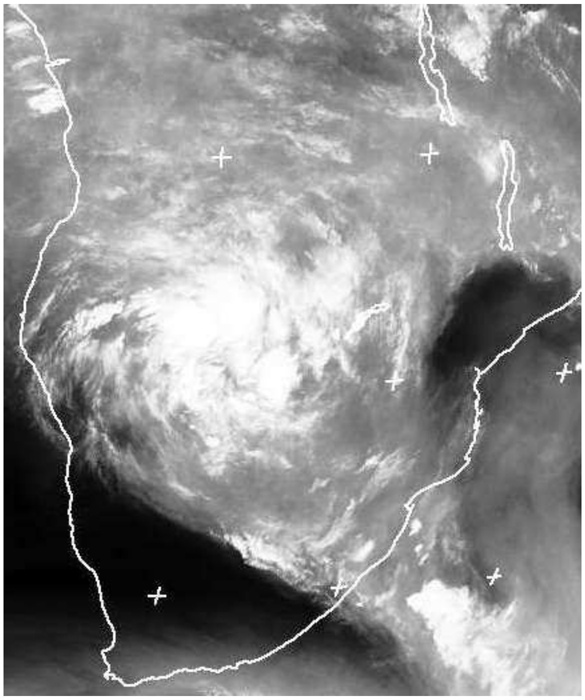

Figure 2.12: A Meteosat Second Generationh water vapor image (channel 5) of a tropical low over southern Africa on 21 February 2006 at 0600Z (copyright Eumetsat @ 2006)

$15-20°S$ from the southwest Indian Ocean. This enhanced moist easterly flow is steered around an anticyclone over the Mozambique Channel across the east coast of southern Africa. Strong subsidence occurred on either side of the tropical-temperate trough. This served to focus the inflow of moisture into the system and contributed to the intensity of the rainfall (Lindesay and Jury, 1991).

2.5.9 Tropical lows and easterly waves

Tropical easterly circulation affects rainfall variability at least over the northern parts of South Africa (Taljaard, 1994; Tyson, 1984). Disturbances in the tropical easterly flow occurring around the northern sector of subtropical anitcyclones take the form of easterly waves and lows (Preston-Whyte and Tyson, 1988). They are barotropic systems and are almost exclusively a summer phenomenon and are usually associated with the inter-tropical convergence zone (ITCZ). Warm, humid easterly winds occur between the ITCZ and the subtropical high pressure belt. A well-defined moisture boundary are therefore easily detected in association with these systems. Warm, moist air occurs northeast ot it while dry air occurs to the southwest. Low-level convergence occurs to the east of these systems. Thunderstorms develop in the convergence zone extending about 200-300 km northeastward of the moisture discontinuity (Preston-Whyte and Tyson, 1988). The low-level convergence results in strong uplift which may sustain rainfall in the absence of pronounced instability. When the air is sufficiently unstable good rains occurring in rainy spells of a few days duration, may occur over wide areas. Winds with a northerly component are associated with these events. To the west of these systems, subsidence and consequently clear skies occur. Divergence are associated with these systems at higher levels of the troposphere. In the case of a tropical low, the divergence occurs at higher levels compared to an easterly wave. (Preston-Whyte and Tyson, 1988).

Easterly waves have been observed in the southwest Indian Ocean (Okoola, 1989) and may affect the east coast of Africa (Lindesay and Jury, 1991). Unlike easterly waves found over the Sahel, the tropical North Atlantic Ocean and Caribbean Sea, easterly waves over southern Africa are semi-stationary (Preston-Whyte and Tyson., 1988). For easterly waves to develop, increasing easterly flow must be present through the troposphere (Riehl, 1954). This condition is seldom met over the southwest Indian Ocean (Padya, 1984) because of the intrusion of westerly flow at upper levels (Lindesay and Jury, 1991). Therefore, easterly waves over the southwest Indian Ocean may only appear in summers when the upper westerlies are situated further poleward. Easterly wave pertubations with wavelengths of approximately 2500 km move westward toward the African east coast, whereafter their propogation speed decrease (Lindesay and Jury, 1991). If the ridge in the Mozambique Channel is present, the easterly wave pertubations are steered in over the continent. They can track as far west as $20°E$ where the Inter Tropical Convergence (ITC) is typically at maximum intensity. Waves that become stationary can supply moist convective energy to the atmosphere further south (Lindesay and Jury, 1991). In the absence of the ridge, the easterly wave pertubations follow a southerly track over Madagascar and the Mozambique Channel (Harrison, 1984).

Tropical lows can affect the weather on the South African plateau to $25°S$, or even $30°S$ (Taljaard, 1995a). According to the synoptic climatology that was constructed by Taljaard (1995b), the centre of the low can usually be located over Botswana or Namibia. A trough extends from the tropical low southwards across the North Cape or the Free State. The skies are usually mostly overcast in the vicinity of the tropical low, the temperature below normal and the air humid (Taljaard, 1995a). Over South Africa the cloudiness is highest over the eastern parts of the country. Tropical lows are associated with the most widespread and occasionally heavy rain in South Africa (Taljaard, 1995b). It has been recognized that it is largely the occurrence of rains associated with tropical lows which distinguish abnormally wet years from dry years (Preston-Whyte and Tyson, 1988).

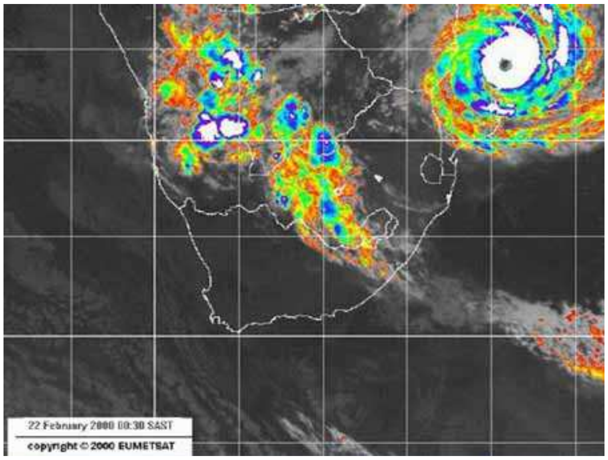

Figure 2.13: A Meteosat 7 false colour image of Tropical Cyclone Eline making landfall just south of Beira on 22 February 2000 at 00:30 SAST.

The centre of the tropical low tends to deepen to 700 hPa but disappears above 500 hPa to be replaced by a ridge or anticyclonic circulation in the upper troposphere (Taljaard, 1995b). Characteristic features of tropical lows are anticyclonic circulation above the low and below normal temperatures in the lower third of the troposphere. These below normal temperatures strengthen the surface low to the 700 or 600 hPa level. Above the low, the saturated adiabatic lapse rate causes upper-tropospheric temperatures to be above normal. Therefore, anticyclonic circulation sets in above about 300 hPa around the central cyclonic gyre. The release of latent heat over the areas where it is raining is responsible for the reversal of the circulation in the lower and upper troposphere. The upper level anticyclone provides the necessary upper divergence to aid in maintaining the system (Taljaard, 1995a). Satellite imagery show typical cloud distributions associated with the uplift to the east of the easterly lows and the clear air resulting from the subsidence over western areas (Preston-Whyte and Tyson, 1988).

2.5.10 Tropical Cyclones

Tropical cyclones are warm cored, intense vortical storms that develop over the tropical oceans in regions of very warm surface water (Holton, 1992). They form in summer and early autumn with the most cyclones occurring in January or February (Preston-Whyte and Tyson, 1988). There are usually between six and twelve storms observed over the southwest Indian Ocean in a year (Preston-Whyte and Tyson, 1988). These storms last for several days and are associated with very high rainfall. Extreme rainfall is not the only danger posed by tropical cyclones. The destructively strong winds and the huge waves that are produced by these storms are characteristic of mature tropical cyclones. The centre of the storm is characterized by the eye (figure 2.13) which is 30-50 km in diameter (Preston-Whyte and Tyson, 1988). The eye is a region of subsidence of warm, dry air and are therefore often cloud-free. Around the eye there are up to 200 cumulonimbus towers within and around the storm (Preston-Whyte and Tyson, 1988). A very striking feature of tropical cyclones are the anticyclonically spiraling high-level cloud.

Tropical cyclones have typically radial scales of several hundred kilometers, similar to those of midlatitude synoptic systems. But the horizontal scale of the region of intense convection and strong winds in a tropical cyclone is typically only about 100 km in radius. Therefore, tropical cyclones are classified as mesoscale systems (Holton, 1992).

The formation of tropical cyclones is still not completely understood and remains therefore a matter of uncertainty (Holton, 1992; Preston-Whyte and Tyson, 1988). What is known, is that it almost always appears that tropical cyclones develop from pre-existing disturbances (Preston-Whyte and Tyson, 1988), however it rarely happens that a tropical cyclone develops from the many tropical disturbances that form each year (Holton, 1992). Tropical cyclones need an extensive ocean area where the sea surface temperature is in excess of $27°C$ to develop. This is one of a number of conditions that are necessary, but not necessarily sufficient, for their formation. Another factor that plays a vital role in tropical cyclone formation is weak wind shear in the mid -and upper troposphere. Upper-level anticyclonic divergence is needed to produce high-level outflow which in turn allows the development of very low pressure and high winds near the surface. For the maintenance of tropical cyclones low-level supply of heat and moisture combined with a low frictional drag at the surface are needed as well as the massive release of latent heat through condensation and the eviction of air aloft. When one of these factors cease, the storm will start to decay rapidly (Preston-Whyte and Tyson, 1988). This typically happens when the storm moves in over land or enters an ocean area where the sea surface temperatures are to low to provide enough moisture that fuels the storm. There is of course the very special cases, such as in 2000, when tropical cyclone Eline (figure 2.13), degraded to a tropical low when it entered the African continent on it's east coast and moved almost right across Africa to reach Namibia (Reason and Keibel, 2004). On it's way it caused heavy rain and devastating floods.

Tropical cyclones in the Indian Ocean west of $95°E$ develops with little exception in the zone 5-$20°S$. Most of them occur between 10 and $15°S$. Very few cyclones ever develop closer to the equator than $7°S$ (Taljaard, 1972). The formation of tropical cyclones is inhibited where the Coriolis force approach zero (Preston-Whyte and Tyson, 1988). Gray (1967) performed a study based on 70 years data. He investigated tropical cycogenesis in the Indian Ocean. He found that tropical cyclones tend to be located south of the mean position of the inter tropical convergence zone. According to Taljaard (1996), tropical cyclones develop along or close to the inter-tropical convergence zone. Gray (1967) found that that the cyclones develop about 5° closer to the equator in November and April than in midsummer. Cyclones are most frequent in the zone 10-15°S east of 60°E, but west of this longitude the highest frequencies are found in the zone 15-25°S. The cyclones are slow-moving in the Mozambique Channel. They accelerate along 25-30°S after recurvature. Tropical cyclones in this region move predominantly westward while they are north of 20°S. Recurvature occurs anywhere between 15 and 25°S. They usually recurve to the south before reaching the land, often moving south along the Mozambique Channel, but sedom reaching 30°S (Preston-Whyte and Tyson, 1988). Less than 5% of tropical cyclones in the southwest Indian Ocean actually make landfall on the east coast of Africa, and even fewer significantly penetrate into the interior (Reason and Keibel, 2004). Only about 1 out of 10 systems moves south with an eastward component immediately after development (Taljaard, 1972).

The influence of tropical cyclones on southern African weather is extremely contrasting (Taljaard, 1996). When they are centred 500 km or more from the east coast or located in the eastern part of the Mozambique Channel (and particularly when they are slow moving), subsident conditions set in over the subcontinent (Taljaard, 1996) causing dry and hot conditions (Taljaard, 1996; Mason and Jury, 1997). These cloud-free areas are referred to as the 'dumping ground'. When tropical cyclones are within less than 200 km from the coast, southeasterly winds produce cloudy weather and variable amounts of rain, depending on it's distance from the coast. When they reach the coast, or move inland, heavy rainfall occurs over the coastal belt up to the escarpment (Taljaard, 1996). The last tropical cyclone that added significantly to South Africa's rainfall was Eline in 2000 (Dyson and van Heerden, 2001; Reason and Keibel, 2004).

2.5.11 Topographically induced weather systems

Meso-scale weather systems or circulation patterns that develop as a result of the influence of topography on flow occur frequently over South Africa. Mountain waves develop in regions where the wind flow is approximately perpendicular to the mountains, where the wind strength is sufficient and increase with altitude and where a stable layer is present above the mountain crests. These conditions occur usually in association with cold fronts in winter. Mountain waves occur most of the time over the mountains of the Western Cape, the Eastern Cape, Lesotho and occasionally the Asbes mountains in the Norhtern Cape.

Topographically induced troughs develop sometimes during the summer over the northeastern interior when a surface high pressure system ridges east or south of the eastern escarpment regions (Taljaard, 1996). When low-level moisture is present, this topographically induced area of low pressure may aid in triggering convective cloud development due to it being a low-level moisture convergence zone. However, these kind of troughs are generally not significant (Taljaard, 1995a). During the winter when relatively high pressure occurs over the plateau side of the main escarpment, a trough or even a shallow low develops to the lee of the escarpment (Taljaard, 1996).

When weak synoptic flow exists over the country, the first convective cloud development occurs usually in the mountainous regions such as the Witwatersrand, the eastern highground and Lesotho. The trigger for this development is the local mountain circulation that develops due to differential heating of the surface. If sufficient moisture and instability is available, thunderstorm development follows.

Chapter 3

The C-CAM forecasting system

3.1 Introduction

Short-range weather forecasts produced by C-CAM are verified in this study. This AGCM has been developed at CSIRO Marine and Atmospheric Research, Australia. C-CAM is formulated on a quasi-uniform grid, derived by projecting the panels of a cube to the surface of the Earth (Rancic et al., 1996; McGregor, 2005a). The model has the capability to run in variable resolution stretched-grid mode to provide high resoltion over the area of interest. In the latter case the model may run in conjunction with another simulation, by using sea-surface temperatures and far-field nudging of winds provided by the host model (McGregor and Dix, 2001). This approach of dynamic downscaling is highly flexible compared to the traditional limited-area modelling approach. It also avoids one of the main problems associated with limited-area models, namely reflections at the lateral boundaries (McGregor and Dix, 2001, 2006). C-CAM is a 2-time-level semi-implicit semi-Lagrangian hydrostatic model. The C-CAM dynamics, numerics and physical parameterization schemes are discussed by McGregor (2005a), McGregor and Dix (2001, 2006) and in section 3.2.

C-CAM has mostly been used to perform multi-year simulations of regional climate. These include simulations of present-day climate over various domains, with SSTs and far-field winds provided by NCEP reanalysis. Climate change simulations have also been carried out, with forcing provided by the CSIRO Mk3 OAGCM (e.g. Engelbrecht, 2005). It has also been used for short-range weather-forecasting and to model the global transport of trace gases.

The highly efficient semi-Lagrangian semi-implicit numerical integration scheme of C-CAM makes it possible to run the model operationally at high resolution on a fast PC. C-CAM became operational at UP on the 1st of December 2004, running in variable resolution mode with the highest resolution over southern Africa. During the course of the forecasting project described in this study, it was initialized once a day with the 0000Z Global Forecasting System (GFS) analysis field and produced a four day forecast. The design of the C-CAM forecasting system over southern Africa is discussed in more detail in section 3.3.

In order to produce operational weather forecasts, the model data is needed in a graphical format. In the operational environment, forecasting is a man-machine mix. Every forecaster has his/her favourite parameters used in formulating a forecast, but there are certain basic fields that all forecasters utilize during the forecasting process. A number of GrADS scripts were developed in order to facilitate the daily operational use of C-CAM. GrADS software is freely available on the internet (http://grads.iges.org/grads/downloads.html) and is widely used by the atmospheric research community. Some of additional variables calculated in the forecasting scripts are discussed in section 3.4.

3.2 Characteristics of C-CAM

C-CAM is formulated on a quasi-uniform grid, derived by projecting the panels of a cube onto the surface of the Earth. The conformal-cubic grid was devised on these panels by Rancic et al. (1996), and is isotropic except at the eight singular vortices themselves (McGregor and Dix, 2006). The model has the capability to run in variable resolution stretched-grid mode to provide high resolution over the area of interest. Compared to the more traditional nested limited-area modelling approach, C-CAM provides great flexibility for dynamic downscaling from any global model, essentially requiring only sea-surface temperatures and far-field winds from the host model. It also avoids other problems that may occur with limited-area models, such as reflections at lateral boundaries (McGregor and Dix, 2001, 2006).

Distinctive features of the C-CAM dynamics as applied in the present study are (McGregor, 2005a; McGregor and Dix, 2001, 2006):

- 2-time-level semi-implicit time-differencing of the hydrostatic primitive equations
- semi-Lagrangian horizontal advection with bi-cubic horizontal interpolation (McGregor, 1993, 1996)
- total-variation-diminishing vertical advection
- unstaggered grid, with winds transformed reversibly to/from C-staggered locations before/after gravity wave calculations to provide improved dispersion characteristics (McGregor, 2005b)
- deformation-based horizontal diffusion

- Cartesian representation used for the calculation of departure points, and also for the advection or diffusion of vector quantities
- time-differencing is made weakly implicit by off-centering (Rivest et al., 1994) in order to avoid "semi-Lagrangian mountain resonances" near steep orography for large Courant numbers
- careful treatment of surface pressure near terrain
- global a posteriori conservation for mass and moisture

The model includes the following physical parameterizations (McGregor and Dix, 2001, 2006):

- new mas-flux cumulus convection scheme, including evaporative downdrafts (McGregor, 2003)
- diurnally varying GFDL parameterization for long-wave and short-wave radiation (Fels and Schwarzkopf, 1975; Schwarzkopf and Fels, 1991)
- interactive diagnosed cloud distributions
- gravity wave drag scheme of Chouinard et al. (1986)
- stability-dependent boundary layer scheme based on Monin Obukhov similarity theory (McGregor et al., 1993) and non-local vertical mixing (Holtslag and Boville, 1993)
- paramaterization to enhance sea-surface temperatures under conditions of low wind speed and large downward solar radiation, for the purpose of calculating surface fluxes
- soil/canopy scheme described by Gordon et al. (2002), having six layers for soil temperatures, six layers for soil moisture using Richard's equation and three layers for snow

3.3 Design of the forecasting experiments

3.3.1 General design, spatial resolution, stretching factor and time step

In order to obtain the high-resolution operational forecasts described in the study, C-CAM ran in variable resolution stretched-grid mode over southern Africa. The model ran in stand-alone mode, that is, no far field wind nudging was supplied from a host simulation. A C100 horizontal resolution was used, that is, each of the six panels has 100 x 100 grid points. The Schmidt stretching factor (Schmidt, 1977) was 0.3, which implies a horizontal resolution of approximately 15 km on the panel of highest resolution, and approximately 200 km on the panel at the opposite side of the cube. The model was integrated with 18 sigma levels in the vertical, the lowest level being located approximately 30 m above the surface.

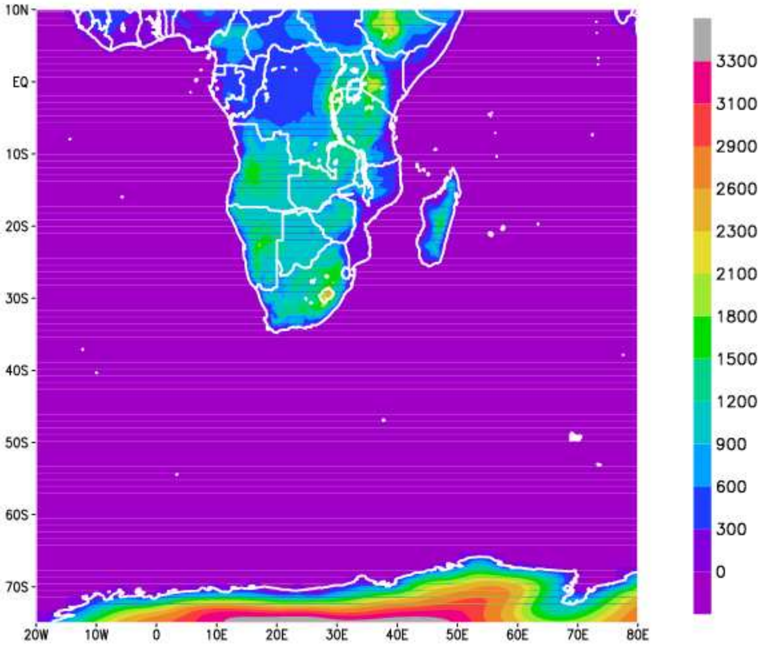

Figure 3.1: C-CAM output domain at 0.3° horizontal resolution with shaded topography.

The model integrations were performed on a PC with a 2000 MHz CPU and 512 MRam. Using an integration time step of 5 min, a four-day model simulation at C100 resolution took 8.5 hours to complete on this computing system. It may be noted that during the first trail runs performed during November 2004, a time step of 15 minutes was used. The forecast fields turned out to be noisy. The 5 min time step that was used during the remainder of the project is more suitable for the high-resolution stretched grid simulations performed. During the trail runs, C-CAM produced an eight day forecast. However, because of time constraints of the operational environment, and a lack of data storage facilities, it was decided to produce only a four day forecast after each initialization during the remainder of the project.

3.3.2 Output domain and model topography

During the forecasting project model output was written to two domains: At 0.3° horizontal resolution over a domain covering 75° S to 10° N and 20° W to 80° E (figure 3.1), and at 0.15° resolution on a smaller domain covering 36° S to 20° S and 10° E to 36° E (figure 3.2). The model topography interpolated to 0.3° and 0.15° resolution are displayed in the respective figures. Output over the larger domain is needed in order to evaluate the synoptic-scale evolution of

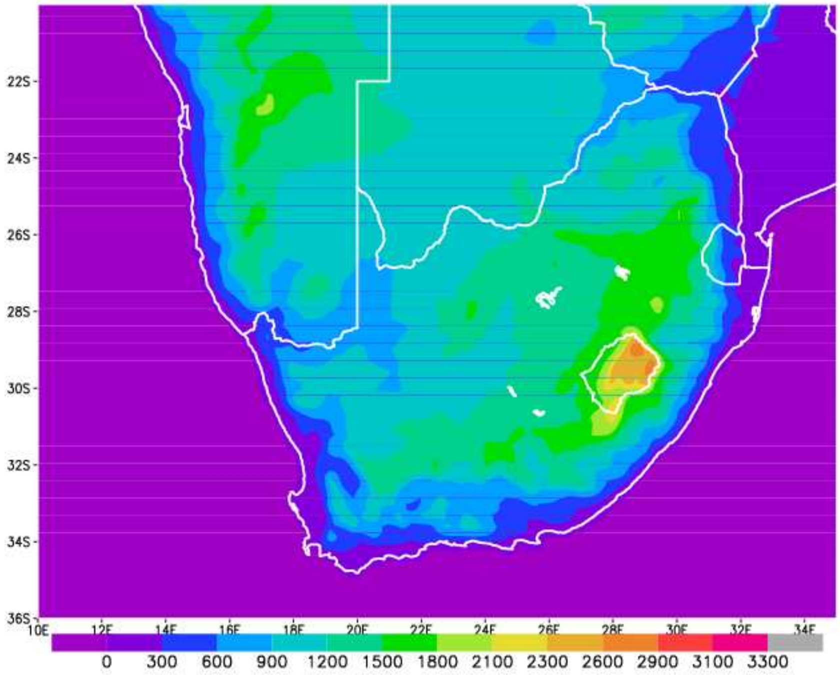

Figure 3.2: C-CAM output domain at 0.15° horizontal resolution with shaded topography.

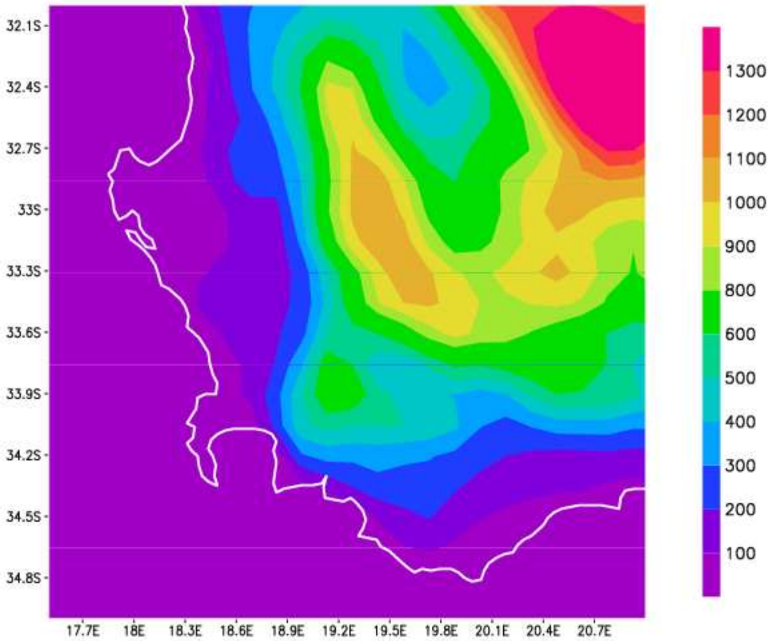

Figure 3.3: Shaded C-CAM topography depicting the southwestern escarpment of South Africa.

weather systems in the C-CAM forecasts, whilst the higher-resolution data over the smaller domain is more useful in verifying the forecasts against obervations made over the subcontinent. The model output were interpolated to selected pressure levels. These levels are 1000 hPa, 950 hPa, 900 hPa, 850 hPa, 800 hPa, 750 hPa, 700 hPa, 600 hPa, 500 hPa, 400 hPa, 300 hPa, 200 hPa and 100 hPa. A range of surface and near-surface variables are also available as standard C-CAM output.

High resolution model topography is required in order to capture the patterns of regional climate and weather over southern Africa in model simulations (Engelbrecht and Rautenbach, 2000). The regions of specific interest in this regard are mountainous areas, which are affected in more than one way. Ridging high pressure systems that move in over a mountainous area may produce extensive cloud development and precipitation, due to the induced topographical lift of the airmass. This process often occurs along the eastern escarpment regions of South Africa. The same process is also important along the southern coastal belt, although here the topographical lift is weaker because the largest component of the moisture flux is aligned parallel to mountain ranges (for maximum topographical lift the ideal wind components must be perpendicular to the mountain ranges). Topographical lift also occurs along the western and southwestern es-

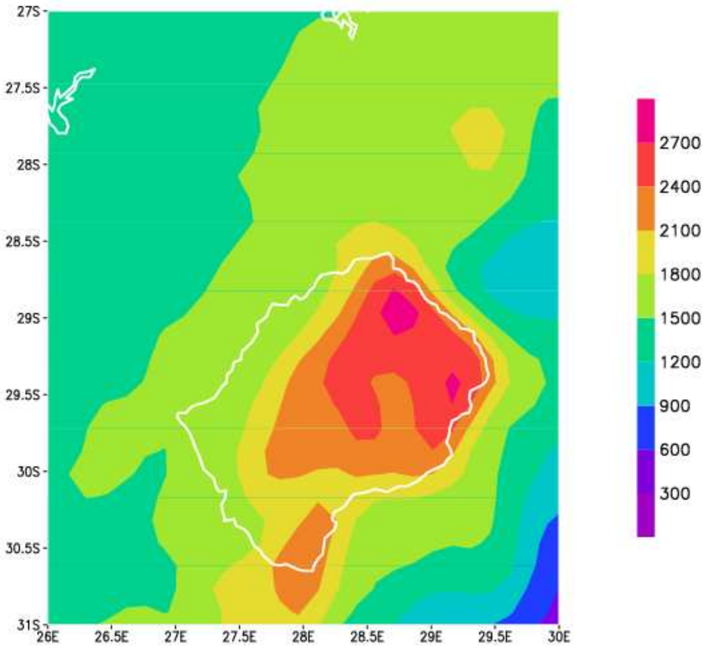

Figure 3.4: Shaded C-CAM topography depicting Lesotho and the adjacent highground.

carpment (figure 3.3) ahead of frontal systems that nears the country. High resolution model topography is required in order to obtain satisfactorily simulations of the topographic-induced rainfall patterns over these regions. High resolution model topography may also contribute to sucessful simulations of heat-driven thunderstorms that often develop over high ground areas in South Africa, such as the Witwatersrand (see Chapter 2, section 2.5.11). The local mountain circulation that develops under weak synoptic flow leads to convective cloud development over these regions.

With an effective resolution of about 15 km over southern Africa, the C-CAM topography field (displayed at 0.15° resolution in figure 3.2) captures many of the features that are characteristic of southern African topography. It can be seen in figure 3.2 that the interior of South Africa is characterized by an elevated plateau, which generally rises from the west to the east. Over the western part of the plateau the altitude is approximately a 1000 m, whilst maximum altitudes in excess of 2700 m occur along the eastern escarpment over Lesotho in the model topography (figure 3.4). Other characteristic topographical features over the interior that are depicted in the model topography include the Waterberg in Limpopo, the Witwatersrand that extends in an east-west direction from the Drakensberg mountain range, the Asbesberg over the Northern Cape and the mountain ranges over the southern interior that forms part of the Great Escarpment (figure 3.2).

The model topography adequately describes the coastal margins along the east and southeast coast of southern Africa, that are narrow and marked by steep topographic gradients with valleys that run into the Great Escarpment (figure 3.2). Two distinct low lying features that extend from the coastal plains into the interior are also present in the model topography. These are the Limpopo valley and the Orange river canyon that are both found along the northern borders of South Africa (figure 3.2).

3.3.3 Initial conditions

The production of high-quality weather forecasts requires the use of a complete and accurate description of the atmosphere's initial state. In this study, the C-CAM forecasts were initialized using the Global Data Assimilation System (GDAS) (Derber et al., 1991). Since the observational network at a given point in time contains large data voids, and the observations, when available, contain errors and may not be representative of a larger-scale region, the global atmospheric state cannot be determined by observations alone. To help overcome this inadequacy in the observational network, data from earlier times are included by the GDAS system through a 6-hour forecast from the previous analysis. Using known error properties of both the observations and the 6-hour forecast, an objective analysis procedure combines the new observations with the 6-hour forecast to produce an estimate of the true atmospheric state. The analysis system used in the GDAS is referred to as Spectral Statistical Interpolation (SSI) (Derber et al., 1991). In this analysis procedure it is not necessary for the analysis variables to be the same as those of the observations. Rather, it is only necessary to be able to calculate observed variables from the analysis variables in order to compare the analysis to the observations. Nonstandard observation types and analysis variables closely related to those used by the forecast model are used easily. The analysis variables in the SSI system are vorticity, divergence, unbalanced heights, and specific humidity, while the input observation variables are wind components, temperature, surface pressure, and specific humidity (Derber et al., 1991).

3.4 Forecasting scripts

GrADS scripts were developed to conveniently display the basic fields that are used during a routine forecasting process. In this section a brief description of these scripts are presented. Most of the scripts function to display a time-animation of a specific atmospheric field. In some cases, it was necessary to first calculate the desired variable before it could be displayed graphically, since it is not part of the standard C-CAM output fields. For these cases, the calculation procedures followed are described in section 3.4.2.

Basic model prognosis fields utilized during the forecasting process include the Mean Sea-Level Pressure (MSLP), the heights of selected pressure levels (usually 850 hPa, 700 hPa, 500 hPa and 300 hPa), moisture fields, vertical velocity and divergence/convergence patterns. By analysing these prognostic fields the synoptic weather pattern and how it's expected evolution may be studied.

3.4.1 Scripts displaying standard output variables of C-CAM

These scripts function to provide animations of the 6-hourly fields of a number of the standard C-CAM output fields. The fields include MSLP, heights of 850 hPa, 700 hPa, 500 hPa and 300 hPa (hereafter referred to as standard levels), winds at the standard levels, temperature at the standard levels, relative humidity at the standard levels, 2 m temperature and mixing ratio.

3.4.2 Scripts displaying derived variables

A number of variables useful in short-range forecasting may be derived from the standard C-CAM output fields. This section describes how some of the derived fields used in the study (see Chapter 5) may be calculated.

3.4.2.1 Equivalent potential temperature

Equivalent potential temperature, designated by θ_e, is the potential temperature that a parcel of air would have if all its moisture were condensed and the resulting latent heat used to warm the parcel (Holton, 1992). It is a useful parameter for studying cumulus convection (Preston-Whyte and Tyson, 1988). Areas where the atmosphere is conditionally stable or unstable are revealed by the vertical profile of the equivalent potential temperature. The atmosphere is conditionally unstable when θ_e decreases with height and conditionally stable when θ^e increases with height. In the presence of sufficient low-level moisture as well as upward vertical motion, convective development takes place when the atmosphere is conditionally unstable.

The θ^e field may be derived from the standard C-CAM output fields. A satisfactory estimate of $\theta^e$is:

$$\theta_e \approx \theta + 3(1000)w, \tag{3.1}$$

where $\theta = T\,(p/p_0)\exp^{R/c_p}$ is the potential temperature; $R = 287\,Jkg^{-1}K^{-1}$ is the gas constant of dry air, $c_p = 1004\,Jkg^{-1}K^{-1}$ is the specific heat at constant pressure and w is the mixing ratio.

In the forecasting script the θ_e difference is calculated between 500 hPa and 700 hPa). Negative values represent areas where the atmosphere is conditionally unstable and positive areas represent areas where the atmosphere is conditionally stable.

3.4.2.2 Moisture Flux Convergence (MFC)

Boundary-layer convergence has proven to be a valuable prognostic tool to forecast thunderstorm initiation (Wilson et al., 1992). In fact, the importance of identifying these low-level convergence zones in initiating has been realized more than 30 years ago (Purdom, 1973). These convergence lines are seen on satellite imagery as lines of cumulus cloud. Since clouds form when there is sufficient moisture available, a useful variable in forecasting and timing the location and timing of convection is the Moisture Flux Convergence (MFC), which may be defined as

$$MFC = -\frac{\partial}{\partial x}\left(\rho q u\right) - \frac{\partial}{\partial y}\left(\rho q v\right). \tag{3.2}$$

Here q is the specific humidity, which may be related to the C-CAM variable mixing ratio by the relationship

$$q = w\left(\frac{m_d}{m_d + m_v}\right). \tag{3.3}$$

3.4.2.3 Bulk shear

There is a relation between the type of storm and the vertical shear of the lower tropospheric environment (Holton, 1992). Vertical wind shear influences the form that the convection might take, i.e., whether the convection evolves as short-lived cells, multicells, or supercells (Weismann and Klemp, 1982; Holton, 1992). In the second case study in chapter 5, the bulk shear (SHR) as documented in Dupilka and Reuter (2006) is calculated in order to determine the nature of the convection, given that convection will occur. Since C-CAM output is written out on pressure levels, the bulk shear was computed using

$$SHR = \frac{\sqrt{(u_2 - u_1)^2 + (v_2 - v_1)^2}}{\mid z_2 - z_1 \mid}.$$

Here z_1 and z_2 denote the heights of the bottom and top of a pressure layer, respectively; $(u_1\,, v_1)$ and $(u_2\,, v_2)$ denote the horizontal wind velocities at levels z_1 and z_2, respectively. The South African terrain varies significantly (see chapter 3), especially over the eastern and southeastern parts of the country. However, over most of the interior the surface pressure values are close to the 850 hPa level. Therefore, the bulk shear was calculated in the layer from 850 hPa to 500 hPa. The geopotential heights at these levels were used in determining the required values of z_1 and z_2.

3.5 Discussion

The computational efficiency of the numerical and physical schemes of C-CAM, in conjunction with using the GFS analysis as initial conditions, facilitates the operational use of C-CAM as a forecasting model using an ordinary PC as computing system. By running the model in variable stetched-grid mode, high resolution was obtained over southern Africa. In fact, the 15 km forecasts described in the study are the highest to ever be performed over the southern Africa region up to date. Another practical advantage of a variable resolution global model in short-range weather forecasting, is that only the set of initial conditions is required to run the model in stand-alone mode. In the case of nested limited-area modelling, lateral boundary conditions from a host model would also be needed at regular time-intervals.

Since the forecasts were not nudged within forecasts from a host model away from the area of interest, an imporant question is whether model errors induced by lower horizontal resolution away from the area of interest, would eventually contaminate the forecasts over southern Africa. This aspect is explored further when the model forecasts are verified in Chapters 4 and 5.

Chapter 4

Objective verification of C-CAM

4.1 Introduction

In order to test quantitatively the ability of C-CAM to forecast atmospheric circulation over southern Africa, several statistical measures are used. Firstly, grid field verification is performed on the C-CAM forecasts of the 500 hPa geopotential height and the vertically integrated moisture flux. This verification is performed on the larger model domain that covers $20°W$ to $80°E$ and $75°S$ to $10°N$, over which the output is available at $0.3°$ horizontal resolution (see chapter 3). The verification is done on a monthly basis, where each 6-hour forecast of all the individual model runs is verified against NCEP reanalysis data (Kalnay et al., 1996). The absolute error, the root mean square error and the pattern correlation are calculated for all the forecast hours (in six-hour intervals) of each model run. The monthly average of these values may then be taken for each of the forecast hours, thereby providing a method of evaluating the growth of the model error in time. It may be noted that the 500 hPa geopotential height is a standard field used in the verification of NWP models over the mid-latitudes of Earth (Bengtson and Hodges, 2006; Elmore et al., 2006). However, in the subtropics and tropics circulation systems are less well defined in terms of geopotential height. Over these regions the wind field, or the moisture flux that is defined in terms of the wind field, are more useful fields to be analysed in the verification process. Over southern Africa, the vertically integrated meridional moisture flux from the tropics plays a crucial role in determining daily weather, seasonality and climate (D' Abreton and Lindesay, 1993). The vertically integrated moisture flux was therefore chosen as a variable to be verified in this study. In addition to the grid field verification, point verification is performed for the 24-hour temperature forecast of C-CAM at selected pressure levels, at one coastal and one interior station. In this case, the high horizontal resolution output at $0.15°$ over the smaller output domain

Station	Pressure levels where temperature verification is performed											
FACT	1000	950	900	850	800	750	700	600	500	400	300	200
FAIR	-	-	-	850	800	750	700	600	500	400	300	200

Table 4.1: Pressure levels at the coastal (FACT) and inland station (FAIR) at which temperature verification was performed

(see chapter 3) is used in the verification process. The model grid point closest to the specific weather station is used for the verification. The observed upper air sounding data at each of the weather stations was obtained from the SAWS.

4.2 Data

As mentioned in chapter 3, C-CAM became operational at UP in December 2004. However, during the following months it happened that some runs were lost, mainly due to insufficient archiving space on the computer where the model was running, power failures and some other logistical challenges. Fortunately, those challenges have been solved and since May 2006 the model has been running smoothly. For this study, the C-CAM data that was generated during 2005 was utilized. For the grid field verification, the C-CAM output written out at 0.3°resolution was utilized while the point verification performed on C-CAM made use of the output written out at 0.15°resolution. A six month period starting January 2005 was chosen to be verified quantitatively. Due to lost model runs, March 2005 and July 2005 did not qualify to be verified since more than a third of the runs were lost. Therefore, the six month period is as follows:

- January 2005
- February 2005
- April 2005
- May 2005
- June 2005
- August 2005

For the grid field verification NCEP reanalysis data was used as the observational data. Due to the scarcity of data over the Southern Ocean, reanalysis fields are the only means of obtaining an accurate depiction of the observed state of the atmosphere. This dataset has a resolution of 2.5°. The domain over which the verification was performed covers 20°W to 80°E and 75°S to 10°N. This is the C-CAM domain where data is written out on a 0.3°grid although the actual resolution is as high as 0.15° over southern Africa.

Point verification was done at two upper-air stations of the SAWS, one coastal station and one interior station. The station at Cape Town International Airport ($33°58'S$, $18°36'E$) was selected as the coastal station and the station at Irene Weather Office ($25°55'S$, $28°13'E$) was selected as the interior station. The 0000Z upper-air ascents of these stations were obtained for the six month period under investigation. The observed temperature at selected pressure levels were obtained from the upper air soundings in order to test C-CAM's 24-hour temperature forecast at these pressure levels. The selected pressure levels differ for the coastal and inland station as seen in table 4.1.

4.3 Methodology

4.3.1 Grid field verification

The horizontal resolution of the NCEP reanalysis data and that of the C-CAM output differs considerably. With the NCEP data having a much coarser resolution of 2.5°, the 0.3° C-CAM data was interpolated to the NCEP grid. For this procedure, a bicubical interpolation scheme was used. The interpolation software was developed by Engelbrecht (2000). However, it had to be expanded upon in order to calculate the different statistical measures after interpolation. An option to calculate 24-hour persistence forecasts and to verify these against the relevant reanalysis fields was also constructed. As mentioned before, the statistical measures included the average absolute error, the root mean square error and the pattern correlation. The monthly average root mean square error and pattern correlation of the NCEP persistence forecasts were also calculated to compare it with the corresponding C-CAM root mean square error and pattern correlation.

4.3.1.1 Average absolute error

The monthly average absolute errors of the 500 hPa geopotential height and vertically integrated moisture flux were calculated over the entire 0.3° grid field for each forecast hour (00-hour forecast to 96-hour forecast at 6-hour intervals) of all the individual model runs. Thus, the result is 17 average absolute error fields for each of the six months that were verified. The absolute error is defined as

$$absolute\,error = \mid f_i - o_i \mid, \tag{4.1}$$

where f_i denotes the C-CAM forecast field and o_i the corresponding NCEP reanalysis value at grid point i.

4.3.1.2 Root mean square error

The root mean square error was also calculated for each forecast hour of all the individual model runs on a monthly basis, and then averaged for each forecast hour over the specific month. The result was 17 root mean square values that represented the average magnitude of the 500 hPa geopotential height error, for each of the 6 months that were verified at each of the 17 forecast hours. The root mean square error, here referred to as RMSE, was calculated as follows:

$$RMSE = \sqrt{\frac{1}{N}\sum_{i=1}^{N}(f_i - o_i)^2} \tag{4.2}$$

where f_i denotes the C-CAM forecast and o_i the corresponding NCEP reanalysis value at grid point i; N is the number of grid points.

4.3.1.3 Pattern correlation

The pattern correlation was, just as the absolute error and the root mean square error, calculated for each forecast hour of all the individual model runs. The monthly average for each forecast hour was then calculated, so that 17 values were obtained that represent the average 500 hPa geopotential height and the vertically integrated moisture flux pattern correlations. This was done for each of the six months studied. The pattern correlation was calculated as follows:

$$Pattern\,correlation = \frac{\sum_{i=1}^{N}(f_i - \bar{f})(o_i - \bar{o})}{\sqrt{\sum_{i=1}^{N}(f_i - \bar{f})^2}\sqrt{\sum_{i=1}^{N}(o_i - \bar{o})^2}}, \tag{4.3}$$

where f_i and o_i represent the forecast and observed values at grid point i, respectively; N is the the number of grid points. The spatial averages of the f and o fields are indicated by $\overline{f}$ and $\bar{o}$, respectively.

4.3.2 Point verification

The C-CAM data written to the 0.15° grid was used for the point verification. The C-CAM grid point closest to the location of the station was determined, and then used to provide the forecast values that were compared to the sounding data. It was decided to use the point closest to the station instead of a weighted average of the four surrounding points, so that the influence of ocean points could be minimized at the coastal station. Software was developed to automate the point verification procedure. The monthly average absolute error as well as the monthly average bias were calculated for the 24-hour temperature forecasts at the selected pressure levels (see tabel 4.1).

4.3.2.1 Average absolute error

The absolute error of the 24-hour temperature forecast was calculated at all the selected pressure levels for each model run. It was then averaged on a monthly basis. That is,

$$Absolute\,error = \mid f_i - o_i \mid . \tag{4.4}$$

Here, f_i and o_i represents the forecast and observed temperatures at pressure level i, respectively.

4.3.2.2 Average bias

The bias of the 24-hour temperature forecast was calculated at all the selected pressure levels for each model run. It was then averaged on a monthly basis. That is,

$$Average\,bias = f_i - o_i. \tag{4.5}$$

Here, $f_i$cand o_i represents the forecast and observed temperatures level i, respectively.

4.3.3 Vertically integrated moisture flux

The vertically integrated moisture flux may be defined as

$$Q = \frac{1}{g}\int_{850}^{300} q\mathbf{V}\,dp \tag{4.6}$$

(after Hastenrath, 1966; D'Abreton and Lindesay, 1993). Here $\mathbf{V} = (u,\, v)$ is the horizontal wind and q is the specific humidity. Note that due to the elevated plateau of South Africa (see chapter 3), it is sensible to calculate the integral in (4.6) from the 850 hPa level upwards.

The components of the vector in (4.6) are the vertically integrated zonal moisture flux

$$Q_u = \frac{1}{g}\int_{850}^{300} qu\,dp \tag{4.7}$$

and the vertically integrated meridional moisture flux

$$Q_v = \frac{1}{g}\int_{850}^{300} qv\,dp. \tag{4.8}$$

Note that, following the definition of the absolute error (4.1), the absolute error of the vector field (4.6) is defined as

$$\epsilon = \frac{1}{g}\int_{850}^{300} \|q_{f_i}V_{f_i} - q_{o_i}V_{0_i}\|\,dp. \tag{4.9}$$

Here V_i^f and V_i^o denotes the forecast and observed (NCEP reanalysis) wind at grid point i, respectively.

In this study the moisture flux is expressed in units of $g\,cm^{-1}\,s^{-1}$.

4.4 Grid field verification results

4.4.1 500 hPa geopotential heights

4.4.1.1 Monthly average absolute error

The monthly average absolute error fields of the 500 hPa geopotential heights, as calculated for each of the forecast hours for the various months studied, are displayed in figures (4.1) to (4.18). During all months the most striking feature is the zonally orientated belt of average absolute errors that develops in the high latitude regions, whilst the errors are small and fairly consistent over the tropical regions. The error belt spreads generally north -and eastward as the forecast time increases, so that by the end of the forecast period the meridional error gradient equatorwards of the error belt is situated between $30° - 40°S$. There exists definite seasonality in the behaviour of the average absolute error of the 500 hPa geopotential height. Errors are larger in the winter -and transitional months compared to the summer months. The spatial coverage of the error belts is also notably larger during the winter months. In January and February errors in excess of 50 gpm, that occur at the end of the forecast period, are confined close to or south of $50°S$. Errors of this magnitude move to the north of $50°S$ during April, and by August are situated over the extreme southern part of South Africa. By this time, most of the ocean that forms part of the responsibility of South Africa for weather forecasts experiences average errors greater than 60 gpm, whereas in January, the average error that exceeds 60 gpm at the end of the forecast period are visible as two enclosed areas in a zonal belt between $50° - 70°S$.

Seasonality is not just evident in the magnitude of the average absolute errors, but also in the origin and location of the errors at the 17 different forecasting times. Seasonality of the magnitude of the errors may be caused by systems that are in general more intense in winter compared to summer, while the location and origin of the errors may be linked to regions where cyclogenesis occures frequently, or where the system density is high (Keable et al., 2002; also see chapter 2). In what follows, the evolution of the errors as a function of integration time is discussed for each of the months studied. Where possible, it is attempted to explain the nature and origin of the errors.

January and February have a similar error pattern. Except that the errors are in general of comparable magnitude, the largest errors occur mostly in the south-western part of the area under investigation - that is off the Antarctic coast and approximately between $20°W - 10°E$. Although the error patterns are similar for these two months, some subtle differences are present. One such a difference is that the largest errors in February are situated more northwards than in January during the first 48 hours of the forecast. The largest January errors occurs then between $60° - 70°S$ while the largest February errors occur between $50° - 60°S$. By the end of the forecast period, the latitudinal position of the largest errors are situated between $50° - 60°S$ for both months. This is also the zonal belt that is occupied by the most intense systems in summer (Keable et al., 2002; also see chapter 2), which may partially explain the presence of the error belt in this region. Another factor that can lead to this striking error pattern, could be the fact that most 500 hPa cyclones and cyclogenesis occur in this region as it is in the vicinity of the surface circumpolar trough (Keable et al., 2002; also see chapter 2). Another difference seen between January and February is that the error belt is slightly narrower in February, and the meridional error gradient equatorwards of the error belt is situated more southward compared to January. A possible explanation for the error belt to be situated more southward during February, is that the southward penetration of tropical airmasses over South Africa is generally greater in February than in January. Tropical airmasses are barotropic in nature, and the high amplitude baroclinic systems with higher associated absolute errors remain further to the south in February.

A prominent feature during April, May, June and August is an area of maximum errors inland of the Antarctica coast between about $20° - 60°E$. These errors occur during all of the forecast hours, and the magnitude of the errors increase as the forecast hour progresses. These errors are most striking in June and August towards the end of the forecast period. The error area is initially isolated, but expands in spacial extent and merge with other error zones (mostly to the north) towards the end of the forecast period. This error area inland of the Antarctica coast between about $20° - 60°E$ is present during January and February as well, but to a much lesser extent and not as an area of maximum errors. Queen Maud Land is an area where maximum system density is found. It is also a favoured area of cyclogenesis (Keable et al., 2002; see chapter 2). This provides a very reasonable explanation for this characteristic error region inland of the Antarctica coast. The fact that these errors are much more striking in the winter months can be due to the systems being more intense during winter months (Keable et al., 2002; also see chapter 2).

Except for the area of maximum errors over Antarctica desribed above, the high latitude error belt in April is characterized by various small enclosed areas of maximum errors. The axis of the error belt is generally between $50° - 60°S$. In May the largest errors occur initially over two areas. Firstly over Antarctica as described above, and secondly to the north of this area between $50° - 60°S$. The latter error has become merged with the maximum error area over Antarctica by the 54-hour forecast, whereafter the error belt becomes more prominent. The largest errors in the error belt occur mostly over the central -and eastern part of the belt. Another notable feature of the error belt is that it's western side is situated slightly northwards of the remainder of the belt. The error belt is situated between $40° - 50°S$ west of $0°E$, and between $50° - 70°S$ further eastwards.

In June, the zone of largest errors is well defined from the start of the forecast. There are two areas where maximum errors occur. The first area is situated between $50° - 60° S$ and westwards of about $20° E$ and the second area is inland of the Antarctica coast as mentioned above. These two error areas occur from the 0-hour forecast and expand east -and northwards during the remainder of the forecast period. The error belt axis remains between $50° - 60° S$ during the whole period. This is the month where the magnitude of the largest errors is mostly larger than the maximim errors of the other months (when comparing at corresponding forecast times). This might be because the most intense systems are found in winter (Keable et al., 2002; see chapter 2).

Except for the error area inland of the Antarctica coast, a secondary error area appears to the southwest and south of South Africa in August. This error area exists independently during some of the forecast hours, before it is entrained into the error belt at the 60-hour forecast. Even when this error area is entrained into the error belt, it remains visible amongst other enclosed areas of large errors present in the belt. This error area gradually moves southeastwards after being entrained into the error belt. It may be the result of a significantly strong system (or a few of them) which presence is reflected in this monthly average absolute error field. Another August feature is that the largest errors occur mostly in the eastern part of the error belt during the last few forecast hours.

Over South Africa the average absolute errors exceed 15 gpm from the 48-hour forecast for January and February. In April and May errors that exceed 15 gpm enter South Africa from the 42-hour forecast, in June from the 30-hour forecast and in August from the 6-hour forecast. Errors that exceed 20 gpm enter South Africa from the 78-hour forecast in January, the 84-hour forecast in February, the 48-hour forecast in April, the 54-hour forecast in May and the 48-hour forecast in June and August. The maximum average absolute errors that occur over South Africa in January and February are 25 gpm, in April it is 30 gpm, in May 35 gpm, in June 40 gpm and in August it is 50 gpm. Further, it is interesting to note that in the winter months (May, June, August and April to a lesser extent) the errors arrive at South Africa in the form of an error-trough during the later forecast hours. This may be attributed to the northward shift of the westerly wind belt. The fact that this error-trough is mostly present during the later forecast hours may be indicative of timing errors in the placement of the troughs by the model.

It may be noted that absolute errors in the 500 hPa height field tend to enter the output domain from the west (note the error fields in the early forecast times for the months January, February and June). This may be related to the fact the the model employs progressively lower resolution as one moves away from the highest-resolution panel over the area of interest. Relatively large errors may be expected to originate over lower resolution areas, and such errors upstream of the area of interest are likely to be transported into the area of interest by

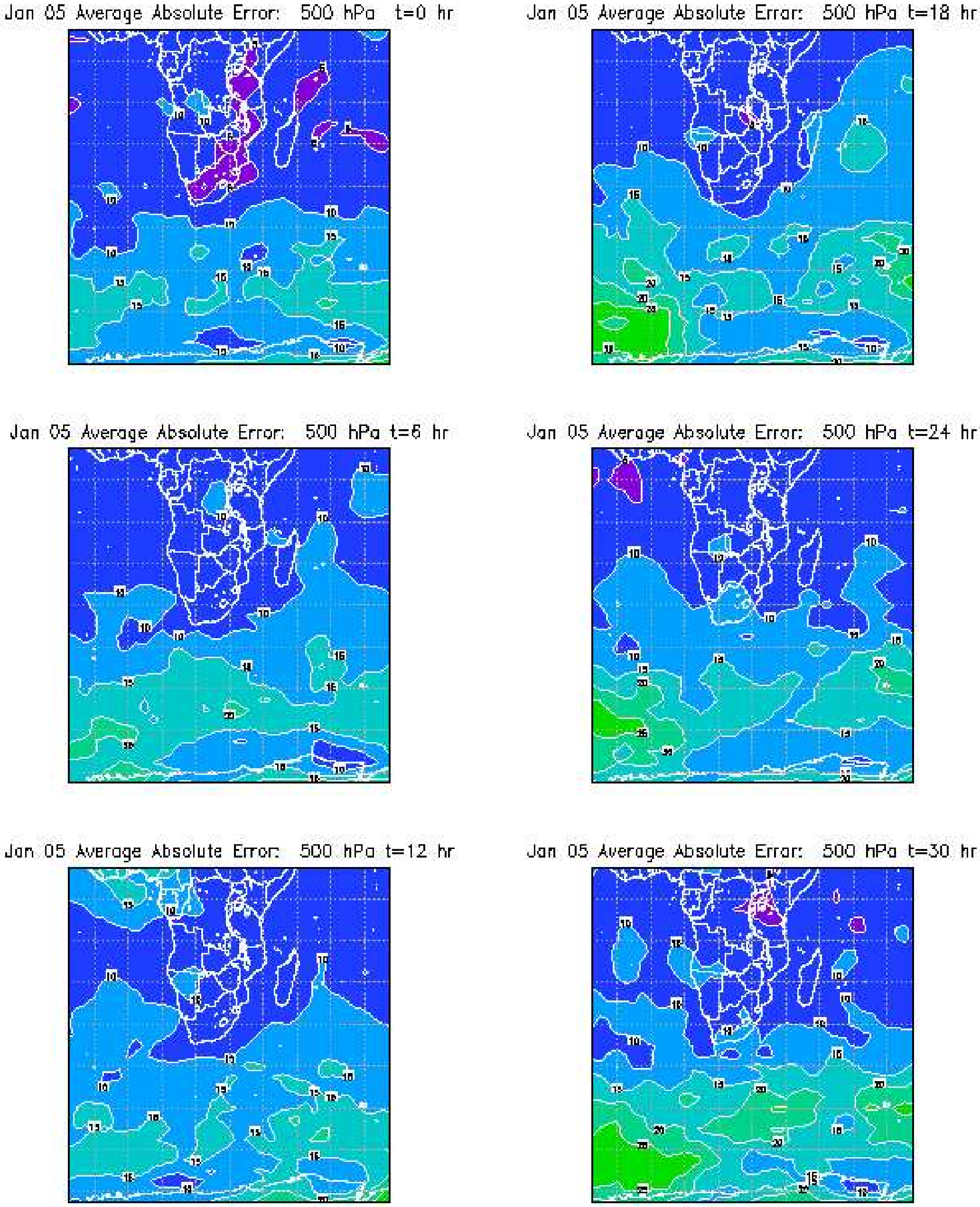

Figure 4.1: Average absolute error in the C-CAM forecasts at 500 hPa geopotential height: January 2005

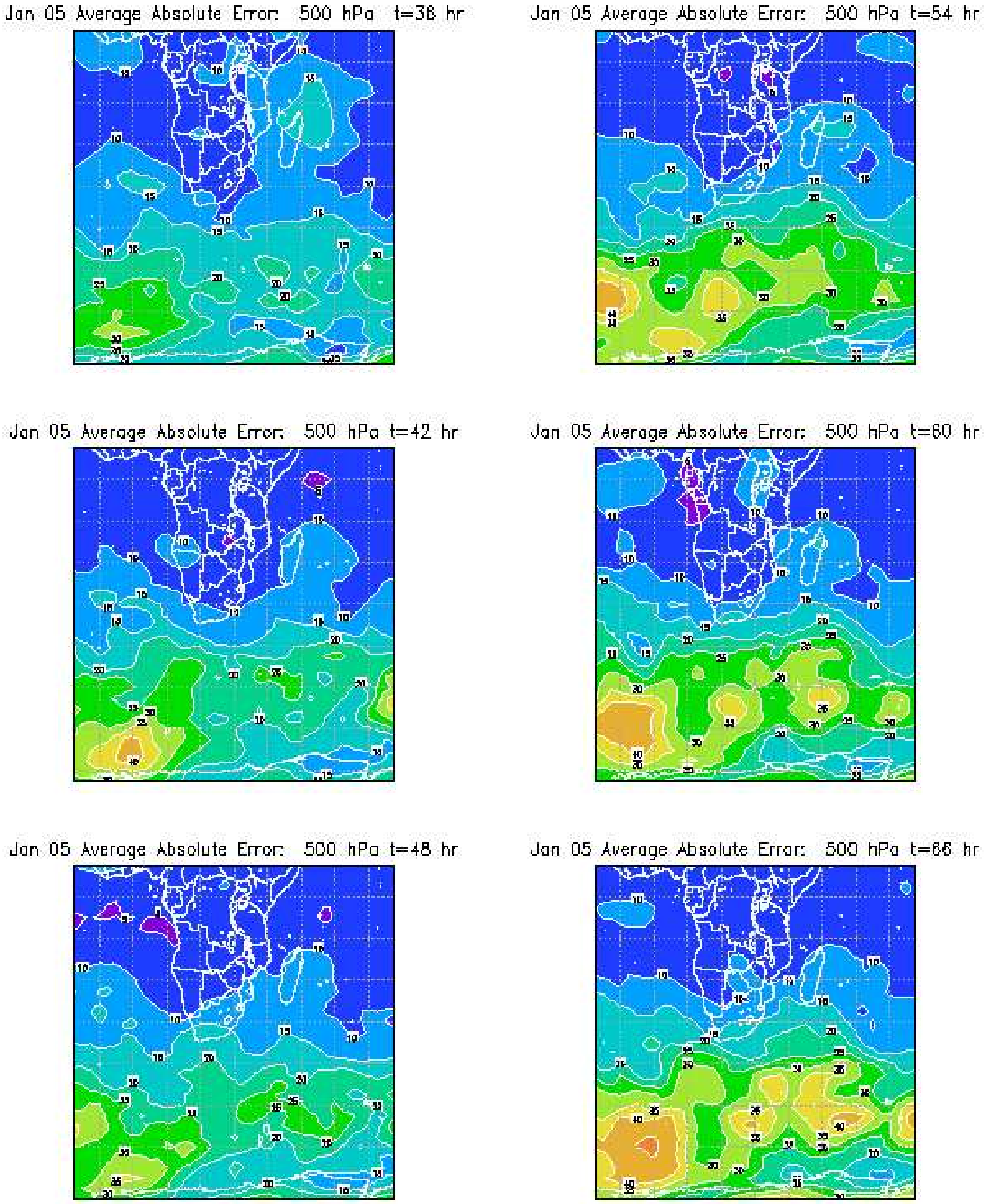

Jan 05 Average Absolute Error: 500 hPa t=36 hr

Jan 05 Average Absolute Error: 500 hPa t=54 hr

Jan 05 Average Absolute Error: 500 hPa t=42 hr

Jan 05 Average Absolute Error: 500 hPa t=60 hr

Jan 05 Average Absolute Error: 500 hPa t=48 hr

Jan 05 Average Absolute Error: 500 hPa t=66 hr

Figure 4.2: Average absolute error in the C-CAM forecasts at 500 hPa geopotential height: January 2005

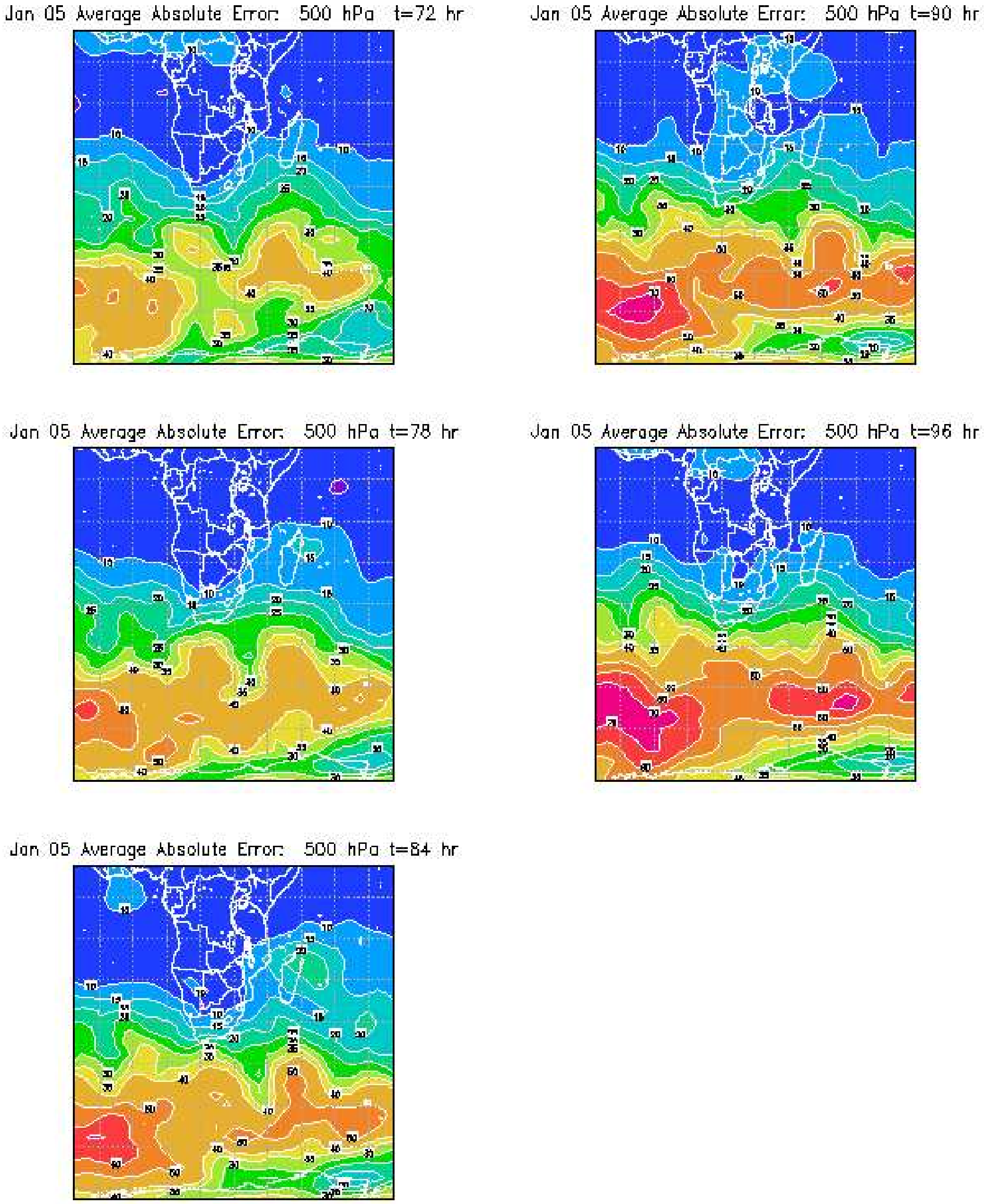

Jan 05 Average Absolute Error: 500 hPa t=72 hr

Jan 05 Average Absolute Error: 500 hPa t=90 hr

Jan 05 Average Absolute Error: 500 hPa t=78 hr

Jan 05 Average Absolute Error: 500 hPa t=96 hr

Jan 05 Average Absolute Error: 500 hPa t=84 hr

Figure 4.3: Average absolute error in the C-CAM forecasts at 500 hPa geopotential height: January 2005

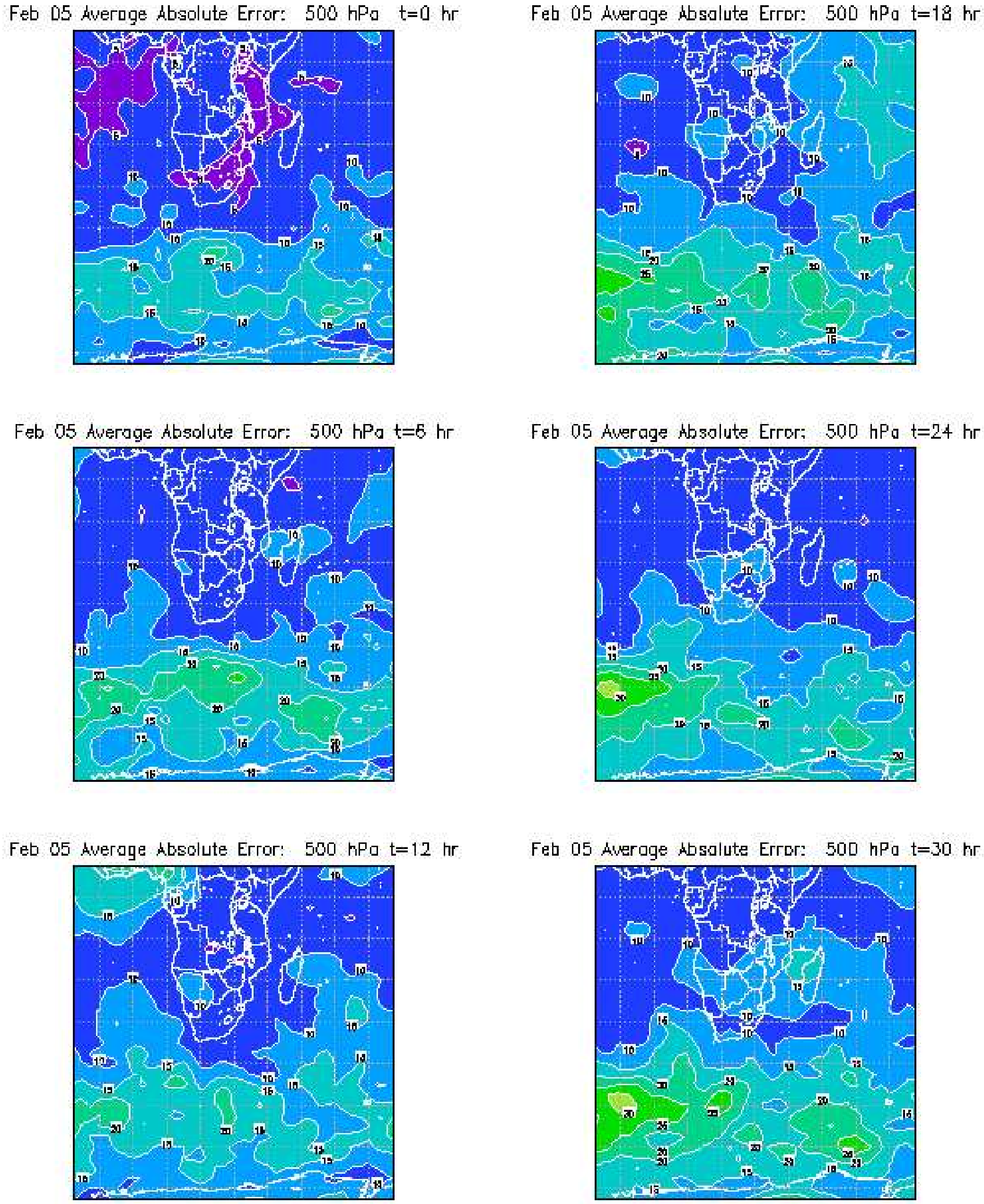

Feb 05 Average Absolute Error: 500 hPa t=0 hr

Feb 05 Average Absolute Error: 500 hPa t=18 hr

Feb 05 Average Absolute Error: 500 hPa t=6 hr

Feb 05 Average Absolute Error: 500 hPa t=24 hr

Feb 05 Average Absolute Error: 500 hPa t=12 hr

Feb 05 Average Absolute Error: 500 hPa t=30 hr

Figure 4.4: Average absolute error in the C-CAM forecasts at 500 hPa geopotential height: February 2005

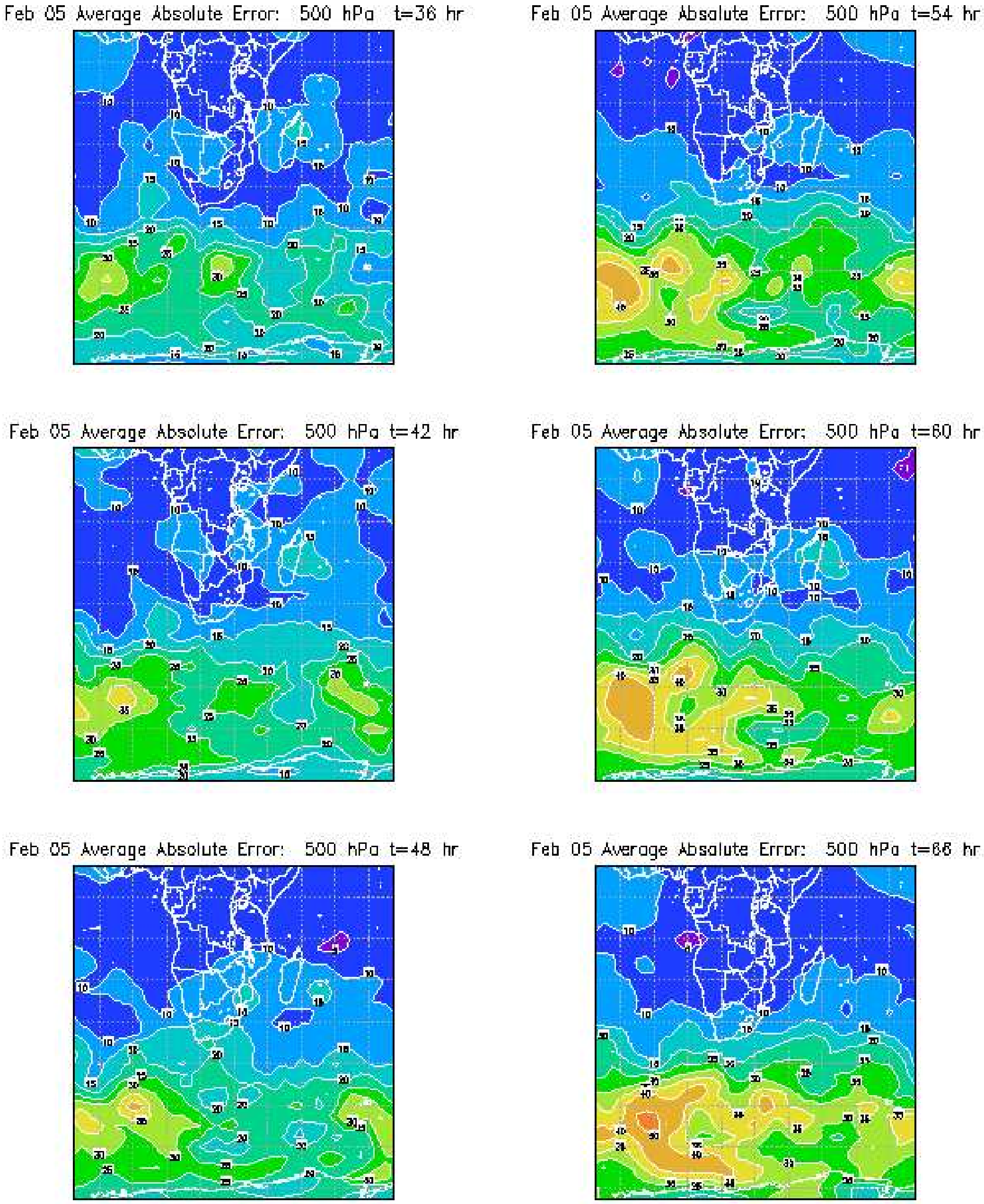

Feb 05 Average Absolute Error: 500 hPa t=36 hr

Feb 05 Average Absolute Error: 500 hPa t=54 hr

Feb 05 Average Absolute Error: 500 hPa t=42 hr

Feb 05 Average Absolute Error: 500 hPa t=60 hr

Feb 05 Average Absolute Error: 500 hPa t=48 hr

Feb 05 Average Absolute Error: 500 hPa t=66 hr

Figure 4.5: Average absolute error in the C-CAM forecasts at 500 hPa geopotential height: February 2005

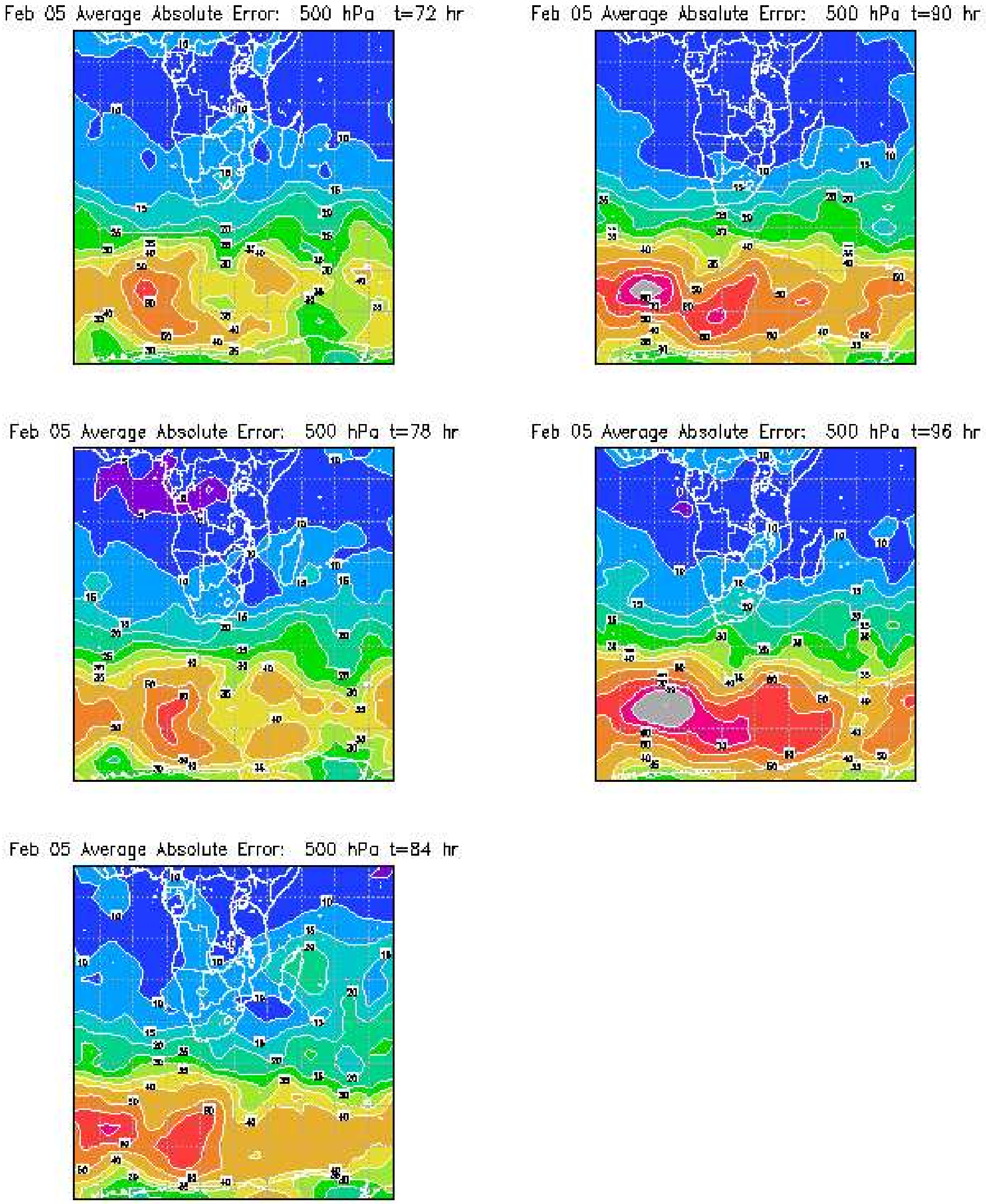

Feb 05 Average Absolute Error: 500 hPa t=72 hr

Feb 05 Average Absolute Error: 500 hPa t=90 hr

Feb 05 Average Absolute Error: 500 hPa t=78 hr

Feb 05 Average Absolute Error: 500 hPa t=96 hr

Feb 05 Average Absolute Error: 500 hPa t=84 hr

Figure 4.6: Average absolute error in the C-CAM forecasts at 500 hPa geopotential height: February 2005

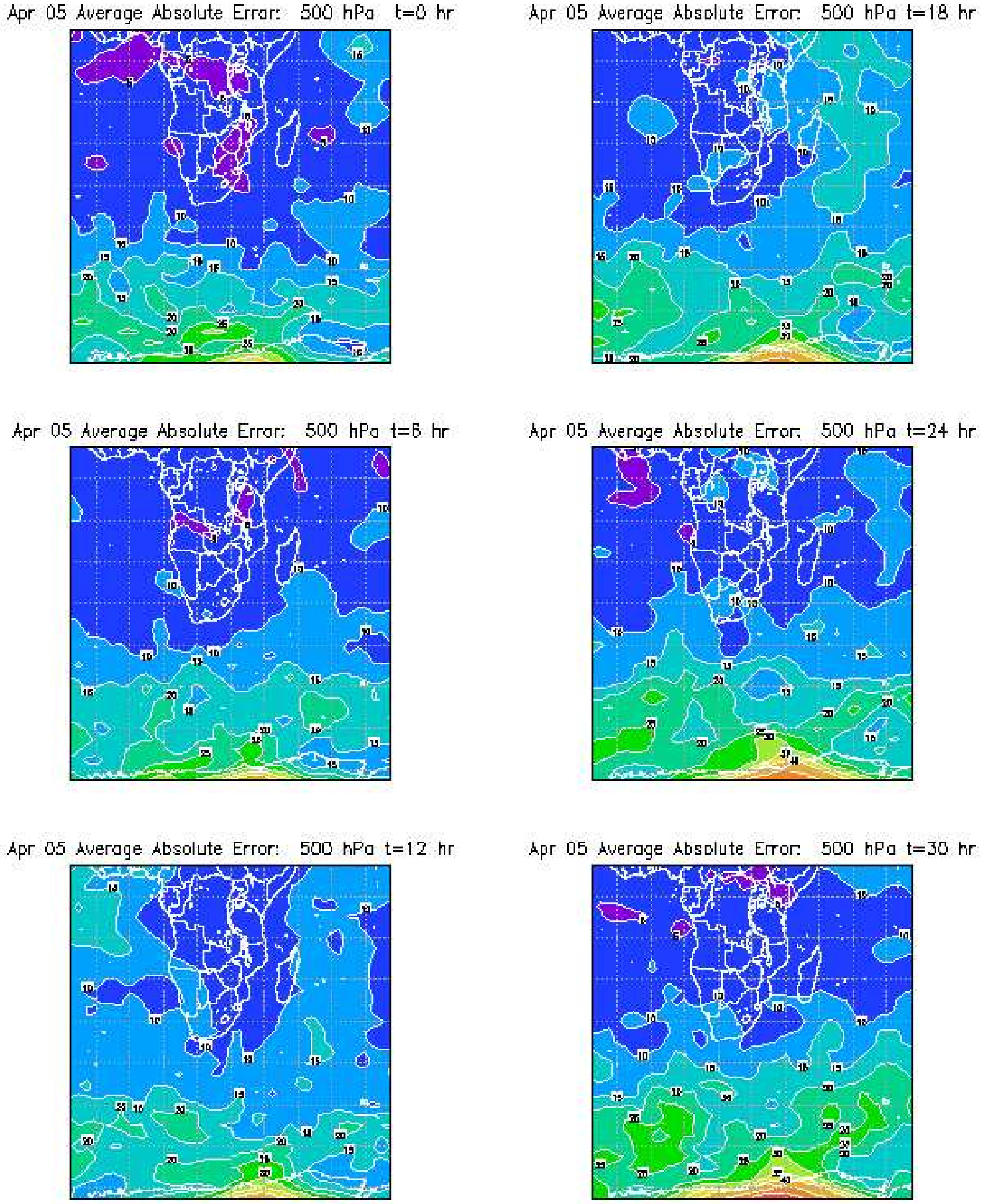

Apr 05 Average Absolute Error: 500 hPa t=0 hr

Apr 05 Average Absolute Error: 500 hPa t=18 hr

Apr 05 Average Absolute Error: 500 hPa t=6 hr

Apr 05 Average Absolute Error: 500 hPa t=24 hr

Apr 05 Average Absolute Error: 500 hPa t=12 hr

Apr 05 Average Absolute Error: 500 hPa t=30 hr

Figure 4.7: Average absolute error in the C-CAM forecasts at 500 hPa geopotential height: April 2005

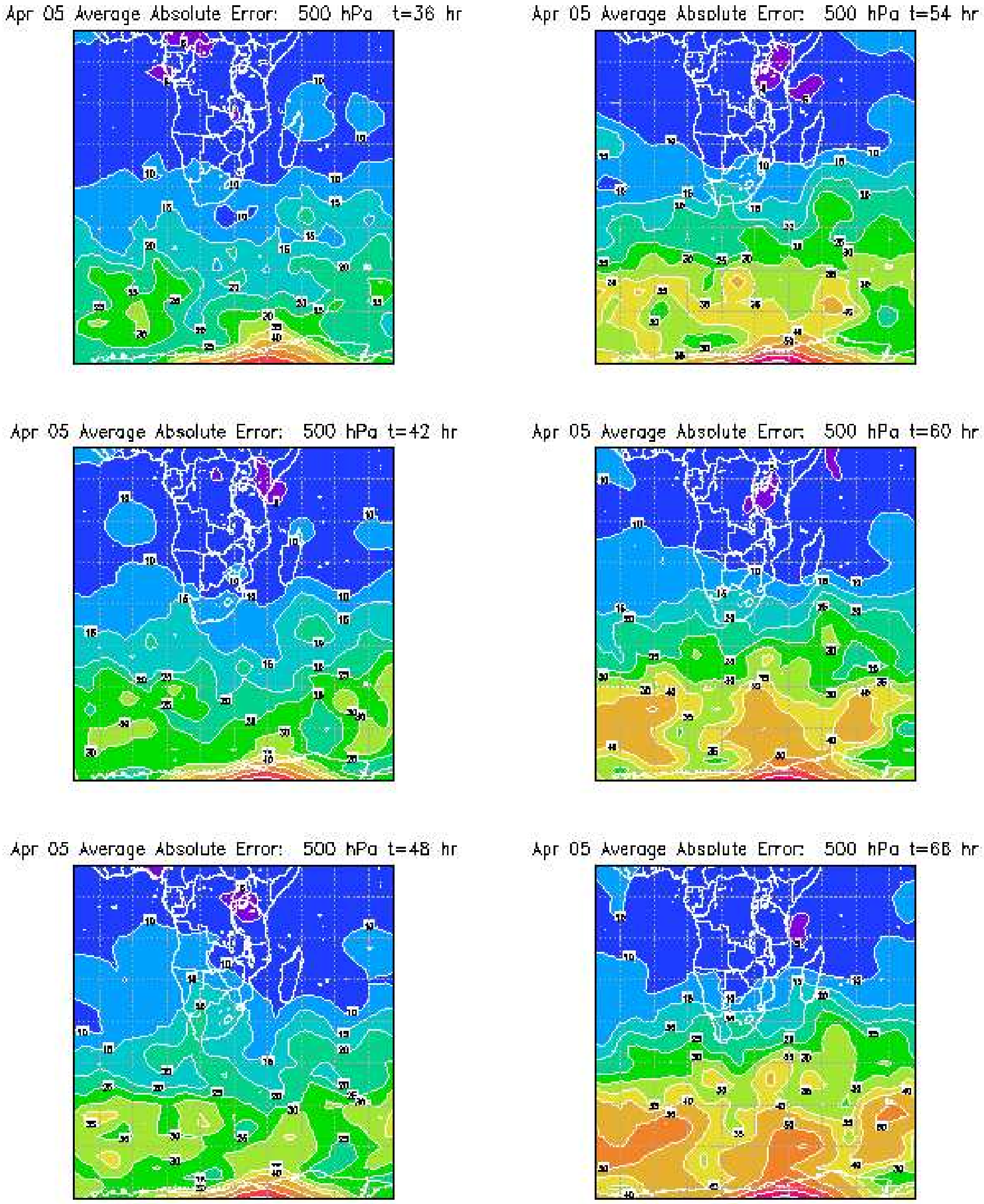

Apr 05 Average Absolute Error: 500 hPa t=36 hr

Apr 05 Average Absolute Error: 500 hPa t=54 hr

Apr 05 Average Absolute Error: 500 hPa t=42 hr

Apr 05 Average Absolute Error: 500 hPa t=60 hr

Apr 05 Average Absolute Error: 500 hPa t=48 hr

Apr 05 Average Absolute Error: 500 hPa t=66 hr

Figure 4.8: Average absolute error in the C-CAM forecasts at 500 hPa geopotential height: April 2005

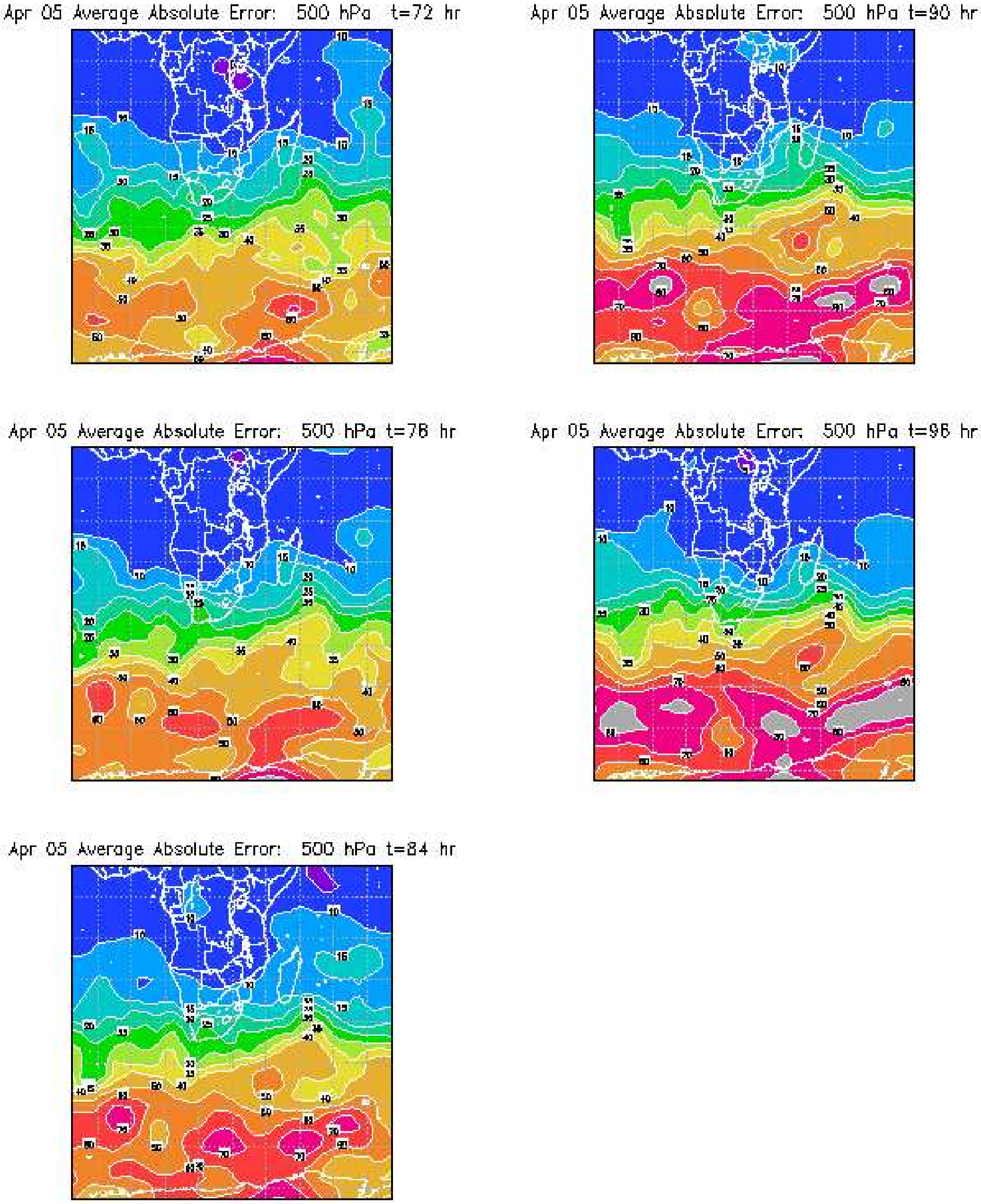

Apr 05 Average Absolute Error: 500 hPa t=72 hr

Apr 05 Average Absolute Error: 500 hPa t=90 hr

Apr 05 Average Absolute Error: 500 hPa t=78 hr

Apr 05 Average Absolute Error: 500 hPa t=96 hr

Apr 05 Average Absolute Error: 500 hPa t=84 hr

Figure 4.9: Average absolute error in the C-CAM forecasts at 500 hPa geopotential height: April 2005

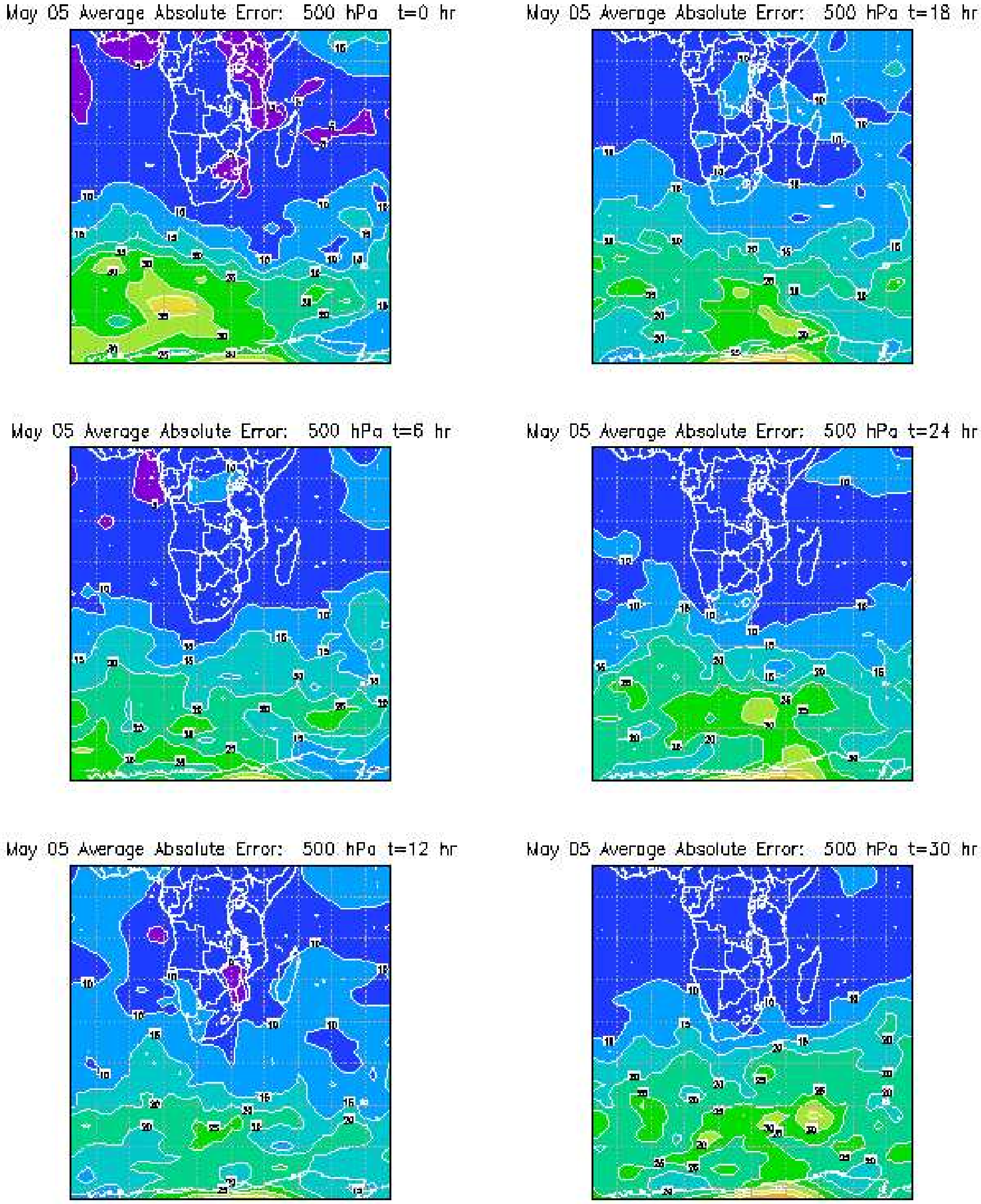

Figure 4.10: Average absolute error in the C-CAM forecasts at 500 hPa geopotential height: May 2005

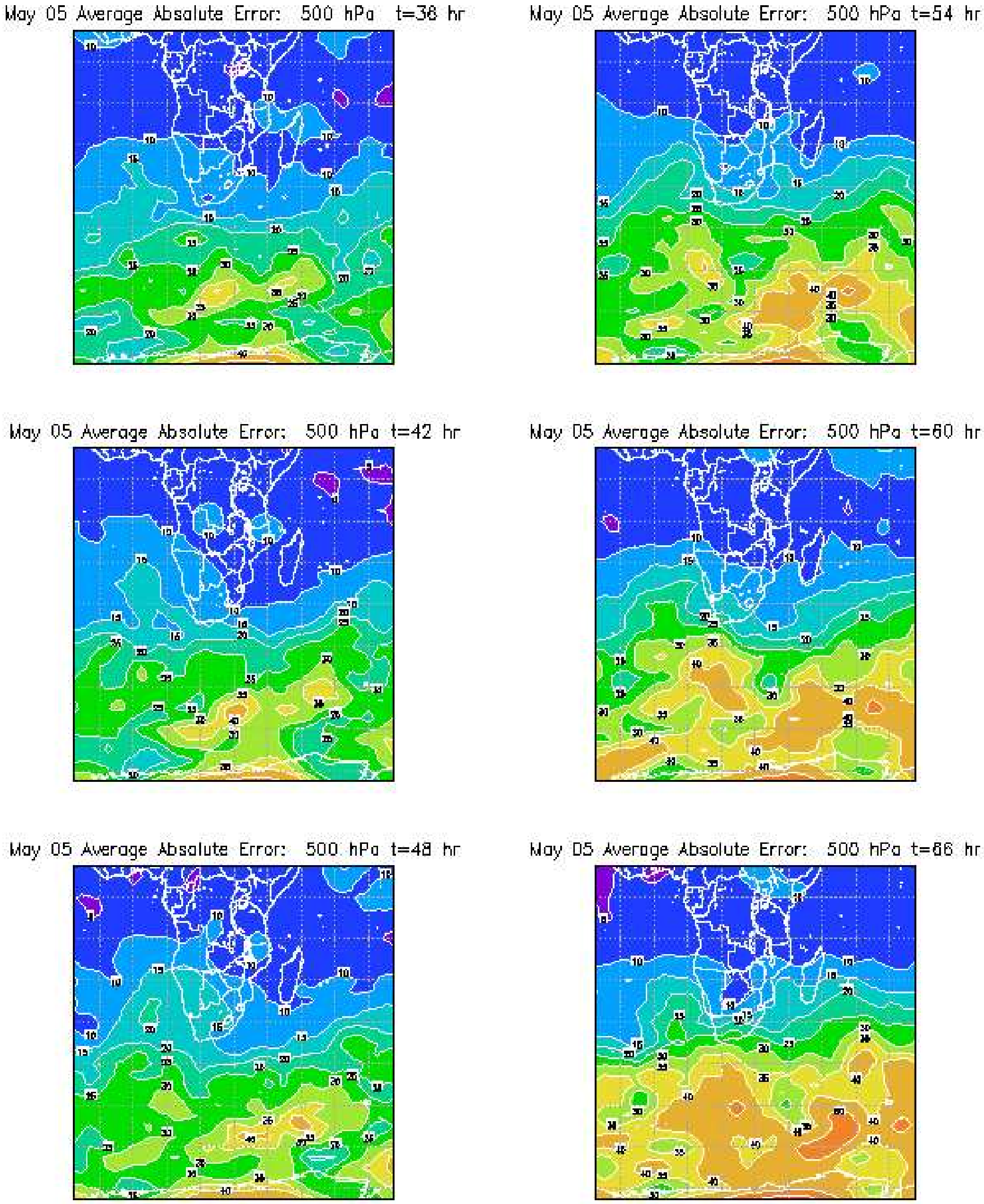

Figure 4.11: Average absolute error in the C-CAM forecasts at 500 hPa geopotential height: May 2005

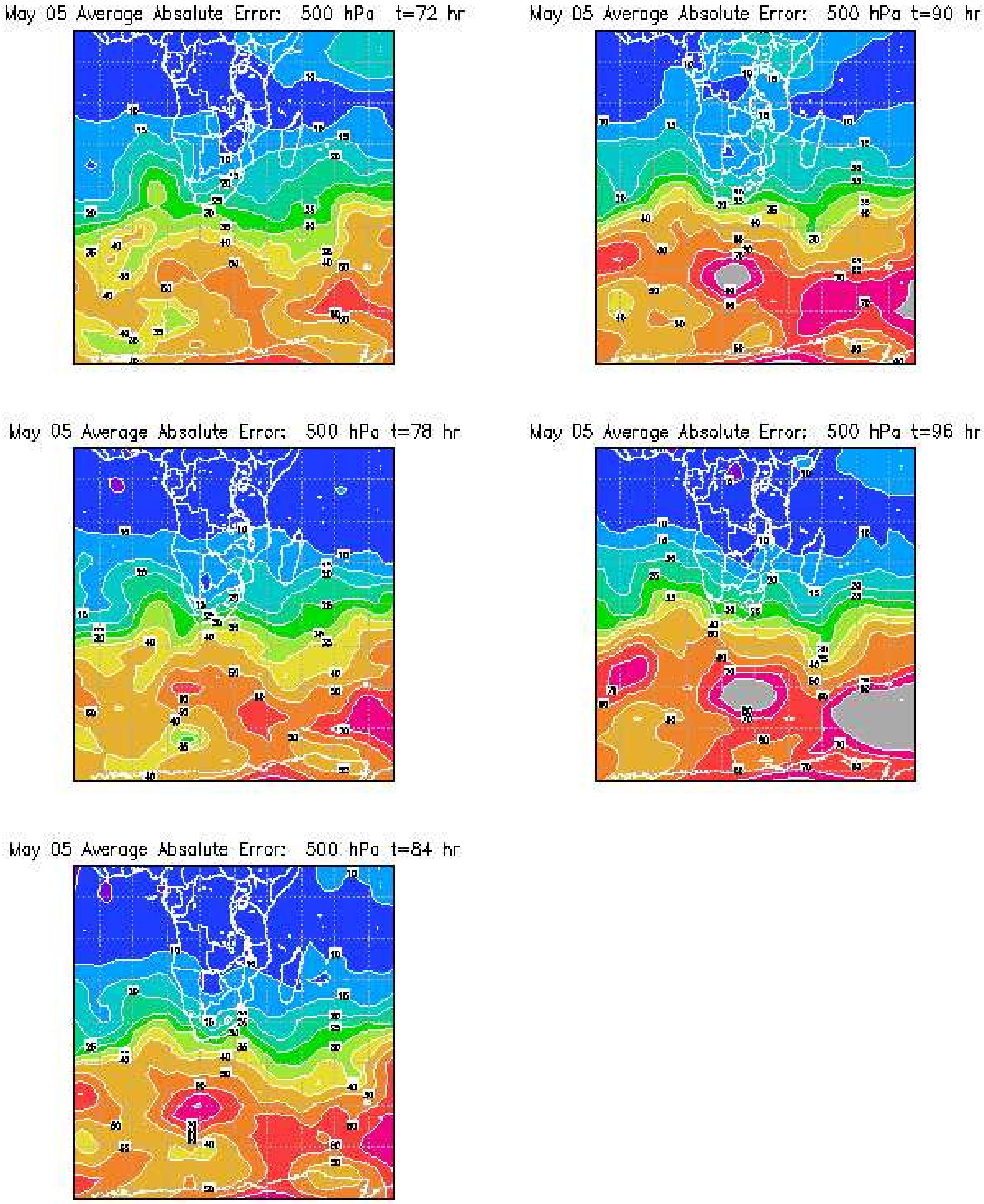

May 05 Average Absolute Error: 500 hPa t=72 hr

May 05 Average Absolute Error: 500 hPa t=90 hr

May 05 Average Absolute Error: 500 hPa t=78 hr

May 05 Average Absolute Error: 500 hPa t=96 hr

May 05 Average Absolute Error: 500 hPa t=84 hr

Figure 4.12: Average absolute error in the C-CAM forecasts at 500 hPa geopotential height: May 2005

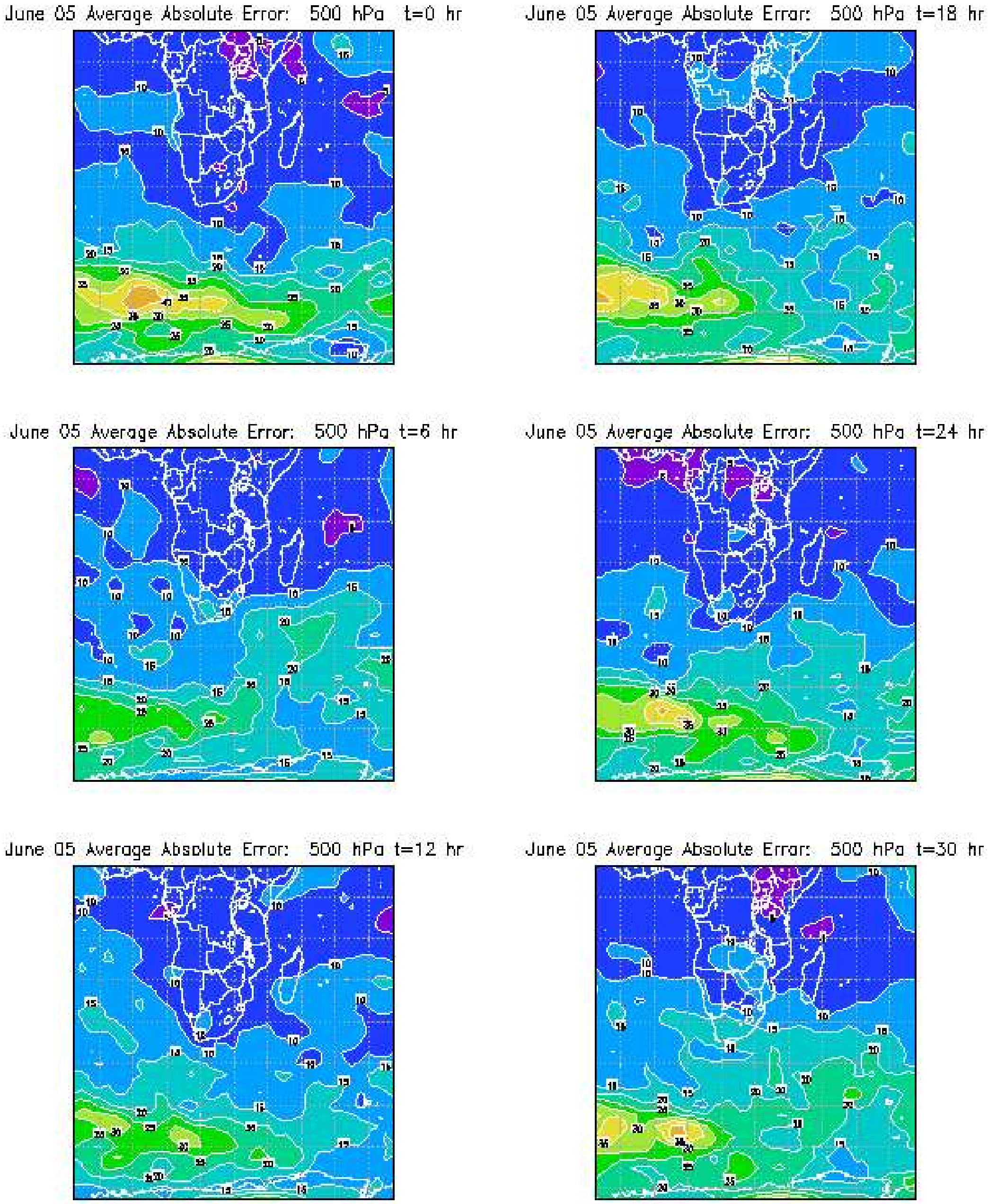

June 05 Average Absolute Error: 500 hPa t=0 hr

June 05 Average Absolute Error: 500 hPa t=18 hr

June 05 Average Absolute Error: 500 hPa t=6 hr

June 05 Average Absolute Error: 500 hPa t=24 hr

June 05 Average Absolute Error: 500 hPa t=12 hr

June 05 Average Absolute Error: 500 hPa t=30 hr

Figure 4.13: Average absolute error in the C-CAM forecasts at 500 hPa geopotential height: June 2005

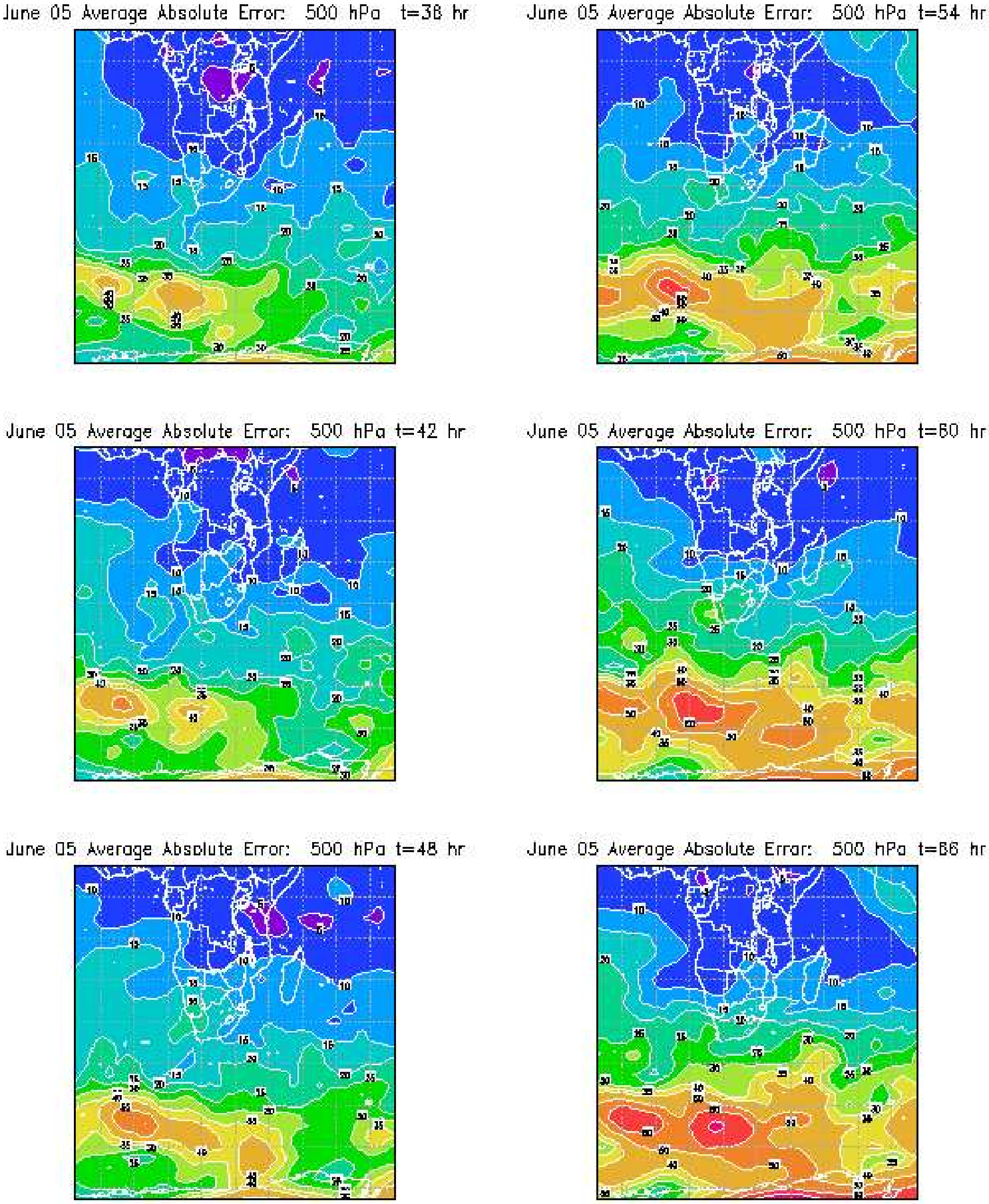

June 05 Average Absolute Error: 500 hPa t=36 hr

June 05 Average Absolute Error: 500 hPa t=54 hr

June 05 Average Absolute Error: 500 hPa t=42 hr

June 05 Average Absolute Error: 500 hPa t=60 hr

June 05 Average Absolute Error: 500 hPa t=48 hr

June 05 Average Absolute Error: 500 hPa t=66 hr

Figure 4.14: Average absolute error in the C-CAM forecasts at 500 hPa geopotential height: June 2005

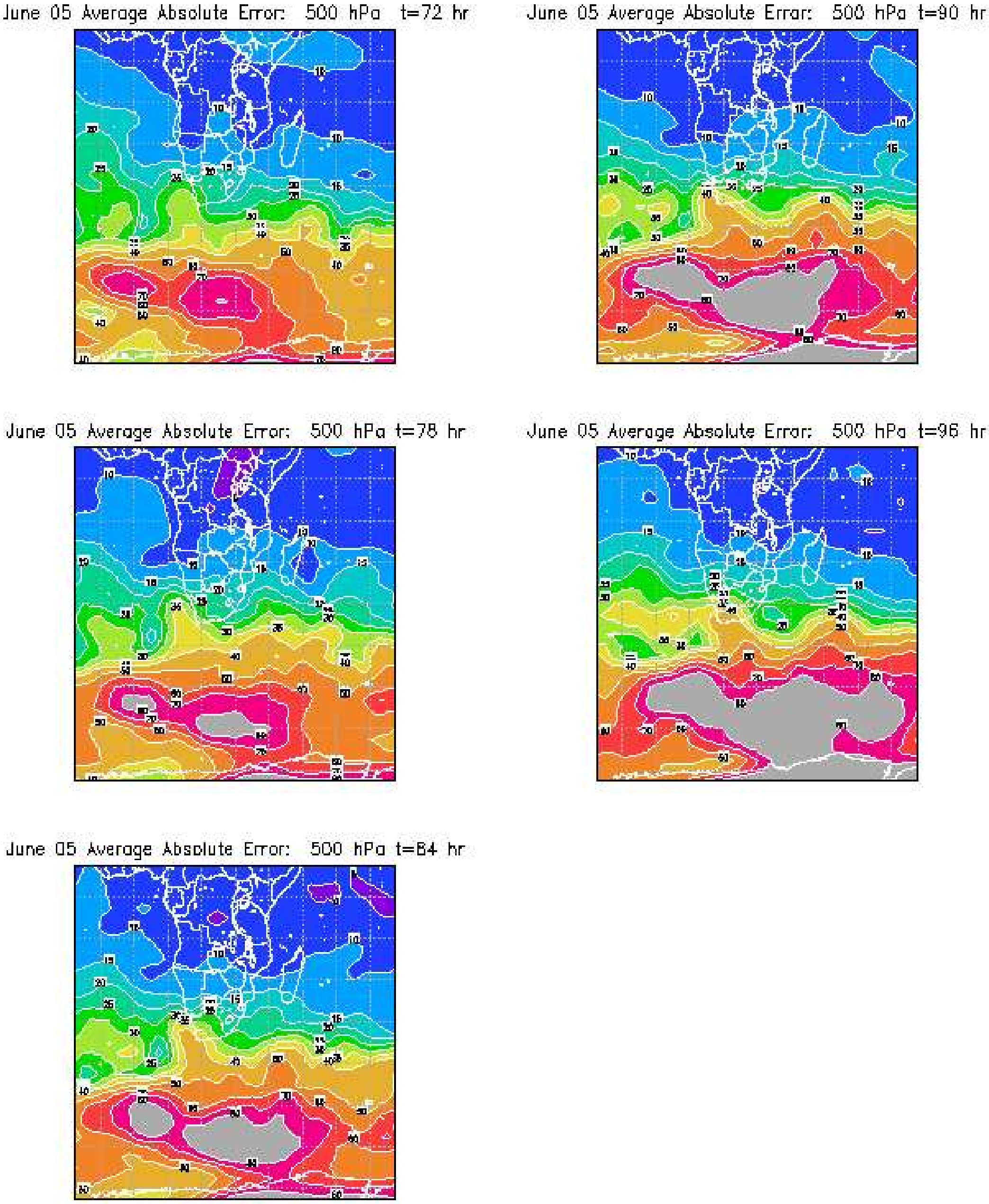

June 05 Average Absolute Error: 500 hPa t=72 hr

June 05 Average Absolute Error: 500 hPa t=90 hr

June 05 Average Absolute Error: 500 hPa t=78 hr

June 05 Average Absolute Error: 500 hPa t=96 hr

June 05 Average Absolute Error: 500 hPa t=84 hr

Figure 4.15: Average absolute error in the C-CAM forecasts at 500 hPa geopotential height: June 2005

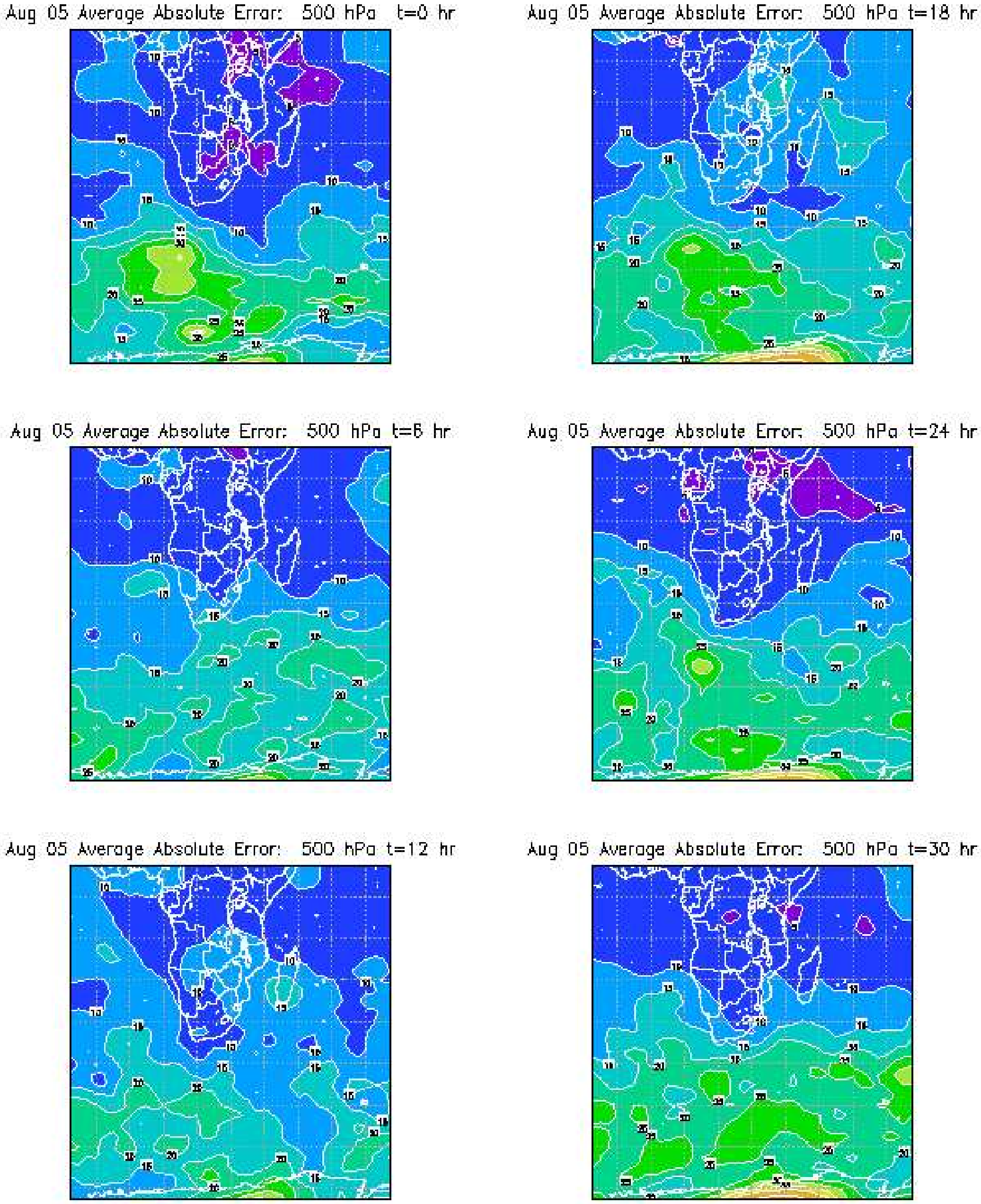

Figure 4.16: Average absolute error in the C-CAM forecasts at 500 hPa geopotential height: August 2005

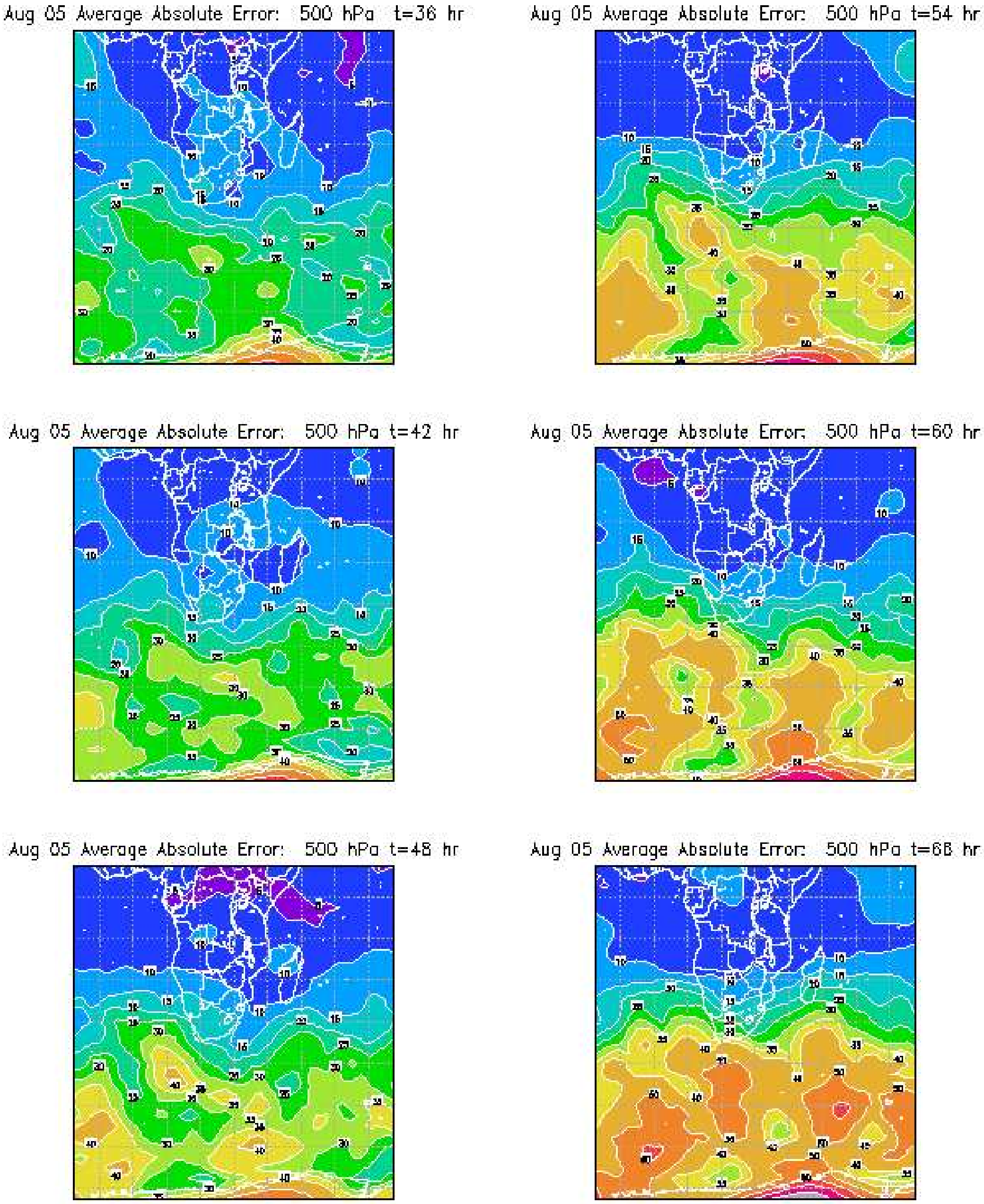

Figure 4.17: Average absolute error in the C-CAM forecasts at 500 hPa geopotential height: August 2005

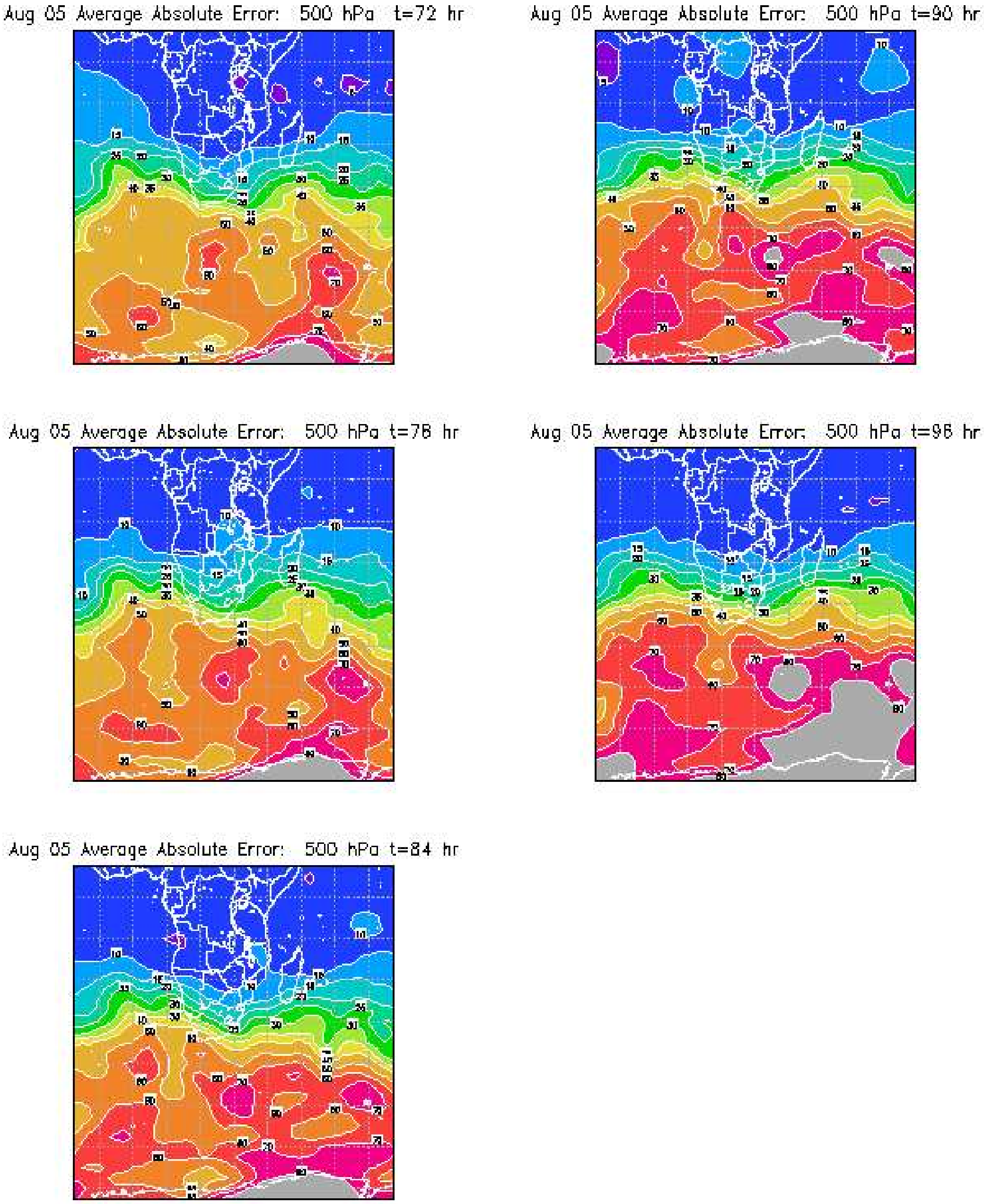

Figure 4.18: Average absolute error in the C-CAM forecasts at 500 hPa geopotential height: August 2005

the advecting westerly winds. Also, an area of favoured cyclogenesis are found between the Weddel Sea and the South Pole, which is situated to the west and south of the area under investigation. Systems that develop in this favoured area of cyclogenesis propogates into the area under investigation and can contribute to the observed absolute errors. Another interesting feature of the absolute error field is the fact that large errors tend to develop over Antarctica. These errors tend to propagate northeastwards into the area of interest (note the error fields in the early forecast hours of the months April, May, June and August). As the model resolution is also relatively lower over Antarctica, relatively large simulation errors may be expected here. The sensitivity of the growth of the model error with respect to Antarctica probably stems from the fact that this in an important area of cyclogenesis (Keable et al., 2002; also see Chapter 2). Cyclones that develop over the Southern Ocean tend to travel northeastwards (Keable et al., 2002; also see Chapter 2), so that the associated error field may also be expected to propagate in a northeasterly direction.

4.4.1.2 Root mean square error

The root mean square error is a widely used statistical measure to quantify the magnitude of an error. As described in the methodology, the monthly average root mean square error of the 500 hPa geopotential height forecasts for all the forecast hours (figure 4.19) was calculated for the six month period under investigation. The NCEP persistence forecasts were calculated as well in order to determine whether the C-CAM forecasts will lose value as a function of the integration time.

The C-CAM forecasts for each specific month outperforms the corresponding NCEP persistence forecast for all the forecast hours. The persistence forecast errors are in general smaller in the summer months and increase in the winter months, with the largest errors in August. June is an exception, as the second smallest errors occur in this month. The same tendency is shown in the C-CAM forecast errors except that June is the month with the second most largest errors. As expected, the C-CAM errors grow as the integration time increases. The growth rate of the errors reveals mostly a similar tendency during all of the months. The errors start to grow more rapidly from about the 9thintegration time - that is from the 48-hour forecast. One can conclude from this that the model forecasts are very valuable for the first two days and must thereafter be used with more caution. However, they have skill and remain valuable as they fare better than the persistence forecast over the full four day integration period.

The magnitude of the root mean square errors during the individual months, confirm what is seen during the analysis of the average absolute errors in the previous section. The months of January and February are characterized by the smallest errors. The errors during these two months, are not comparible with

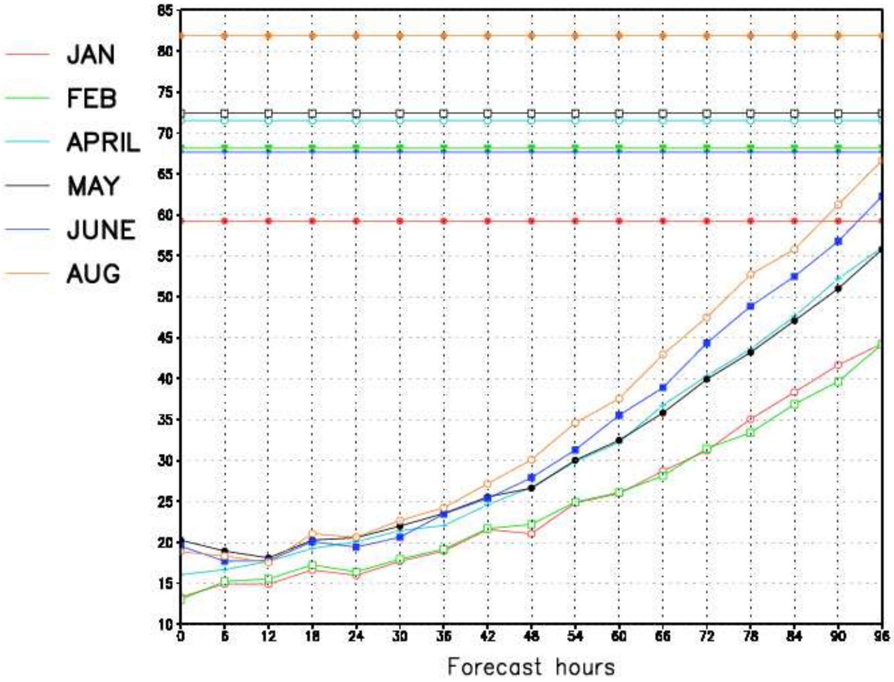

Figure 4.19: The monthly root mean square errors of the NCEP persistence (horizontal lines) and C-CAM forecasts of the 500 hPa geopotential height

the remaining four months, which have very similar error patterns up until the 8th integration time. After this, April and May still show similar error magnitude and error-growth patterns. June and August show the largest errors after the 8th integration time. This tendency for the errors to be larger in magnitude during the intermediate and winter months can be explained by systems being more variable in the intermediate months, and more intense during winter months. The propagation speed of the weather systems are also greater during these months compared to the summer months, and this may also attribute to the larger errors that occur.

4.4.1.3 Pattern correlation

Pattern correlations were calculated for the simulated 500 hPa geopotential height fields and the corresponding NCEP reanalysis data to gain more insight into how the accuracy of the simulated geopotential height pattern decreases as a function of the integration time. As described in the methodology, the monthly average pattern correlation were calculated for all the forecast hours (figure 4.20), for all of the six months under investigation. The pattern correlations of the NCEP persistence forecasts were also calculated in order to gain more insight in the skill of the C-CAM forecasts. As with the root mean square error, the C-CAM forecasts outperform the NCEP persistence forecasts during all of the forecast hours. During all of the months under investigation, the C-CAM pattern correlation starts to deteriorate more rapidly from approximately the 9thintegration time. This corresponds with when the root mean square error starts to increase more rapidly (see the previous section).

The pattern correlations of the NCEP persistence forecasts show very similar behaviour compared to the corresponding root mean square errors. The tendency is again for the summer months to have the better pattern correlation compared to the winter and intermediate months. However, June is again an exception, having the best pattern correlation of all the months investigated. The monthly average pattern correlations of the C-CAM forecasts are the highest for the month of February. Interestingly, the January and May C-CAM pattern correlations are very similar. They are higher than the pattern correlations for April, June and August, which may be grouped together, with August having the worst pattern correlation.

4.4.2 Vertically integrated moisture flux

4.4.2.1 Monthly average absolute error

The monthly average absolute error fields of the vertically integrated moisture flux for the various months studied are shown in figures 4.21 to 4.38. The absolute error field for January (figures 4.21, 4.22 and 4.23) shows that large model errors are present during model initialization over tropical Africa. As time progresses in the model simulation, two distinct meridional error bands develop.

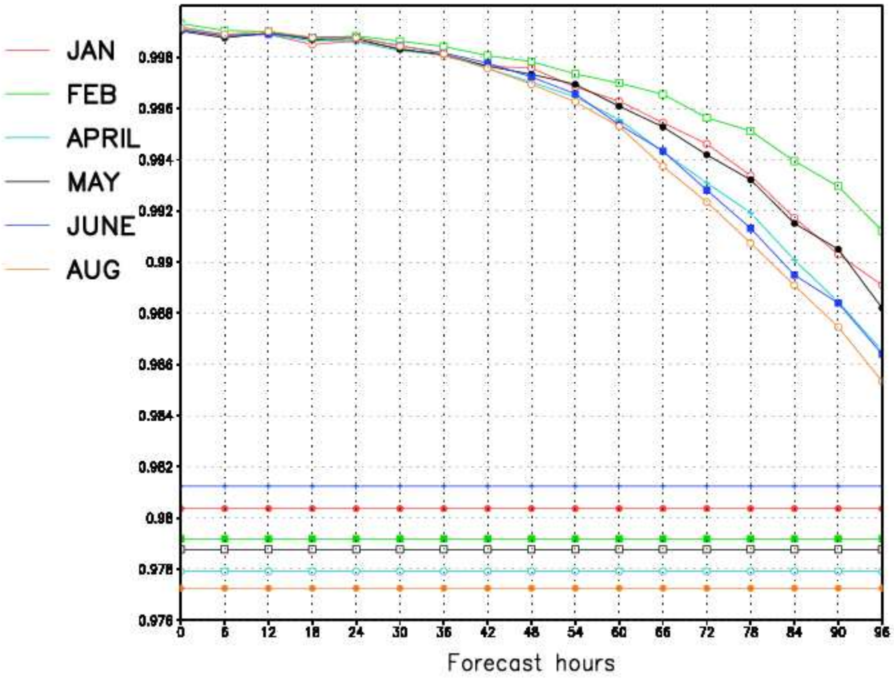

Figure 4.20: The monthly average pattern correlations of the NCEP persistence (horizontal lines) and C-CAM forecasts of the 500 hPa geopotential height

The one is located from Mozambique southeastwards over Madagascar into the Indian Ocean, whilst the second band is orientated from Angola southeastwards over Botswana and South Africa into the Indian Ocean. These two error bands co-incide with the typical average location of tropical-temperate cloudbands over this region (Tyson, 1986; Jury, 1992; Jury and Pathack, 1993, Jury et al., 1994; Washington and Todd, 1999; also see chapter 2). Another distictive feature of the January error pattern is the development of a zonal error band over the Southern Ocean where errors propagate eastwards. A second zonal error band is present over the northern Indian Ocean where errors propogate westward in the prevailing easterly flow.

During February (figures 4.24, 4.25 and 4.26) the average moisture flux errors over southern Africa are generally higher than in January, in particular in the meridional band stretching from Angola over Botswana into South Africa. The meridional error band that stretches from Mozambique to Madagascar in the January error field is not well defined in February. This error band now only originates over Madagascar extending into the southern Indian Ocean. The zonal error band over the Southern Ocean is more well defined than in January but the westward propogating errors over the northern Indian Ocean are much smaller in February compared to January.

In April (figures 4.27, 4.28 and 4.29) the largest errors in the moisture flux over southern Africa propogate into the region from the north, similar to what happens in January and February. The April error field is generally very similar to the February error field.

The May error field (figures 4.30, 4.31 and 4.32) shows interesting differences compared to the previously discussed error fields. The model error at model initialization over subtropical Africa is much smaller compared to the months discussed above. This is related to the northward displacement of the ITCZ in May. The meridional error band over the subcontinent is weaker than in the months discussed previously. In fact, two distinct zonal error bands are now the dominant features. The one error band stretches over the northern Indian Ocean into the subcontinent. It signifies the growth and propagation of model errors in the easterly wind regime north of the subtropical high pressure belt. The second error band is located over the Southern Ocean in the westerly wind regime. This band is located further to the north than in the months discussed previously and represents an important source of errors over South Africa by the end of the integration period.

The error field for June (figures 4.33, 4.34 and 4.35) is very similar to that of May. The two zonal error bands are even better defined and the meridional error band over the subcontinent is shifted to the far west. Errors from the zonal band over the Southern Ocean gradually moves into South Africa as the

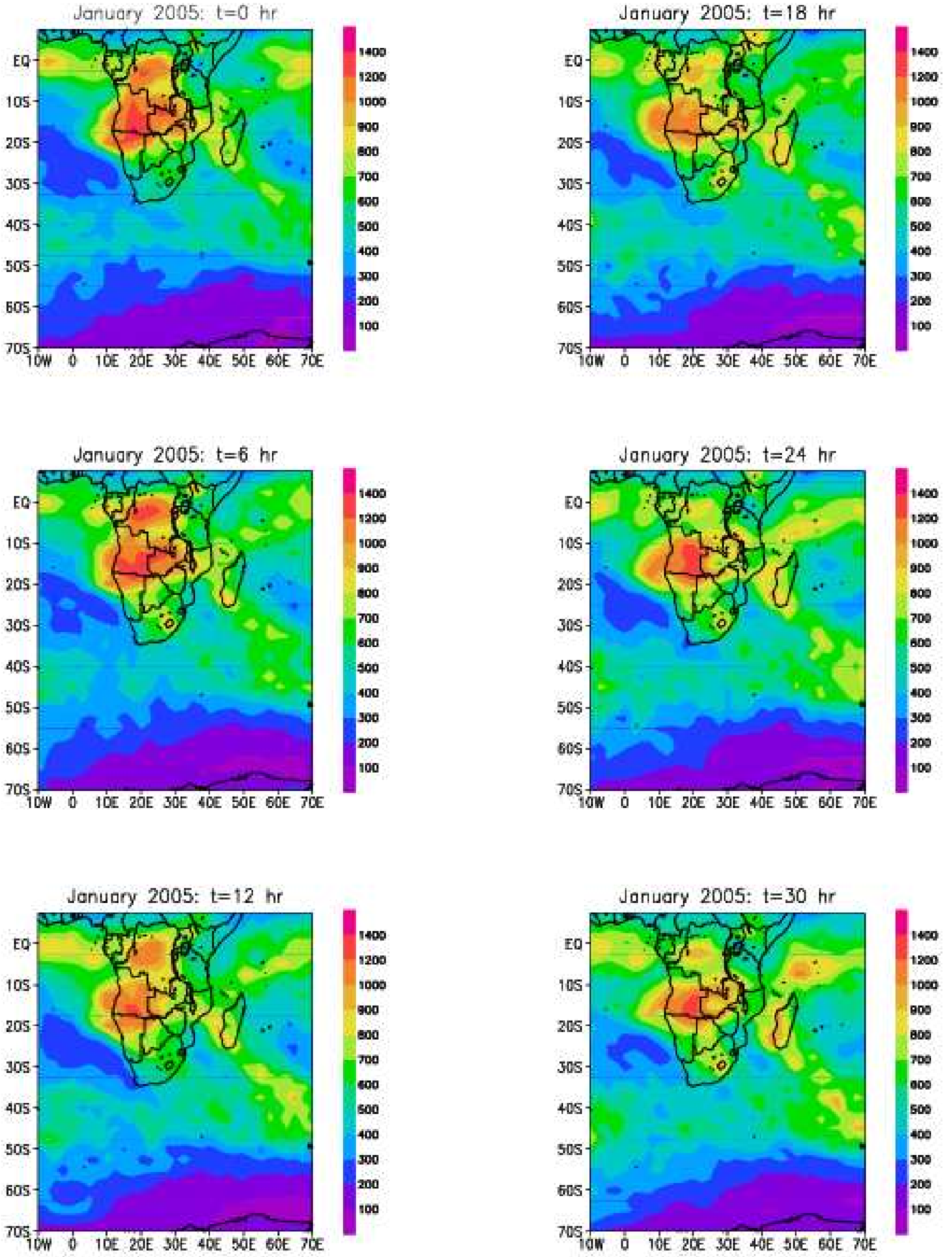
January 2005: t=0 hr

January 2005: t=18 hr

January 2005: t=6 hr

January 2005: t=24 hr

January 2005: t=12 hr

January 2005: t=30 hr

Figure 4.21: Average moisture flux error ($g\,cm^{-1}\,s^{-1}$) in the C-CAM forecasts: January 2005

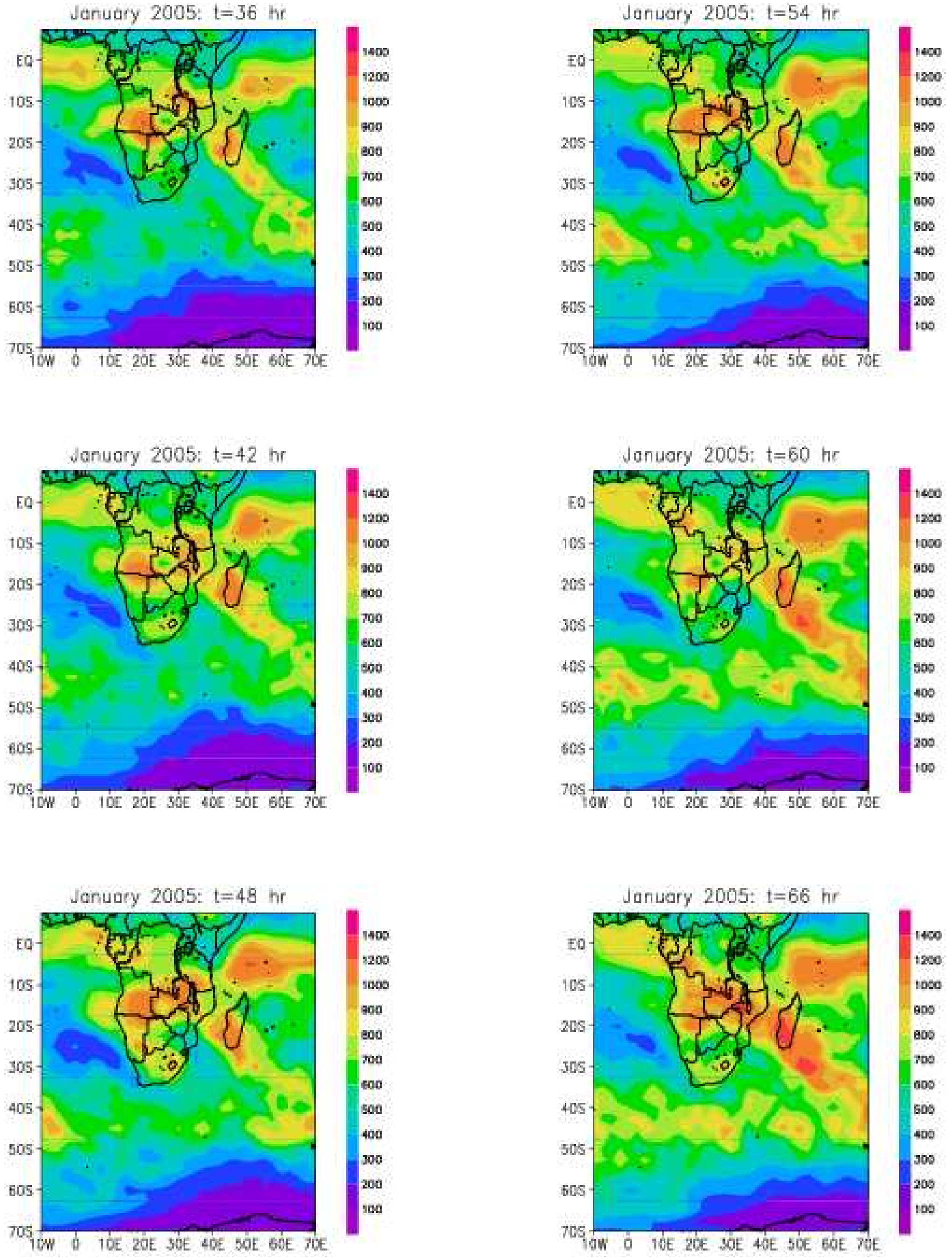

Figure 4.22: Average moisture flux error ($g\,cm^{-1}\,s^{-1}$) in the C-CAM forecasts: January 2005

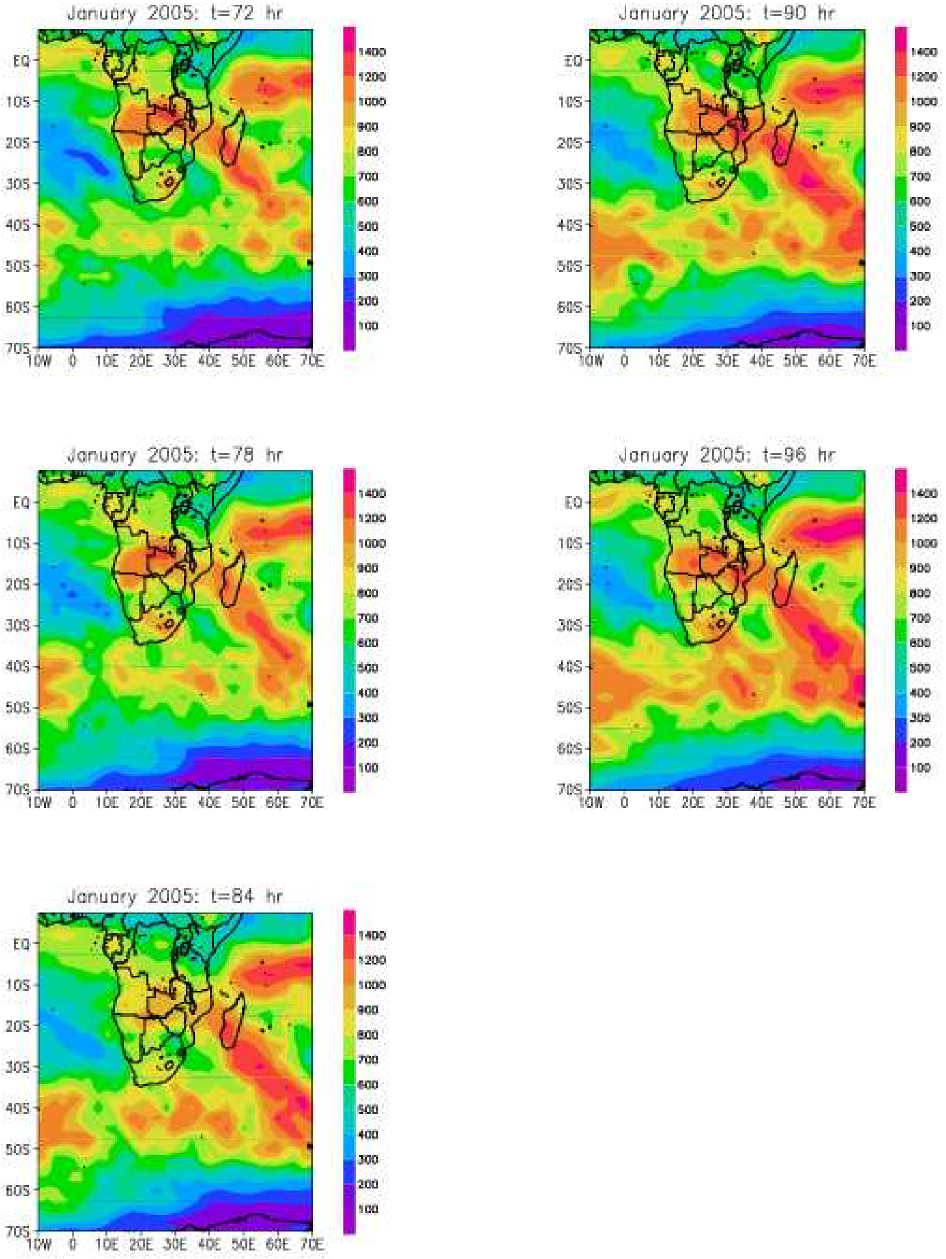

Figure 4.23: Average moisture flux error ($g\,cm^{-1}\,s^{-1}$) in the C-CAM forecasts: January 2005

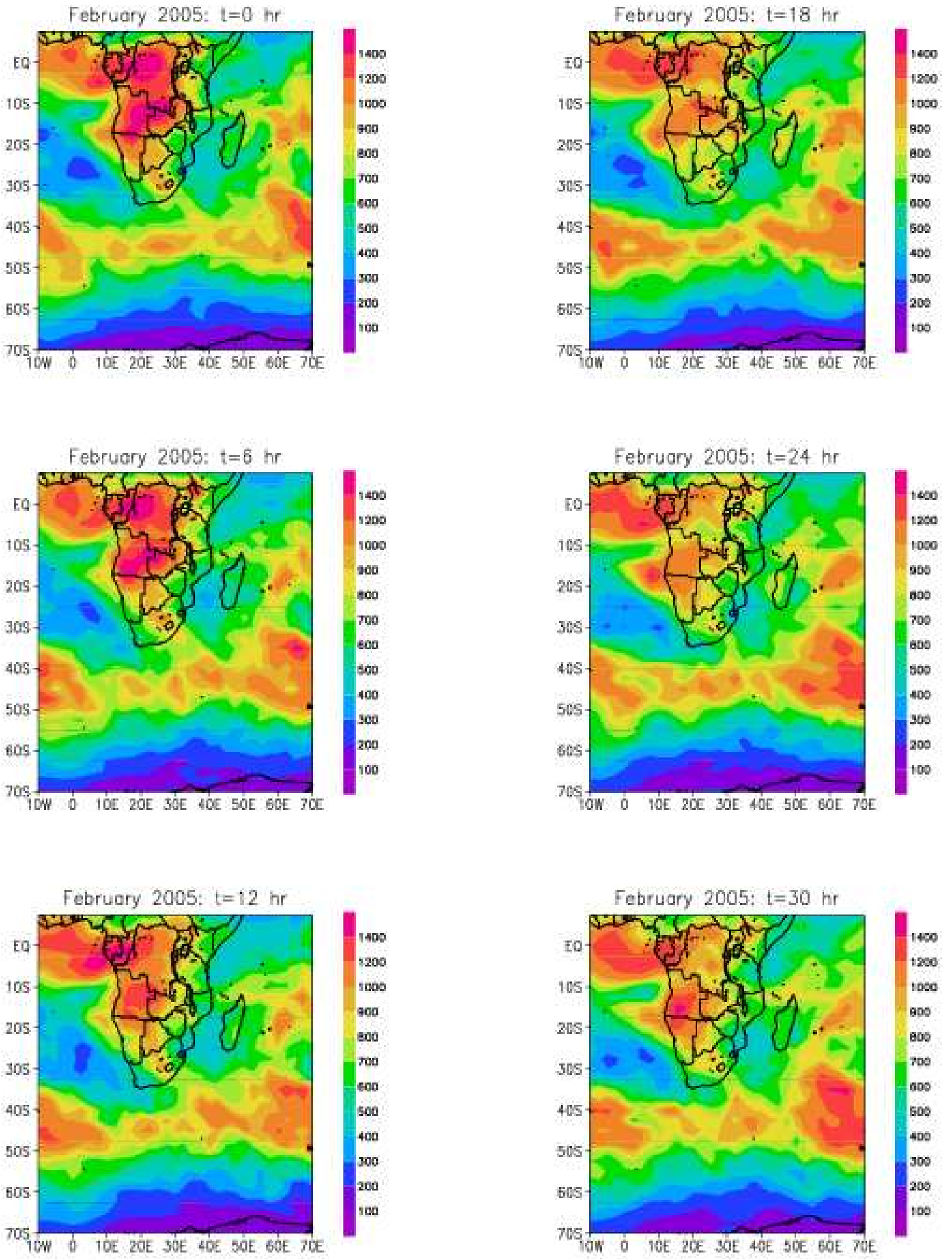
February 2005: t=0 hr

February 2005: t=18 hr

February 2005: t=6 hr

February 2005: t=24 hr

February 2005: t=12 hr

February 2005: t=30 hr

Figure 4.24: Average moisture flux error ($g\,cm^{-1}\,s^{-1}$) in the C-CAM forecasts: February 2005

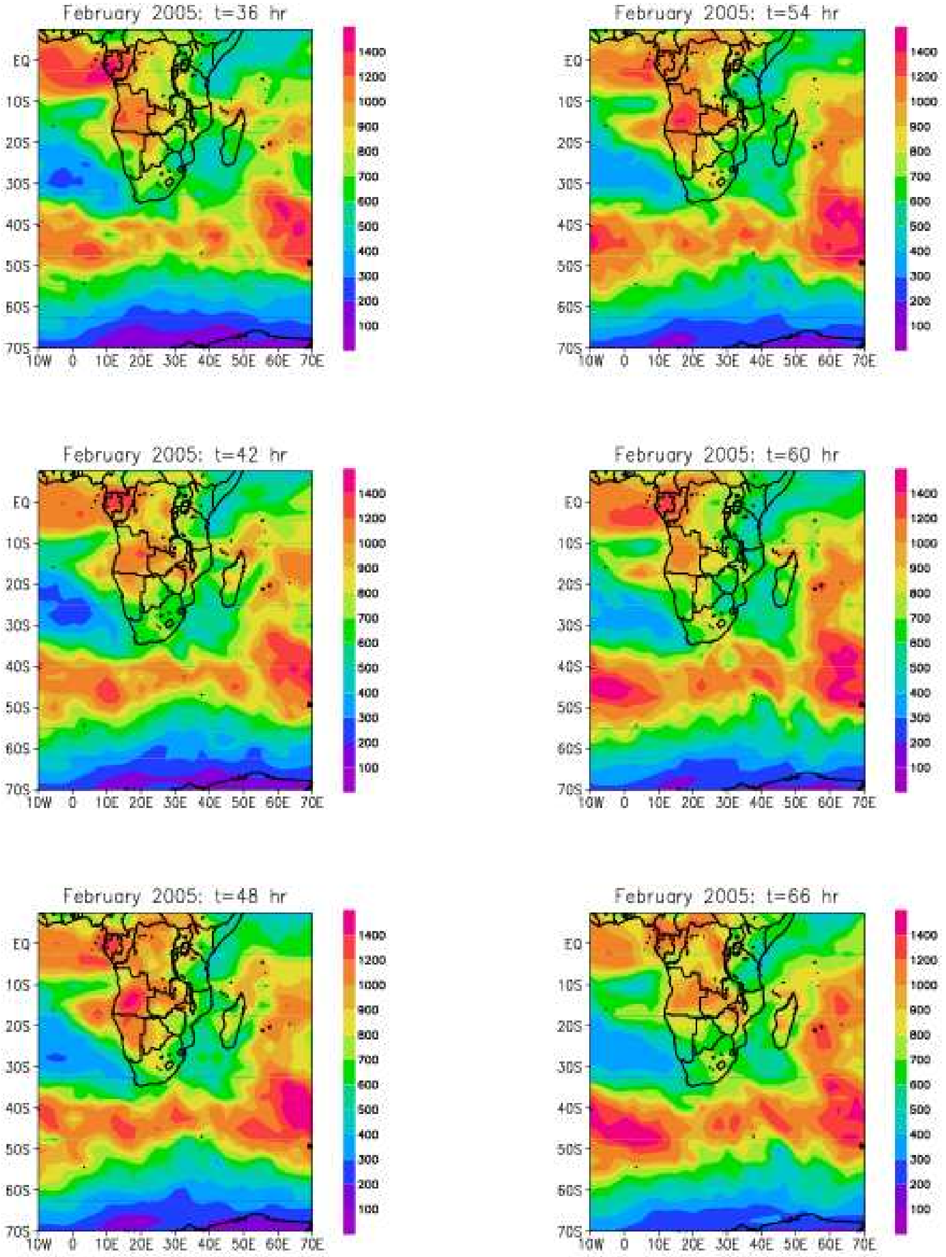

Figure 4.25: Average moisture flux error ($g\,cm^{-1}\,s^{-1}$) in the C-CAM forecasts: February 2005

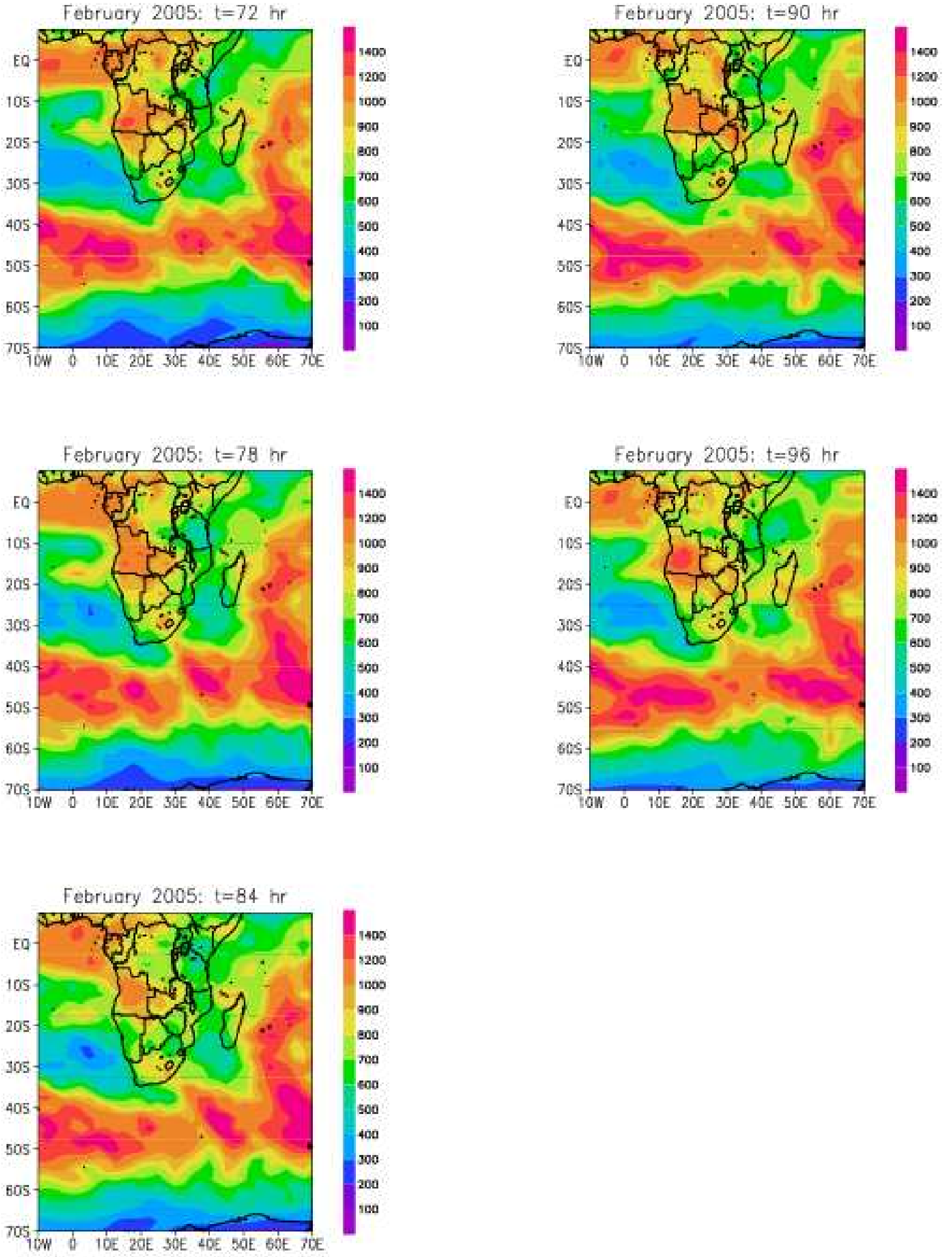

February 2005: t=72 hr

February 2005: t=90 hr

February 2005: t=78 hr

February 2005: t=96 hr

February 2005: t=84 hr

Figure 4.26: Average moisture flux error ($g\,cm^{-1}\,s^{-1}$) in the C-CAM forecasts: February 2005

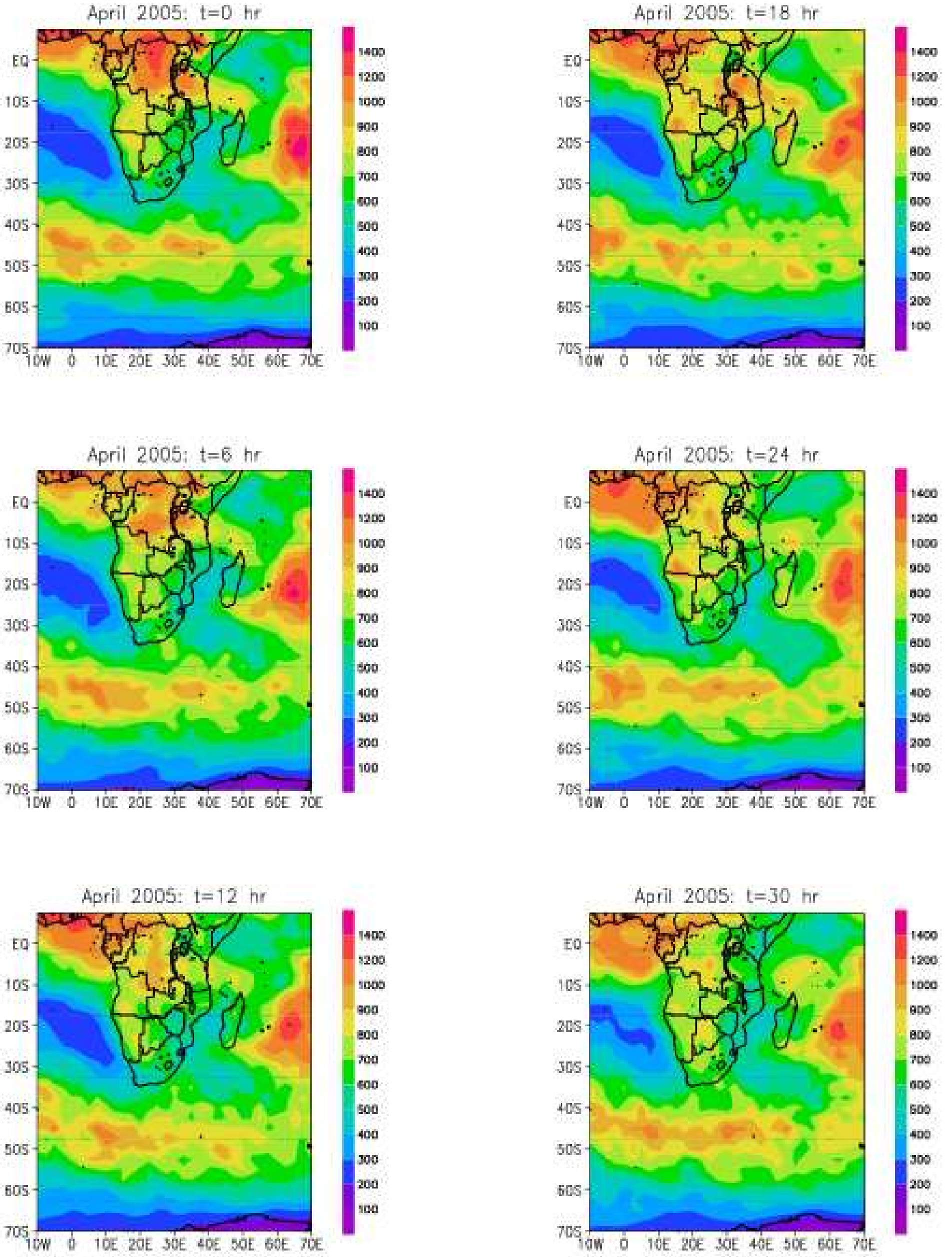

Figure 4.27: Average moisture flux error ($g\,cm^{-1}\,s^{-1}$) in the C-CAM forecasts: April 2005

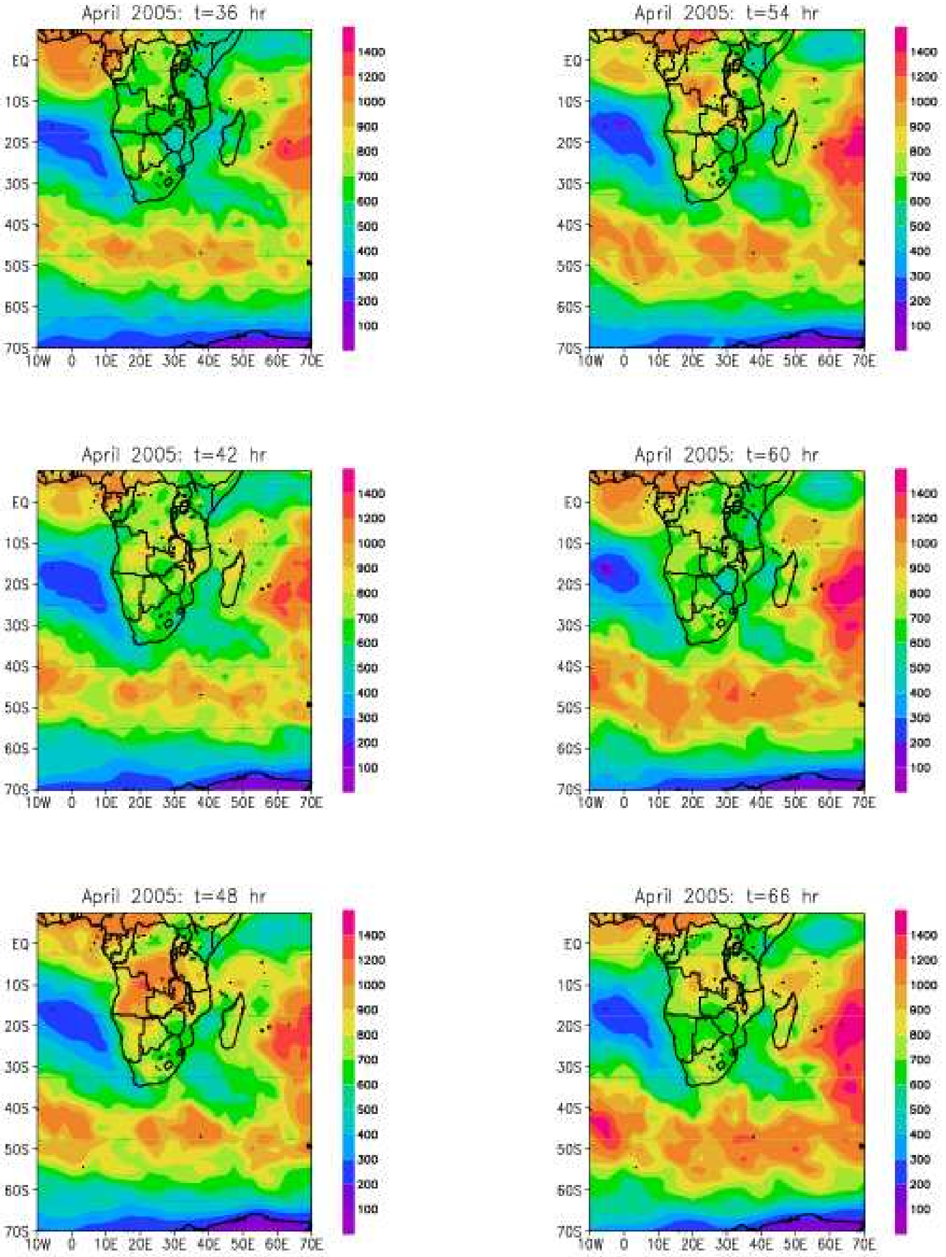

Figure 4.28: Average moisture flux error ($g\, cm^{-1}\, s^{-1}$) in the C-CAM forecasts: April 2005

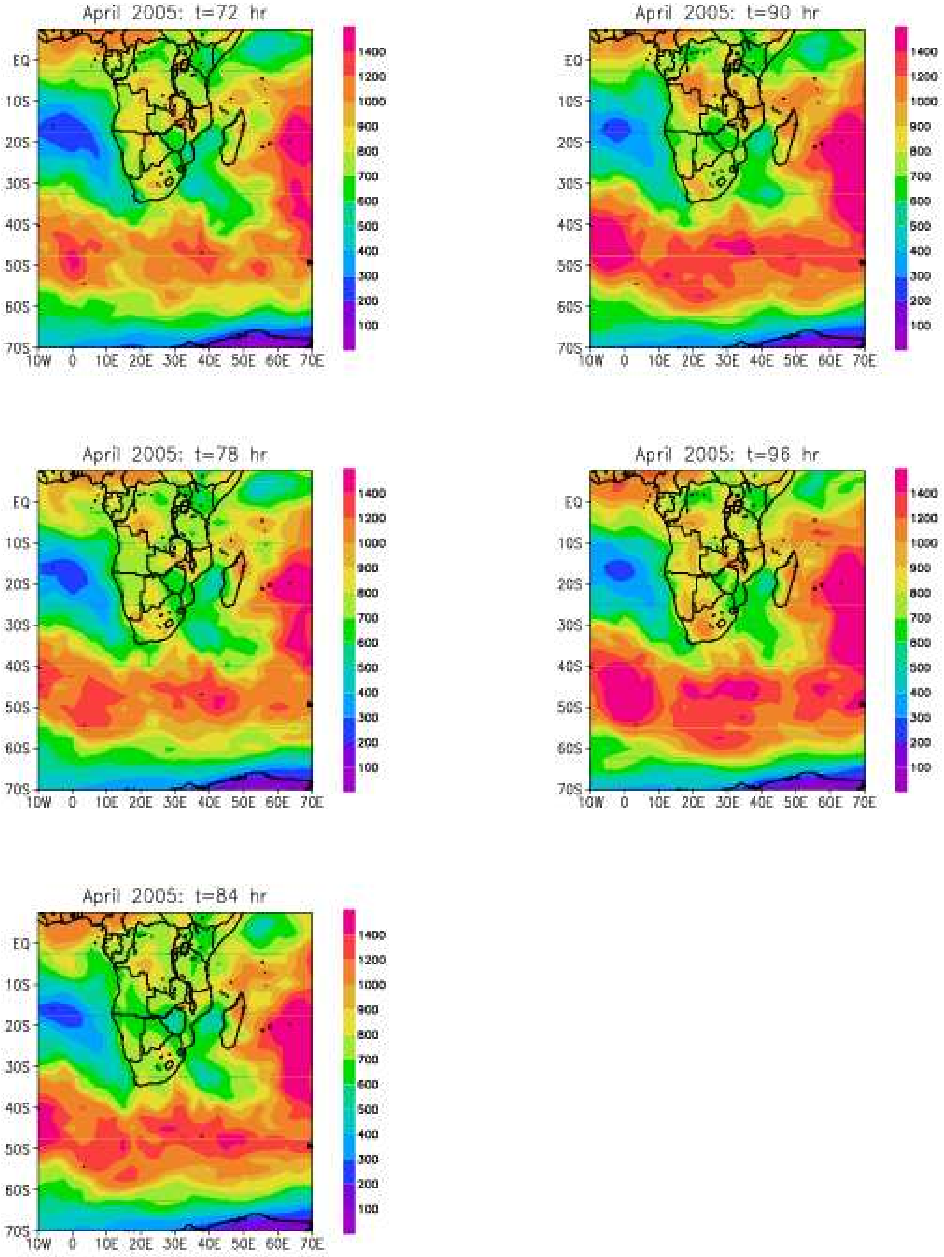

Figure 4.29: Average moisture flux error ($g\,cm^{-1}\,s^{-1}$) in the C-CAM forecasts: April 2005

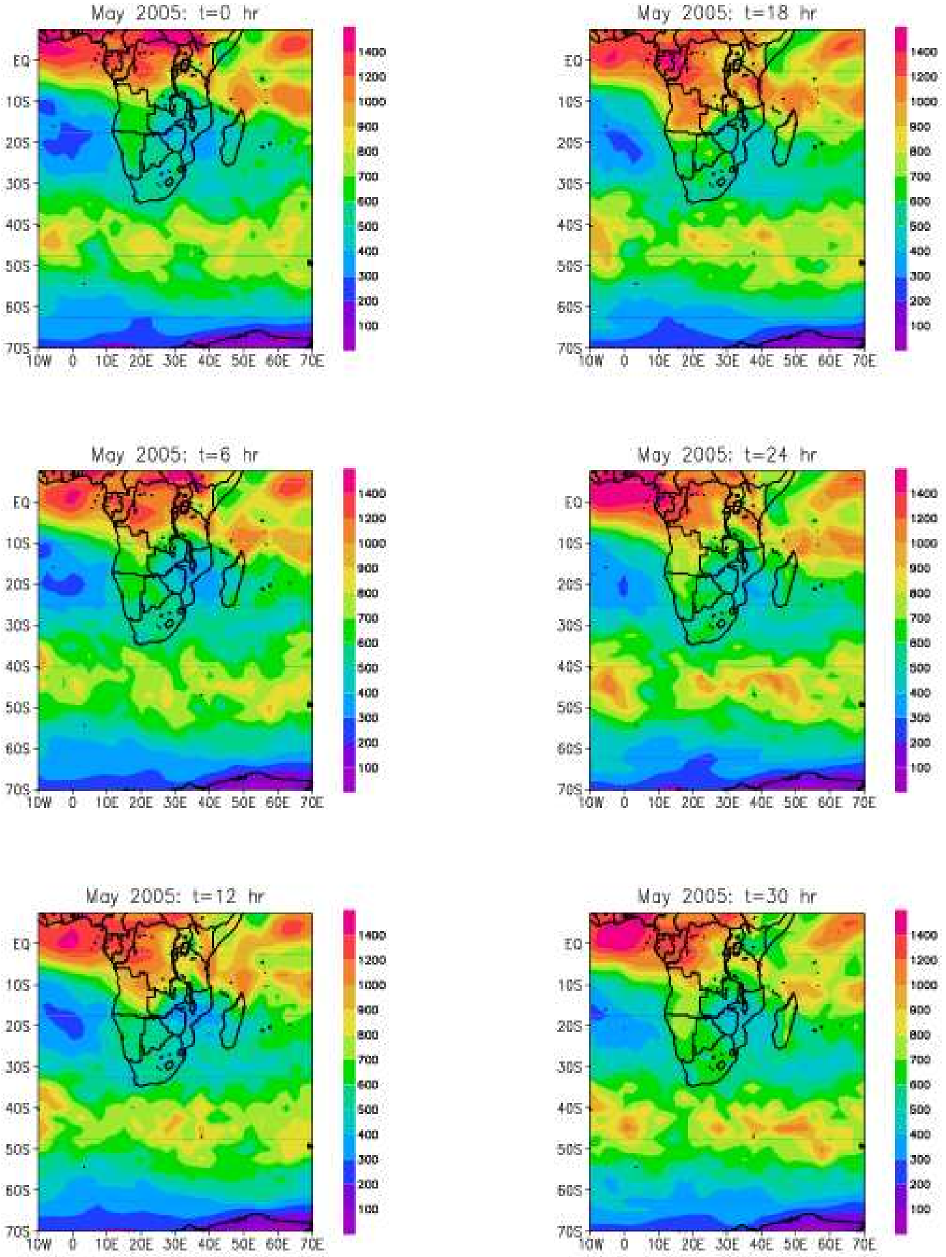

Figure 4.30: Average moisture flux error ($g\,cm^{-1}\,s^{-1}$) in the C-CAM forecasts: May 2006

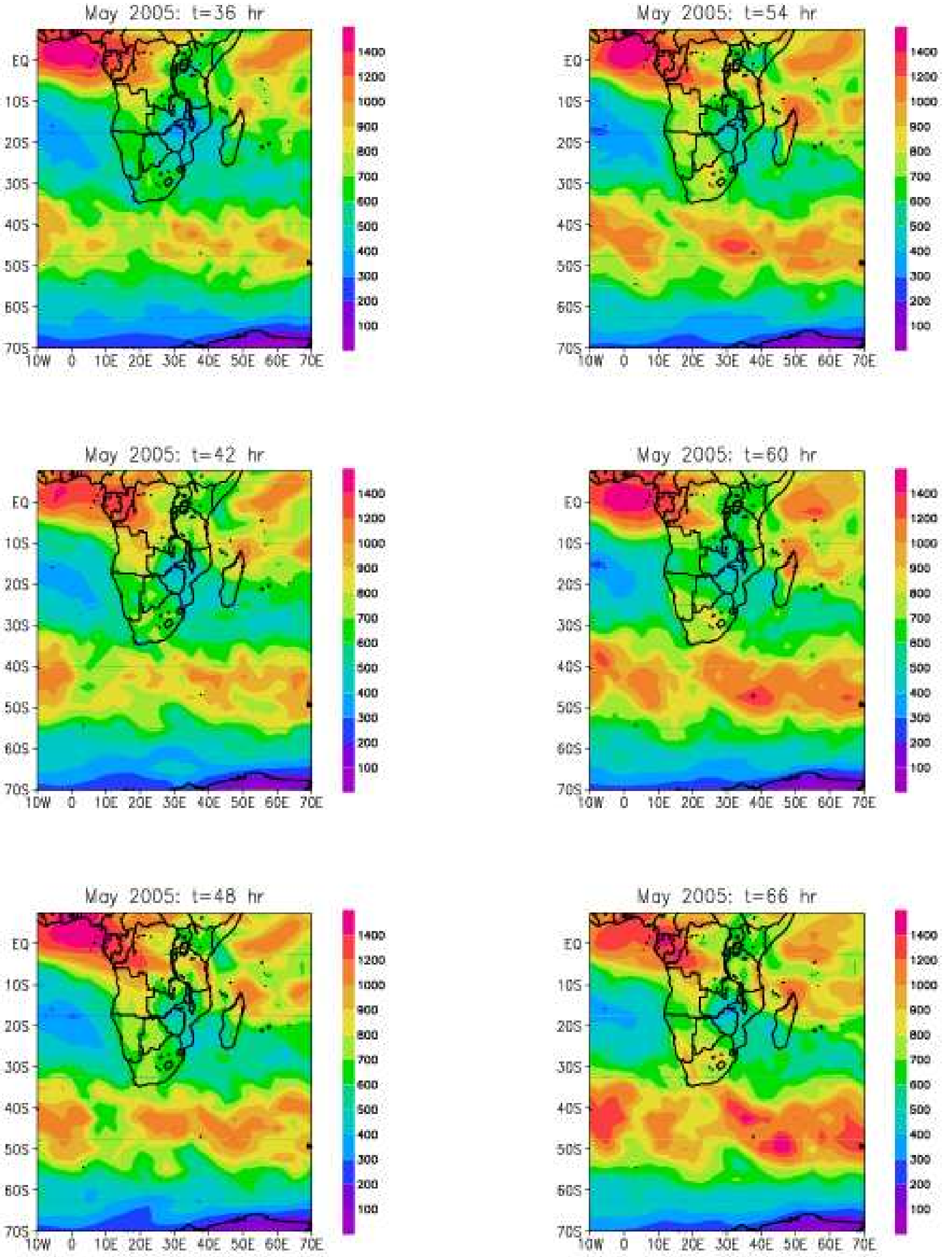

Figure 4.31: Average moisture flux error ($g\,cm^{-1}\,s^{-1}$) in the C-CAM forecasts: May 2006

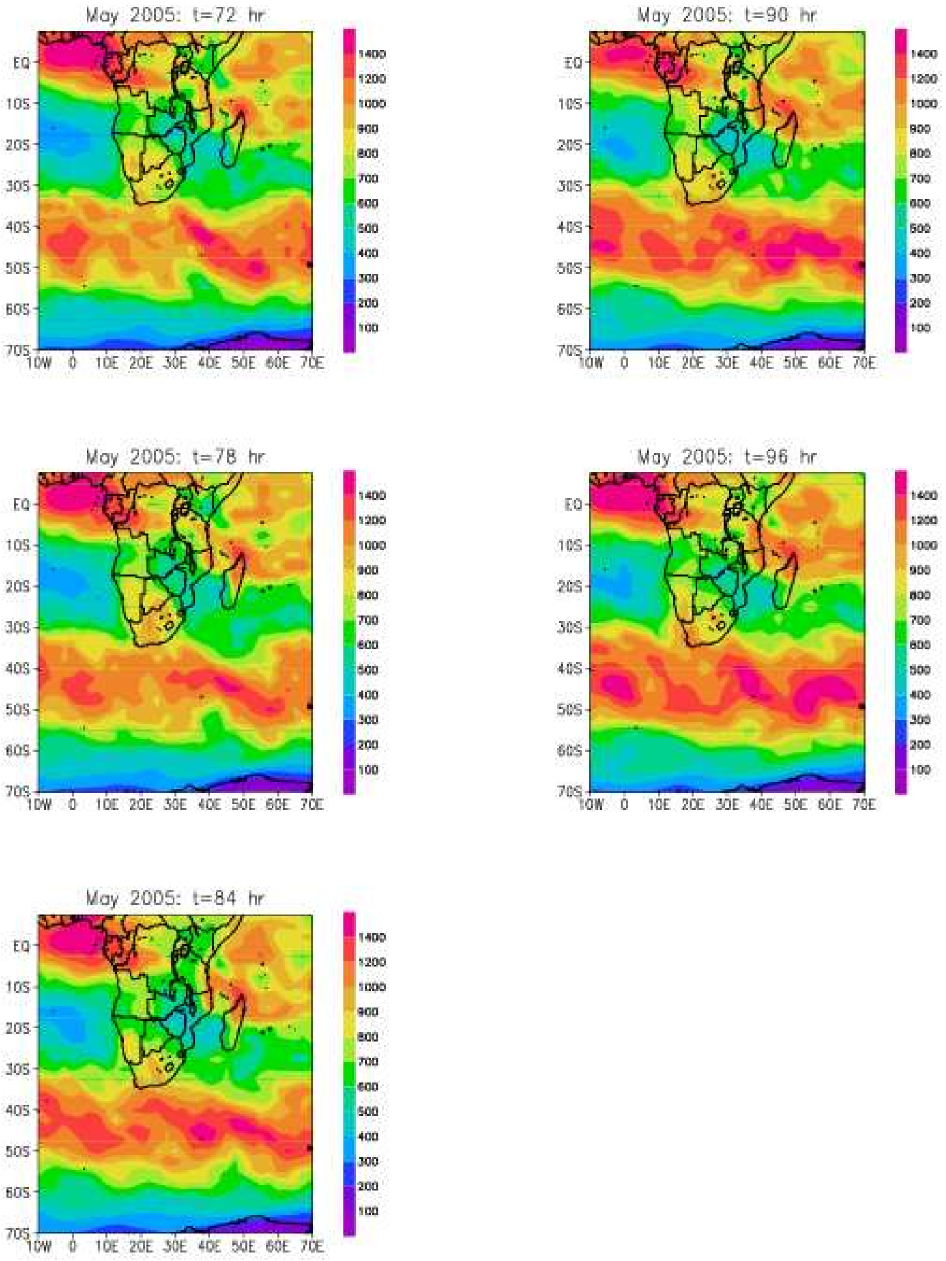

Figure 4.32: Average moisture flux error ($g\,cm^{-1}\,s^{-1}$) in the C-CAM forecasts: May 2005

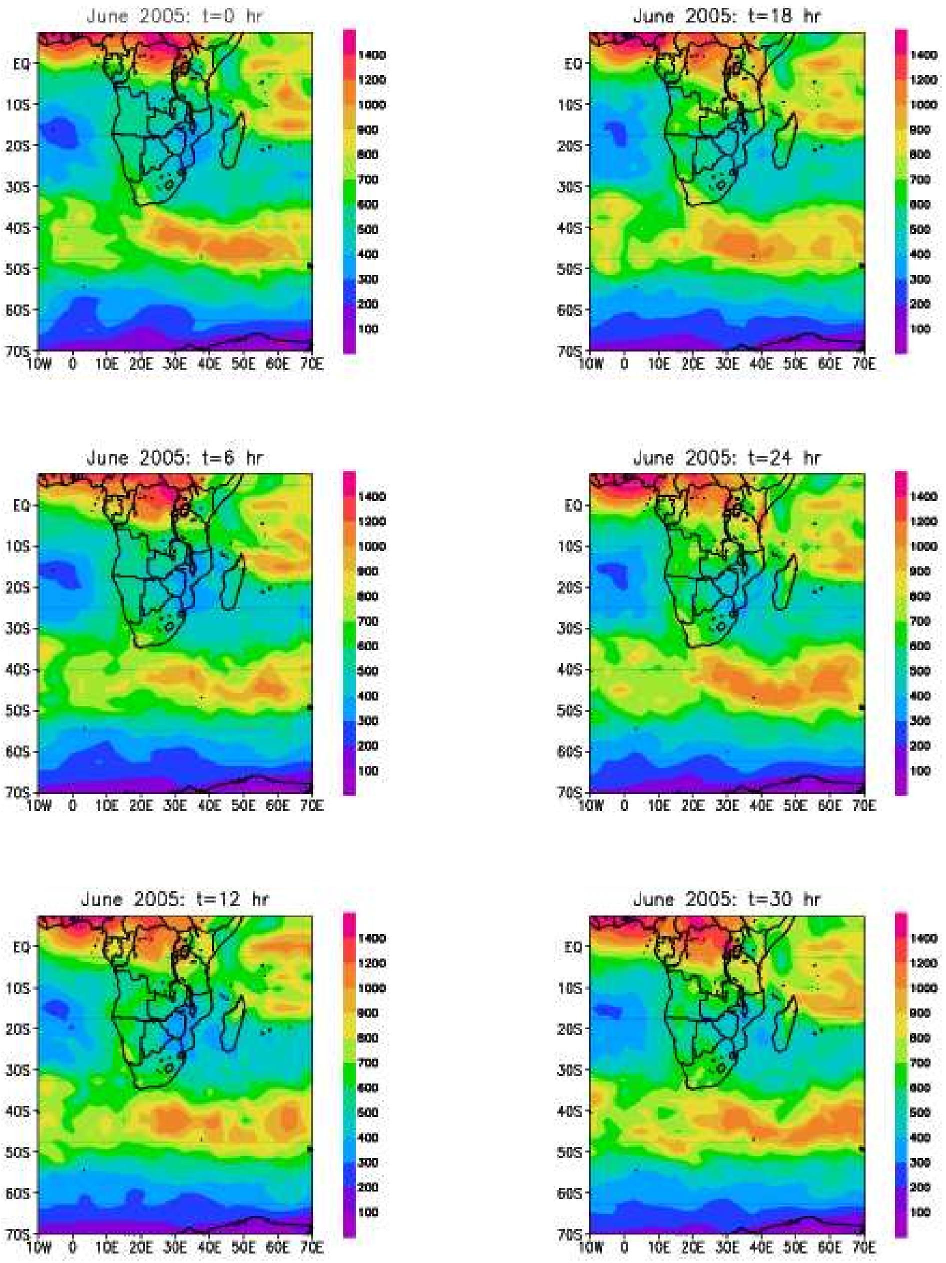
June 2005: t=0 hr

June 2005: t=18 hr

June 2005: t=6 hr

June 2005: t=24 hr

June 2005: t=12 hr

June 2005: t=30 hr

Figure 4.33: Average moisture flux error $(g\,cm^{-1}\,s^{-1})$ in the C-CAM forecasts: June 2005

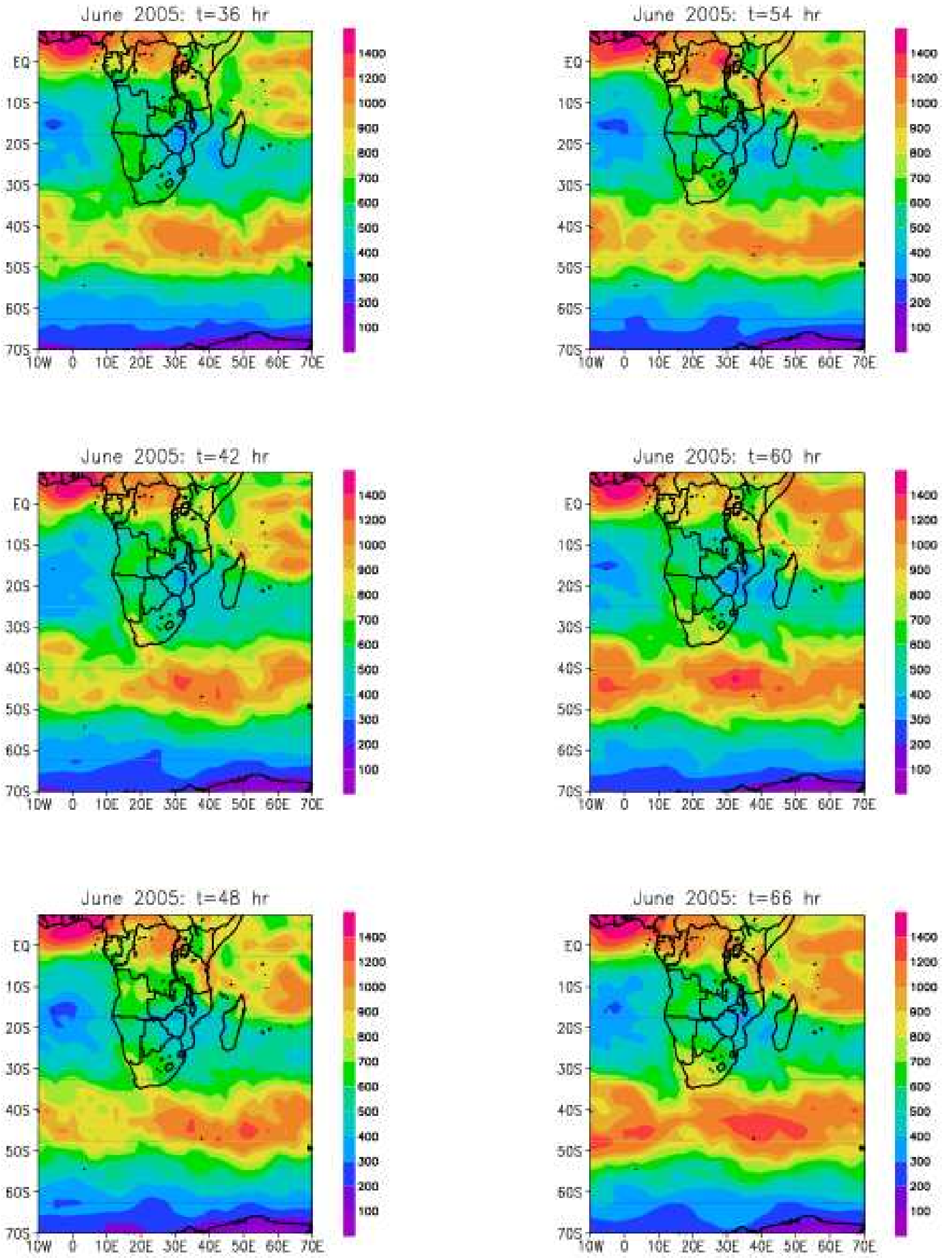

June 2005: t=36 hr

June 2005: t=54 hr

June 2005: t=42 hr

June 2005: t=60 hr

June 2005: t=48 hr

June 2005: t=66 hr

Figure 4.34: Average moisture flux error ($g\,cm^{-1}\,s^{-1}$) in the C-CAM forecasts: June 2005

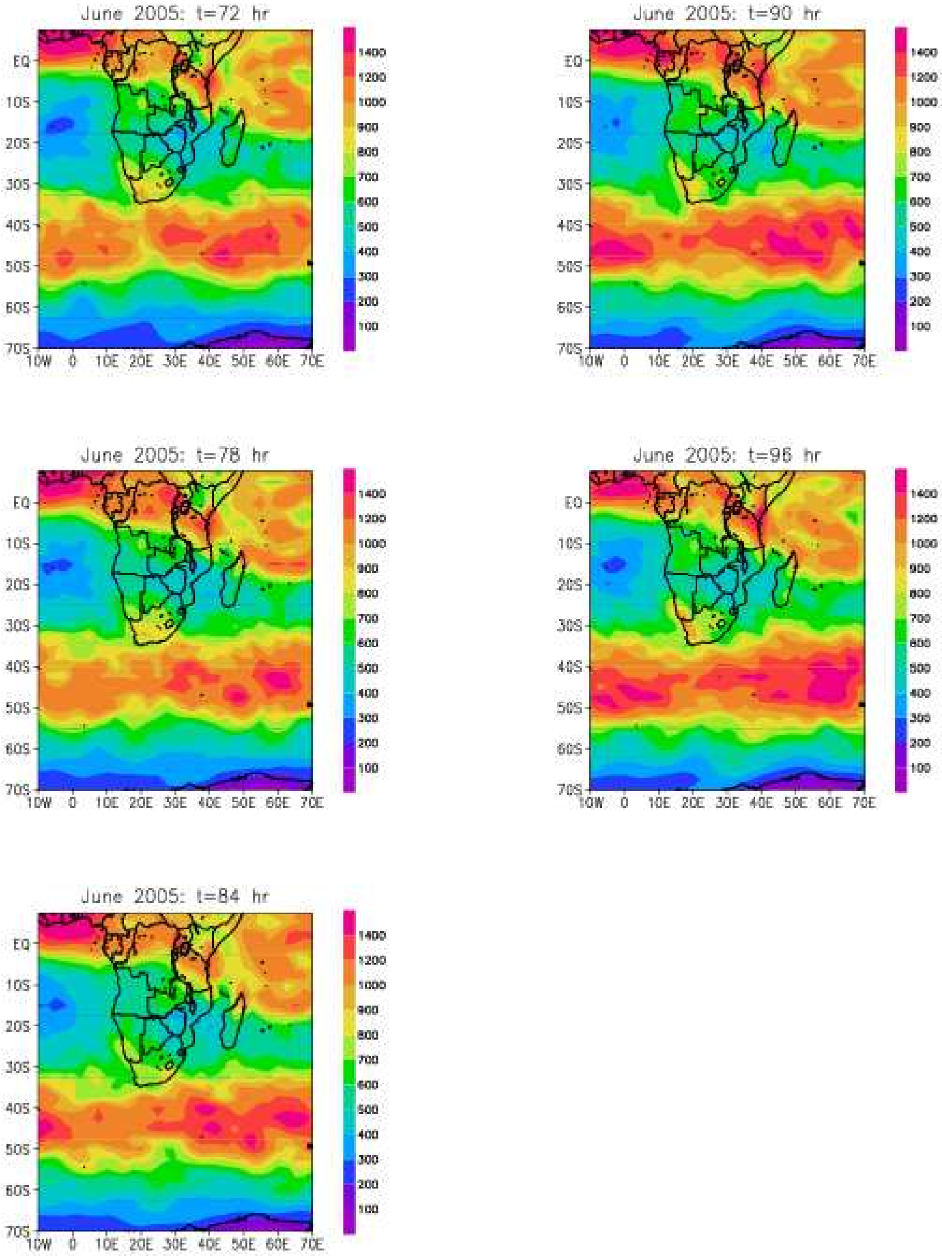

Figure 4.35: Average moisture flux error ($g\,cm^{-1}\,s^{-1}$) in the C-CAM forecasts: June 2005

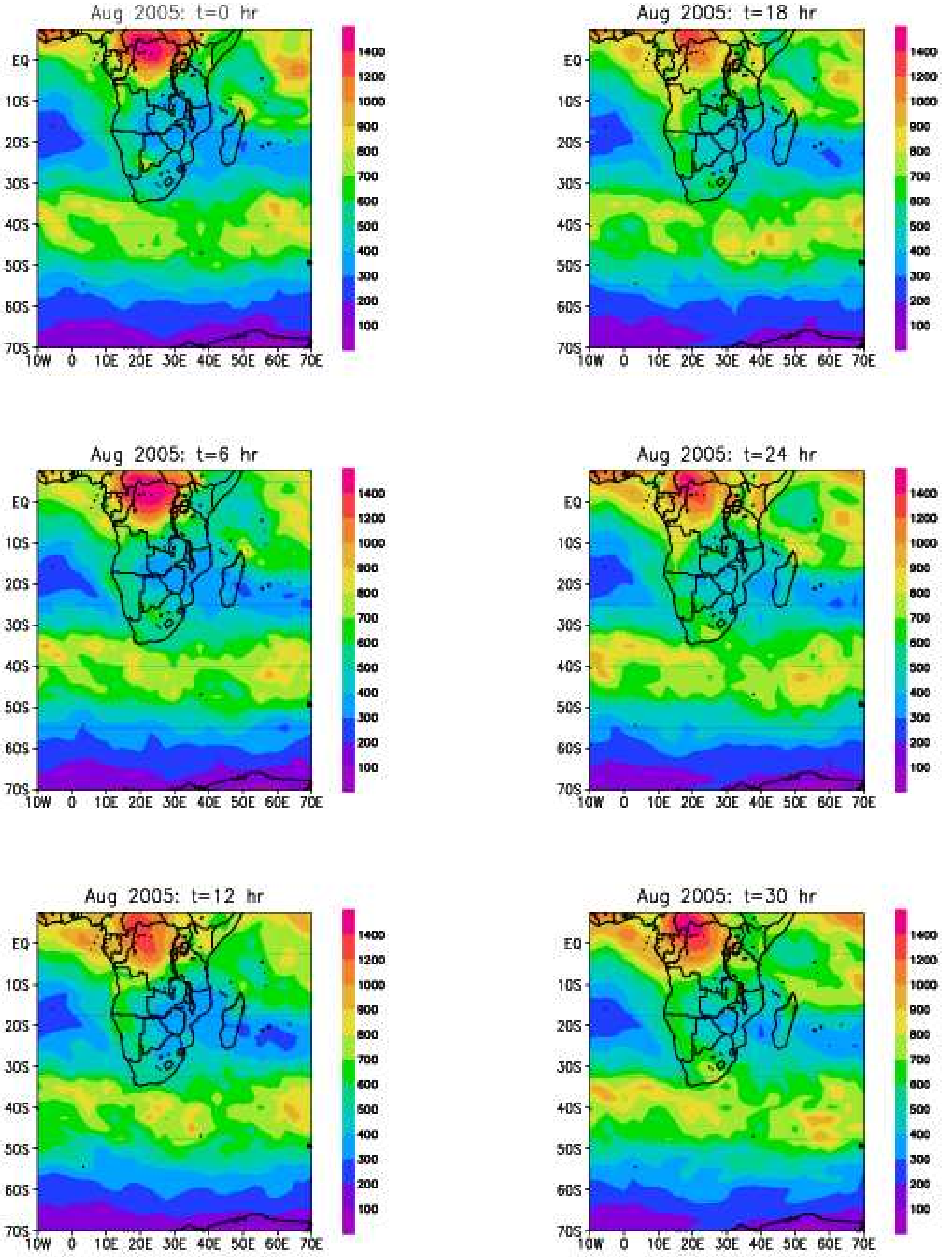

Figure 4.36: Average moisture flux error ($g\,cm^{-1}\,s^{-1}$) in the C-CAM forecasts: August 2005

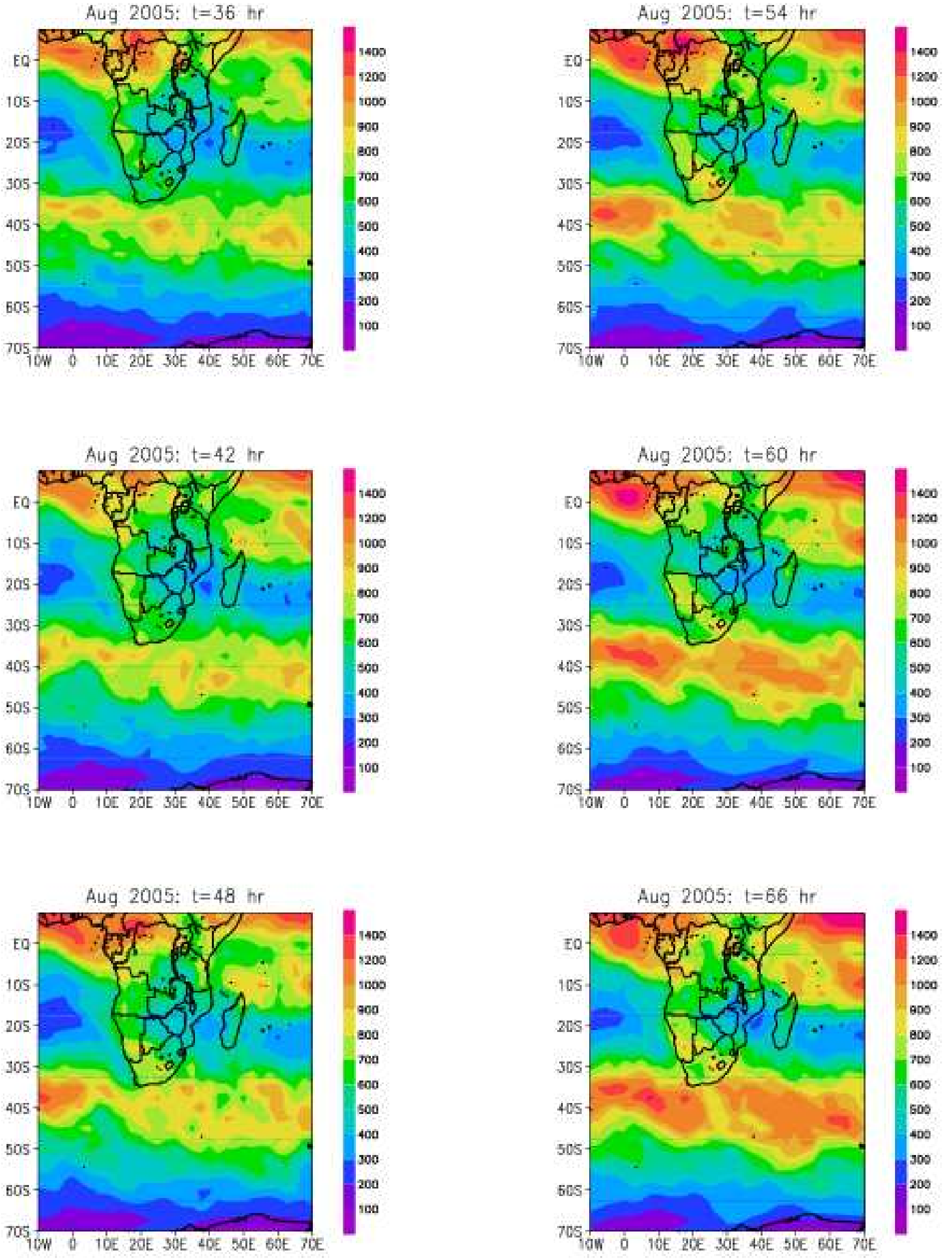

Aug 2005: t=36 hr

Aug 2005: t=54 hr

Aug 2005: t=42 hr

Aug 2005: t=60 hr

Aug 2005: t=48 hr

Aug 2005: t=66 hr

Figure 4.37: Average moisture flux error ($g\,cm^{-1}\,s^{-1}$) in the C-CAM forecasts: August 2005

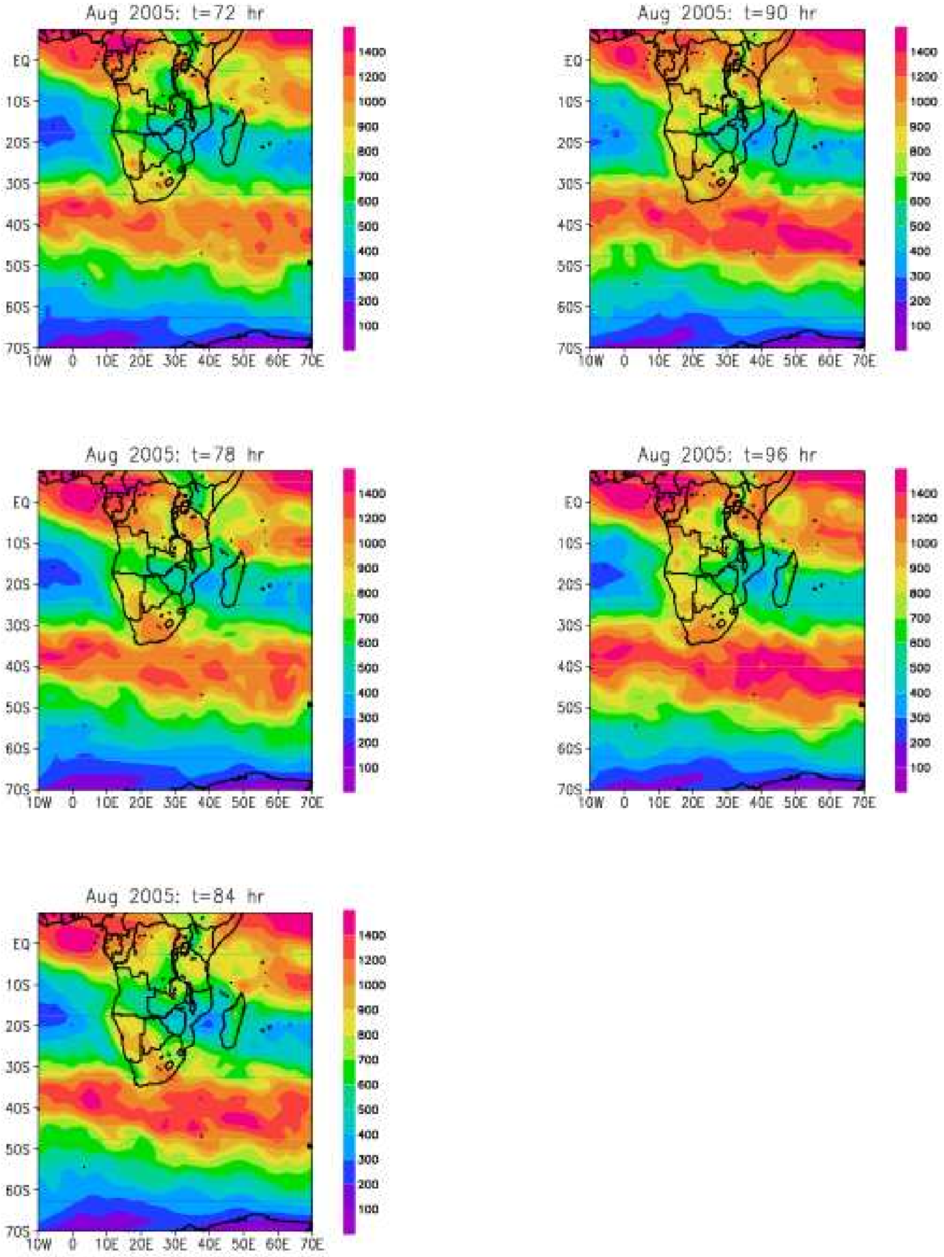

Figure 4.38: Average moisture flux error ($g\,cm^{-1}\,s^{-1}$) in the C-CAM forecasts: August 2005

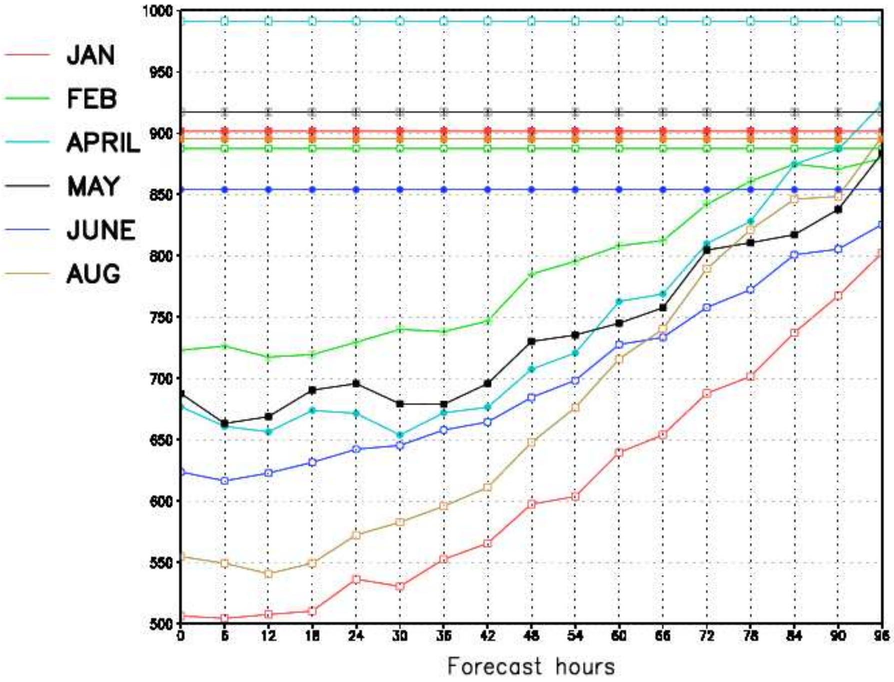

Figure 4.39: The monthly root mean square error ($g\,cm^{-1}\,s^{-1}$) of the NCEP persistence (horizontal lines) and C-CAM forecasts of the zonal moisture flux

model integration progesses. This is clearly the greatest source of error over the country during this month.

The error fields observed in August (figures 4.36,4.37 and 4.38), show close resemblance to that of May and June. The most striking feature is again the two zonal error bands. With regard to the meridional error band, there is closer correspondence between the fields of August and May than between August and June. During August and May, the meridional error band is visibly better defined than during June. Further, the contribution of errors from the north in over South Africa is larger during August than in May. This can probably be explained by the fact that conditions become less subsident during August while it becomes more subsident during May.

4.4.2.2 Root mean square error

The root mean square error has been seperately calculated for the zonal (figure 4.39) and the meridional (figure 4.40) moisture flux components. In both cases the C-CAM forecasts of the vertically integrated moisture flux were better than the 24-hour persistence forecasts over the full four day integration period. The

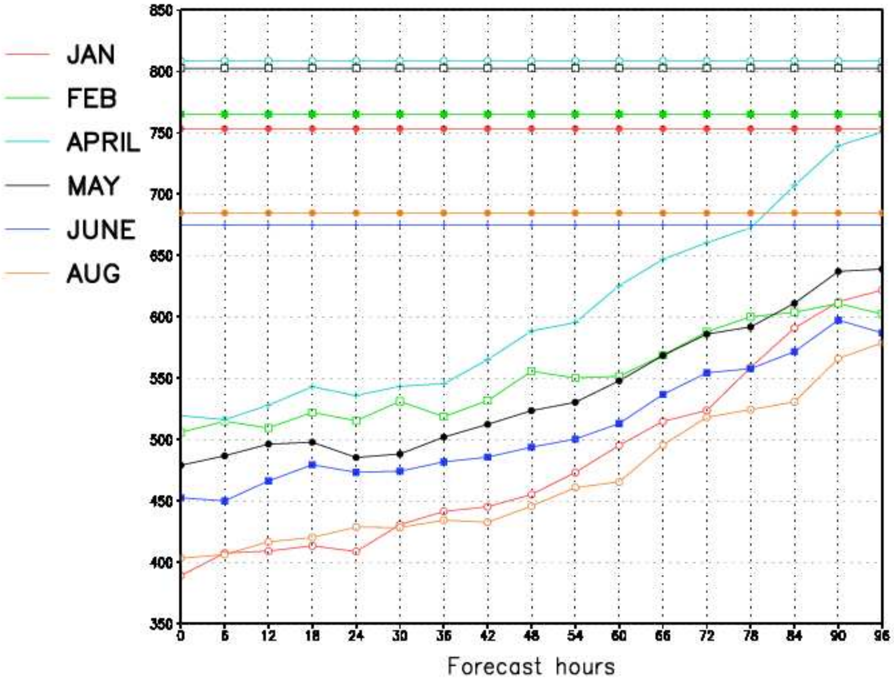

Figure 4.40: The monthly root mean square error ($g\,cm^{-1}\,s^{-1}$) of the NCEP persistence (horizontal lines) and C-CAM forecasts of the meridional moisture flux

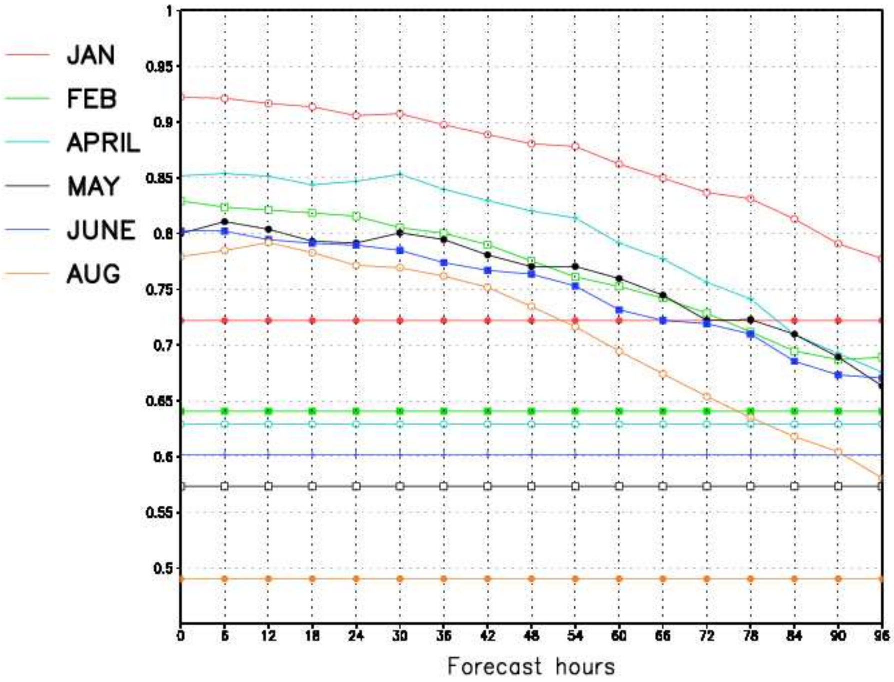

Figure 4.41: The monthly pattern correlation of the NCEP persistence (horizontal lines) and C-CAM forecasts of the zonal moisture flux

errors started to grow more rapidly at about the 8th integration time (42-hour forecast). The meridional errors were in general smaller than the zonal errors. This is because, seen over the whole output domain, the zonal transport of moisture is much larger than the meridional transport of moisture (e.g. D'Abreton and Lindesay, 1993).

4.4.2.3 Pattern correlation

The pattern correlations calculated for the zonal (figure 4.41) and meridional (figure 4.42) moisture fluxes, as the corresponding root mean square errors, indicates that the C-CAM forecasts are better than the 24-hour persistence forecasts for the full four day integration period. The rate at which the errors grow, started to increase significantly after 54-hours. The pattern correlations for the meridional fluxes were considerably less than those for the zonal fluxes. This suggest that the model simulated the meridional moisture transport patterns less well than the zonal patterns.

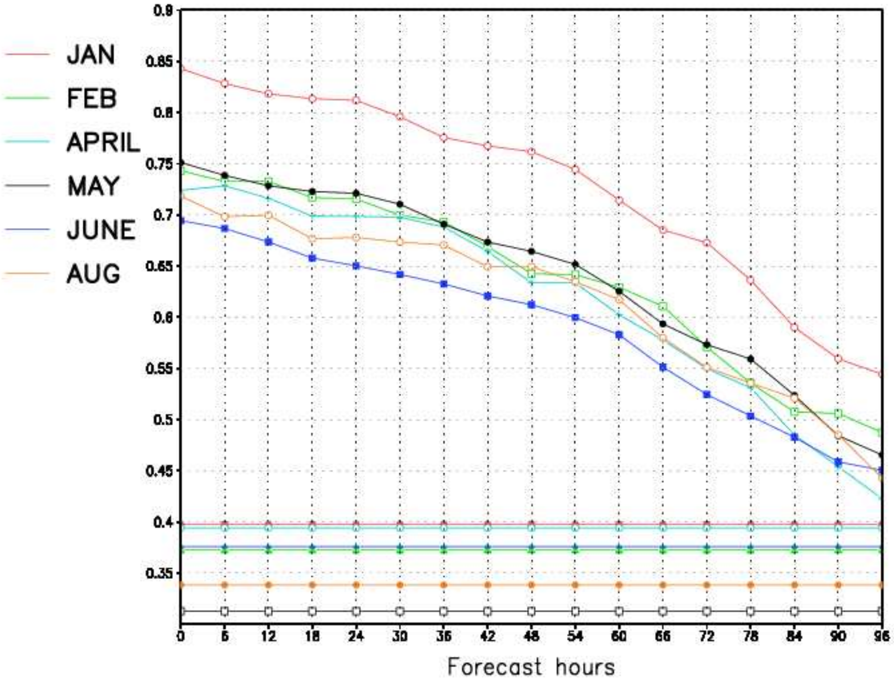

Figure 4.42: The monthly pattern correlation of the NCEP persistence (horizontal lines) and C-CAM forecasts of the meridional moisture flux

4.5 Point verification

4.5.1 Point verification at the Cape Town weather office station

4.5.1.1 Average absolute error

The largest average absolute errors occurred during all of the months near the surface and at 200 hPa in the vicinity of the troposphere. The tendency for larger errors to occur near the surface can probably be explained by topographical influences. The larger errors at 200 hPa are probably linked to being in the vicinity of the troposphere. During January and February, the errors near the surface were larger than those at 200 hPa, while the opposite was true for April, May, June and August. Also, the errors in the low-levels were generally larger in January and February compared to the other months. Both these features are probably linked to the characteristic easterly winds that occur often over this region during summer. This happens as a surface high pressure system ridges in over the eastern part of the country and a tight pressure gradient is established from the interior towards the coast. The easterly flow created in this way has to decent over the escarpment to reach the coastal regions. The larger errors can probably be linked to this physical process that is not fully captured in the model simulation.

In the mid -and upper levels, January and February had generally the smallest errors. This is probably because during these months the weather systems are mostly barotropic in nature. At 200 hPa, April, May and June are the months with the largest errors. May and June are winter months while April is a transitional month. During these months, the westerly wind belt is situated more northwards compared to the other months under investigation. Jet streams are also located more frequently over the country during the winter months. They are characterised by tight temperature gradients, which are likely to contribute to the larger errors observed at these levels.

4.5.1.2 Average bias

The largest monthly average bias occurres near the surface and at 200 hPa, in the vicinity of the tropopause, except for one month (August) where it occurres at 300 hPa. For all of the months the largest low-level bias occurred at 1000 hPa, except for January and February where the largest low-level bias occurred at 950 hPa. In all of these months a cold bias (about $1-2°C$) occurred from 1000 hPa to 900 hPa. From 900-800 hPa all months had a cold bias except for June and August which had a small warm bias. It is interesting to note that the two summer months, January and February, were the last months to move over to a warm bias at 700 hPa. This characteristic cold bias observed in January and February from the surface to about 700 hPa is most likely due to easterly winds and the resultant adiabatic warming that is not captured fully by the model

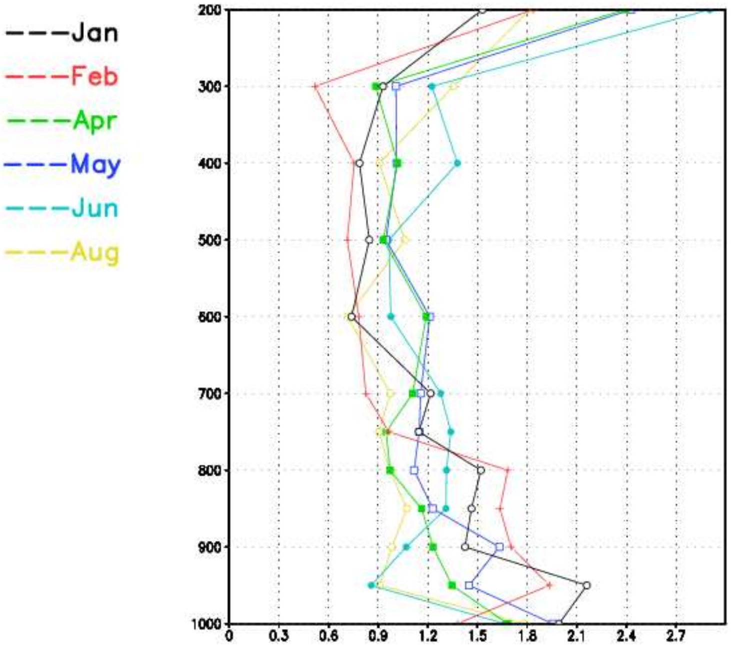

Figure 4.43: The monthly average absolute error of the 24-hour temperature C-CAM forecasts (^{O}C) at Cape Town

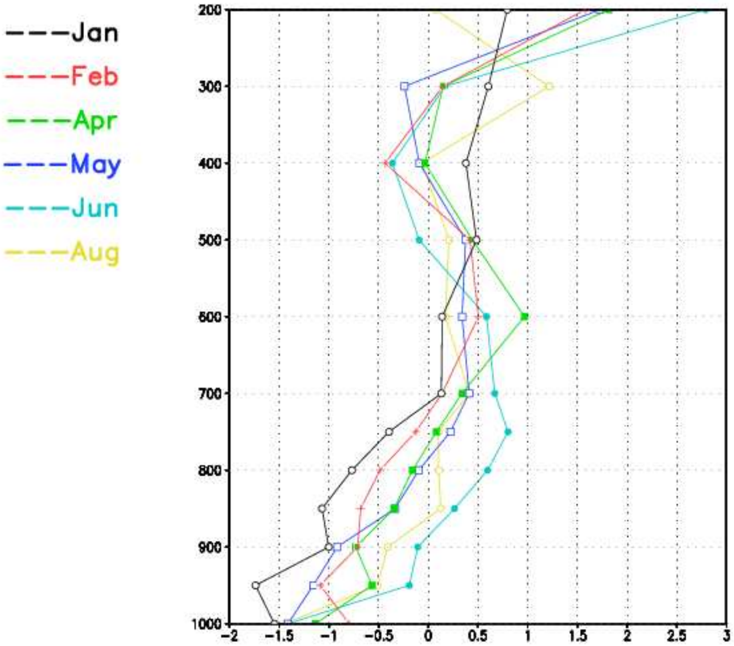

Figure 4.44: The monthly average bias of the 24-hour temperature C-CAM forecasts (^{O}C) at Cape Town

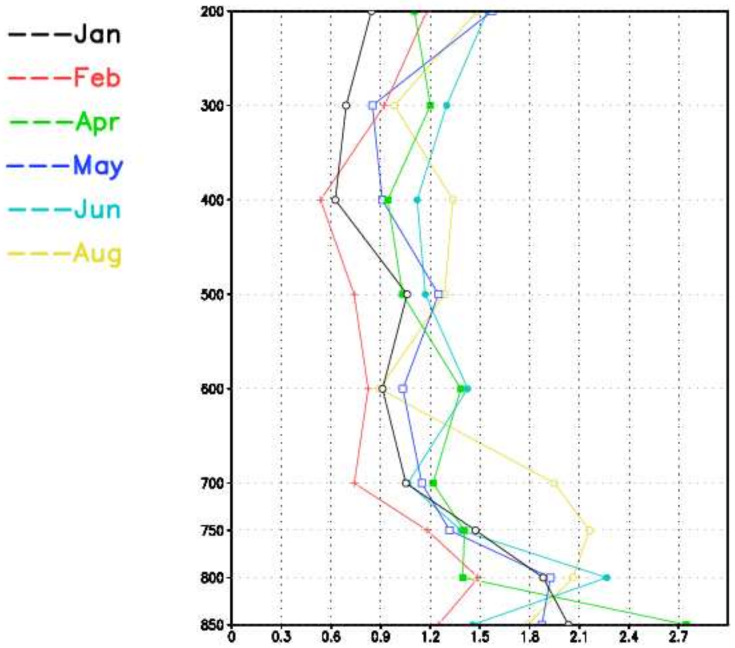

Figure 4.45: The monthly average absolute error of the 24-hour temperature C-CAM forecasts (^{O}C) at Irene

simulation (as described in 4.5.1.1). A warm bias ($< 1°C$), is characteristic of the mid-troposphere. There is a tendency towards a cold bias again at 400 hPa. Only January had a warm bias at that level. Towards the top of the troposphere, a warm bias is dominant. This is most likely due to tropopause height characteristics that are not fully captured in the model forecast.

4.5.2 Point verification at the Irene weather office station

4.5.2.1 Average absolute error

The largest errors occurred in the low-levels while a secondary maximum occurred during 4 of the 6 months at 200 hPa. It was quite striking that the errors at 200 hPa are much smaller than the errors at this level at Cape Town ($1.5 - 3°C$). The reason for this is probably because Cape Town is more under the influence of upper westerly waves, and therefore the height of the tropopause vary more frequently, while Irene is situated in the region where the mean circulation is anticyclonic (see chapter 2).

The larger errors close to the surface can again be due to topographical influences. The most striking feature of the errors in the low-levels is probably the August error that had it's maximum at 750 hPa. The magnitude of the August

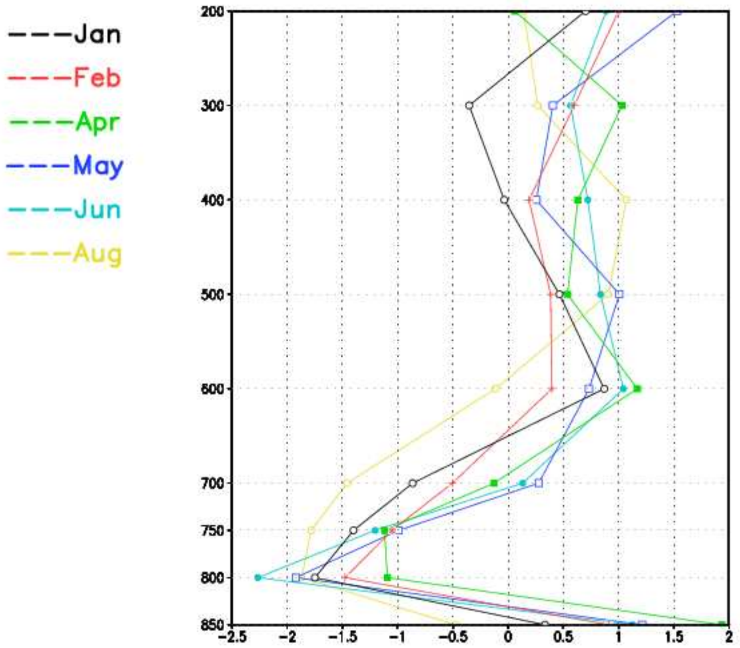

Figure 4.46: The monthly average bias of the 24-hour temperature C-CAM forecasts (^{O}C) at Irene

error is strikingly larger at 750 hPa and 700 hPa compared to the other months. Errors were generally the smallest in the mid-levels.

4.5.2.2 Average bias

A significant cold bias occurred at 800 hPa and 750 hPa as well as for four of the six months at 700 hPa. Except for August and January, all of the months had a warm bias (about $< 1.5°C$) from 600 hPa to 200 hPa. August had a very small cold bias at 600 hPa while January had a small cold bias at 400 hPa and 300 hPa. The cold bias at 800 hPa ($between\ -2.5°C\ and\ -1.5°C$) was the largest in magnitude compared to the other levels, for all of the months with the exception of April. This appears to be a significant bias because it is observed in all of the months. The implication of this bias as well as the warm bias that occurs most of the time in the mid -and upper tropospere is that a model sounding can under-estimate the instability of the environment.

Chapter 5

Subjective verification of C-CAM

5.1 Introduction

In this chapter C-CAM forecasts are verified subjectively by means of case studies. The objective is to determine the usefulness of C-CAM for operational short-term weather forecasting over South Africa. The weather events studied include a cut-off low that moved over the southwestern part of South Africa and a thunderstorm event that occurred over the eastern interior of South Africa. In the case of the cut-off low event, heavy rainfall occurred in places along the Cape south coast. The thunderstorm event that is discussed in the second case study, exhibited a wedge shape on satellite images which is indicative of a severe storm. In this chapter it is determined whether prognostic C-CAM fields, that would typically be used by a weather forecaster in the operational environment, could have been used to predict the mentioned severe weather events. The C-CAM forecasts are verified at the synoptic scale by means of a subjective comparison to NCEP reanalysis data. Observational data such as METARs, SYNOPs and upper air soundings obtained from the SAWS was also used in the verification process. A discussion on the subjective verification results are given in section 5.2.7 and 5.3.6.

5.2 Case study 1: The cut-off low of 10-11 April 2005

5.2.1 Introduction

A cut-off low system occured over the southwestern part of South Africa on the 10th and 11th of April, 2005. The vortex of the system was confined to the Western -and Eastern Cape. The 24-hour rainfall totals as recorded at 0600Z

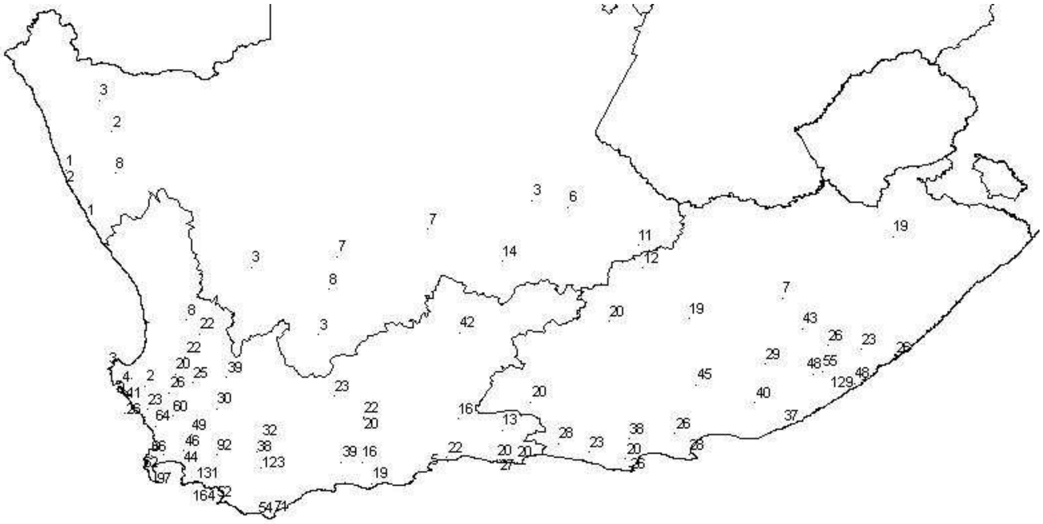

Figure 5.1: The observed rainfall for the period 0600Z 10 April 2005 to 0600Z 11 April 2005 (data obtained from the South African Weather Service)

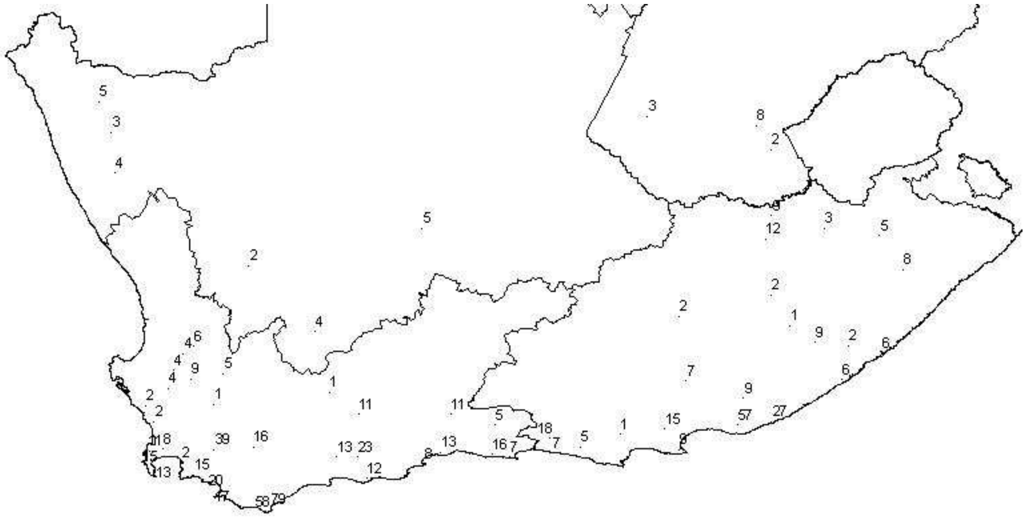

Figure 5.2: The observed rainfall for the period 0600Z 11 April 2005 to 0600Z 12 April 2005 (data obtained from the South African Weather Service)

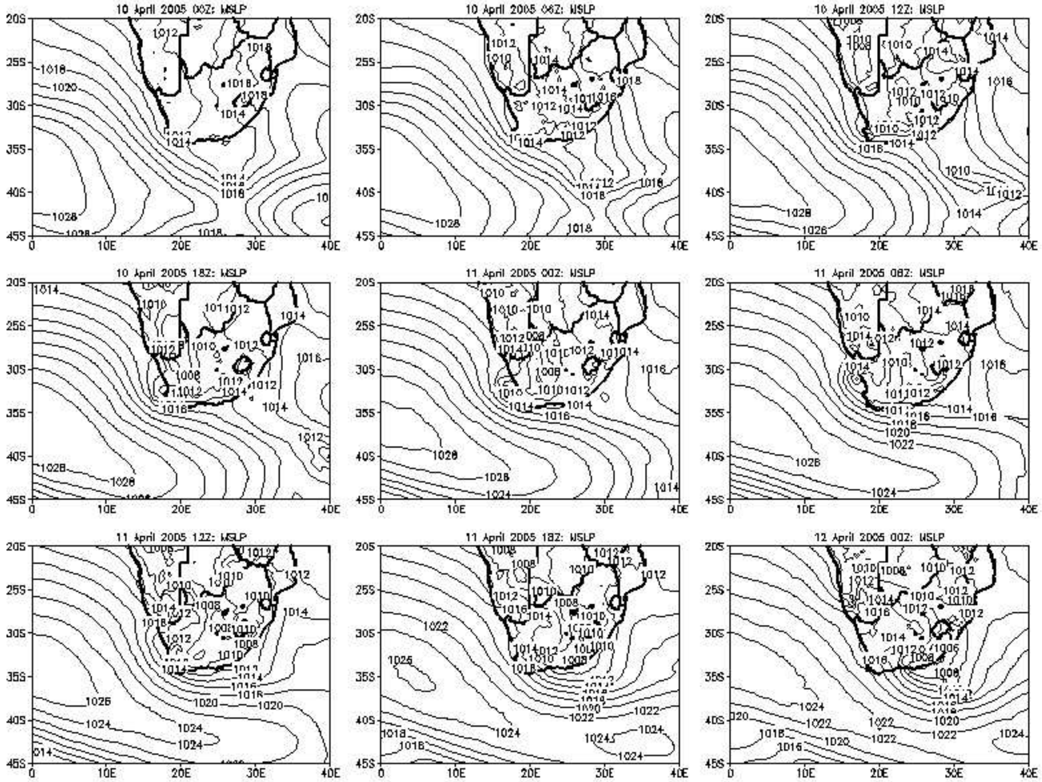
10 April 2005 00Z: MSLP
10 April 2005 06Z: MSLP
10 April 2005 12Z: MSLP
10 April 2005 18Z: MSLP
11 April 2005 00Z: MSLP
11 April 2005 06Z: MSLP
11 April 2005 12Z: MSLP
11 April 2005 18Z: MSLP
12 April 2005 00Z: MSLP

Figure 5.3: C-CAM prognosis of the sea level pressure for 10 April 2005 0000Z to 12 April 2005 0000Z

on the 10th and 11th are displayed in figures 5.1 and 5.2 respectively. The highest falls occurred along the coastal areas of the Western -and Eastern Cape, while good falls were experienced over the southwestern and southern interior as well (figure 5.1 and figure 5.2). Along the coast, more than 100 mm fell at Hermanus (164 mm), Kleinmond (131 mm), Tygerhoek (123 mm) and Kidds Beach (129 mm) for the 24 hour period ending at 0800 SAST on the 11th of April 2005. The rainfall totals recorded for the succeeding 24 hour period were smaller, with the highest falls at Struisbaai (79 mm), Cape Agulhas (58 mm), Alexandria (57 mm) and Tygerhoek (41 mm).

5.2.2 Description of the synoptic pattern as simulated by the 20050410 0000Z C-CAM run

5.2.2.1 Sea-level pressure (SLP)

On the 10^{th} of April at 0000Z, the Atlantic Ocean High was situated southwest of South Africa at about $38°S$, with a central pressure of 1028 hPa (figure 5.3). It extended an elongated ridge eastwards south of the country on the 10^{th}, whilst a surface trough that was initially situated over the extreme western part of South Africa, moved eastwards towards the central interior. This surface trough stretched from Namibia southeastwards. At 0000Z on the 10^{th}, this surface trough was linked to an area of low pressure off the coast in the vicinity of Port Elizabeth. This area of low pressure moved away to the southeast, as the Atlantic Ocean High extended its ridge eastwards south of the country, but maintained a link with the surface trough over the interior of South Africa. By 1800Z on the 10^{th} the formation of a new low pressure area was visible off the west coast, in the vicinity of Cape Columbine. This weak low moved slightly northwards on the 11^{th} while weakening, and by 1800Z it has filled up. The surface trough moved further eastwards and was situated over the eastern interior by 0000Z on the 12^{th}. During this whole time it extended northwestwards over parts of Botswana and Namibia. Although the surface trough moved in an easterly direction, it lagged over the eastern parts of the Western Cape as well as the Eastern Cape. Between 1800Z (11^{th}) and 0000Z (12^{th}) it spilled off the Eastern Cape coast. This circulation pattern was obviously linked to the cut-off low higher up in the troposphere. The effect of this area of low pressure along and off the southeast coast, was to prevent the ridge of the Atlantic Ocean High to move in over the country. A new high pressure centre formed in the forward part of the ridge by 1800Z. This centre was situated far off the southeast coast of South Africa (see chapter two, section 2.5.5). The center of the Atlantic Ocean High southwest of South Africa weakened to 1024 hPa by 0000Z on the 12^{th} and has moved slightly northwards from its original position.

5.2.2.2 700 hPa

At this level the temperature trough and associated cold pool was situated just west of the geopotential height trough on the 10^{th} (figure 5.4). A closed low has formed by 1800Z (3080 gpm). By 0000Z on the 11^{th}, it has deepened to 3040 gpm. The position of this low corresponded to that of the surface low described above. Hereafter, the low weakened gradually as it moved southeastwards. During the 11^{th}, the temperature trough was more in sync with the geopotential height trough.

5.2.2.3 500 hPa

A well defined cold pool accompanied the geopotential height trough at 500 hPa (figure 5.5). A closed low (5680 gpm) has formed by 1800Z on the 10^{th}. It moved in over the southwestern part of South Africa by 0000Z on the 11^{th} . By that time, the low has deepened slightly to 5670 gpm, with a significant increase in the intensity of the cold pool, from $-22°C\ to\ -16°C$. The position of the low corresponded with the position of the surface low described above

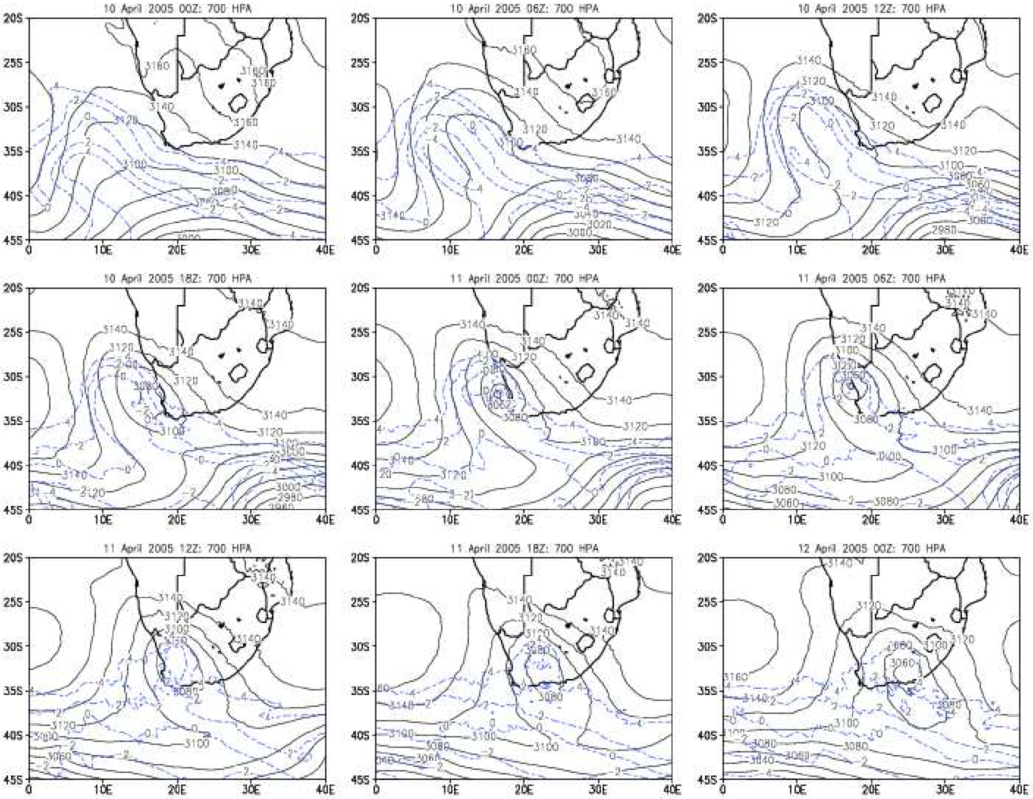

Figure 5.4: C-CAM prognosis of the 700 hPa geopotential heights and temperature for 10 April 2005 0000Z to 12 April 2005 0000Z

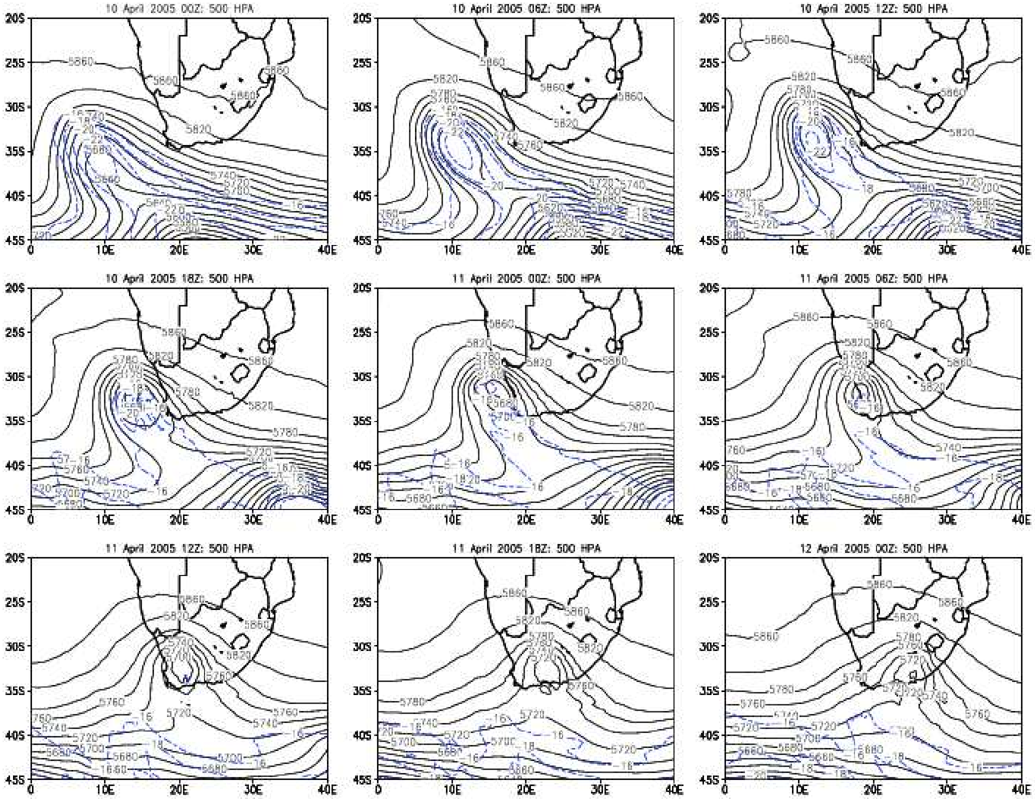
10 April 2005 00Z: 500 HPA
10 April 2005 06Z: 500 HPA
10 April 2005 12Z: 500 HPA
10 April 2005 18Z: 500 HPA
11 April 2005 00Z: 500 HPA
11 April 2005 06Z: 500 HPA
11 April 2005 12Z: 500 HPA
11 April 2005 18Z: 500 HPA
12 April 2005 00Z: 500 HPA

Figure 5.5: C-CAM prognosis of the 500 hPa geopotential heights and temperature for 10 April 2005 0000Z to 12 April 2005 0000Z

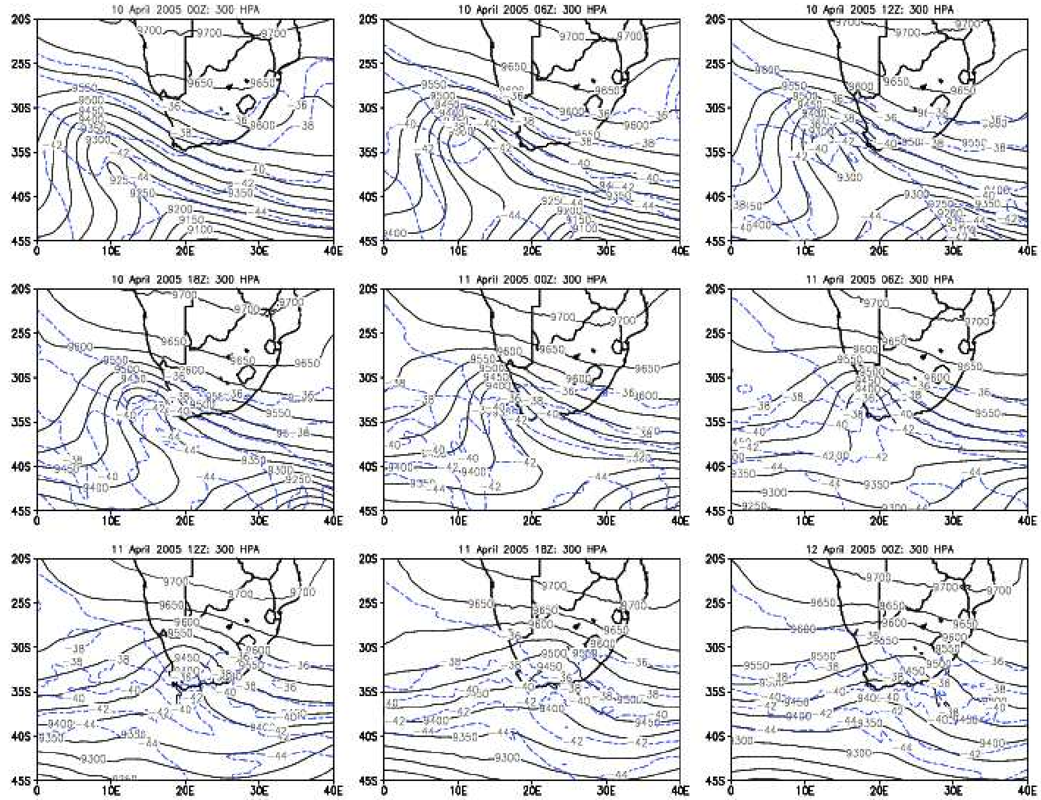

Figure 5.6: C-CAM prognosis of the 300 hPa geopotential heights and temperature for 10 April 2005 0000Z to 12 April 2005 0000Z

(see 5.2.2.1). During the remainder of the day the low moved southeastwards while slightly weakening. It was situated in the Port Elizabeth area by 0000Z on the 12th. The cold pool dissapeared by then.

5.2.2.4 300 hPa

At 300 hPa, a sharp trough was situated west of South Africa with a closed low of 9250 gpm at $37°S$, $10°E$. This trough moved in over the southwestern part of the country at 0000Z on the 11th, while weakening. During the rest of the day it weakened further while moving in a southeasterly direction. It exited the country in the vicinity of Port Elizabeth at 0000Z on the 12th. There was an absence of a well defined cold pool on this level. Instead, multiple temperature troughs were seen in the vicinity of the geopotential height trough. An interesting feature was seen in the temperature prognosis. By 0000Z on the 11th a warm tongue was entrained into the trough just west of the country. This warm tongue weakened whilst moving eastwards with the weakening trough.

5.2.3 Comparison of the C-CAM synoptic prognosis that was initialized on 10 April 2005 0000Z to NCEP reanalysis data

5.2.3.1 Sea-level pressure (SLP)

As expected the analysis field of C-CAM (see figure 5.3) corresponds very well with the corresponding NCEP field (see figure 5.7). The sequence of events during the remainder of the period under investigation as captured by C-CAM corresponds very satisfactorily to the NCEP data. The C-CAM prognosis of the ridging process of the Atlantic Ocean High is very good in terms of timing and position, throughout the forecast period. With regard to intensity, the difference between the forecasted and observed strength of the Atlantic Ocean High is less than 2 hPa throughout the forecasting period.

Other features of special interest are the surface trough and the low that developed in the vicinity of Cape Columbine. Especially the latter, as it is associated with the cut-off low system higher up in the troposphere. The movement of the surface trough was in general well simulated by C-CAM. However, it had the tendency to simulate the trough deeper (by about 2 hPa) and broader than indicated by the NCEP fields. The low that started to develop as indicated by C-CAM at 1800Z in the Cape Columbine area is suggested in the NCEP field as well. It is not indicated as a closed at 0000Z on the 11th as in the C-CAM simulation, but the shape of the isobars suggests that a weak low was present. It is very likely that the resolution of the NCEP data is too coarse to resolve the low pressure system explicitly. At 0600Z and 1200Z on the 11th, C-CAM simulated this low to have moved slightly northwards while weakening. In the NCEP fields, this weak low was no longer suggested. Instead, a low pressure is indicated over the Western Cape's interior at 0600Z, and moved eastwards to be situated over the Eastern Cape coast and surrounding areas by 1200Z. C-CAM simulated a mimima over the southwestern interior at 0600Z, which formed part of the surface trough. This minima in the surface trough is not as distinct as the low pressure area indicated in the NCEP field for the corresponding time. The well defined low pressure that is situated over the Eastern Cape and adjacent ocean as indicated in the 1200Z NCEP field, is absent in the C-CAM forecast. However, the C-CAM surface trough aligned to the area where the NCEP low was situated and linked with a coastal minima just off the coast. It is also noteworthy to mention that the low pressure indicated by NCEP was deeper than the minimas that was associated with the simulated C-CAM surface trough (1006 hPa vs 1008 hPa). Just off the Eastern Cape coast the pressure difference between NCEP and C-CAM was - 4 hPa. By 0000Z on the 12th, C-CAM simulated an area of low pressure (1006 hPa) along the southeast coast and adjacent areas extending southeastwards out to the sea. In the NCEP

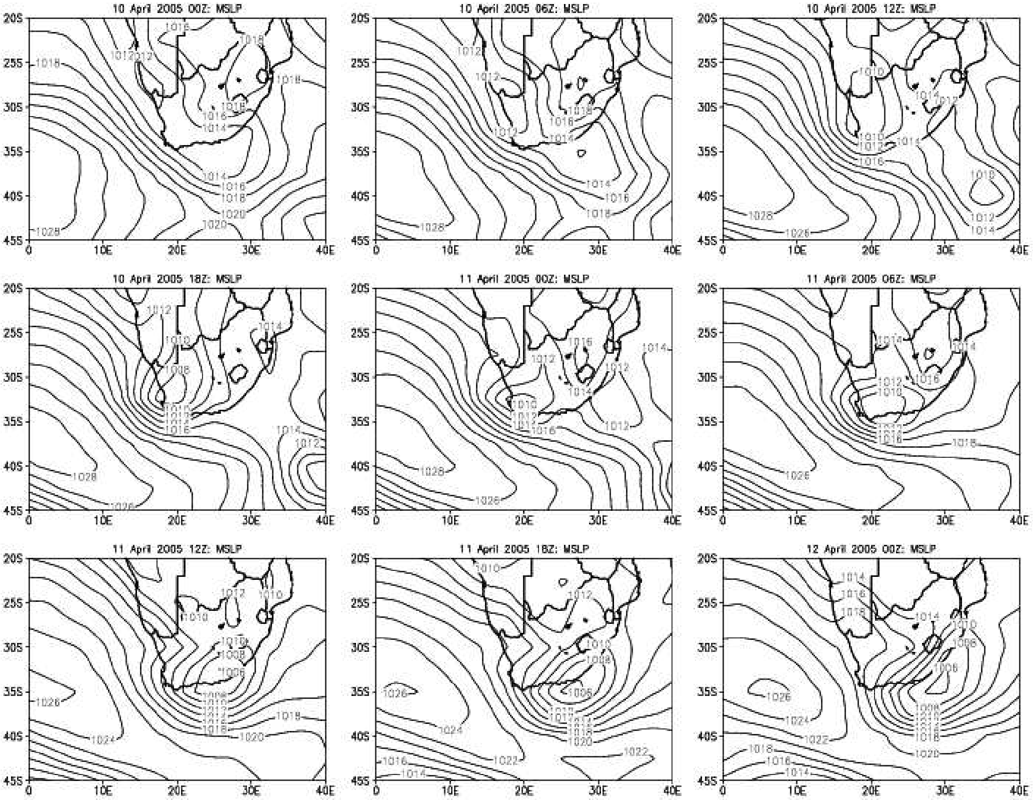

Figure 5.7: NCEP sea level pressure for 10 April 2005 0000Z to 12 April 2005 0000Z

field, the low (1006 hPa) was indicated off the southeastern coast.

5.2.3.2 700 hPa

The C-CAM simulation of the 700 hPa heights (figure 5.4) are generally in good agreement with the NCEP fields (figure 5.8). The following points are noted:

- A closed low is indicated by NCEP from 1200Z on the 10th, while C-CAM indicated the closed low from 1800Z on the 10th.
- The intensity and position of the cut-off low at 1800Z on the 10th is the same for both C-CAM and NCEP.
- The most striking deviation between C-CAM and NCEP occur at 0000Z and 0600Z on the 11th. C-CAM intensified the cut-off low to 3040 gpm, whilst NCEP indicated the height of the cut-off low to be 3090 gpm. NCEP intensified the cut-off low to 3060 gpm at 0600Z. The C-CAM simulation indicated then that the low had a height of 3050 gpm. Another striking feature at 0000Z and 0600Z on the 11th, was the more northward position of the cut-off low as simulated by C-CAM, compared to the NCEP position.
- At 1200Z on the 11th C-CAM weakened the cut-off low. The indicated height of the cut-off low was then 3080 gpm and this was maintained at 1800Z. NCEP maintained the depth of the cut-off low as at 0600Z (3060 gpm) but moved it southeastwards. At 1800Z NCEP weakened the cut-off low to 3080 gpm. At 0000Z on the 12th, the cut-off low has weakened to a trough (3080 gpm) according to NCEP. Interestingly, C-CAM simulated the cut-off low to have deepened to 3060 gpm by this time.
- C-CAM recovered at 1800Z and 0000Z on the 11th with it's simulated movement of the cut-off low. It moved the cut-off low in a southeasterly direction, which corresponds with the movement as indicated by NCEP. However, C-CAM simulated the cut-off low still more northwards compared to the actual position as indicated by NCEP.

5.2.3.3 500 hPa

The general movement of the trough and cut-off low is captured well by C-CAM during the first 18 hours of the forecast. Both C-CAM and NCEP indicated the cut-off low from 1200Z on the 10th (figures 5.5 and 5.9). It is then situated west of southern Africa. Both C-CAM and NCEP indicated that the cut-off low has moved in over South Africa at 0000Z on the 11th. C-CAM's simulation of the movement of the cut-off low had a northern component at 0000Z on the 11th, whereas the actual movement had a dominant easterly component. During the remainder of this period the cut-off low was placed further northwards by C-CAM compared to NCEP. This can be seen in figures 5.5 and 5.9. The placement

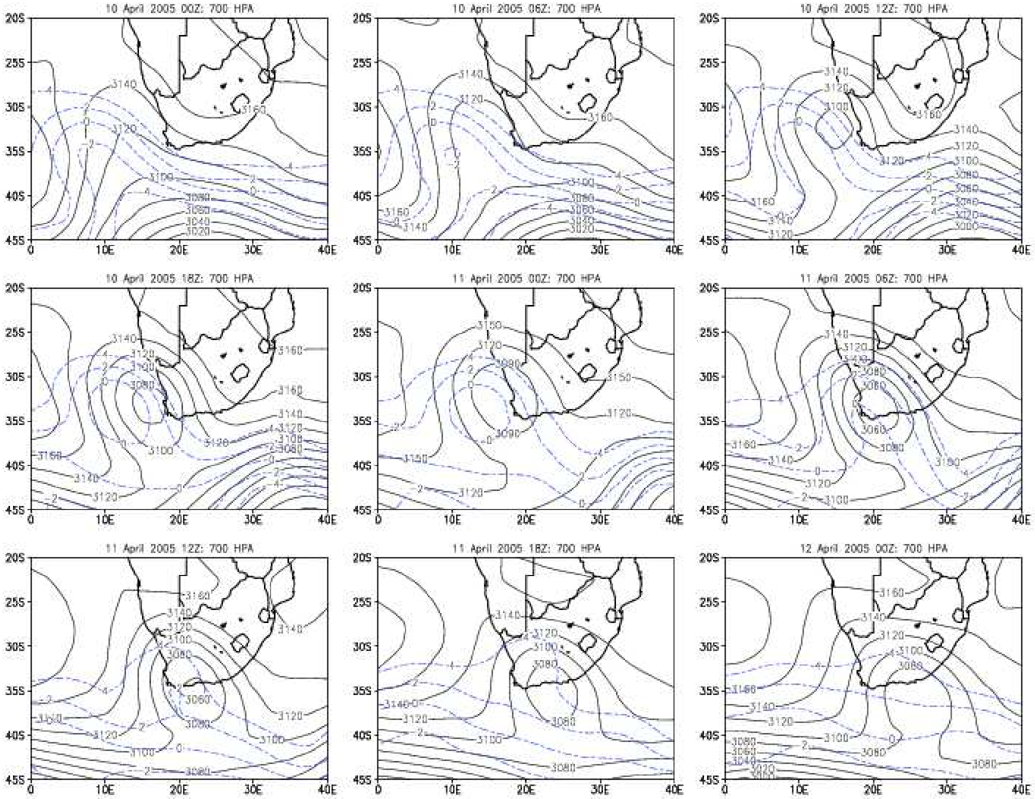

10 April 2005 00Z: 700 HPA
10 April 2005 06Z: 700 HPA
10 April 2005 12Z: 700 HPA
10 April 2005 18Z: 700 HPA
11 April 2005 00Z: 700 HPA
11 April 2005 06Z: 700 HPA
11 April 2005 12Z: 700 HPA
11 April 2005 18Z: 700 HPA
12 April 2005 00Z: 700 HPA

Figure 5.8: NCEP 700 hPa geopotential height and temperature fields for 10 April 2005 0000Z to 12 April 2005 0000Z

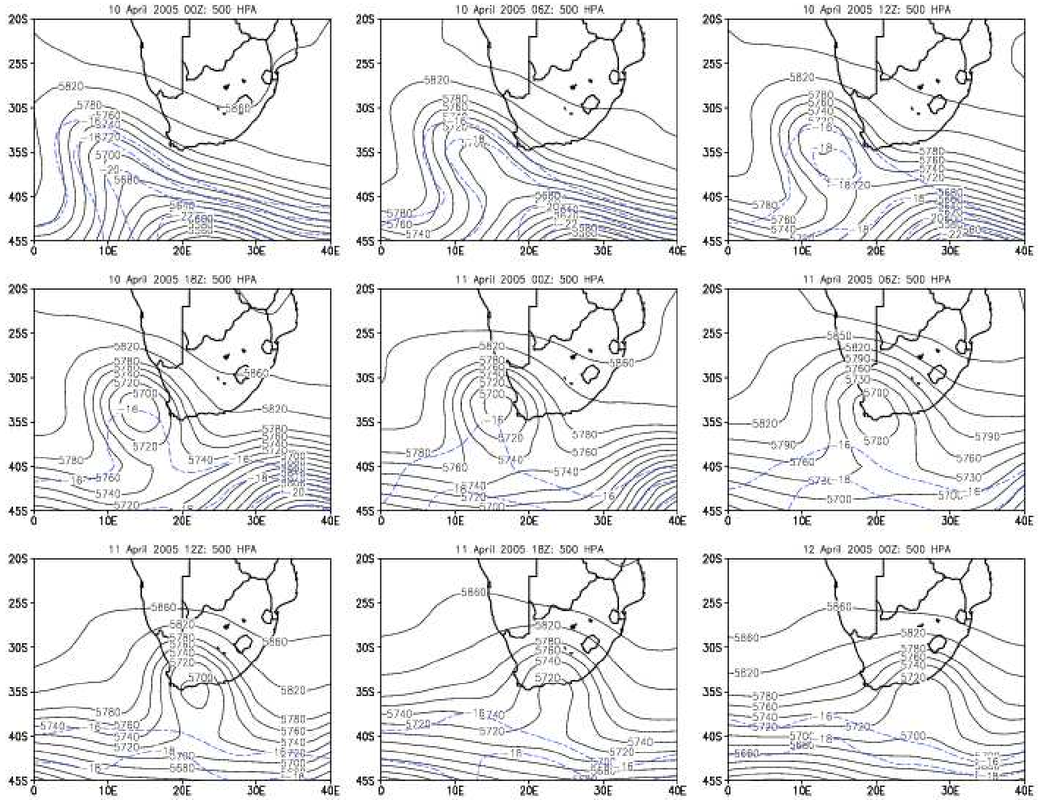
10 April 2005 00Z: 500 HPA
10 April 2005 06Z: 500 HPA
10 April 2005 12Z: 500 HPA
10 April 2005 18Z: 500 HPA
11 April 2005 00Z: 500 HPA
11 April 2005 06Z: 500 HPA
11 April 2005 12Z: 500 HPA
11 April 2005 18Z: 500 HPA
12 April 2005 00Z: 500 HPA

Figure 5.9: NCEP 500 hPa geopotential height and temperature fields for 10 April 2005 0000Z to 12 April 2005 0000Z

of the cut-off low affects a rainfall forecast, especially the area in close proximity of the cut-off low. C-CAM simulated the position of the cut-off low to be over the Eastern Cape in the vicinity of Port Elizabeth by 0000Z on the 12th, while the actual position as indicated by NCEP was just off the coast in the vicinity of Port Elizabeth. NCEP had by then also weakened the cut-off low system so that no closed low was present anymore.

The intensity of the cut-off low at 500 hPa was slightly overestimated by C-CAM during most of this forecast period. The difference at 1200Z on the 10th was 20 hPa, when C-CAM indicated the height of the cut-off low to be 5680 gpm while NCEP indicated it to be 5700 gpm. This difference was maintained up to 0600Z on the 11th, as the depth of the cut-off low was indicated to remain unchanged by C-CAM and NCEP. At 1200Z on the 11th, the cut-off low simulated by C-CAM weakened to 5700 hPa, whilst NCEP still indicated it to be 5700 hPa. Thereafter, the cut-off low weakened to a trough (5720 hPa) for the remainder

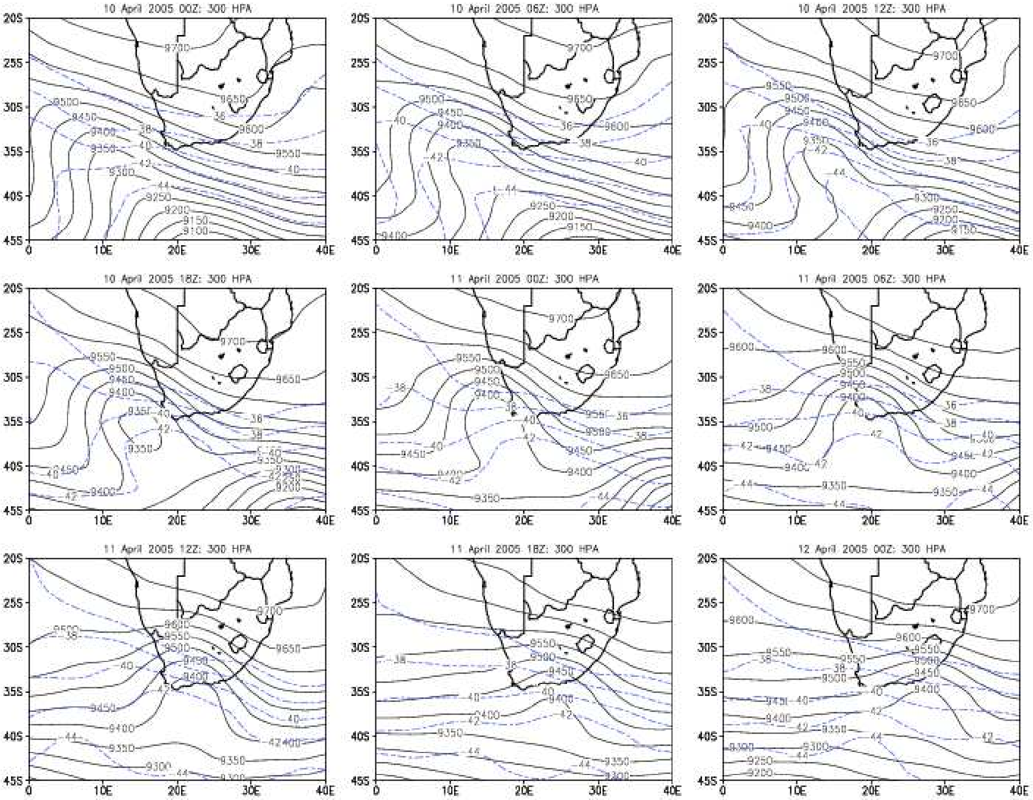

Figure 5.10: NCEP 300 hPa geopotential and temperature fields for 10 April 2005 0000Z to 12 April 2005 0000Z

of this forecast period according to NCEP and exited the country along the Eastern Cape coast. The C-CAM simulation weakened the cut-off low to 5720 hPa at 1800Z, and deepened it slightly at 0000Z on the 12th.

5.2.3.4 300 hPa

A steep trough was indicated west of southern Africa at 0000Z on the 10th according to the NCEP data (figure 5.10). A similar trough was simulated by C-CAM, except that it was more intense, as a closed low was indicated in this trough system. The time evolution of the 300 hPa trough in the C-CAM forecasts shows close agreement to the time evolution of the system in the corresponding NCEP fields. The only significant difference occured at 0600Z on the 11th. Here C-CAM indicated the trough to be deeper than in the corresponding NCEP field. Also, the centre of the trough was placed further to the west than in the corresponding NCEP field. This difference would have had some obvious forecasting implications with regard to the rainfall area as well as the prediction of the ceasure of rainfall.

5.2.4 The track of the cut-off low system: Comparison between different C-CAM simulations and NCEP data

The track that the cut-off low folowed over southern Africa at 500 hPa, accorrding to NCEP reanalysis data, is indicated in figure 5.11 (black line). Only points where a definite closed low was indicated were used in constructing the figure. C-CAM forecasts of the track followed by the cut-off low are also shown. Forecasts initialized at differecnt times are shown, in order to evaluated the forecasted tracks for different lead times. The details of the C-CAM forecasts displayed in figure 5.11 are:

- 20050407 0000Z run, day 4 forecast valid for 10 April 2005
- 20050408 0000Z run, day 3 and 4 forecast valid for 10 and 11 April 2005 respectively
- 20050409 0000Z run, day 2 and 3 forecast valid for 10 and 11 April 2005 respectively
- 20050410 0000Z run, day 1 and 2 forecast valid for 10 and 11 April 2005 respectively
- 20050411 0000Z run, day 1 forecast valid for 11 April 2005

The 20050407 0000Z C-CAM run forecast a cut-off low on the 11th of April. However, the position of the cut-off low was way far to the west of the actual position of the cut-off low at the corresponding times. Also, it is interesting to note that in the 20050407 0000Z model run the cut-off low is simulated to retrogate in a northerly direction. The northward movement of the cut-off low is also simulated in the 20050408 0000Z model run. Again, the position of the cut-off low is significantly westward compared to the actual position of the cut-off low at the corresponding times.

The 20050409 0000Z model run positions the cut-off low eastwards of its actual position during it's initial formation stage. The track of the cut-off low as simulated by this run, is shorter than the actual track the cut-off low system has followed. The final position of the simulated cut-off low is significantly west -and northwards of the actual position.

The simulated cut-off low track of the 20050410 0000Z model run generally shows the same tendency with regard to the directional changes in the movement of the system as compared to the actual track it followed. However, the simulated track is most of the time placed significantly northwards of the actual track. This

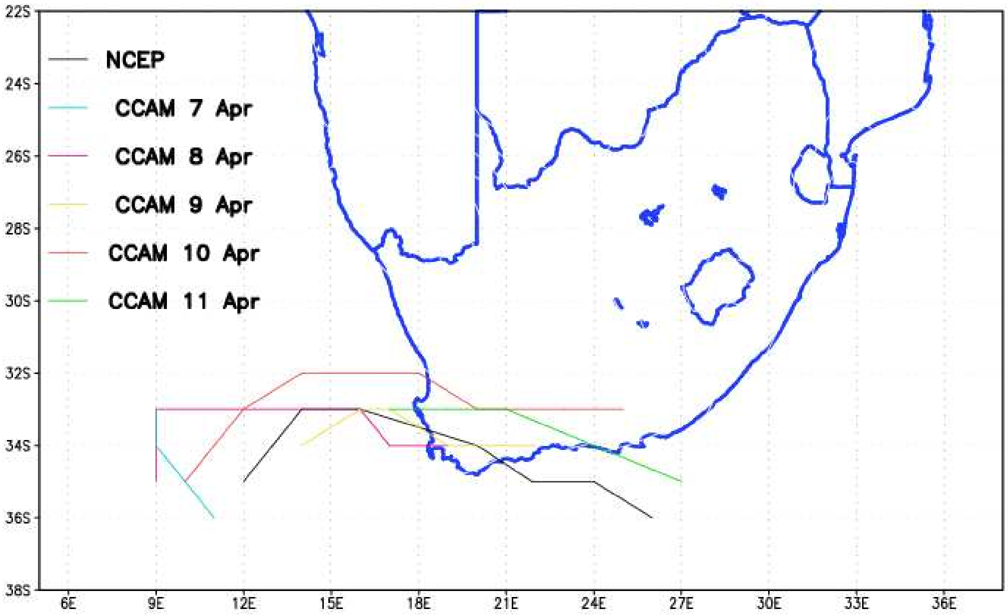

Figure 5.11: The position of the cut-off low system as indicated by NCEP reanalysis data and as simulated by 5 different C-CAM runs. C-CAM runs of 7 to 11 April 2005 are compared to each other and to NCEP reanalysis data.

northward displacement of the track is also seen in the 20050411 0000Z model run, although not as far northwards as the simulated track of the 20050410 0000Z model run.

In summary, all of the 5 different C-CAM runs indicated the development of the cut-off low system, even the day 4 forecast of the 20050407 0000Z model run. However, the prognosis of the position of the cut-off low by the different C-CAM runs varied with each run. It is quite clear that the 20050407 0000Z and the 20050408 0000Z runs struggled the most to capture the movement of this cut-off low. These were day 3 and day 4 forecasts of those model runs. This result confirms the results obtained in chapter 4, where it was shown that from about day 3 the forecast errors start to grow more rapidly.

5.2.5 Comparison of the simulated rainfall intensity to data of selected weather stations

The arial coverage of rainfall as simulated by C-CAM during this weather event compares satisfactorily with what actually occurred (compare figures 5.1 and 5.12). However, by visual inspection of the rainfall totals that occurred during the 48-hour period 0600Z 10 April 2005 to 0600Z 12 April 2005, it is seen

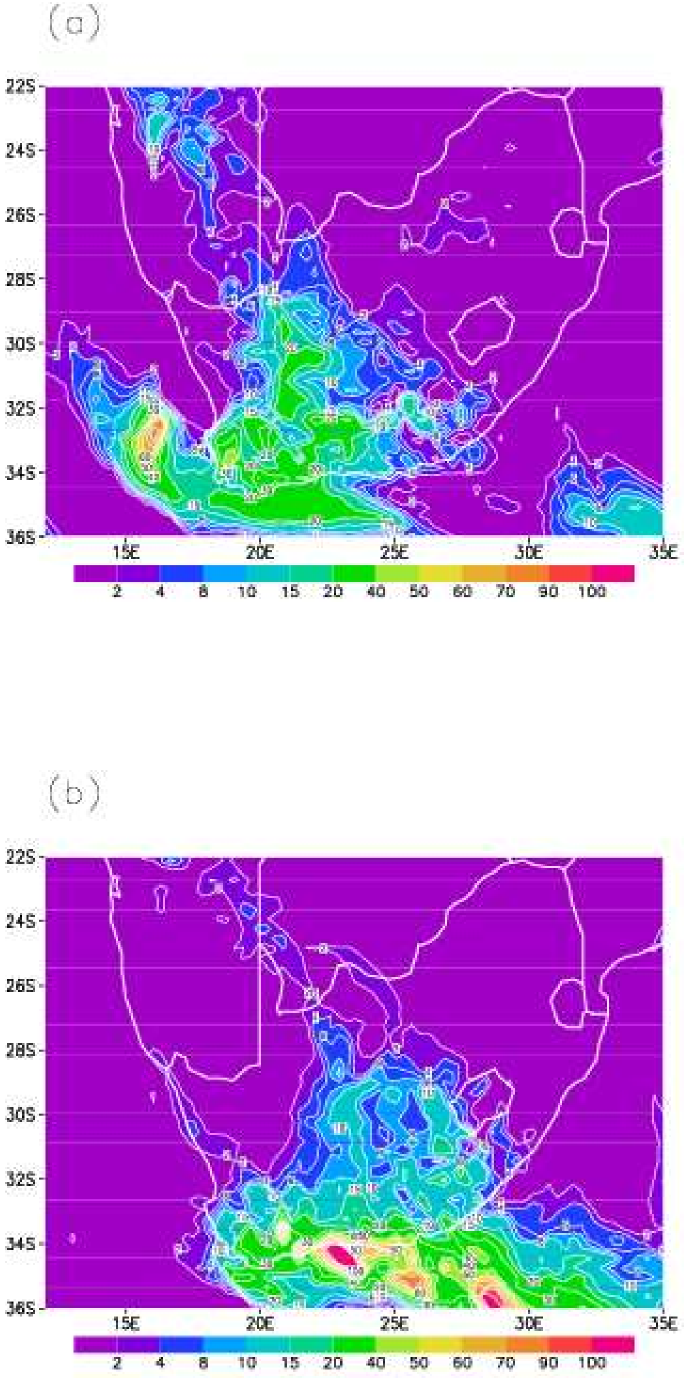

Figure 5.12: The C-CAM simulated rainfall for the periods 0600Z 10 April 2005 - 0600Z 11 April 2005 (a) and 0600Z 11 April 2005 - 0600Z 12 April 2005 (b)

that the C-CAM simulation is in many places not a good reflection of what was actually measured. In this section, a few stations are selected to perform a subjective analysis on the rainfall totals as well as the rainfall intensity. This is done for two 24-hour periods, with the first period from 0600Z 10 April 2005 to 0600Z 11 April 2005 and the second period from 0600Z 11 April 2005 to 0600Z 12 April 2005. C-CAM forecasts of the 20050410 0000Z run for Hermanus $(34^\circ 26' S, 19^\circ 13' E)$, Tygerhoek $(34^\circ 9' S, 19^\circ 54' E)$, Struisbaai $(34^\circ 48' S, 20^\circ 4' E)$, Cape Town $(33^\circ 58' S, 18^\circ 36' E)$ and Port Elizabeth $(33^\circ 59' S, 25^\circ 37' E)$ are compared to SAWS station data. Coastal stations were selected because the highest rainfall totals clearly occurred along the coastal belt. This is a typical characteristic of cut-off low systems - when they produce heavy rainfall, it tends to be along the Cape south coast and adjacent interior regions (see chapter 2). The selection of these specific stations were further based on data availability, as well as the availability of most of the SYNOP data for these stations. The latter was essential to calculate the observed rainfall intensities. Rainfall intensity was calculated for 6-hourly intervals, and are compared to the corresponding C-CAM forecasts (see Tables 5.1 and 5.2).

Main SYNOPs are issued four times a day, namely at 0000Z, 0600Z, 1200Z and 1800Z. Rainfall are reported for different time intervals in each of the SYNOP reports. At 0000Z rainfall is reported for a 6-hour period (1800Z - 0000Z), at 0600Z rainfall is reported for a 24-hour period (0600Z - 0600Z), at 1200Z rainfall is reported for a 6-hour period (0600Z - 1200Z) and at 1800Z rainfall is reported for a 12-hour period (0600Z - 1800Z). By using this information, the rainfall for succeeding 6-hourly intervals starting at 0600Z are obtained. The 6-hourly rainfall for 0600Z - 1200Z and 1800Z - 0000Z is obtainded from the 1200Z and 0000Z SYNOPs respectively. The 6-hourly rainfall for 1200Z - 1800Z is calculated by subtracting the rainfall reported in the 1200Z SYNOP from the rainfall reported in the 1800Z SYNOP. For the 6-hour period, 0000Z - 0600Z, the rainfall reported in the 1800Z SYNOP and the 0000Z SYNOP is added and then subtracted from the rainfall reported in the 0600Z SYNOP. Unfortunately, most of the 0000Z SYNOPs on the 11th of April 2005 appear not to have been issued. Therefore, rainfall for these mentioned stations was not available for the 6-hour period 1800Z - 0000Z, and consequently the rainfall fo the 6-hour period 0000Z - 0600Z could not be calculated.

As mentioned above, the arial coverage of rainfall as simulated by C-CAM is very satisfactorily but the simulated rainfall amounts are not a true reflection of what was actually measured. For the 5 chosen stations under investigation, the rainfall totals were severely under-estimated by C-CAM for the first 24-hour period (0600Z 10 April - 0600Z 11 April). At Hermanus, the measured rainfall total was 164 mm, while C-CAM predicted only 15 mm. Further, C-CAM failed to indicate in which 6-hour interval significant amounts of rain would fell. The forecasted rainfall amounts in all of the 6-hour intervals (for the first 24-hour period) were of comparible magnitude for each station. In reality, the most rain

SAWS Station data	**Time interval**	**SYNOP data**	**C-CAM forecast**
Hermanus	06Z - 12Z	10	4.28862
	12Z - 18Z	12	3.97785
	18Z - 00Z	58	1.95785
	00Z - 06Z	84	5.17769
	Total	164	15.40201
Tygerhoek	06Z - 12Z	10	9.75815
	12Z - 18Z	24	9.16769
	18Z - 00Z	63	4.98785
	00Z - 06Z	26	13.2111
	Total	123	37.12479
Struisbaai	06Z - 12Z	0.4	6.30862
	12Z - 18Z	13.6	4.30415
	18Z - 00Z	32	3.40292
	00Z - 06Z	25	9.45077
	Total	71	23.46646
Cape Town WO	06Z - 12Z	6 from 06Z - 18Z	8.37523
	12Z - 18Z	6 from 06Z - 18Z	9.94461
	18Z - 00Z	34	13.0523
	00Z - 06Z	4	16.6606
	Total	44	48.03274
Port Elizabeth	06Z - 12Z	no rain	1.75585
	12Z - 18Z	< 1	1.86462
	18Z - 00Z	26	1.33631
	00Z - 06Z	$> 1, < 2$	3.04892
	Total	28	8.0057

Table 5.1: Comparison of rainfall intensity and rainfall totals as reported in SYNOP data with C-CAM forecasts for the 24-hour period from 0600Z 10 April 2005 to 0600Z 11 April 2005

SAWS Station data	**Time interval**	**SYNOP data**	**C-CAM forecast**
Hermanus	06Z - 12Z	13	6.23092
	12Z - 18Z	1	5.31415
	18Z - 00Z	not available	0
	00Z - 06Z	can't calculate	0
	Total	20	11.54507
Tygerhoek	06Z - 12Z	16	21.7383
	12Z - 18Z	5	11.0478
	18Z - 00Z	not available	4.52169
	00Z - 06Z	can't calculate	0.687078
	Total	41	37.994868
Struisbaai	06Z - 12Z	68	10.0534
	12Z - 18Z	9	5.99785
	18Z - 00Z	not available	0.637077
	00Z - 06Z	can't calculate	0.00338565
	Total	79	16.69171265
Cape Town WO	06Z - 12Z	7	10.6128
	12Z - 18Z	0	3.57384
	18Z - 00Z	not available	0.559385
	00Z - 06Z	can't calulate	0.00338565
	Total	8	14.74941065
Port Elizabeth	06Z - 12Z	no rain	12.4152
	12Z - 18Z	6	6.77477
	18Z - 00Z	not available	6.63492
	00Z - 06Z	can't calculate	21.5863
	Total	9	47.41119

Table 5.2: Comparison of rainfall intensity and rainfall totals as reported in SYNOP data with C-CAM forecasts for the 24-hour period from 0600Z 11 April 2005 to 0600Z 12 April 2005

was measured in the 1800Z - 0000Z and 0000Z - 0600Z periods (see tables 5.1 and 5.2).

C-CAM fared better during the second 24-hour period (0600Z 11 April - 0600Z 12 April). At Hermanus, Tygerhoek and Cape Town the measured and forecast rainfall figures differ by less than 10 mm. At Struisbaai, heavy rainfall was measured (79 mm) while C-CAM predicted only about 17 mm. At Port Elizabeth, C-CAM over-estimated the rainfall by nearly 40 mm. This is clearly because C-CAM positioned the cut-off low system northwards of where it was actually located during this period. This illustrates the importance of the location of such a system in order to identify the relevent areas to be affected.

5.2.6 Comparison of upper air ascent data at selected stations to the corresponding C-CAM forecast

Two upper air ascent stations were in the region that was directly affected by the passage of the cut-off low system. These stations are located at the airfields in Cape Town ($33°58^{'}S$, $18°36^{'}E$) and Port Elizabeth ($33°59^{'}S$, $25°37^{'}E$). Upper air ascents are done twice daily, at 0000Z and 1200Z. Among the data that is collected and calculated during upper air ascents are the geopotential heights and the relatively humidity at different pressure levels. In this section, the geopotential height and temperature as simulated by C-CAM at Cape Town and Port Elizabeth, are verified against the sounding data. The 00-hour, 12-hour, 24-hour, 36-hour and 48-hour forecasts of the 20050410 0000Z run are verified. The C-CAM grid point closest to the location of the upper air stations is used in order to compare the forecast to the sounding data. This verification is performed on 850 hPa, 700 hPa, 500 hPa and 300 hPa.

In general, the C-CAM forecasts capture the trend of the actual event very satisfactorily, especially with regard to the geopotential height. However, as expected, the model prognosis is smooth in comparison to the observed data. In the geopotential height prognosis, the intensity of the system is mostly under-estimated by C-CAM. This is seen at the Cape Town ascent at 700 hPa (20050411 1200Z) where the C-CAM prognosis is about 30 gpm lower than the observed height (figure 5.13). Unfortunately, the 20050411 0000Z ascent had no data at 500 hPa and 300 hPa, but if we assume that the minimum height at these levels occurred also at 1200Z on the 11th, then this tendency of C-CAM to under-estimates the intensity is detected again. At 500 hPa, C-CAM under-estimates the height by about 20 gpm and at 300 hPa by about 40 gpm. At the Port Elizabeth ascent, it seems by visual inspection that the C-CAM prognosis fared better than at Cape Town. This can be explained by the fact that the cut-off low system was situated westward of Port Elizabeth most of the time, and by the time it moved into the Port Elizabeth vicinity it had weakened.

C-CAM over-estimated the relative humidity at 850 hPa at both Cape Town an Port Elizabeth during all of the ascents. This could be indicative of a model bias, but more data need to be analysed in order to confirm this suspicion. At the other levels, it seems that there are no specific tendency to under -or over-estimate the relative humidity. It is clear though, that sudden decreases and increases are not well simulated by C-CAM (see figures 5.14, figure 5.16).

It is interesting to note that for these forecasts that covers a 48-hour period, it seems that the largest errors are not found at the larger integration times. In fact, for both the geopotential height and temperature prognosis, a visible recovery took place at the 48-hour forecast, especially at Cape Town. The recovery at Cape Town is probably more spectacular because the cut-off low system has moved out of that area before the end of this forecast period. This is

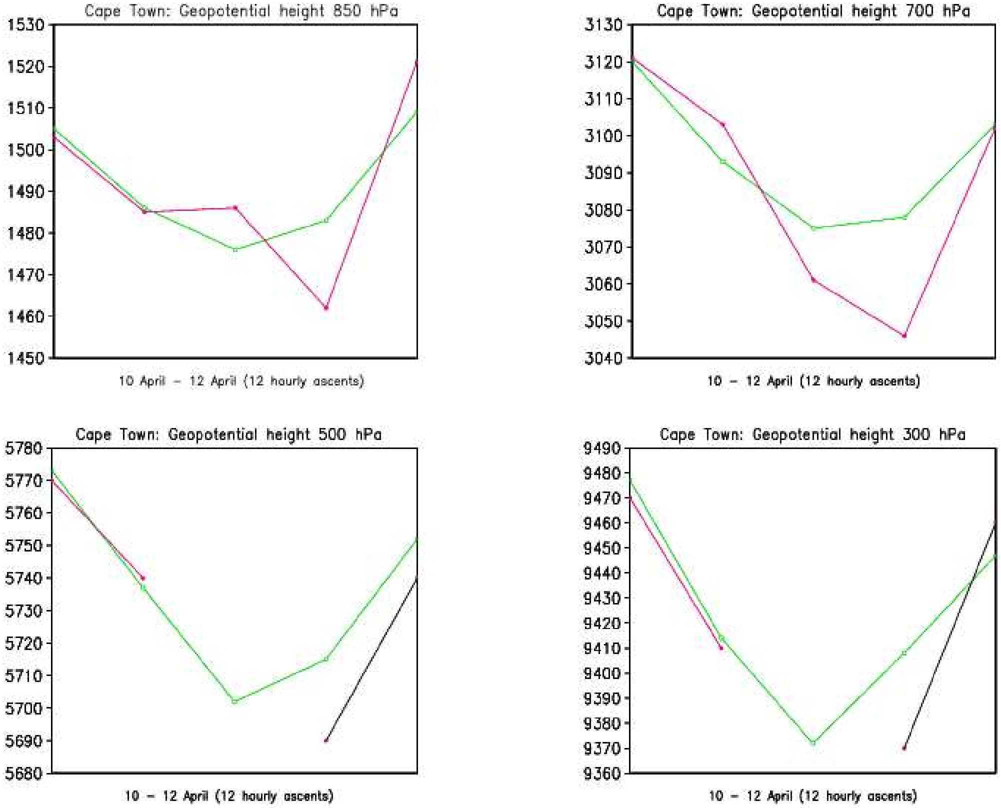

Figure 5.13: The 0000Z and 1200Z geopotential heights at 850 hPa, 700 hPa, 500 hPa and 300 hPa from 10 April 2005 0000Z to 12 April 2005 0000Z as simulated by C-CAM (green) are compared to the corresponding sounding data obtained from the SAWS. The sounding data is presented in magenta or in black following a gap in the observed data.

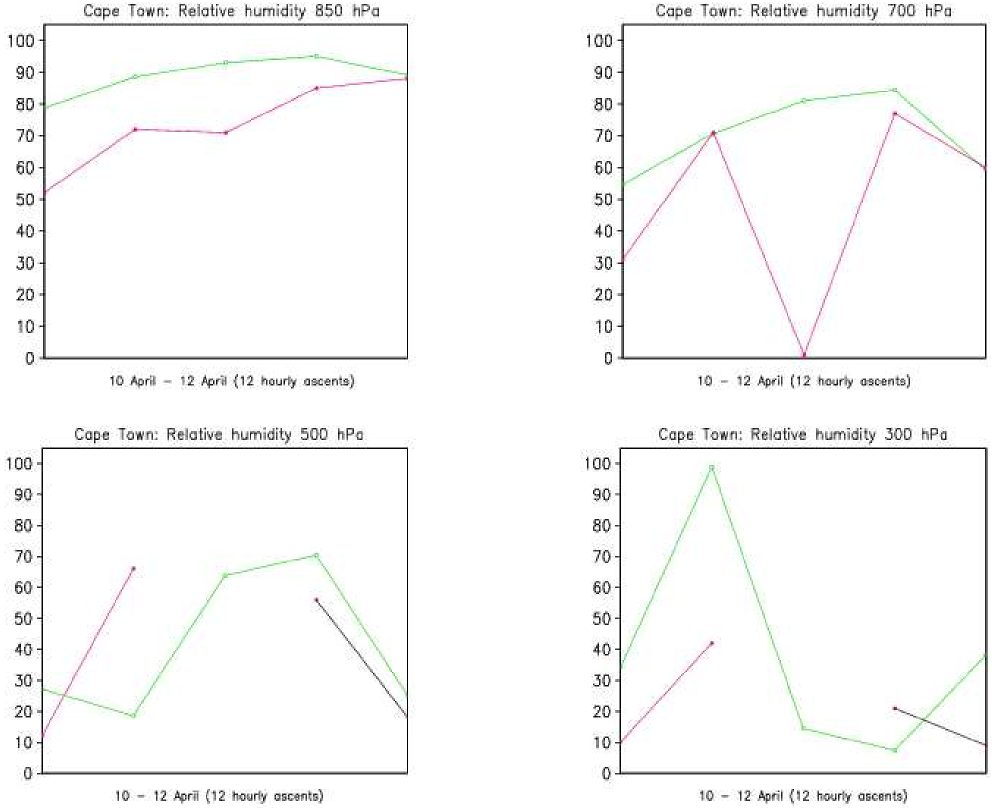

Figure 5.14: The 0000Z and 1200Z relative humidity at 850 hPa, 700 hPa, 500 hPa and 300 hPa from 10 April 2005 0000Z to 12 April 2005 0000Z as simulated by C-CAM (green) are compared to the corresponding sounding data obtained from the SAWS. The sounding data is presented in magenta or in black following a gap in the observed data.

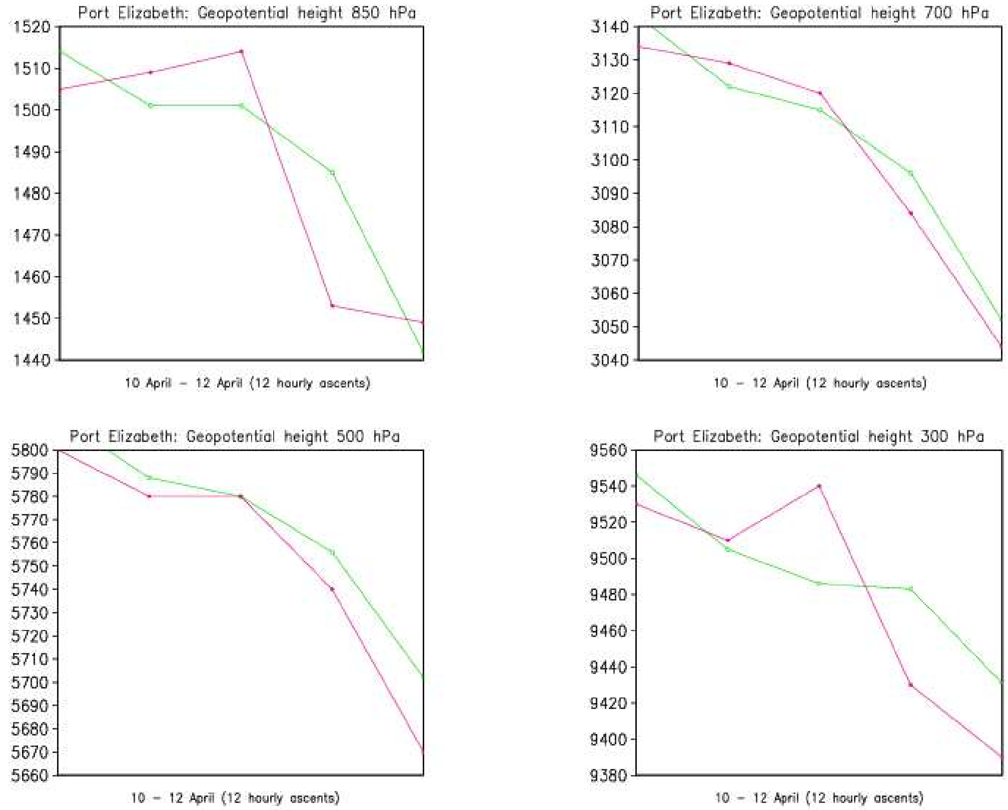

Figure 5.15: The 0000Z and 1200Z geopotential height at 850 hPa, 700 hPa, 500 hPa and 300 hPa from 10 April 2005 0000Z to 12 April 2005 0000Z as simulated by C-CAM (green) are compared to the corresponding sounding data obtained from the SAWS. The sounding data is presented in magenta or in black following a gap in the observed data.

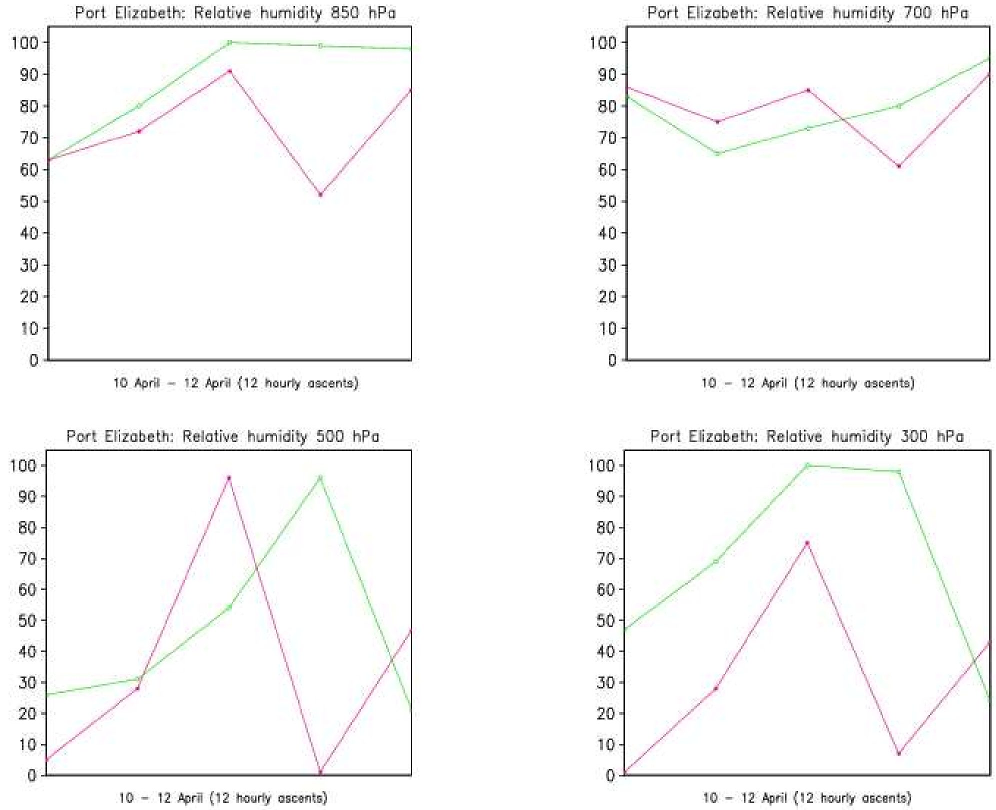

Figure 5.16: The 0000Z and 1200Z relative humidity at 850 hPa, 700 hPa, 500 hPa and 300 hPa from 10 April 2005 0000Z to 12 April 2005 0000Z as simulated by C-CAM (green) are compared to the corresponding sounding data obtained from the SAWS. The sounding data is presented in magenta or in black following a gap in the observed data.

an important point to realize, since it suggests that the behavior of an individual weather system (e.g. the intensity or movement), contributes more to model forecast errors than the effect of the integration time when the integration time is not large. It has been determined in chapter 4 that with the current C-CAM setup, the model errors start to grow more rapidly from approximately the 54-hour forecast.

5.2.7 Discussion

The main aim of this case study was to determine whether C-CAM was successful in forecasting this cut-off low event. The cut-off low moved over the southwestern part of the country on the 10th and the 11th of April 2005. Rainfall associated with the cut-off low occurred over the southwestern and southern parts of the country, whith heavy falls of rain occurring in places along the coastal regions. The highest falls occurred mostly from 1800Z on the 10th to 0600Z on the 11th. This was during the time that the cut-off low moved in over the country and that the surface low associated with it became well defined (see figure 5.7 and figure 5.9). Also, this was during the developing stages of the cut-off low system. According to Taljaard (1995a) this is when heavy rainfall typically occurs (see chapter 2). The rainfall totals were generally smaller on the 11th as the cut-off low system weakened while exiting the country during the latter part of the day.

The questions asked in this case study are whether the model guidance succeeded in capturing the cut-off low event, and if so, was the guidance successful in indicating the areas where heavy rainfall occurred. To answer these questions, typical prognostic fields used by operational forecasters from the 20050410 0000Z model run were subjectively verified against NCEP reanalysis data. These fields include the sea-level pressure prognosis, the 700 hPa, 500 hPa and 300 hPa geopotential height prognosis as well as the model rainfall forecast for these 2 days. In the verification of the sea-level pressure prognosis it was seen that in general C-CAM captured the sequence of events very satisfactorily. The simulation of the high pressure system was good in terms of timing and positioning. At most, there was an absolute difference of 2 hPa between C-CAM and NCEP. There was a tendency in the simulation of the surface trough to be 2 hPa deeper and broader than indicated in the NCEP fields. However, this would not make any significant difference with regard to the rainfall forecast as issued by a forecaster. The main deviation in the sea-level pressure prognosis was found in the simulation of the low that developed in response to the cut-off low higher up in the troposphere. This low was placed more northwards in the model simulation than was actually observed in the NCEP fields. Also, towards the end of the period, this low was not captured satisfactorily, especially as it exited the country along the Eastern Cape coast. The depth of this surface low was under-estimated by C-CAM. The northward positioning of the low was also detected in the 700 hPa, 500 hPa and 300 hPa geopotential height prognosis.

This is the most striking difference between the simulated cut-off low and the actual cut-off low. More subtle differences were detected in the intensity of the cut-off low simulated by C-CAM and the actual intensity as shown by NCEP. Of these, it's worth mentioning that C-CAM started to weaken the cut-off low 6 hours before it actually started to weaken on the 11th. It is also interesting to note that at the 48 hour forecast, C-CAM momentarily intensified the cut-off low just before exiting the country. This was not the case as seen in the NCEP fields.

The verification of the simulated tracks by the different C-CAM runs revealed that even the day 4 forecast was successful in forecasting the cut-off low event. However, the placement of the cut-off low verified unsatisfactorily. The day 3 and day 4 forecasts struggled the most to capture the position of the cut-off low.

In the point verification that was performed at Cape Town and Port Elizabeth, it was seen that at 850 hPa, the relative humidity was over-estimated by C-CAM. It was also clear that sudden decreases and increases in the relative humidity were not successfully forecast by C-CAM. Further, the maximum depth of the system was under-estimated by C-CAM, especially at Cape Town. At first, this seems not sound, since the C-CAM geopotential height prognosis was most of the time over-estimating the intensity of the system (on 500 hPa), but it can be due to the fact that the cut-off low was not positioned correctly. At Port Elizabeth, the geopotential height point verification fared better, and this can be explained by the fact that the system was already weakening when it arrived there. The most valuable result from the point verification is probably the outcome that it is suggested that the behaviour of an individual weather system, contributes more to model forecast errors at a specific point, than the effect of the integration time when the integration time is within the natural boundaries of acceptable errors.

To conclude, even though there are deviations in terms of the movement and intensity of the cut-off low system as described above, it can be said that the simulation of the 20050410 0000Z model run, captured the general characteristics of this event satisfactory. To return to one of the initial questions regarding the ability of the model to provide guidance to forecast this cut-off low event, the answer is positive. It did provide sufficient guidance to forecast this cut-off low event. However, the areas where heavy rainfall occurred was not indicated by the model. Instead, other areas have been indicated by the model to receive heavy rainfall. What is important though, is the fact that the model would have alerted a forecaster of the cut-off low event, and that it indicated the development of a surface low in response to the cut-off low system higher up in the troposphere. Any experienced forecaster will immediately know that this combination nearly always result in heavy rainfall along the coast and will then monitor the evolution of the system by analysing actual data such as satellite imagery. In this way, warnings can still be issued in time, even though the heavy rainfall areas were not indicated correctly by the model.

5.3 Case study 2: Thunderstorms of 24 April 2005

5.3.1 Introduction

On Sunday, 24 April 2005, a line of isolated, independently-formed convective cells developed in the region of the Witwatersrand during the afternoon and merged into a multicell storm towards the evening (figure 5.17). This multicell storm tracked over the eastern-most part of North-West, southern Gauteng, the northeastern Freestate and southern Mpumalanga. Surprisingly, this storm did not produce large amounts of rainfall. The most rain that was measured at SAWS stations, occurred at the Johannesburg International airport and at Springs where 31 mm and 24 mm were measured, respectively. However, this storm produced hail in places and motorists in the Johannesburg region had to pull their vehicles from the road due to reduced visibility (personal communication). The author believes that the significance of this storm lies in the fact that it persisted for a number of hours. This is characteristic of multi-cell storms which can have lifetimes of many hours although individual cells in the storm have lifetimes of about 30 minutes (Holton, 1992). The development of multicell storms are associated with characteristic vertical wind shear patterns. According to Holton (1992), they develop when the wind shear is $2.5 - 5\ ms^{-1}km^{-1}$ in the lower troposphere.

In this case study, the C-CAM prognosis valid for 24 April 2005, of the run initialized at 20050423 0000Z is verified. This implies that a lead-time of approximately 36-42 hours would have been given in the case that the model prognosis was successful in indicating this multicell storm. In the verification of the model forecast we are firstly evaluating the synoptic pattern to determine whether the synoptic systems were simulated correctly. This is done by visual comparison of the model prognosis to the synoptic pattern as constructed from NCEP reanalysis data. Secondly, the prognostic fields of variables that are utilised for forecasting convective development are discussed. The question asked in this case study is whether the C-CAM run could have given quidance in predicting this storm's occurence and nature.

5.3.2 Discussion of satellite imagery and observational data

By visual inspection of satellite imagery (MSG, channel 1 and 9) it was seen that convection was initiated in a characteristic line from about 0900Z. This line of convective cloud followed the terrain of the Witwatersrand (see figure 3.2, chapter 3), and extended to the highground of Mpumalanga. Small, isolated thunderstorms started to develop from about 1200Z according to the satellite

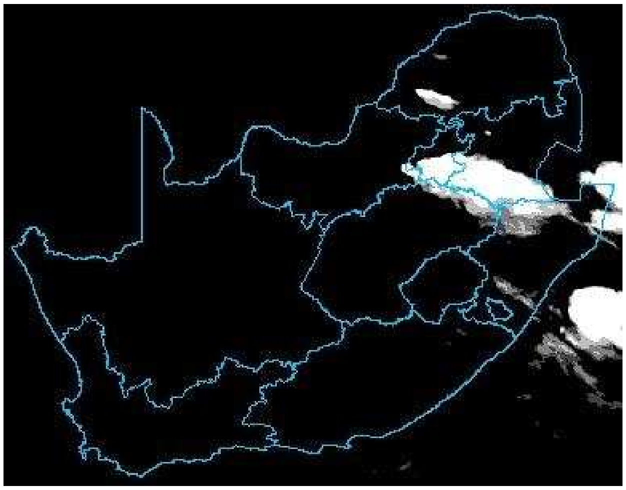

Figure 5.17: The wedge shape thunderstorm can be seen over the northeastern interior in this Meteosat Second Generation (MSG) false color (channel 9) image valid at 24 April 2005 1800Z

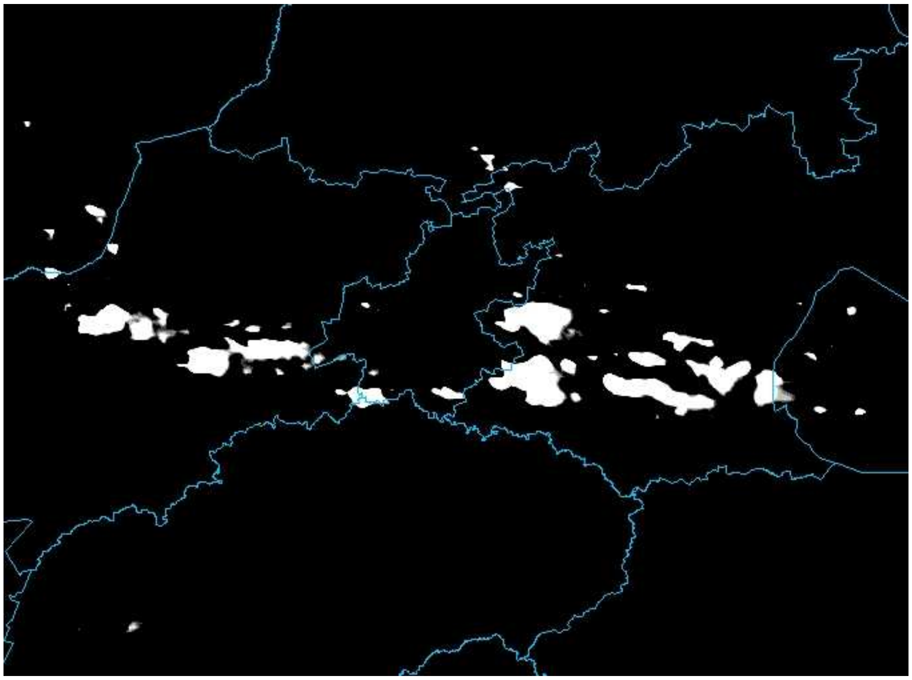

Figure 5.18: The line of individual thunderstorms can be seen along the Witwatersrand on this Meteosat Second Generation (MSG) false color (channel 1) image valid at 24 April 2005 1330Z

images. Most of these thunderstorms were situated in the eastern portion of this line of convective clouds. From 1300Z thunderstorms started to develop in the western portion of this characteristic line of convective clouds. This is also seen in the routine meteorological reports (METARs) as a thunderstorm was reported at Irene. The line of individual thunderstorms can be seen in the 1330Z false color MSG (channel 1) satellite image (figure 5.18). This line of thunderstorms intensified during the next hour and by 1500Z it seemed that they have merged according to the satellite images. This multi-cell storm tracked in an east-southeasterly direction whilst new cells developed on its western and northern side. From about 1700Z this thunderstorm started to exhibit a well defined wedge shape. It is at this time that Johannesburg International airport reported a thunderstorm while it reported in the previous two hours a CB to its southwest. This cell that arrived at the airport was probably one of the most intense cells in this multi-cell storm as is seen in the METARs from 1700Z to 2200Z, since it was the only station that has reported thunderstorms/showers non-stop during the mentioned period. This storm intensified, and small hail was reported in the 1800Z METAR at the airport. The temperature decreased from $17°C$ to $11°C$ between 1700Z and 1800Z. Thunderstorms and rain were reported in the succeeding METARs untill 2100Z. It seems it was the most intense around 1900Z, since the minimum visibility as well as the lowest temperature during the time of the storm occurred then. Also, according to SYNOP data, 28 mm was reported for the 6 hour period that covered 20050424 1800Z to 20050425 0000Z, while 3mm was reported for the 12 hour period that covered 20050424 0800Z to 20050424 1800Z. The 2200Z METAR reported recent thunderstorms and rain as well as a CB to the east of the airport. According to the satellite images, the storm advanced further in an easterly direction whilst weakening.

5.3.3 Synoptic pattern

5.3.3.1 NCEP synoptic pattern

The SLP pattern (figure 5.19) was characterised by an area of low pressure southeast of South Africa on the 23rd and the 24th. There is an indication that this area of low pressure consists actually of three individual low pressure systems. The first and most intense of these lows was situated southeast of the country, whilst the other two were situated just off the Cape south coast and off the east coast respectively (see figure 5.19). The main low pressure was initially situated just off the southeastern coast but moved gradually southeastwards to be situated south of $40°S$ by the end of this period. The low pressure off the Cape south coast, between $35°S$ and $40°S$, lingered in the vicinity of the Eastern Cape coast during most of this period before it followed in the track of the more intense low pressure system while it seemed that the low pressure off the east coast gradually filled up. The other two low pressure systems were initially slowed down in their southeastward track by a high pressure system to the south of them. As the high pressure system made way for an approaching frontal system to its west, the blocking effect it had on the two low pressure systems

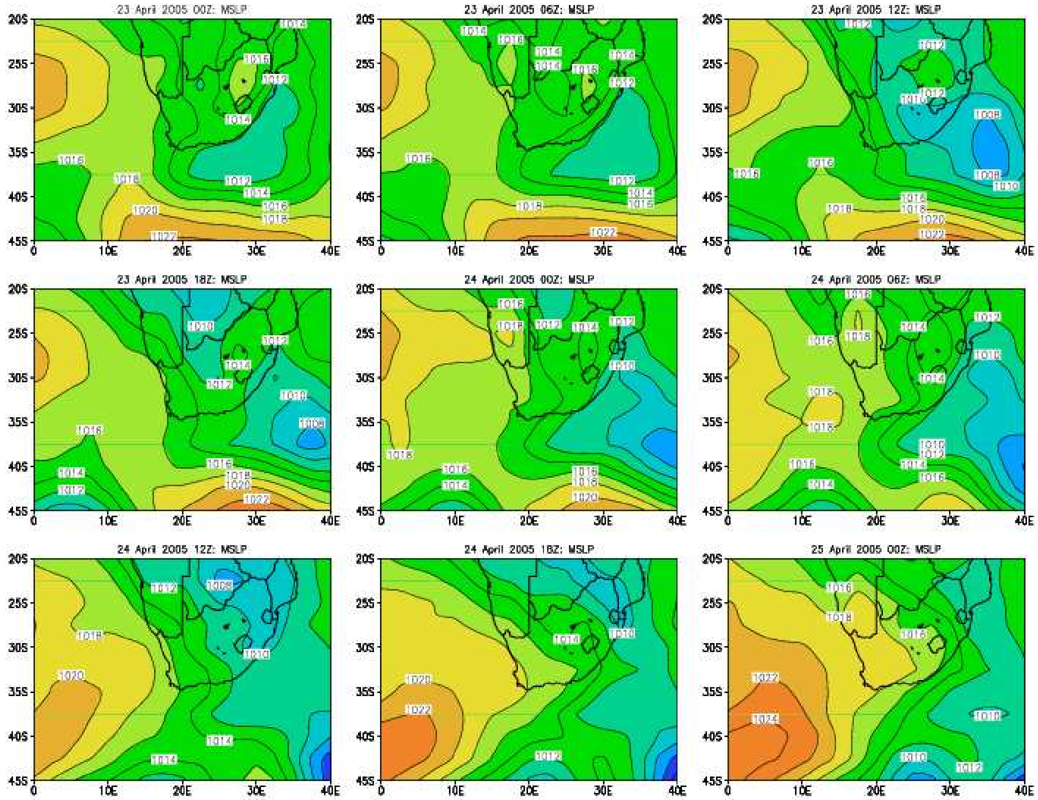

Figure 5.19: NCEP sea-level pressure field for 23 April 2005 0000Z to 25 April 2005 0000Z

weakened. These two low pressure systems were linked to the surface trough over the land. The flow over the land was generally weak and characterised by a slack gradient on the 23rd. The gradient tightened from the southwest on the 24th due to a high pressure system that started to extend a ridge in over the country. This caused for the surface trough over the country to become well defined. It was situated over the eastern half of the country at 1200Z on the 24th, and moved northeastwards during the remainder of this period.

The mid-tropospheric flow on the 23rd and 24th of April 2005 was characterised by the passage of two upper air geopotential height troughs and their associated temperature troughs (figure 5.20, temperature trough not shown). The first trough was situated over the western part of South Africa early on the 23rd. The amplitude of this trough decreased as it progressed eastwards over the country while at the same time the second trough was in the process to build just off the west coast. By 0000Z on the 24th, the second trough has moved

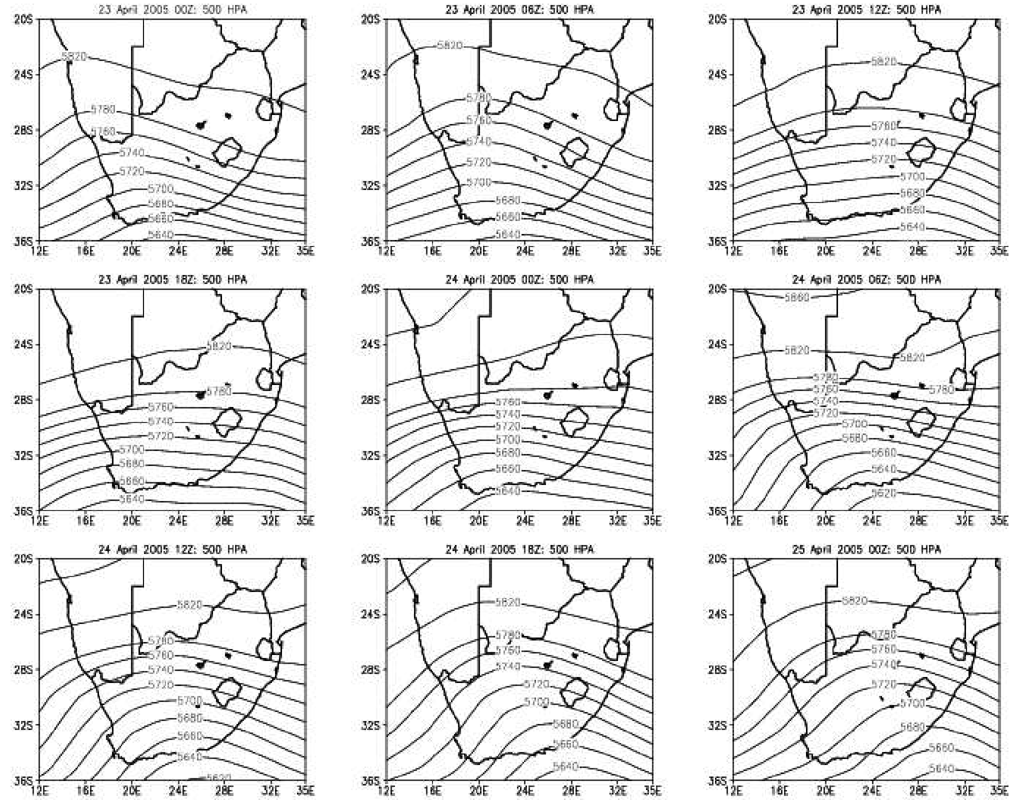

Figure 5.20: NCEP 500 hPa geopotential height field for 23 April 2005 0000Z to 25 April 2005 0000Z

in over the western and southern part of the country, while remnants of the first trough was observed over the northern part of the east coast. During the remainder of the 24th, the second trough moved eastward towards the eastern part of the country while its amplitude steepened slightly, reaching a maximum at about 1800Z.

5.3.3.2 C-CAM synoptic pattern

The C-CAM simulations of SLP and 500 hPa geopotential height for the 23rdand 24th of April are displayed in figures 5.21 and 5.22, respectively. The synoptic pattern as simulated by C-CAM shows close resemblance to the NCEP synoptic pattern and the major systems and sequence of events are generally captured well, especially at 500 hPa. However, a few subtle differences may be identified. Those worth mentioning, include:

- The main low pressure system southeast of the country is moved more rapidly southeastwards in the C-CAM simulation as compared to its actual movement as represented in the NCEP fields. Also, the C-CAM prognosis indicates the depth of this low to be 1010 hPa before leaving the study area (figure 5.21, 23 April 2005 1800Z), while it's actual depth is 1008 hPa.

- The surfuce trough over the land is more defined and slightly deeper in the C-CAM simulation for the 23rd, compared to the actual surface trough as represented by NCEP. Therefore, the pressure gradient over the country is not as relaxed as indicated in the NCEP field. During the latter half of the 24th, the C-CAM simulation is underestimating the strenth of the trough slightly. Generally, the trough-depth is underestimated by about 2 hPa in the C-CAM simulation. Another subtle difference is seen in the simulation of the surface trough for the 24th. Apart from the trough over the northeastern part of the country, the C-CAM prognosis indicates a secondary trough that stretches from southeastern Botswana southeastwards into the Northwest province of South Africa. The position of the surface trough as simulated by C-CAM compares otherwise very satisfactory with the actual position of the trough during this forecast period.

- The ridging of the high pressure system over the country from the southwest, is indicated to be slightly stronger in the C-CAM simulation compared to the NCEP data.

- At 500 hPa, a small pertubation is seen in the vicinity of Lesotho in the C-CAM simulation, while the NCEP field is very smooth. This could be a result of the higher resolution of C-CAM (0.15° compared to the lower resolution of NCEP, 2.5°), whith the C-CAM simulation capturing the effect of the mountains on the flow.

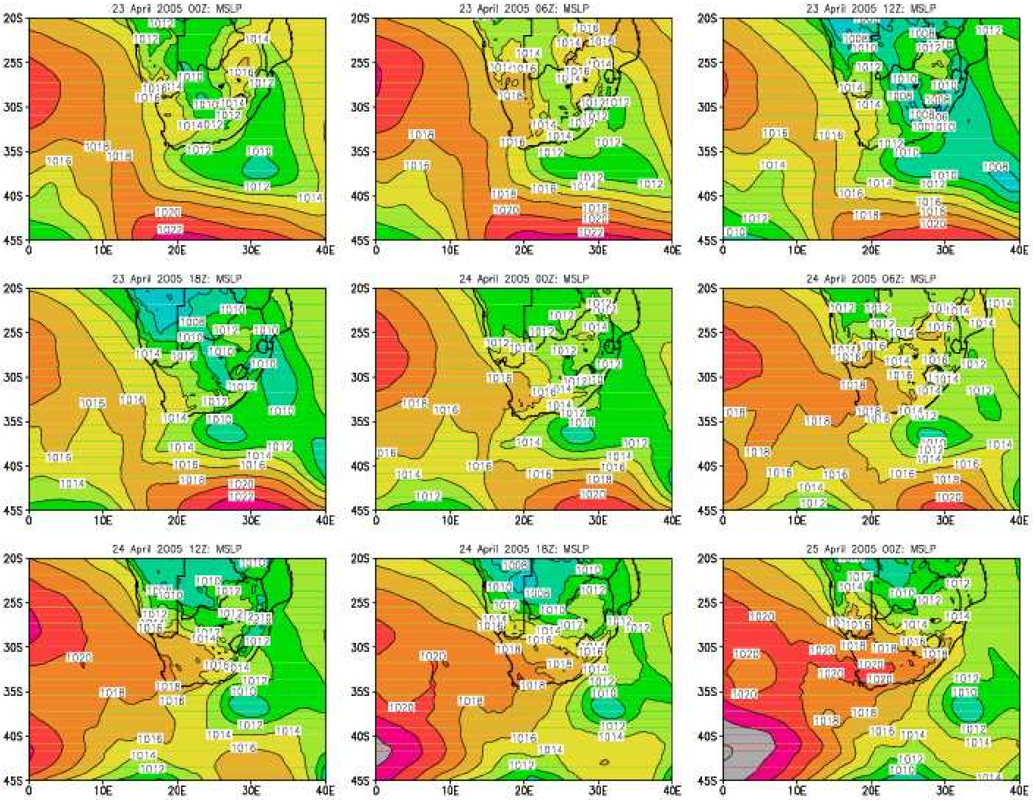

Figure 5.21: C-CAM sea-level pressure field for 23 April 2005 0000Z to 25 April 2005 0000Z

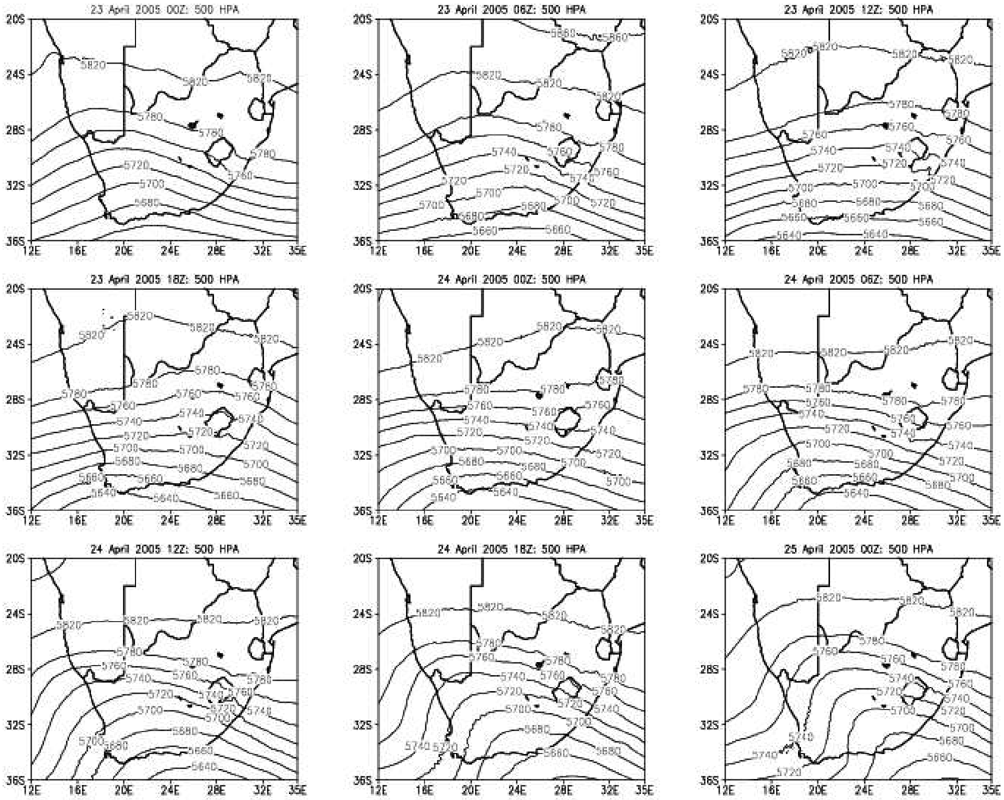

Figure 5.22: C-CAM 500 hPa geopotential height field for 23 April 2005 0000Z to 25 April 2005 0000Z

5.3.4 Sounding data: 500 hPa temperature

Mid-tropospheric cooling or warming in the low-levels can lead to more unstable conditions and convective development is promoted in this way. Very often, forecasters use the 500 hPa temperature of atmospheric soundings to determine whether cooling has taken place in the mid-troposphere. In addition to this, model soundings may also be utilised to determine how the 500 hPa temperatures will change during the forecast period. If cooling is indicated by the model forecast, the forecaster knows that the environmental temperature profile is getting more favourable for convective developent. In this section, the 500 hPa temperature as measured by the 12-hourly soundings at the Irene weather station between 20050423 0000Z to 20050425 0000Z, is compared to the 500 hPa temperature prognosis as simulated by the 20050423 0000Z model run. This is done in order to determine whether C-CAM captures the warming and cooling trends that one will expect considering that two upper air troughs (figure 5.20) made their way over the country during this forecast period. Also, the actual tropospheric temperature profile valid for 20050424 1200Z is compared to the corresponding model sounding. The Irene sounding is the closest sounding to the region where the storm occurred. This sounding should be representative of the environmental temperature profile in the vicinity of the storm.

The observed and simulated soundings are displayed in figure 5.23. C-CAM captured the temperature tendency satisfactorily. Except for the 1200Z sounding on the 23rd, where C-CAM overestimated the cooling by $0.8°C$, the remainder of the model soundings were within $0.5°C$ from the actual soundings. C-CAM gave very good guidance for the 500 hPa temperature tendency valid for the 24th. The cooling from the 1200Z sounding on the 24th to the 0000Z sounding on the 25th is captured very satisfactorily. However, a short-coming may be seen in the model soundings that are 24 hours apart. From the 1200Z sounding on the 23rd to the 1200Z sounding on the 24th the model sounding shows an increase in the temperature of $1.8°C$ while the actual increase was only $0.8°C$. The model sounding of 0000Z on the 24th to 0000Z on the 25th shows an increase in temperature of $0.4°C$, while the actual sounding shows a decrease of $0.2°C$.

After careful inspection of the actual 500 hPa temperature during this forecast period, it is noted that cooling took place twice but that there was generally not much variation in the temperature. The cooling took place in the beginning of this forecast period and again right at the end of the forecast period. The cooling that took place was slight, and one can therefore assume that the cooling on this pressure level did probably not aid in destabilizing the environmental air and consequently the developement of the multicell storm under discussion. The whole troposperic temperature profile for all of the soundings during this period will need to be analysed in order to identify the mechanism responsible for the increase in atmospheric instability that contributed to the thunderstorm

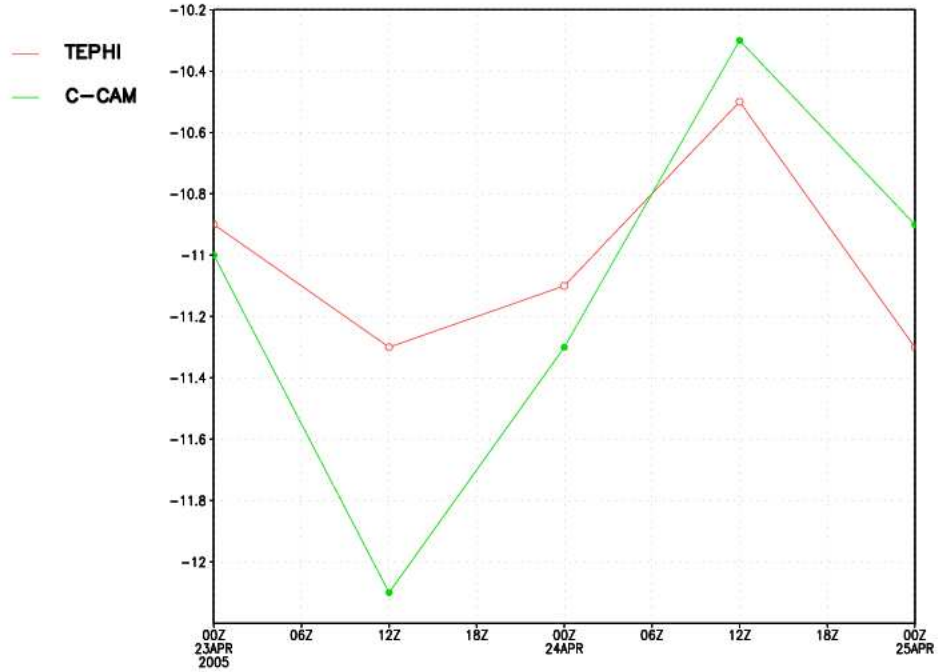

Figure 5.23: Time section (23 April 2005 0000Z to 25 April 2005 0000Z) of the 500 hPa temperature as by actual atmospheric soundings (red) and C-CAM soundings (green). Atmospheric soundings are taken at 0000Z and 1200Z.

develoment. However, this will not be attempted in this study, as the focus is rather on the verification of the 20050423 0000Z model run and not on analysing why the storm developed.

As a next step in the model verification, the model sounding of temperature valid for 20050424 1200Z at Irene is compared against the actual Irene sounding (figure 5.24). The model gridpoint closest to the location of the Irene weather station was used to create the temperature profile. The levels at which model output is written out are verified. These levels are 850 hPa, 800 hPa, 750 hPa, 700 hPa, 600 hPa, 500 hPa, 400 hPa, 300 hPa and 200 hPa. Where necessary, the actual sounding data was interpolated to these levels. A weighted interpolation procedure was used.

It is clearly seen that the model fared the best in the top half of the troposphere. From 500 hPa upwards, the absolute difference between the actual temperature and the forecast temperature is less than $1°C$. Below 500 hPa, the absolute difference ranged between $0.8°C$ to $3°C$. At 850 hPa C-CAM underestimated the temperature by $2.9°C$, at 800 hPa by $0.8°C$, at 750 hPa by $2.9°C$ and at 700 hPa by $0.9°C$. At 600 hPa C-CAM overestimated the temperature by $3°C$. As mentioned earlier, cooling in the mid-troposphere or warming in the low-levels contribute to the destabilization of the environmental air. With C-CAM underestimating temperatures between 850 and 700 hPa, but overestimating temperatures between 600 and 500 hPa, the environmental lapse rate as simulated by the model ends up being less favourable for convective development than the lapse rate that was actually observed. However, the fact that C-CAM indicated cooling from 1200Z on the 24th to 0000Z on the 25th would have shown a forecaster that mid-tropospheric conditions will become more unstable. This would have alerted any forecaster to anticipate convective developent if other conditions that favour convective development are also present. Generally, the C-CAM sounding compared very satisfactory to the actual sounding - especially if it is taken into account that this C-CAM sounding is a 36-hour forecast.

It may be noted that the errors in the temperature profile simuated in this case study show resemblence to the monthly average biases identified for simulations of the vertical temperature profile in chapter 4. Here a general cold bias was identified in the model simulations of the lower tropospheric tempertures, whilst a general warm bias was identified for the middle and upper troposphere.

5.3.5 Thunderstorm potential as simulated by C-CAM

5.3.5.1 Equivalent potential temperature difference

The vertical gradient of the equivalent potential temperature can be used as an indicator of conditional instability. The conditional stability criterion for a satu-

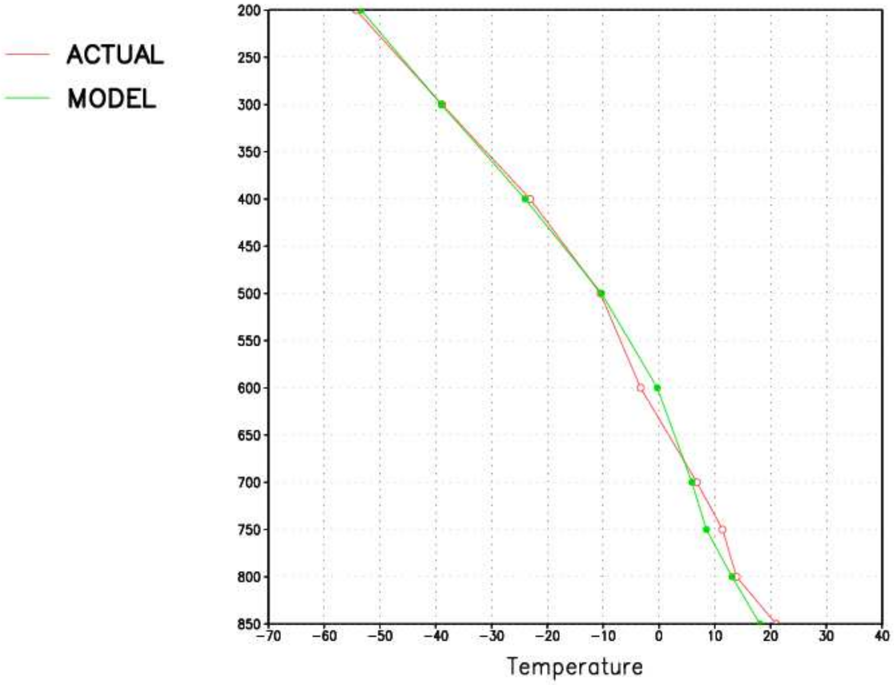

Figure 5.24: Actual vertical temperature profile (red) and vertical temperature profile as simulated by C-CAM (green) valid at 24 April 2005 1200Z

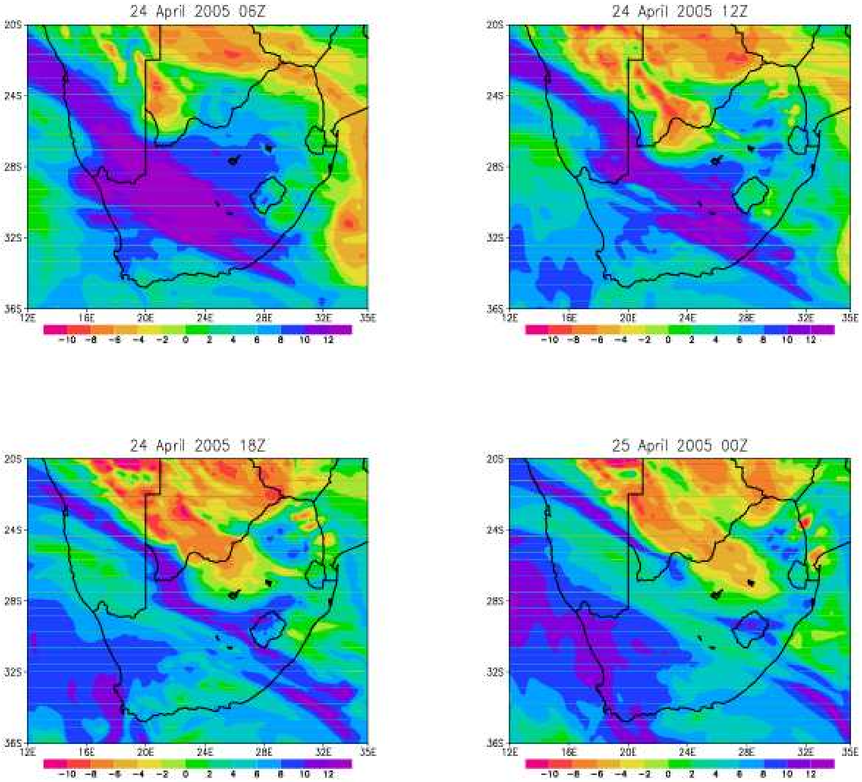

Figure 5.25: Equivalent potential temperature difference (500 hPa - 700 hPa) as simulated by C-CAM, valid for the times as indicated on the figure

rated parcel is (Holton, 1992; also see chapter 3):

$$\frac{\partial \theta_e}{\partial z} < 0, \; conditionally\, unstable$$

$$\frac{\partial \theta_e}{\partial z} = 0, \; neutral$$

$$\frac{\partial \theta_e}{\partial z} > 0, \; conditionally\, stable.$$

The equivalent potential temperature difference is calculated for the 700 hPa to 500 hPa layer. Negative values (reddish) indicate regions where conditionally unstable conditions exist. It can be seen on figure 5.25 that stable conditions are forecast over the area of interest at 0600Z, but that progressively more conditionally unstable conditions moved into that area during the remainder of the day.

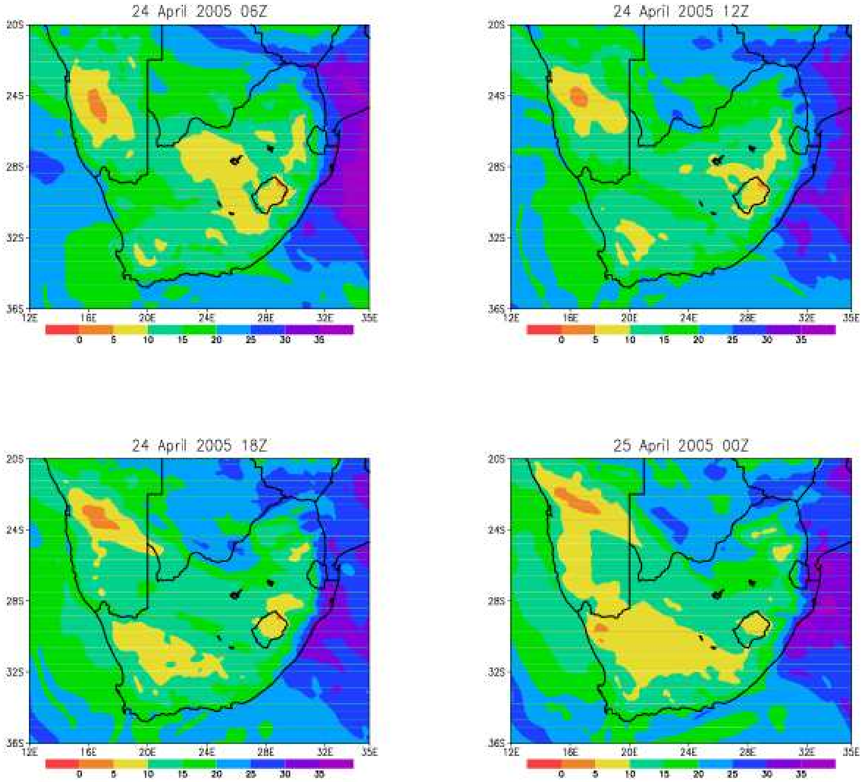

Figure 5.26: Precipitable water (mm) as simulated by C-CAM, valid for the times as indicated on the image

5.3.5.2 Precipitable water

The precipitable water is used as a measure of the atmospheric moisture content. It is the amount of surface rainfall that would result if all the moisture in an atmospheric column condenses and rain out. However, maximum values of precipitable water can be associated with no rainfall. There are processes needed to convert the moisture to rainfall. As precipitable water increases above a certain minimum value, atmospheric stability decreases and there is a progressive tendency for larger storms to develop (Harrison, 1988). Dyson (2000) determined that for heavy rainfall over South Africa the precipitable water must be at least 20 mm.

At 0600Z, the forecast precipitable water in the vicinity where the storm occurred , ranged from 5-15 mm (figure 5.26). A plume with higher precipitable water values (15-25 mm) can be seen at 1200Z to the northwest of the region where the storm occurred. This plume shifted gradually southeastward during

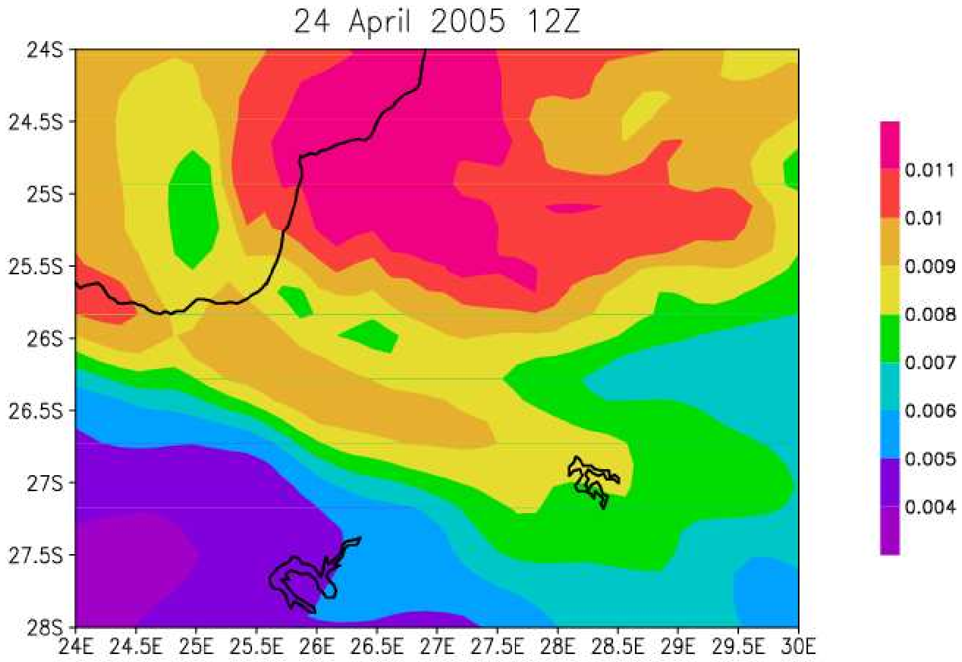

Figure 5.27: Mixing ratio (kg/kg) as simulated by C-CAM valid at 24 April 2005 1200Z

the remainder of the forecast hours towards the area where the storm occurred. By 1800Z, the forecast precipitable water in the region where the storm occurred was 15-20 mm.

5.3.5.3 Mixing ratio

The mixing ratio is a very valuable parameter of the moisture content of the air because it is independent of temperature and vary only with the addition and removal of water vapour (Preston-Whyte and Tyson, 1988). For thunderstorms to develop, sufficient low-level moisture must be present. It has been found that severe convection develop due to mesoscale boundary forcing, like drylines (Moller et al., 1994; Bluestein and Crawford, 1998).

The 850 hPa mixing ratio as simulated by C-CAM valid at 20050424 1200Z can be seen in figure 5.27. The most striking feature seen in this forecast of the mixing ratio, is the relatively tight gradient that was aligned southeasterly from just south of the Botswana border towards the Vaal Dam. This gradient seperated drier air to the south from more moist air to the north. A tongue of more moist air was situated just north of this moisture gradient, in the vicinity of the Witwatersrand. From this model prognosis of the 850 hPa mixing ratio,

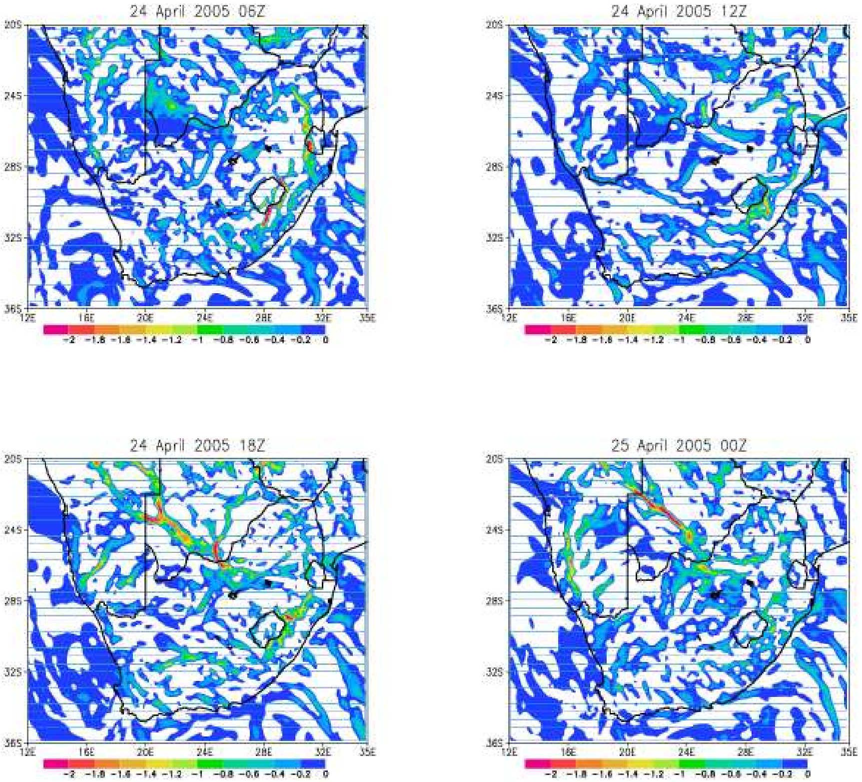

Figure 5.28: Moisture flux convergence (g. $m^{-3}.s^{-1}$) as simulated by C-CAM, valid for the times as indicated on the figure

the low-level moisture pattern seemed favourable for convective development.

5.3.5.4 Moisture flux convergence (MFC)

Studies by Hudson (1971) and Newman (1971) have shown that MFC (see chapter 3) can be used as a short-range predictive parameter. They found the best association between maxima of MFC and convective storms occurred three hours after the time of the MFC analysis. In this case study, MFC has been calculated for the 850 hPa pressure level. It can be seen in figure 5.28 that an increase took place in the MFC from 0600Z to 1800Z in the region where the multi-cell storm developed. What is especially encouraging is the well defined zone of MFC that is shown in the 1200Z prognosis (figure 5.29).

5.3.5.5 Bulk shear

There is a relation between the type of storm and the vertical shear of the lower tropospheric environment (Holton, 1992). Vertical wind shear influences the

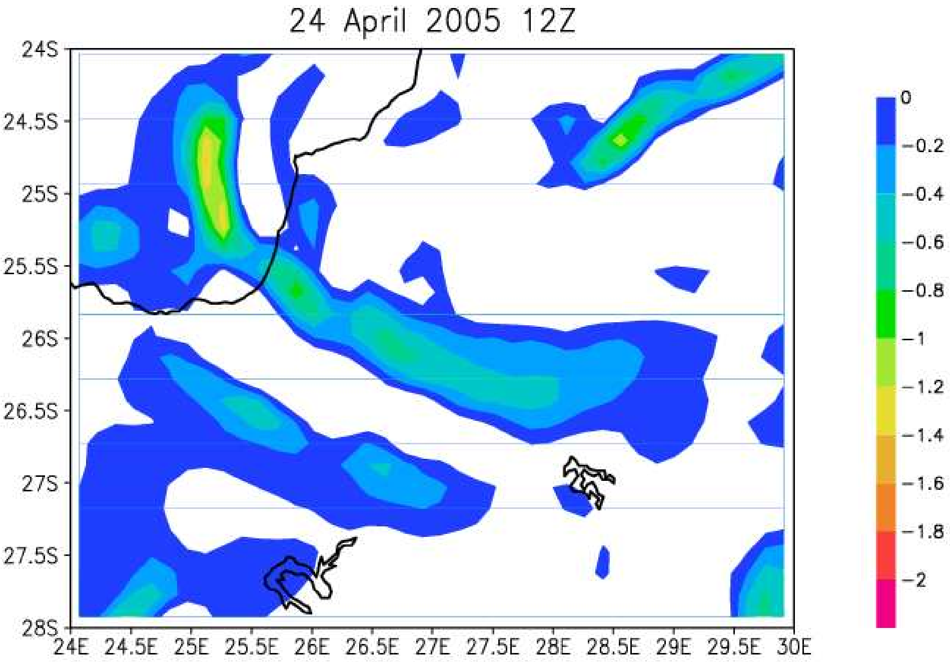

Figure 5.29: Moisture flux convergence ($g.m^{-3}.s^{-1}$) as simulated by C-CAM, valid at 24 April 2005 1200Z

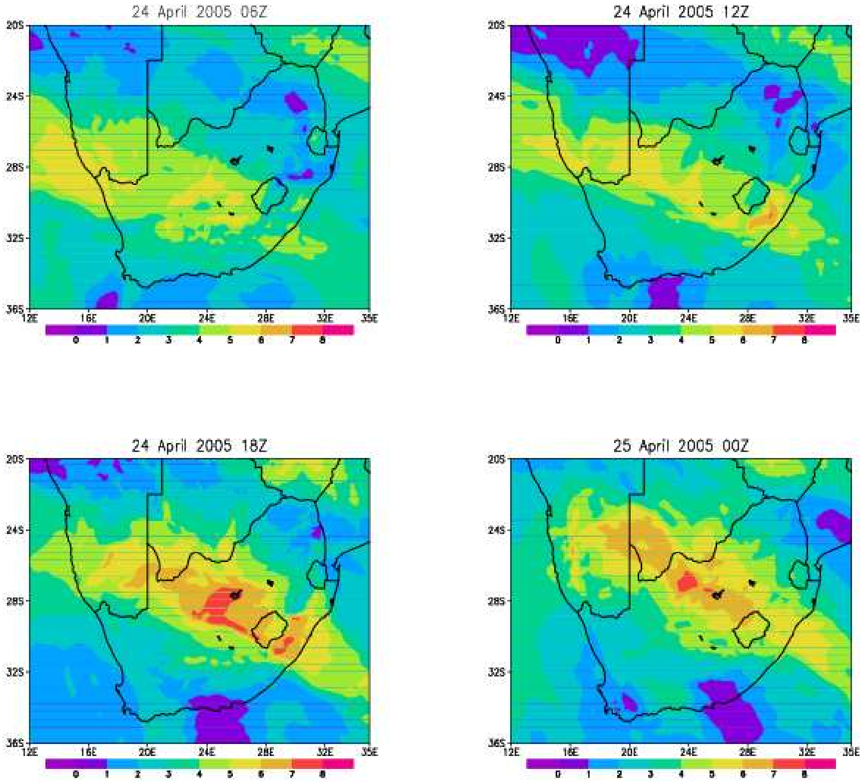

Figure 5.30: Bulk shear (ms^{-1}km^{-1}) for the 850-500 hPa layer as simulated by C-CAM, valid for the times as indicated on the figure

form that the convection might take, i.e., whether the convection evolves as short-lived cells, multicells, or supercells (Weisman and Klemp, 1982; Holton, 1992). In this case study, the bulk shear (SHR) as discussed in chapter 3 is calculated in order to determine the nature of the convection, given that convection will occur. Since over most of the interior the surface pressure values are about 850 hPa, the bulk shear was calculated in the layers from 850 hPa to 500 hPa (see chapter 3).

It can be seen on figure 5.30, that the shear increased in the region where the storm developed as the day progressed. Initially, the shear was $2-3\ ms^{-1}km^{-1}$ (0600Z) and increased to $3-5\ ms^{-1}km^{-1}$at 1800Z. According to Weisman and Klemp (1982), values of $3-5\ ms^{-1}km^{-1}$are associated with supercell formation while Dupilka and Reuter (2006) found that over Alberta, values of greater than 3 ms^{-1}, are mostly associated with non-tornadic severe hail events as well as significant tornadic events. Holton (1992) found that shear of $2.5-5\ ms^{-1}km^{-1}$is associated with multicell storms. Studies that investigate the relationship between the environmental shear and the type of convective storm over South Africa, are unfortunately not well documented. We rely therefore on the results of overseas studies. Based on these results, it seems that in this case the environmental wind shear got progressively favourable for the development of potentially severe convective storms.

5.3.6 Discussion

On Sunday afternoon, the 24th of April 2005, organised convection took place in the region of the Witwatersrand and extended to the highground of Mpumalanga. Towering cumulus clouds were reported from late morning over these areas, and from midday cumulonimbus clouds were reported. The first thunderstorm as reported in the METARs occurred at 1300Z at Irene, although a few thunderstorm cells were visible on the satellite imagery prior to 1300Z. These cells were obviously not close to stations where observations were done. According to the satellite images, the first thunderstorm cells appeared on the Mpumalanga highground. Soon thereafter, small thunderstorm cells started to develop further west. Some of these cells intensified and according to the satellite images, their cold outflow regions aided in the development of new thunderstorms. By late afternoon a multicell storm was visible on the satellite images and new cells developed on the western and northern side of this multicell storm. It was one of these cells that caused hail at the Johannesburg International airport as well as thundershowers that persisted for quite a while.

The question asked in this case study is whether C-CAM could give adequate guidance in anticipating a storm of this nature. As mentioned earlied, the 20050423 0000Z C-CAM run was used in this case study. This multicell storm developed therefore between 36 and 42 hours after the model initialization time. Based on the SLP and 500 hPa geopotential height prognosis for the afternoon and evening of the 24th, at least isolated convective development was expected over the central and eastern interior of South Africa. On the surface, a trough was simulated over the eastern part of the country, while a secondary trough was simulated further westwards. This latter trough extended southeastwards from southern Botswana to the eastern highground of the country. The region where the convective development took place was situated not too far north of this trough that was aligned in a southeasterly direction. The upper air trough was situated over the western part of the country but moved eastwards during the day to be situated over the central part of the country by 0000Z on the 25th. The movement and position of the upper air trough was generally favourable to promote convective development. Therefore, it can be assumed that provided that sufficient moisture was available, isolated thunderstorm development would have been forecast by most operational forecasters, based on just the prognostic synoptic pattern. The next step in the forecasting process was to focus on this area where convective activity may be expected in order to be more precise on the location and nature of the expected activity. This was done by analysing specific prognostic fields used in convective forecasting, in particular, atmospheric instability, moisture availability, moisture flux convergence and wind shear.

In the analysis of these prognostic fields it was seen that there was an increase of atmospheric instability, precipitable water, moisture flux convergence as well as wind shear in the region where the convective development occurred. Also, the 850 hPa mixing ratio prognosis for 1200Z on the 24th, showed a tongue of moist air with a tight moist-dry gradient (dry line) on it's southern side. The dry line is often associated with the initiation of thunderstorms over Texas and Oklahoma (Schaefer, 1986). It has been found by Preston-Whyte and Tyson (1988) that line storms, which are mostly multicellular, form preferentially ahead of a moisture discontinuity. It can therefore be assumed that this dry line that is detected in the 850 hPa mixing ratio prognosis, aided in the initial development of the convective activity. The surface moisture flux convergence provided a further trigger to initiate convective activity while the atmospheric instability present as indicated by the equivalent potential temperature difference (500-700 hPa) aided to sustain the convective activity. The wind shear which is associated with the nature of the convection, fell in the catagory where it is indicative of multicell storms. To summarise, all these prognostic fieds, gave good quidance in the anticipation of multicellular convection.

Chapter 6

Conclusions

The numerical model C-CAM is being used for short-range weather forecasting at UP. The model became operational in December 2004, and forecasts issued during 2005 are verified in this study. During this period the model was initialized once a day at 0000Z from GFS analysis and a 4-day forecast was produced with each model run. The model ran in variable resolution stretched-grid mode over southern Africa. The effective resolution over southern Africa was about 15 km, whilst over the panel of lowest resolution the resolution was in the order of 200 km. The model employed 18 sigma levels in the vertical. Model output was written to two domains: at 0.3 horizontal resolution over a larger domain that contained the subcontinent and surrounding oceans and at 0.15 horizontal resolution over a domain covering South Africa. Model output was available for a large number of variables at different pressure levels at 6-hourly intervals (see chapter 3 for a detailed description of the C-CAM forecasting system).

An important objective of the study, was to determine the accuracy and skill of C-CAM in forecasting synoptic-scale weather systems over southern Africa. This was achieved by comparing the C-CAM forecasts of 500 hPa geopotential height and the vertically integrated moisture flux against NCEP reanalysis data. The absolute error, root mean square error and the pattern correlation were determined for every 6-hour interval of each model run and was then averaged monthly. Corresponding error fields were calculated for 24-our persistence forecasts obtained using NCEP reanalysis data. The root mean square error and pattern correlation results show that the model has higher skill than 24-hour persistence forecasts for the full 4-day integration period for all the months studied. However, the results suggests that the day 3 and day 4 forecasts, must be used more carefully since the errors start to grow more rapidly from about the 9th integration time (48-hour forecast).

In the average absolute errors of the 500 hPa geopotential heights, the most striking feature during all al the months was a zonal error belt that developed in the high latitude regions while the errors were small and fairly consistent over the tropical regions. The high latitude error belt generally spread north -and eastwards as the forecast time increased. By the end of the forecast period (96-hour forecast), the meridional error gradient equatorwards of the error belt was situated between 30-40S. It was seen that there exists a definite seasonality in the behaviour of the average absolute error of the 500 hPa geopotential height. Errors are larger in the winter -and transitional months compared to the summer months. The spatial coverage of the error belts is also notably larger during the winter months. The amplitude and evolution of the 500 hPa geopotential height error pattern can be linked to the areas characteristic of cyclogenesis (e.g. the Weddel Sea and Queen Maud land), the most intense westerly wind systems (e.g. larger errors during winter months when systems are more intense) as well as the track of the systems (e.g. the mostly northeastward propogation of errors can be linked to the fact that upper-level cyclones tend to move northeastwards) (see chapter 4 for details).

Root mean square errors and pattern correlations calculated for the zonal and meridional moisture fluxes, as for the 500 hPa geopotential heights, indicate that C-CAM performs better than 24-hour persistence forecasts over the full four day integration period. The pattern correlation for the meridional moisture flux, is generally lower than that of the zonal moisture flux. This indicates that the model simulates the circulation patterns responsible for the meridional transport of moisture less well than the zonal patterns. The absolute errors indicate that in the summer and late summer months studied (January, February and April), relatively large errors in the moisture flux occur in a northwest to southeast directed band over the subcontinent. In the winter months (May and June), zonal errors are more important. These errors propagate into South Africa from the zonal error band located over the Southern Ocean.

Point verification was performed at one coastal (Cape Town) and one interior station (Irene). Twenty-four hour C-CAM forecasts of the vertical temperature profile at specific pressure levels were compared against the corresponding upper-air sounding data obtained from the SAWS. Where necessary, a weighted interpolation procedure was applied on the sounding data in order to obtain temperature values at the pressure levels on which C-CAM output is written. The absolute error and the bias were determined at all the selected pressure levels for the 24-hour forecast of each model run and then averaged on a monthly basis. At Cape Town and Irene the largest errors occurred in the low-levels and again near 200 hPa. The errors near 200 hPa were much more striking at Cape Town. This can probably linked to the fact that Cape Town is more prone to the passage of westerly waves and therefore it can be assumed that the height of the troposphere vary there more frequently. At both locations, the larger errors in the low-levels can be due to topographical influences. The average bias patterns at Cape Town and Irene show each their own characteristic features that are generally observed in all of the months. The average bias at Cape Town show a cold bias in the low-levels, a near-neutral to small warm bias in the mid-levels, a small cold bias during some of the months between 400 hPa to 300 hPa and a distinct warm bias during all of the months at 200 hPa. The average bias at Irene shows a warm bias at 850 hPa, a very distinct cold bias in the remainder of the low-levels (up to 700 hPa, except for two of the months at this level) and a warm bias (mostly small) for the remainder of the profile except for one of the months at 300 hPa and 400 hPa.

Another objective of this study was to determine the usefulness of C-CAM in the forecasting of specific weather events over southern Africa. In the first case study, a cut-off low event was verified while a thunderstorm event was investigated in the second case study. Both these case studies were approached from a forecasters perspective. Typical prognostic fields utilized by forecasters were verified. The synoptic sequence of events was subjectively verified by means of visual inspection against NCEP reanalysis data. In both these case studies, the synoptic sequence of events were captured satisfactory by the model prognosis. In the cut-off low event, heavy rainfall occurred along the Cape south coast. C-CAM captured the rainfall area satisfactory but failed to forecast the heavy rainfall in the correct locations. However, the model gave good guidance that the cut-off low event could be expected which will alert any experienced forecaster. In the thunderstorm event, which showed severe characteristics on satellite imagery, the question asked was whether the model guidance would have been suffient to indicate the probability of a potentially severe storm. In the analysis of prognostic fields it was seen that conditions were favourable for convective development in the region where the storm developed. Also, the forecast wind shear by C-CAM, showed that convective development with a multicellular nature, could be expected.

Generally, C-CAM provided satisfactory forecasts that are better than 24-hour persistence forecasts over the full four day integration period although the day one and day two forecasts are much better than the day three and the day four forecasts. The case studies illustrate that C-CAM can provide very usefull guidance in operation short-range weather forecasting.

Bibliography

[1] Bengtsson L and Hodges KI (2006) A note on atmospheric predictability. *Tellus* **58A** 154-157.

[2] Bjerknes V (1904) Das problem von der wettervorhersage, betrachtet vom standpunkt der mechanic und der physic. *Meteor. Z.* **21** 1-7.

[3] Bluestein HB and Crawford TM (1998) *On the forecasting of severe convection along te dryline: The role of topography.* Preprints of 16th Conf. on Weather Anal. and Forecasting. Phoenix, Arizona. American Meteorol. Soc. 281-282.

[4] Charney JG (1948) On the scale of atmospheric motions. *Geofys. Publ.* **17 (2)** 1-17.

[5] Charney JG, Gilchrist B and Shuman F (1956) The prediction of general quasi-geostrophic motions. *J. Meteor.* **13** 489-499.

[6] Chouinard C, Beland M and McFarlane N (1986) A simple gravity wave drag parameterization for use in medium-range weather forecasts models. *Atmos.-Ocean* **24** 91-110.

[7] CLW (Coastal Low Workshop) (1984) *Coastal Lows, S.A.* Institute of Maritime Technology, 67 pp.

[8] Crimp SJ, Van den Heever SC, D'Abreton PC, Tyson PD and Mason SJ (1997) *Mesoscale Modelling of Tropical-Temperate Troughs and Associated Systems over Southern Africa.* WRC Report **595/1/97** 395 pp.

[9] D'Abreton PC and Lindesay JA (1993) Water vapour transport over southern Africa during wet and dry early and late summer months. *Int. J. Climatol.* **13** 151-170.

[10] Davies T, Cullen MJP, Malcolm AJ, Mawson MH, Staniforth A, White AA and Wood N (2005) A new dynamical core for the Met Office's global and regional modelling of the atmosphere. *Quart. J. Roy. Meteor. Soc.* **131** 1759-1782.

[11] Derber JC, Parrish DF and Lord SJ (1991) The new global operational analysis system at the National Meteorological Center. *Weather and Forecasting* **6** 538-547.

[12] Dupilka ML and Reuter GW (2006) Forecasting tornadic thunderstorm potential in Alberta using environmental sounding data. Part I: Wind shear and Buoyancy. *Weather and Forecasting* **21** 325-335.

[13] Dyson LL (2000) *A dynamical forecasting perspective on synoptic scale weather systems over southern Africa.* MSc Thesis, University of Pretoria, 90 pp.

[14] Dyson LL and van Heerden J (2001) The heavy rainfall and floods over the northeastern Interior of South Africa during February 2000. *S. Afr. J. Sci.* **97** 80-86.

[15] Elmore KL, Schultz DM and Baldwin ME (2006) The behavior of synoptic-scale errors in the Eta Model. *Mon. Wea. Rev.* **134** 3355-3366.

[16] Estie KE (1981) The Laingburg flood disaster of 25/1/1981. *News Letter* No. **383,** Weather Bureau, Pretoria.

[17] Engelbrecht FA (2000) *Nested climate modelling over southern Africa with a semi-Lagrangian limited area model.* MSc-thesis, University of Pretoria, 134 pp.

[18] Engelbrecht FA (2005) Simulations of climate and climate change over southern and tropical Africa with the conformal-cubic atmospheric model. In *Potential Impacts and Vulnerabilities of Climate Change on Hydrological Responses in southern Africa,* ed. R.E. Schulze, chap. 4. WRC Report **1430/1/05**. Water Research Commission, Pretoria.

[19] Engelbrecht FA (2006) *Theory and application of quasi-elastic equations in terrain-following coordinates based on the full pressure field.* Ph. D. thesis, University of Pretoria, 234 pp.

[20] Engelbrecht FA and Rautenbach CJ deW (2000) Perspective for nested climate modelling over southern Africa. *SA Tydskrif vir Natuurwetenskap en Tegnologie* **19** 47-51.

[21] Engelbrecht FA, Rautenbach CJ deW, McGregor JL and Katzfey JJ (2002) January and July climate simulations over the SADC region using the limited-area model DARLAM. *Water SA,* **28**, 361-374.

[22] Fels SB and Schwarzkopf MD (1975) The simplified exchange approximation: a new method for radiative transfer calculations. *J. Atmos. Sci.* **32** 1475-1488.

[23] Gray WM (1967) *Global view of the origin of tropical disturbances and storms.* Atmos. Sci. Paper No 114, Dept. of Atmos. Sci., Colorado State University, Fort Collins, 105 pp.

[24] Gordon HB, Rotstayn LD, McGregor JL, Dix MR, Kowalczyk EA, OâFarrell SP, Waterman LJ, Hirst AC, Wilson SG, Collier MA, Watterson IG and Elliott TI (2002) *The CSIRO Mk3 climate simulation model.* Technical Report 60, CSIRO Atmospheric Research, 130 pp.

[25] Haltiner GJ and Williams RT (1980) *Numerical prediction and Dynamic Meteorology* (2nd edition). John Wiley and sons. 477 pp.

[26] Harangozo S and Harrison MSJ (1983) On the use of synoptic data in indicating the presence of cloud bands over southern Africa. *S. Afr. J. Sci.* **79** 413-414.

[27] Harrison MSJ (1984) A generalized classification of South African summer rain-bearing synoptic systems. *Int. J. Climatol.* **4** 547-560.

[28] Harrison MSJ (1986) *A synoptic climatology of South African rainfall variations.* Ph.D. thesis, University of the Witwatersrand.

[29] Harrison MSJ (1988) Rainfall and precipitable water relationships over the central interior of South Africa. *South African Geographical Journal* **70 (2)** 100-111.

[30] Hastenrath SL (1966) The flux of atmospheric water vapour over the Caribbean Sea and the Gulf of Mexico. *J. Appl. Meteorol.* **5** 778-788.

[31] Hayward LQ and van den Berg HJC (1968) Die Port Elizabeth stortreens van 1 Septermber 1968. *Nuusbrief* No. **234**, Weerburo, Pretoria.

[32] Holton JR (1992) *An Introduction to Dynamic Meteorology* (3rd edition). Academic Press. 511 pp.

[33] Holtslag AAM and Boville BA (1993) Local versus non-local boundary layer diffusion in a global climate model. *J. Climate* **6** 1825-1843.

[34] Hudson HR (1971) On the relationship between horizontal moisture convergence and convective cloud formation. *J. Appl. Meteor.* **10** 755-762.

[35] Hunter I (1987) The weather of the Agulhas Bank and the Cape south coast. *CSIR Research Report* **634**.

[36] Janjic ZI, Gerrity JP Jr and Nickovic S (2001) An alternative approach to nonhydrostatic modeling. *Mon. Wea. Rev.* **129** 1164-1178.

[37] Johnson DH (1970) The role of the tropics in the global circulation. *The Global Circulation of the Atmosphere* (GA Corby, Ed) London, Roy. Meteor. Soc., 113-136.

[38] Jones DA and Simmonds I (1993) A climatology of Southern Hemispheric extratropical cyclones. *Climate Dynamics* **9** 131-145.

[39] Jury MR (1992) A climatic dipole governing the interannual variability of convection over the SW Indian Ocean and SE Africa region. *Trends Geophys. Res.* **1** 165-172.

[40] Jury MR and Pathack BMR (1993) Composite climatic patterns associated with the 1992 drought over southern Africa: 1975-1984. *Theor. Appl. Climatol.* **47** 137-145.

[41] Jury MR, McQueen CA and Levey KM (1994) SOI and QBQ signals in the African region. *Theor. Appl. Climatol.* **50** 103-115.

[42] Jury MR, Pathack B, Rautenbach CJ deW and Van Heerden J (1996) Drought over South Africa and Indian Ocean SST: Statistical and GCM results. *The Global Atmosphere and Ocean System* **4** 47-63.

[43] Jury MR, Mulenga H and Rautenbach CJ deW (2000) Tropical Atlantic variability and Indo-Pacific ENSO: Statistical analysis and numerical simulation. *The Global Atmosphere and Ocean System* **7** 107-124.

[44] Kalnay, E, and Coauthors (1996) The NCEP/NCAR 40-Year Reanalysis Project. *Bull. Amer. Meteor. Soc.* **77** 437-471.

[45] Keable M, Simmonds I, and Keay K (2002) Distribution and temporal variability of 500 hPa cyclone characteristics in the southern hemisphere. *Int. J. Climatol.* **22** 131-150.

[46] Lamb HH, and Britton GP (1955) General atmospheric circulation and weather variations in the Antarctic. *Geogr. J.* **121** 334-349.

[47] Lindesay JA and Jury MR (1991) Atmospheric circulation controls and characteristics of a flood event in central South Africa. *Int. J. Climatol.* **11** 609-627.

[48] Mason SJ and Jury MR (1997). Climatic variability and change over southern Africa: A reflection on underlying processes. *Prog. Phys. Geogr.* **21** 23-50.

[49] McGregor JL (1993) Economic determination of departure points for semi-Lagrangian models. *Mon. Wea. Rev.* **121** 221-230.

[50] McGregor JL (1996) Semi-Lagrangian advection on conformal-cubic grids. *Mon. Wea. Rev.* **124** 1311-1322.

[51] McGregor JL (2003) A new convection scheme using simple closure. *BMRC Research Report* **93** 33-36.

[52] McGregor JL (2005a) C-CAM: *Geometric aspects and dynamical formulation* [electronic publication]. Technical Report 70, CSIRO Atmospheric Research, 43 pp.

[53] McGregor JL (2005b) Geostrophic adjustment for reversibly staggered grids. *Mon. Wea. Rev.* **133** 1119-1128.

[54] McGregor LL, Gordon HB, Watterson IG, Dix MR and Rotstayn LD (1993) *The CSIRO 9-level atmospheric general circulation model.* Technical Report 26, CSIRO Atmospheric Research, 89 pp.

[55] McGregor JL and Dix MR (2001) *The CSIRO conformal-cubic atmospheric GCM.* IUTAM Symposium on Advances in Mathematical Modelling of Atmosphere and Ocean Dynamics, P.F. Hodnett, Ed., Kluwer, 197-202.

[56] McGregor JL and Dix MR (2006) An updated description of the Conformal-Cubic Atmospheric Model.

[57] Moller AR, Doswell III CA, Foster MP and Woodall GR (1994) The operational recognition of supercell thunderstorm environments and storm structures. *Weather and Forecasting* **9** 327-347.

[58] Newman WR (1971) *The relationship between horizontal moisture convergence and severe storm occurrences.* M.S. thesis, School of Meteorology, University of Oklahoma, 54 pp.

[59] Okoola RE (1989) Westward moving disturbances in the southwest Indian Ocean. *Meteorol. Atmos. Phys.* **41** 35-44.

[60] Olwoch JM, Rautenbach CJ deW, Erasmus BFN, Engelbrecht FA and Van Jaarsveld AS (2003) Simulating ticks distributions over sub-Saharan Africa: the use of observered and simulated climate surfaces. *Journal of Biogeography* **30** 1221-1232.

[61] Olwoch JM, Reyers B, Engelbrecht FA and Erasmus BFN (2007) Climate change and the tick-borne disease, Theileriosis (East Coast fever) in sub-Saharan Africa. *Journal of Arid Environments. Accepted.*

[62] Padya BM (1984) The Climate of Mauritius, Meteorological Office, Vacoas, Mauritius Meteorological Office Report, 217 pp.

[63] Preston-Whyte RA and Tyson PD (1988) The Atmosphere and Weather of Southern Africa. Oxford University Press, Cape Town. 374 pp.

[64] Purdom JFW (1973) *Satellite imagery and the mesoscale convective forecast problem.* Preprints, 8thconference on Severe Local Storms, Denver, Amer. Meteor. Soc. 244-251.

[65] Rancic M, Purser RJ and Mesinger F (1996) A global shallow-water model using an expanded spherical cube: Gnomic versus conformal coordinates. *Quart. J. Roy. Meteor. Soc.* **122** 959-982.

[66] Rautenbach CJ deW (2003) *Seasonal climate predictions with a coupled atmosphere-ocean general circulation model.* Water Research Commission Report, No **904/1/03** 82 pp.

[67] Rautenbach CJ deW, Engelbrecht FA, Potgieter-Engelbrecht CJ, Ndarana T and McGregor JL (2005) *Regional model development for simulating atmospheric behavior and rainfall over southern Africa.* Water Research Commission, Pretoria, RSA, Report **1261/1/05**.

[68] Reason CJC and Keibel A (2004) Tropical Cyclone Eline and Its Unusual Penetration and Impacts over the Southern African Mainland. *Weather and Forecasting* **19** 789-805.

[69] Richardson LF (1922) *Weather prediction by numerical process.* Cambridge University Press, reprinted Dover, 1965, 236 pp.

[70] Riehl H (1954) *Tropical Meteorology.* McGraw-Hill, New York, 392 pp.

[71] Riphagen HA (1999) The Eta model in South Africa. *International Eta Model Newsletter* no. 2, February 1999.

[72] Riphagen HA, Bruyere CL, Jordaan W, Poolman ER and Gertenbach JD (2002) Experiments with the NCEP regional Eta model at the South African Weather Bureau, with emphasis on terrain presentation and its effect on precipitation predictions. *Mon. Wea. Rev.* **130** 1246-1263.

[73] Rivest C, Staniforth A and Robert A (1994) Spurious resonant response of semi-Lagrangian discretizations to orographic forcing: Diagnostics and solution. *Mon. Wea. Rev.* **122** 366-376.

[74] Rubin MJ (1956) The associated precipitation and circulation patterns over southern Africa. *Notos* **5** 53.

[75] Schaefer JT (1986) The dryline. *Mesoscale Meteorology and Forecasting,* PS Ray, Ed., Amer. Meteor. Soc., 549-572.

[76] Schmidt F (1977) Variable fine mesh in spectral global model. *Beitr. Phys. Atmos.* **50** 211-217.

[77] Schwarzkopf MD and Fels SB (1991) The simplfied exchange method revisted: an accurate, rapid method for computation of infrared cooling rates and fluxes. *J. Geophys. Res.* **96** 9075-9096.

[78] Simmonds I and Keay K (2000) Mean Southern Hemisphere extratropical cyclone behaviour in the 40-year NCEP-NCAR reanalysis. *Journal of Climate* **13** 873-885.

[79] Streten NA (1973) Some characteristics of satellite-observed bands of persistent cloudiness over the Southern Hemisphere. *Mon. Wea. Rev.* **101** 486.

[80] Taljaard JJ (1953) The mean circulation in the lower troposphere over southern Africa. *S. Afr. Geogr. J.* **35** 33.

[81] Taljaard JJ (1959) S*outh African airmasses: their properties, movement and associated weather*. Ph.D. Thesis, University of the Witwatersrand, 221 pp.

[82] Taljaard JJ and van Loon H (1960) *The construction of 500 mb contour maps over the Southern Ocean.* In Antarctic Meteorology, Pergamon Press, Melbourne, 96-114.

[83] Taljaard JJ and Van Loon H (1962) Cyclogenesis, cyclones and anticyclones in the Southern Hemisphere during the Winter and Spring of 1957. *Notos* **11** 3-20.

[84] Taljaard JJ, and Van Loon H (1963) Cyclogenesis, cyclones and anticyclones in the Southern Hemisphere during Summer 1957/58. *Notos* **12** 37-50.

[85] Taljaard JJ (1964) Cyclogenesis, cyclones and anticyclones in the Southern Hemisphere during autumn, 1958. *Notos* **13** 31-36.

[86] Taljaard JJ and Van Loon H (1964) Southern Hemisphere weather maps for the International Geophysical Year. *Bull. Amer. Meteor. Soc.* **45** 88-95.

[87] Taljaard JJ (1965) Cyclogenesis, cyclones and anticyclones in the Southern Hemisphere during the period June to December 1985. *Notos* **14** 73-84.

[88] Taljaard JJ (1967) Development, Distribution and Movement of Cyclones and Anticyclones in the Southern Hemisphere during the IGY. *J. Appl. Meteor.* **6** 973-987.

[89] Taljaard JJ (1972) Synoptic Meteorology of the Southern Hemisphere. In: *Meteorology of the Southern Hemisphere. C.W. Newton (Editor), Meteorological Monographs*, no. **35**, American Meteorological Society, Boston, 263 pp.

[90] Taljaard JJ (1994) Atmospheric circulation systems, synoptic climatology and weather phenomena of South Africa. Part 1. Controls of the weather and climate of South Africa. *Technical Paper* **27**, SA Weather Bureau, Department of Transport, Pretoria.

[91] Taljaard JJ (1995a) Atmospheric circulation systems, synoptic climatology and weather phenomena of South Africa. Part 2. Atmospheric circulation systems in the South African region. *Technical Paper* **28**, SA Weather Bureau, Department of Transport, Pretoria.

[92] Taljaard JJ (1995b) Atmospheric circulation systems, synoptic climatology and weather phenomena of South Africa. Part 3. The synoptic climatology of South Africa in January and July. *Technical Paper* no. **29**, SA Weather Bureau, Department of Transport, Pretoria.

[93] Taljaard JJ (1995c) Atmospheric circulation systems, synoptic climatology and weather phenomena of South Africa. Part 4. Surface pressure and wind phenomena in South Africa. *Technical Paper* no. **30**, SA Weather Bureau, Department of Transport, Pretoria.

[94] Taljaard JJ (1996) Atmospheric circulation systems, synoptic climatology and weather phenomena of South Africa. Part 6. Rainfall in South Africa. *Technical Paper* no **32**, SA Weather Bureau, Department of Transport, Pretoria.

[95] Todd MC, Washington R and Palmer PI (2004) Water vapour transport associated with tropical-temperate trough systems over southern Africa and the southwest Indian ocean. *Int. J. Climatol.* **24** 555-568.

[96] Tyson PD (1984) The atmospheric modulation of extended wet and dry spells over South Africa, 1958-1978. *J. Climatol.* **4** 621-635.

[97] Tyson PD (1986) Climatic Change and Variability in southern Africa, Oxford University Press, Cape Town, 220pp.

[98] Van Loon H (1965) A climatological study of the atmospheric circulation in the Southern Hemisphere during the IGY, Part I: 1 July 1957-31 March 1985. *J. Appl. Meteor.* **4** 479-491.

[99] Washington R and Todd MC (1999) Tropical temperate links in southern African and southwest Indian Ocean daily rainfall. *Int. J. Climatol.* **19** 1601-1616.

[100] Weismann ML and Klemp JB (1982) The dependence of numerically simulated convective storms on vertical wind shear and buoyancy. *Mon. Wea. Rev.* **110** 504-520.

[101] Wilson JW, Foote G, Crook NA, Fankhauser JC, Wade CG, Tuttle JD, Mueller CK and Krueger SK (1992) The role of boundary layer convergence zones and horizontal rolls in the initiation of thunderstorms: A case study. *Mon. Wea. Rev.* **120** 1785-1815.